8-1-2013

BIFURCATION AND CHAOS OF NONLINEAR VIBRO-IMPACT SYSTEMS

Yu Guo
Southern Illinois University Carbondale, gary.rain@gmail.com

BIFURCATION AND CHAOS OF NONLINEAR VIBRO-IMPACT SYSTEMS

by

Yu Guo

M.S., Southern Illinois University Edwardsville, 2008
B.S., South China University of Technology, 2006

A Dissertation
Submitted in Partial Fulfillment of the Requirements for the
Doctor of Philosophy in Engineering Science

Department of Engineering Science
In the Graduate School
Southern Illinois University Carbondale and Edwardsville
August/2013

DISSERTATION APPROVAL

BIFURCATION AND CHAOS OF NONLINEAR VIBRO-IMPACT SYSTEMS

by

Yu Guo

A Dissertation Submitted in Partial

Fulfillment of the Requirements

for the Degree of

Doctor of Philosophy

in the field of Mechanical Engineering

Approved by:

Albert C.J. Luo, Chair

Fengxia Wang

Tsuchin Philip Chu

Om Agrawal

Mohammad Sayeh

Chunqing Lu

Graduate School

Southern Illinois University Carbondale

06/07/2013

ABSTRACT

AN ABSTRACT OF THE DISSERTATION OF

Yu Guo, for the Doctor of Philosophy degree in Mechanical Engineering, presented on 06/07/2013, at Southern Illinois University Carbondale.

TITLE: BIFURCATION AND CHAOS OF NONLINEAR VIBRO-IMPACT SYSTEMS

MAJOR PROFESSOR: Dr. Albert C.J. Luo

Vibro-impact systems are extensively used in engineering and physics field, such as impact damper, particle accelerator, etc. These systems are most basic elements of many real world applications such as cars and aircrafts. Such vibro-impact systems possess both the continuous characteristics as continuous dynamical systems and discrete characteristics introduced by impacts at the same time. Thus, an appropriately developed discrete mapping system is required for such vibro-impact systems in order to simplify investigation on the complexity of motions.

In this dissertation, a few vibro-impact oscillators will be investigated using discrete maps in order to understand the dynamics of vibro-impact systems. Before discussing the nonlinear dynamical phenomena and behaviors of these vibro-impact oscillators, the theory for nonlinear discrete systems will be applied to investigate a two-dimensional discrete system (Henon Map). And the complete dynamics of such a nonlinear discrete dynamical system will be presented using the inversed mapping method. Neimark bifurcations in such a discrete system have also drawn a lot of interest to the author. The Neimark bifurcations in such a system have actually formed a boundary dividing the stable solution of positive and negative maps (inversed mapping). For the first time, one is able to obtain a complete prediction of both stable and unstable solutions in such a discrete dynamical system. And a detailed parameter map will be

presented to illustrate how changes of parameters could affect the different solutions in such a system.

Then, the theory of discontinuous dynamical systems will be adopted to investigate the vibro-impact dynamics in several vibro-impact systems. First, the bouncing ball dynamics will be analytically discussed using a single discrete map. Different types of motions (periodic and chaotic) will be presented to understand the complex behavior of this simple model. Analytical condition will be expressed using switching phase of the system in order to easily predict stick and grazing motion. After that, a horizontal impact damper model will be studied to show how complex periodic motions could be developed analytically. Complete set of symmetric and asymmetric periodic motions can also be easily predicted using the analytical method. Finally, a Fermi-Accelerator being excited at both ends will be discussed in detail for application. Different types of motions will be thoroughly studied for such a vibro-impact system under both same and different excitations.

DEDICATION

I would like to make some important dedications with this research work.

First, I would like to dedicate this work to my wife who always stays by my side, supporting me when the hard times come. Without your love and support, I could never have achieved what I had. To my kids in the future, I would also like to dedicate this work to you. I would like to let you know that you are always loved by your parents even before you are born. And I would like you to understand, whatever you want in this world, you will need to work hard for it.

I would like to further dedicate this research to my parents who taught me to be independent and responsible. Thanks to you that I could have the chance to study abroad and work on such an interesting research. Thanks to you for all your physical and mental supports that helped me get through difficulties.

I would like to dedicate this work to all my important family members. To my grandfather and maternal grandfather who have passed away, how I wish you could see this work and celebrate with me. To my grandmother and maternal grandmother, thank you for your kind love. I know you missed me when I couldn't visit you for years. I love and miss you all forever.

Finally, I would like to dedicate this research to all the people who have supported it. I gratefully appreciate for your advices and supports. This research would not have gone smoothly without your helps.

ACKNOWLEDGMENTS

First I would like to give grateful thanks to my advisor Dr. Albert C.J. Luo, who gave me all the advices and support during the entire process of this research. I could never have achieved what I have without the intuitive guiding of Dr. Luo. Also as the dissertation advisory committee chair, Dr. Luo kindly provided a lot of help through the whole preparing process of this dissertation. Herein, I would like to express my deepest appreciation to Dr. Albert C.J. Luo once again.

Also I would like to especially thank all the dissertation advisory committee members: Professor Fengxia Wang, Professor Tsuchin Philip Chu, Professor Om Agrawal, Professor Mohammad Sayeh, Professor Chunqing Lu. Thanks to you for all the advices and suggestions you gave me. Without all these helps I couldn't have completed this dissertation so smoothly.

I would like to gratefully thank the Department of Mechanical and Industrial Engineering for their financial support. Also I wish to express my appreciation to all the faculty and staff at Southern Illinois University for the cooperative efforts during my years of graduate study. Nevertheless, the guidance from all the professors in class leads me to the successful completion of this dissertation.

Finally, I would like to express my greatest appreciation to the members in our research group for their helps. Thanks to all my friends for their helps, supports, and valuable hints that make the tough work easier.

TABLE OF CONTENTS

LIST OF TABLES

LIST OF FIGURES

CHAPTER 1

INTRODUCTION

In this chapter, a brief review of the discrete and discontinuous dynamical systems will be provided, and a brief history of researches on different vibro-impact systems will be introduced. The layout of this dissertation and the chapter summary will also be described.

1.1. Objectives

Vibro-impact systems are extensively investigated in both engineering and physics field. Such systems possess the continuous characteristics as continuous dynamical systems, and carry the discrete characteristics introduced by impacts at the same time. Thus, appropriately developed discrete mapping structures are required for such vibro-impact systems in order to investigate the complexity of motions. In this dissertation, a few vibro-oscillators will be investigated in order to understand the dynamics of vibro-impact systems. Before discussing the nonlinear dynamical phenomena and behaviors of these vibro-impact oscillators, the theory for nonlinear discrete systems will be applied to a two-dimensional discrete system (Henon Map), and the complete dynamics of such nonlinear discrete dynamical systems will be presented. Then, the theory of discontinuous dynamical systems will be adopted to research the vibro-impact dynamics in several vibro-impact systems. First, bouncing ball dynamics will be analytically discussed using a single discrete map. And then, a horizontal impact damper will be presented to show how complex periodic motions could be developed and predicted analytically. Finally, a double excited Fermi-Accelerator under same or different excitations will be discussed in detail for application.

1.2. Henon Map

The nonlinear discrete systems are usually obtained from the nonlinear difference equations of dynamical systems. These systems provide a convenient way to easily describe the behavior of a complex dynamical system by looking only at the initial and final states. The complex dynamical behaviors in such systems can be observed through the cascade of stable solutions.

Among different nonlinear discrete systems, Henon map is a typical example that's of great interests to researchers. In 1976, a one-dimensional discrete map was used to describe the dynamical processes in biological, economic, and social science (May, 1976). In the same period, a discrete-time dynamic system was introduced to simplify the 3-dimensional Lorenz equations as a Poincare map (Henon, 1976), from which one can observe chaos numerically. This discrete system was latter on well known as Henon map. The existence of chaotic behavior in Henon map was later mathematically proved (Marotto, 1979) for certain parameters. At the same time, the chaotic behavior of Henon map was measured using Lyapunov characteristic exponent and frequency spectrum (Curry, 1979). In 1988, the topologic properties and multifractality of Henon map was investigated (Cvitanovic, Gunaratne, & Procaccia, 1988). In 1992, a geometric approach for the period doubling bifurcation was presented by Luo and Han (Luo & Han, Period Doubling and Multifractals in 1-D Iterative Maps, 1992). And they investigated the multifractality of a general one-dimensional iterative map. In 1993, numerical investigation of parameter maps was also performed (Gallas, 1993) for Henon map. Later in 2000, Zhusubaliyev et al numerically conducted the bifurcation analysis of Henon map and presented a more detailed parameter map (Zhusubaliyev, Rudakov, Soukhoterin, & Mosekilde, 2000).

All the aforementioned investigations were based on the numerical iterations of the discrete map. In 2006, Gonchenko et al (Gonchenko, Meiss, & Ovsyannikov, Chaotic Dynamics of Three-Dimensional Henon Maps that Originate from a Homoclinic Bifurcation, 2006) investigated the 3-dimensional Henon map generated from a homoclinic bifurcation. Later in 2007 they further studied the bifurcation of periodic solution of the generalized Henon map. They also proved the existence of infinite cascades of periodic solutions in such a system (Gonchenko, Gonchenko, & Tatjer, Bifurcations of Three-Dimensional Diffeomorphisms with Non-Simple Quadratic Homoclinic Tangencies and Generalized Henon Maps, 2007). In 2008, the parameter maps of periodic windows embedded in chaotic solutions of Henon map was determined with a random searching procedure (Lorenz, 2008). Recently, the Ying-Yang theory in nonlinear discontinuous dynamics was presented (Luo, A Ying-Yang theory in Nonlinear Discrete Dynamical Systems, 2010). In his theory, Luo divided the solutions of nonlinear discrete dynamical systems into three states: “Yang”, “Ying”, and “Ying-Yang” states. Through his approach one can obtain the complete solution states for all the entire parameter regions. Also he and Guo applied the approach to Henon map and investigated the parameter characteristics of the stable and unstable solutions in such a nonlinear discrete system (Luo & Guo, Parameter characteristics for stable and unstable solutions in nonlinear discrete dynamical systems, 2010).

Using the same theory (Luo, A Ying-Yang theory in Nonlinear Discrete Dynamical Systems, 2010) proposed by Luo, the complete solution states in the entire parameter space for Henon map will be presented in chapter 2. The stable and unstable periodic solutions of the Henon map will be investigated for demonstrations, and the corresponding eigenvalues analysis of periodic solutions will be carried out. The parameter map beyond the existing results for different solutions will be developed. The Poincare mapping relative to Neimark bifurcation will

be presented and the separatrix of solutions will be illustrated. The idea of discrete mappings will be further applied to dynamical systems such as bouncing ball, impact pair, and double excited Fermi accelerator later to help describe different types of motions easily in these systems.

1.3. Bouncing Ball System

The bouncing ball problem is a simple model that has been attracting the interest of many researchers from early days. Although the model seems simple, it contains rich motions with complexity that has not yet been fully understood. One of the earliest researches on bouncing ball problem was carried out by Schnurmann focusing on the rate of energy loss of a bouncing steel ball (Schnurmann, 1941). In 1982, the dynamics of repeated impacts with a sinusoidal vibrating table was investigated (Holmes, 1982). In 1985, the chaotic dynamics of a bouncing ball was studied using mapping technique and the behavior of Lyapunov exponents was discussed (Everson, 1986). In 1987, a near-resonant perturbation method was used to investigate the suppression of period doubling bifurcation in a bouncing ball system (Wiesenfeld & Tufillaro, 1987). In 1988, experimental evidence of the suppression of period doubling was observed by near-resonant perturbations (Pieranski, 1988). In 1996, the dynamics of a bouncing ball with a sinusoidal vibrating table was investigated (Luo & Han, The dynamics of a bouncing ball with a sinusoidally vibrating table revisited, 1996). Luo and Han presented an exact model to obtain a wider range of stable motion with more accurate stability results. In 2002, the dynamics of a bouncing ball under the effect of air-damping was investigated, and some bifurcation scenario results were provided (Naylor & Sanchez, 2002). In 2004, the asynchronous sampling method was used to study the dynamical behaviors of a bouncing ball system in reduced impact representation (Giusepponi, Marchesoni, & and Borromeio, 2005). Recently in 2009, the dynamics of a bouncing ball system modeled with discrete maps was investigated

(Barroso, Carneiro, & Macau, 2009). Barroso et al also presented some periodic motion with stability, chaotic motion, and stick motion without analytical conditions. In 2011, the chaotic behavior of the bouncing ball system was studied (Matyas & Barna, 2011). Also Matyas and Barna tried giving a semi-analytical estimation of chaotic motions in such a system. In 2012, a modified Lyapunov method was presented to study the stability of periodic motions in a bouncing ball system (Leine & Heimsch, 2012). At the same time, the effect of phase on different types of motions of a bouncing ball system was studied with perturbation (Joseph, Marino, & Sanjuan, 2012). However, Joseph, Marino, and Sanjuan's research did not provide an analytical explanation of why such effect exists. The effect of phase is very important on motion switching in a bouncing ball system, and thus, affects different types of motions. This will be analytically explained later in chapter 3. All these previous researches did not consider the switching of motion, and transition between impact chatter and stick. Thus, they were either not able to catch the complexity periodic motions caused by chatter and stick or simply took them as chaotic motions.

On the other hand, in 2002, the stability and bifurcation for the asymmetric periodic motion in a periodically excited horizontal impact pair was investigated with generic mappings technique (Luo, An unsymmetrical motion in a horizontal impact oscillator, 2002). Later in 2005, Luo investigated the mapping dynamics of periodic motions in a piecewise linear system (Luo, The mapping dynamics of periodic motions for a three-piecewise linear system under a periodic excitation, 2005); And later, he summarized the work and developed a theory to analytically investigate the non-smooth dynamical systems on connectable and accessible sub-domains (Luo, A theory for non-smooth dynamic systems on the connectable domains, 2005). In 2008, Luo further improved the theory and presented the theory for flow switchability in

discontinuous dynamical systems (Luo, A theory for flow switchability in discontinuous dynamical systems, 2008). From 2009 to 2011, Luo and Guo applied this theory on different systems such as Fermi-acceleration oscillator and horizontal impact pair under periodic excitation (Luo & Guo, Motion switching and chaos of a particle in a generalized Fermi-acceleration oscillator, 2009; Luo & Guo, Switching mechanism and complex motions in an extended Fermi-acceleration oscillator, 2010; Guo & Luo, 2011; Luo & Guo, Bifurcation analysis of a fermi-acceleration oscillator under different excitations, 2011). In these works they provided complete parameter maps, prediction of periodic motions, and investigated the complexity caused by impact chattering and stick motion.

In chapter 3, the flow switchability theory of discontinuous dynamical systems will be used to investigate the bifurcation and chaos in a bouncing ball system. The analytical conditions for stick and grazing motion will be developed, which provide criterions of motion switchability related to switching phase of the system. Switching sets and mapping structures will be introduced for such a system. Simulation of periodic and chaotic motions will also be illustrated based on the generic mappings. Complex periodic motion caused by impact chattering and stick will also be predicted.

1.4. Horizontal Impact Pair

Phenomena in the impact pair problem are extensively investigated in the field of mechanical engineering. i.e., a typical application that has drawn great interest of researchers is the impact damper. A better understanding of this vibro-impact problem is very useful to study vibration and noise in engineering. Early in 1983, Bapat and Popplewell studied the asymptotically stable periodic motions of an impact-pair consisting of two rigid masses separated by a clearance (Bapat & Popplewell, Stable periodic motions of an impact-pair, 1983). In this

work, the asymmetric period-1 motions are observed. Also Shaw and Holmes studied periodic motion bifurcations and chaotic motions in a single-degree of freedom non-linear oscillator (Shaw & Holmes, 1983). In 1987, Heiman et al used the local bifurcation theory to study the periodic motions and stability of an inclined impact pair (Heiman, Sherman, & Bajaj, On the dynamics and stability of an inclined impact pair, 1987). Later in 1988, Heiman et al further investigated the periodic and chaotic motions through bifurcation analysis and Poincare maps (Heiman, Bajaj, & Sherman, Periodic motions and bifurcations in dynamics of an inclined impact pair, 1988). Also the stability region of two equal-spaced impact motions of an impact-pair was investigated (Bapat, Impact-pair under periodic excitation, 1988) using Fourier series and perturbation methods. In 1991, Nordmark studied grazing impacts in one-degree of freedom impact oscillator (Nordmark, 1991). In 1995, Bapat studied the motion of an inclined impact damper with friction and collisions on both sides (Bapat, The general motion of an inclined impact damper with friction, 1995). Han et al investigated the periodic and chaotic motion of a horizontal impact pair and initialized an idea of using discrete mapping structures to describe complex motions in an impact pair (Han, Luo, & Deng, 1995). Recently, Park et al investigated the resonant vibrations of a single unit impact damper experimentally and numerically (Park, Wang, & Crocker, 2009). For analytical investigation, Luo investigated the stability and bifurcation for the unsymmetrical periodic motion in a periodically excited horizontal impact oscillator (Luo, An unsymmetrical motion in a horizontal impact oscillator, 2002) using the method of generic mappings. Then in 2005, he presented the mapping dynamics of periodic motions in a piecewise linear system (Luo, The mapping dynamics of periodic motions for a three-piecewise linear system under a periodic excitation, 2005).

From these previous researches, the motion switchability and impact chattering was not considered. Thus, the dynamical behavior complexities of the impact pair systems were not discussed completely. In 2005, Luo developed a local singularity theory for the switchability of flows in discontinuous dynamical systems (Luo, A theory for non-smooth dynamic systems on the connectable domains, 2005) (also see (Luo, Singularity and Dynamics on Discontinuous Vector Fields, 2006) and (Luo, Discontinuous Dynamical Systems on Time-varying Domains, 2009)). Then Luo and Chen applied such a theory to investigate periodic motions and grazing bifurcation of an idealized gear transmission system with impacts (Luo & Chen, Grazing bifurcation and periodic motion switching in a piecewise linear, impacting oscillator under a periodical excitation, 2005). However in their research, it was assumed that the locations of impact are fixed and the plastic impact condition was applied. Based on such assumptions, the model may not be very useful for real gear transmission systems because it eliminated impact chatters. Thus in 2007, Luo and O'Connor adopted the time-varying impact location to study the nonlinear dynamics of a gear transmission system described with an impact model with possible stick (Luo & O'Connor, Nonlinear dynamics of a gear transmission system part I: mechanism of impacting chatter with stick, 2007) and (Luo & O'Connor, Nonlinear dynamics of a gear transmission system part II: periodic impacting chatter and stick, 2007). Later, Luo and Guo systematically investigated the switching bifurcation and chaos in a double excited Fermi oscillator accelerated with periodic excitation. The achieved results seem very complicated, which is very difficult to explain the physical phenomena of vibro-impact problems (Luo & Guo, Switchability and bifurcation of motions in a double-excited Fermi-acceleration oscillator, 2010).

Thus, to help one further understand the switching mechanism of vibro-impact problems, the flow switchability theory of discontinuous dynamical systems with time varying boundaries

will be adopted to investigate the switching bifurcation and chaos of a ball in a periodically shaken horizontal impact pair in chapter 4. The analytical conditions for stick and grazing motions will be developed. Switching sets and mapping structures will be introduced. Analytical prediction of complex motions in the periodically shaken impact pair will be carried out using the analytical conditions and discrete mapping structures.

1.5. Dual Excited Fermi Accelerator

The Fermi acceleration oscillator is a very important physical model, and such impact phenomena extensively exist in physics and engineering field. The Fermi acceleration was first introduced by Fermi to explain the origin of cosmic radiation (Fermi, 1949). In 1964, Zaslavskii and Chirikov provided the criterion of the Fermi accelerator in one-dimensional case to explain the existing chaotic motion (Zaslavskii & Chirikov, 1964). In 1983, the harmonic, sub-harmonic, and chaotic motions of a single-degree of freedom non-linear oscillator were investigated (Shaw & Holmes, 1983). To further understand the nonlinear dynamical behaviors of the Fermi oscillator, the dynamics of the Fermi accelerator with a viscous friction were investigated (Luna-Acosta, 1989). In 1998, Lopac and Dananic further investigated the chaotic dynamics and energy conservation in a gravitationally driven Fermi accelerator (Lopac & Dananic, 1998). At the same time, Saif et al discussed the classical and quantum dynamics of a Fermi accelerator and determined the existence of dynamical localization for both position and momentum in a window of the modulation amplitude (Saif, Bialynicki-Birula, Fortunato, & Schleich, 1998). In 2004, a simple stochastic system was presented to generate anomalous diffusion of both position and velocity in the Fermi accelerator (Bouchet, 2004). And the discrete dynamical systems formalism was adopted to investigate the effect of a time-dependent perturbation on a Fermi accelerator model (Leonel, da Silva, & Kamphorst, On the dynamical properties of a Fermi accelerator

model, 2004). In 2005, Leonel and McClintock studied the dynamical and chaotic properties of a Fermi-Ulam bouncer model (Leonel & McClintock, A hybrid Fermi-Ulam-bouncer model, 2005). In 2006, a two-dimensional nonlinear area-contracting map was used to study the Fermi accelerator model with inelastic collisions (Leonel & de Carvalho, A family of crisis in a dissipative Fermi accelerator model, 2006). Also Leonel and Silva studied the dynamical properties of a bouncing ball model with a nonlinear excitation force (Leonel & Silva, A bouncing ball model with two nonlinearities: a prototype for Fermi acceleration, 2008). The aforementioned studies did not consider the motion switchability and impact chatters, which cause the dynamical behavior complexity.

On the other hands, in 2002, Luo discussed the stability and bifurcation analysis for the unsymmetrical periodic motion in a periodically excited horizontal impact oscillator (Luo, An unsymmetrical motion in a horizontal impact oscillator, 2002). In 2005, the mapping dynamics method was proposed to determine periodic motion in a piecewise linear system (Luo, The mapping dynamics of periodic motions for a three-piecewise linear system under a periodic excitation, 2005). For a better understanding of such dynamical systems, Luo developed a theory for the non-smooth dynamical systems on connectable and accessible sub-domains (Luo, A theory for non-smooth dynamic systems on the connectable domains, 2005). Such a theory was applied to investigate the flows and grazing bifurcations of an idealized gear transmission system with impacts (Luo & Chen, Grazing bifurcation and periodic motion switching in a piecewise linear, impacting oscillator under a periodical excitation, 2005). In 2006, Luo and Gegg applied this theory again to develop the force criteria for stick and non-stick motions in the friction-induced oscillator (Luo & Gegg, Stick and non-stick periodic motions in periodically forced oscillators with dry friction, 2006). In 2007, Luo and O'Connor studied the nonlinear dynamics

of a gear transmission system through an impact model with possible stick (Luo & O'Connor, Mechanism of impacting chatter with stick in a gear transmission system, 2007) and (Luo & O'Connor, Periodic motion and chaos with impacting chatter and stick in a gear transmission system, 2007). Luo and Guo systematically investigated the switching bifurcation and chaos in a generalized Fermi oscillator accelerated with a simple excitation (Luo, Resonance and Chaotic Dynamics, 2008), (Luo & Guo, Motion switching and chaos of a particle in a generalized Fermi-acceleration oscillator, 2009), and (Luo & Guo, Switchability and bifurcation of motions in a double-excited Fermi-acceleration oscillator, 2010). Under dual excitations, the complexity of chaos and periodic motions for the particles in the Fermi oscillators will be a lot different from the single excitation. The initial studies of the complex switch dynamics in such a system were completed considering same excitation (Luo & Guo, Switchability and bifurcation of motions in a double-excited Fermi-acceleration oscillator, 2010). Then in 2011, different excitation with one excitation proportional to the other was considered for such a dual excited Fermi oscillator (Luo & Guo, Bifurcation analysis of a fermi-acceleration oscillator under different excitations, 2011), and further analysis on bifurcation and switchability was presented

In chapter 5, motion complexity in the Fermi oscillator with dual excitations will be investigated using same and different excitations. The analytical conditions for switchability of the motions in such a system will be developed. Generic mappings will be introduced to describe different types of motions in such oscillators. Analytical predictions of periodic motions will then be presented through the mapping structures. Finally, periodic and chaotic motions in such an oscillator will be simulated, and Poincare mappings for the Neimark bifurcation will be presented as well.

1.6. Conclusions

In this chapter, a brief description of the objectives is presented for this dissertation. A brief history of researches on discrete dynamical systems and vibro-impact systems is provided. A layout of content for each chapter is included and concise introductions of each chapter are presented.

CHAPTER 2

DISCRETE DYNAMICAL SYSTEM

This chapter studies the complete stable and unstable periodic solutions states of Henon Map as a typical example for *n*-dimensional nonlinear discrete dynamical systems. Using Luo's theory for nonlinear discrete dynamical systems (Luo, A Ying-Yang theory in Nonlinear Discrete Dynamical Systems, 2010), a comprehensive investigation on the Henon map is carried out for a better understanding of complexity in nonlinear discrete systems. First, the bifurcation scenario based on positive and negative mappings of the Henon map will be given. Then the analytical predictions of the corresponding periodic solutions are achieved, and the corresponding eigenvalue stability analysis is conducted for the periodic solutions. The Poincare mapping sections of Neimark bifurcations of periodic solutions are also presented. Finally, a parameter map for periodic and chaotic solutions is provided. The complete unstable and stable periodic solutions in such a nonlinear discrete system are presented for the first time. These results provide a novel view for one to rethink the existing theory.

2.1. Problem Introduction

Consider the Henon map given as follow

$$\left.\begin{aligned} f_1(\mathbf{x}_k, \mathbf{x}_{k+1}, \mathbf{p}) &= x_{k+1} - y_k - 1 + ax_k^2 = 0, \\ f_2(\mathbf{x}_k, \mathbf{x}_{k+1}, \mathbf{p}) &= y_{k+1} - bx_k = 0 \end{aligned}\right\} \tag{2.1}$$

where $\mathbf{x}_k = (x_k, y_k)^{\mathrm{T}}$, $\mathbf{f} = (f_1, f_2)^{\mathrm{T}}$ and $\mathbf{p} = (a, b)^{\mathrm{T}}$. Consider both positive and negative mapping structures as follow:

$$\begin{aligned}\mathbf{x}_{k+N} &= P_+^{(N)}\mathbf{x}_k = \underbrace{P_+ \circ \cdots P_+ \circ P_+}_{N\text{-terms}}\mathbf{x}_k, \\ \mathbf{x}_k &= P_-^{(N)}\mathbf{x}_{k+N} = \underbrace{P_- \circ \cdots P_- \circ P_-}_{N\text{-terms}}\mathbf{x}_{k+N}.\end{aligned} \tag{2.2}$$

Equations (2.1) and(2.2) give

$$\left.\begin{aligned}&\mathbf{f}(\mathbf{x}_k, \mathbf{x}_{k+1}, \mathbf{p}) = 0, \\ &\mathbf{f}(\mathbf{x}_{k+1}, \mathbf{x}_{k+2}, \mathbf{p}) = 0, \\ &\vdots \\ &\mathbf{f}(\mathbf{x}_{k+N-1}, \mathbf{x}_{k+N}, \mathbf{p}) = 0\end{aligned}\right\} \tag{2.3}$$

and

$$\left.\begin{aligned}&\mathbf{f}(\mathbf{x}_{k+N-1}, \mathbf{x}_{k+N}, \mathbf{p}) = 0, \\ &\mathbf{f}(\mathbf{x}_{k+N-2}, \mathbf{x}_{k+N-1}, \mathbf{p}) = 0, \\ &\vdots \\ &\mathbf{f}(\mathbf{x}_k, \mathbf{x}_{k+1}, \mathbf{p}) = 0.\end{aligned}\right\} \tag{2.4}$$

Eqs.(2.3) and (2.4) are identical to each other except that the order of equations in Eq.(2.4) is different. For periodic solutions of both the positive and negative maps, the periodicity requires

$$\mathbf{x}_{k+N} = \mathbf{x}_k \quad \text{or} \quad \mathbf{x}_k = \mathbf{x}_{k+N}. \tag{2.5}$$

Thus, the periodic solutions $\mathbf{x}_{k+j}^*$ ($j = 0,1,\cdots,N$) for the positive and negative mapping structures are the same, which can be obtained by solving Eqs.(2.3) and (2.5). However the stability and bifurcation are different because $\mathbf{x}_{k+j}$ varies with $\mathbf{x}_{k+j-1}$ for the *j*th positive mapping and $\mathbf{x}_{k+j-1}$ varies with $\mathbf{x}_{k+j}$ for the *j*th negative mapping. Using a small perturbation, equation (2.1) for the positive mapping gives

$$[\frac{\partial \mathbf{f}}{\partial \mathbf{x}_{k+j-1}}] + [\frac{\partial \mathbf{f}}{\partial \mathbf{x}_{k+j}}] \cdot [\frac{\partial \mathbf{x}_{k+j}}{\partial \mathbf{x}_{k+j-1}}]\Big|_{(\mathbf{x}_{k+j-1}^*, \mathbf{x}_{k+j}^*)} = 0, \tag{2.6}$$

where

$$[\frac{\partial \mathbf{f}}{\partial \mathbf{x}_{k+j-1}}]_{(\mathbf{x}^*_{k+j-1},\mathbf{x}^*_{k+j})} = \begin{bmatrix} \frac{\partial f_1}{\partial x_{k+j-1}} & \frac{\partial f_1}{\partial y_{k+j-1}} \\ \frac{\partial f_2}{\partial x_{k+j-1}} & \frac{\partial f_2}{\partial y_{k+j-1}} \end{bmatrix}_{(\mathbf{x}^*_{k+j-1},\mathbf{x}^*_{k+j})} = \begin{bmatrix} 2ax^*_{k+j-1} & -1 \\ -b & 0 \end{bmatrix}, \tag{2.7}$$

$$[\frac{\partial \mathbf{f}}{\partial \mathbf{x}_{k+j}}]_{(\mathbf{x}^*_{k+j-1},\mathbf{x}^*_{k+j})} = \begin{bmatrix} \frac{\partial f_1}{\partial x_{k+j}} & \frac{\partial f_1}{\partial y_{k+j}} \\ \frac{\partial f_2}{\partial x_{k+j}} & \frac{\partial f_2}{\partial y_{k+j}} \end{bmatrix}_{(\mathbf{x}^*_{k+j-1},\mathbf{x}^*_{k+j})} = \begin{bmatrix} 1 & 0 \\ 0 & 1 \end{bmatrix}. \tag{2.8}$$

So one obtains

$$\begin{aligned} DP_+(\mathbf{x}^*_{k+j-1}) &= [\frac{\partial \mathbf{x}_{k+j}}{\partial \mathbf{x}_{k+j-1}}]_{\mathbf{x}^*_{k+j-1}} = [\frac{\partial \mathbf{f}}{\partial \mathbf{x}_{k+j}}]^{-1}[\frac{\partial \mathbf{f}}{\partial \mathbf{x}_{k+j-1}}]_{\mathbf{x}^*_{k+j-1}} \\ &= \begin{bmatrix} 2ax^*_{k+j-1} & -1 \\ -b & 0 \end{bmatrix}. \end{aligned} \tag{2.9}$$

Similarly, for the negative mapping,

$$[\frac{\partial \mathbf{f}}{\partial \mathbf{x}_{k+j}}] + [\frac{\partial \mathbf{f}}{\partial \mathbf{x}_{k+j-1}}] \cdot [\frac{\partial \mathbf{x}_{k+j-1}}{\partial \mathbf{x}_{k+j}}]\big|_{(\mathbf{x}^*_{k+j-1},\mathbf{x}^*_{k+j})} = 0. \tag{2.10}$$

With Eqs.(2.7) and (2.8), the foregoing equation gives

$$DP_-(\mathbf{x}^*_{k+j}) = [\frac{\partial \mathbf{x}_{k+j-1}}{\partial \mathbf{x}_{k+j}}]_{\mathbf{x}^*_{k+j}} = [\frac{\partial \mathbf{f}}{\partial \mathbf{x}_{k+j-1}}]^{-1}[\frac{\partial \mathbf{f}}{\partial \mathbf{x}_{k+j}}]_{\mathbf{x}^*_{k+j}} = -\frac{1}{b}\begin{bmatrix} 0 & 1 \\ b & 2ax^*_{k+j-1} \end{bmatrix}. \tag{2.11}$$

Thus, the resultant perturbation of the mapping structure in Eq.(2.2) gives

$$\begin{aligned} \delta \mathbf{x}_{k+N} &= DP_+^{(N)} \mathbf{x}_k = \underbrace{DP_+ \cdot \cdots \cdot DP_+ \cdot DP_+}_{N\text{-terms}} \delta \mathbf{x}_k, \\ \delta \mathbf{x}_k &= DP_-^{(N)} \delta \mathbf{x}_{k+N} = \underbrace{DP_- \cdot \cdots \cdot DP_- \cdot DP_-}_{N\text{-terms}} \delta \mathbf{x}_{k+N} \end{aligned} \tag{2.12}$$

where

$$\left.\begin{aligned} DP_+^{(N)} &= \prod_{j=1}^{N} DP_+(\mathbf{x}^*_{k+N-j}), \\ DP_-^{(N)} &= \prod_{j=1}^{N} DP_-(\mathbf{x}^*_{k+N-j+1}). \end{aligned}\right\} \tag{2.13}$$

Consider the eigenvalues λ^+ and λ^- of $DP_+^{(N)}(\mathbf{x}_k^*)$ and $DP_-^{(N)}(\mathbf{x}_{k+N}^*)$ for positive and negative maps, respectively. The following statements hold.

(i) If $|\lambda_{1,2}^+|<1$ (or $|\lambda_{1,2}^-|<1$), the periodic solutions of $P_+^{(N)}(\mathbf{x}_k)$ (or $P_-^{(N)}(\mathbf{x}_{k+N})$) are stable.

(ii) If $|\lambda_{1\text{ or }2}^+|>1$ (or $|\lambda_{1\text{ or }2}^-|<1$), the periodic solutions of $P_+^{(N)}(\mathbf{x}_k)$ (or $P_-^{(N)}(\mathbf{x}_{k+N})$) are unstable.

(iii) If real eigenvalues $\lambda_1^+=-1$ and $|\lambda_2^+|<1$ (or $\lambda_1^-=-1$ and $|\lambda_2^-|<1$), the period-doubling (PD) bifurcation of the periodic solutions of $P_+^{(N)}(\mathbf{x}_k)$ (or $P_-^{(N)}(\mathbf{x}_{k+N})$) occurs.

(iv) If real eigenvalues $|\lambda_1^+|<1$ and $\lambda_2^+=1$ (or $|\lambda_1^-|<1$ and $\lambda_2^-=-1$), then the saddle-node (SN) bifurcation of the periodic solutions relative to $P_+^{(N)}(\mathbf{x}_k)$ (or $P_-^{(N)}(\mathbf{x}_{k+N})$) occurs.

(v) If two complex eigenvalues of $|\lambda_1^+|<1$ and $|\lambda_2^+|=1$ (or $|\lambda_1^-|<1$ and $|\lambda_2^-|=1$), the Neimark bifurcation (NB) of the periodic solutions of $P_+^{(N)}(\mathbf{x}_k)$ (or $P_-^{(N)}(\mathbf{x}_{k+N})$) occurs.

2.2. Bifurcations and Predictions

A bifurcation of the periodic solutions for the Henon map is presented with varying parameter *b* for $a=0.85$, as shown in Figure 2.1. This bifurcation is obtained through numerical iterations. The solutions for P_+ are presented in Figure 2.1 in black, while the solutions for P_- are in red. The dashed vertical lines in Figure 2.1 (a) indicate the location where bifurcations occur. The acronyms “PD”, “SN” and “NB” correspond to period-doubling bifurcation, saddle-node bifurcation, and Neimark bifurcation, respectively. It is observed that the stable periodic solutions for positive mapping P_+ always lie in $b\in(-1.0,1.0)$. For

$b \notin (-1.0, 1.0)$, the positive mapping P_+ would not converge. The stable period-1 solution of P_+ is in $b \in (-1.0, -0.07)$. At $b = -1.0,$ the Neimark bifurcation (NB) of the period-1 solution occurs. At $b \approx -0.07$, the period-doubling bifurcation (PD) of the period-1 solution takes place. This point is also the saddle-node bifurcation (SN) for the period-2 solution of P_+ (i.e. $P_+^{(2)}$). The periodic solution of $P_+^{(2)}$ is in the range of $b \in (-0.07, 0.39)$. Similarly, at $b \approx 0.39$, there is a period-doubling bifurcation (PD) of the period-2 solution, which corresponds to the saddle-node bifurcation (SN) for the period-4 solution $P_+^{(4)}$. The periodic solution of $P_+^{(4)}$ exists for $b \in (0.39, 0.80)$. This solution ends at $b \approx 0.80$, where a $P_+^{(4)}$ saddle-node bifurcation (SN) occurs, corresponding to the period-doubling bifurcation (PD) of another branch of $P_+^{(2)}$ solution. This $P_+^{(2)}$ runs until $b = 1$, where another Neimark bifurcation takes place. After the Neimark bifurcation, the stable periodic solutions for positive mapping P_+ do not exist anymore. On the other hand, the stable solutions for negative mapping P_- lie in $b \in (-\infty, -1.0)$ and $b \in (-1, +\infty)$. Similarly, for $b \in (-1.0, 1.0)$, the negative mapping P_- would not converge. At $b = -1,$ the Neimark bifurcation (NB) of the periodic solution of mappings P_- exists which overlap with the one for positive mapping P_+. The period-1 solution of P_- is in $b \in (-\infty, -1.0)$ and $b \in (2.07, +\infty)$. The period-doubling bifurcation (PD) of the period-1 solution of P_- and the saddle-node bifurcation (SN) for the period-2 solution of P_- (i.e., $P_-^{(2)}$) occurs at $b \approx 2.07$. The stable periodic solution of $P_-^{(2)}$ exists in $b \in (1.0, 2.07)$. At $b = 1,$ the Neimark bifurcation (NB) of the periodic solution of $P_-^{(2)}$ occurs. Again, this bifurcation overlaps with the one for the positive mapping P_+. Finally, a 3-dimesional view of this bifurcation scenario is also presented in Figure 2.1 (b) for a better imagination of the solutions.

The numerical iteration can only provide stable solutions of the system. In some cases, it even fails to provide the complete stable solution due to the sensitive dependency on initial conditions. Thus, to provide complete set of stable and unstable solutions, analytical predictions are adopted for both positive and negative mappings of the Henon maps. The analytical predictions are then solved numerically for both stable and unstable solutions. The predicted periodic solutions are presented in Figure 2.2 and Figure 2.3 for positive and negative mapping, respectively. The acronyms “PD”, “SN” and “NB” will be used to represent the stable period-doubling bifurcation, stable saddle-node bifurcation and Neimark bifurcation, respectively. On the other hand, the acronyms “UPD”, “USN” will be used to represent the unstable period-doubling bifurcation relative to unstable nodes and unstable saddle-node bifurcation, respectively. It can be observed from these figures that the positive and negative mappings connect with each other through the Neimark bifurcations. When looking at positive maps, the negative maps overlaps with part of the unstable positive mapping solutions for $b \notin (-1.0, 1.0)$, which cannot be provided by numerical iteration of the Henon maps. On the other hand, when looking at the negative maps, the positive maps overlaps with part of the unstable negative mapping solutions for $b \in (-1.0, 1.0)$. Again, these unstable solutions cannot be obtained using the numerical iterating method. Finally, some of the unstable solutions (indicated by dotted curves) stay unstable for both positive and negative mappings.

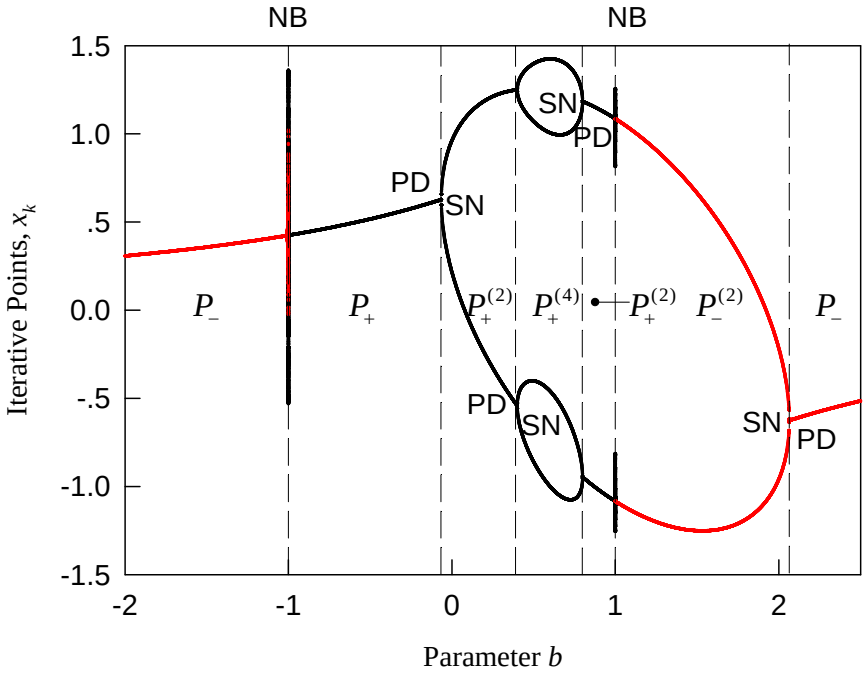

(a)

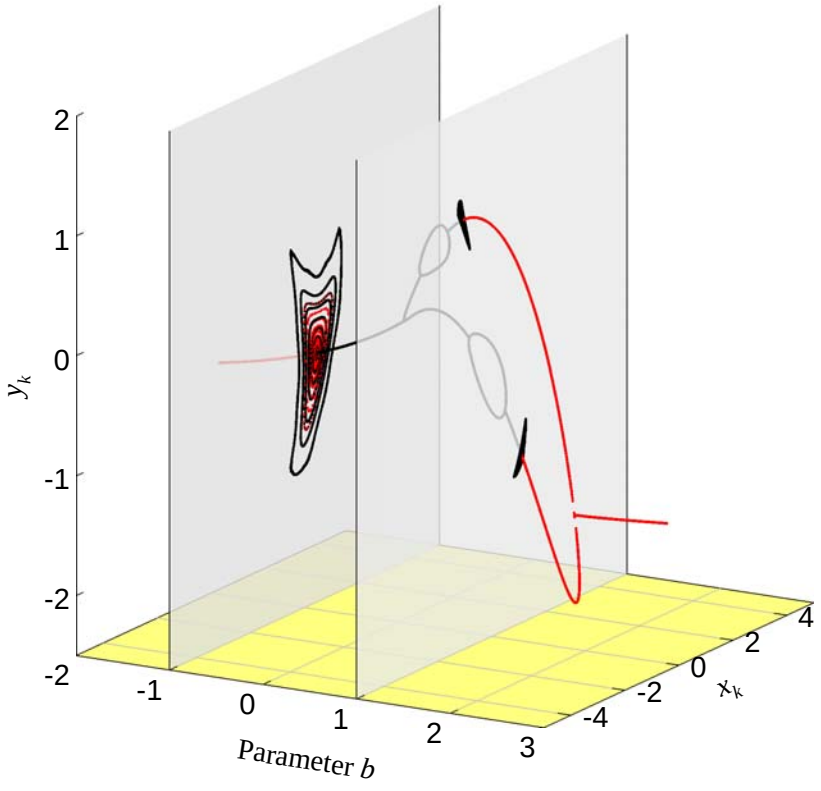

(b)

Figure 2.1: Numerical predictions of periodic solutions of the Henon mapping: (a) complete negative and positive mappings and (b) 3-D view of the scenario. ($a = 0.85$).

The analytical prediction of positive mapping P_+ for $a = 0.85$ and $b \in (-\infty, +\infty)$ is presented in Figure 2.2 (a)-(d). The periodic solutions of the positive mapping are arranged in Figure 2.2 (a). The real part, imaginary part, and magnitude of the eigenvalues for such periodic solutions are provided in Figure 2.2 (b)-(d), respectively. The stable period-1 solutions $P_+^{(1)}$ for positive mapping lie in $b \in (-1.0, -0.07)$. For $b \in (-0.07, +\infty)$, the unstable $P_+^{(1)}$ solution is saddle. For $b \in (-\infty, -1.0)$, the unstable $P_+^{(1)}$ solution is relative to the unstable focus. The corresponding bifurcations of the period-1 solution $P_+^{(1)}$ are Neimark bifurcation (NB) at $b = 1.0$ and period-doubling bifurcation (PD) at $b \approx -0.07$. For $b \in (2.07, +\infty)$, the $P_+^{(1)}$ solution is unstable node. For $b \in (-\infty, 2.07)$ the unstable $P_+^{(1)}$ solution is saddle. Thus, the unstable period-doubling bifurcation (UPD) of the $P_+^{(1)}$ solution occurs at $b \approx 2.07$. At this point, the unstable periodic solution is from an unstable node to saddle. Because of the unstable period-doubling bifurcation, the unstable period-2 solution of $P_+^{(2)}$ for the unstable node is obtained for $b \in (1.0, 2.07)$. This unstable $P_+^{(2)}$ solution is from unstable focus to unstable node. At $b \approx 2.07$, the bifurcation of the unstable $P_+^{(2)}$ solution is from the unstable node to unstable saddle. This is called the unstable saddle-node bifurcation, where the bifurcation for the mapping of $P_-^{(2)}$ is from the stable node to saddle. The stable $P_+^{(2)}$ solution exist for $b \in (-0.07, 0.39)$ and $b \in (0.8, 1.0)$. The unstable solution of $P_+^{(2)}$ is saddle for $b \in (0.39, 0.8)$. At $b \approx 0.39$ and $b \approx 0.8$, the period doubling bifurcations of the $P_+^{(2)}$ solution exists, which are from the stable to unstable state. In addition, these points are the saddle-node bifurcation for the stable $P_+^{(4)}$ solution. The stable $P_+^{(4)}$ solution exists for $b \in (0.39, 0.8)$.

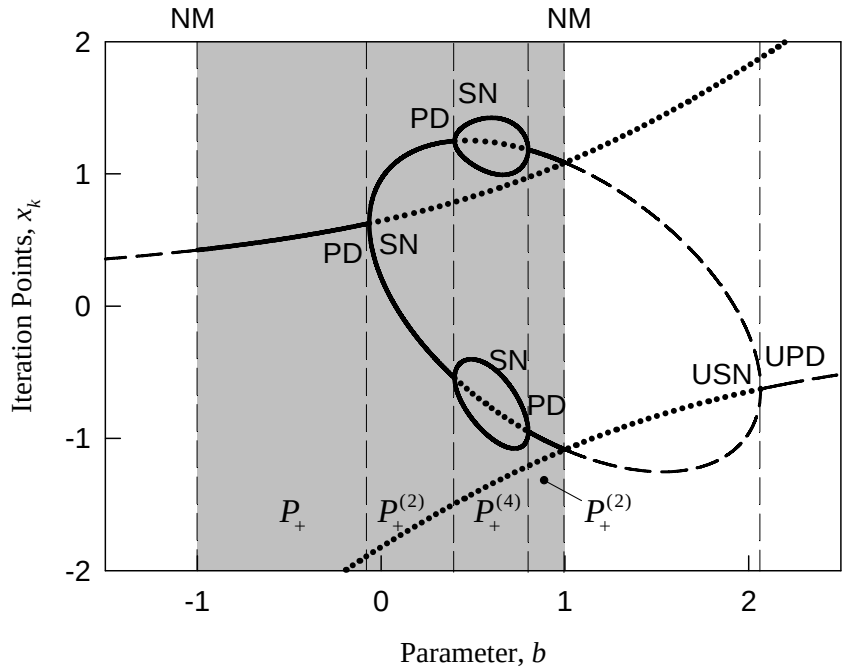

(a)

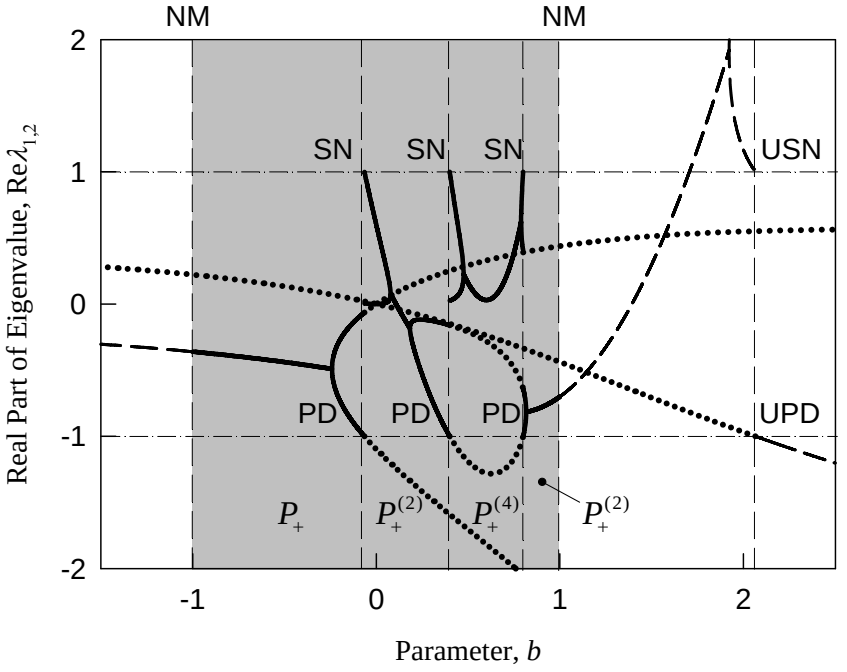

(b)

Figure 2.2: Analytical predictions of *stable* and *unstable* periodic solutions for positive mapping (P_+) of the Henon map: (a) periodic solutions, (b) Real part of eigenvalues, (c) Imaginary part of eigenvalues, (d) Magnitude of eigenvalues. ($a = 0.85$ and $b \in (-\infty, +\infty)$).

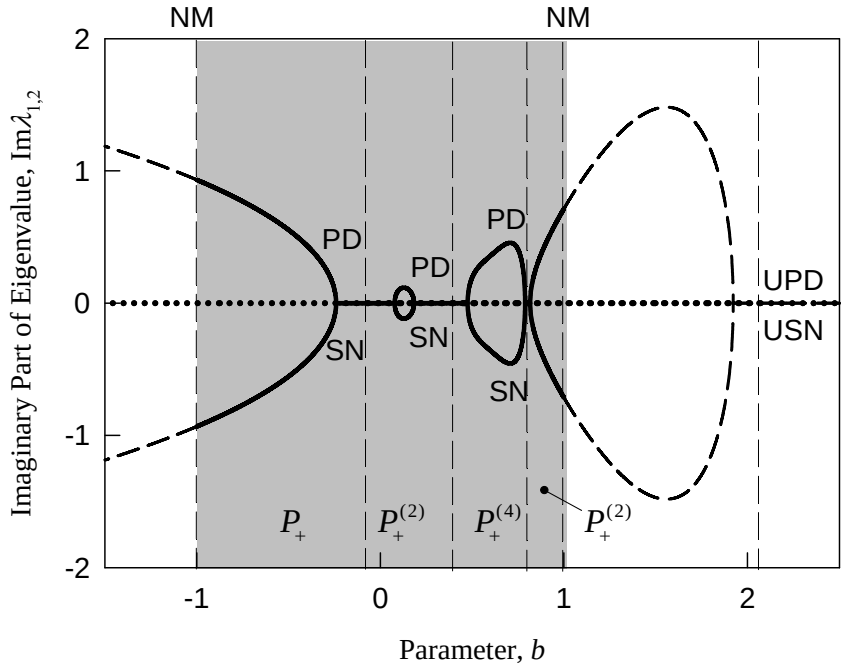

(c)

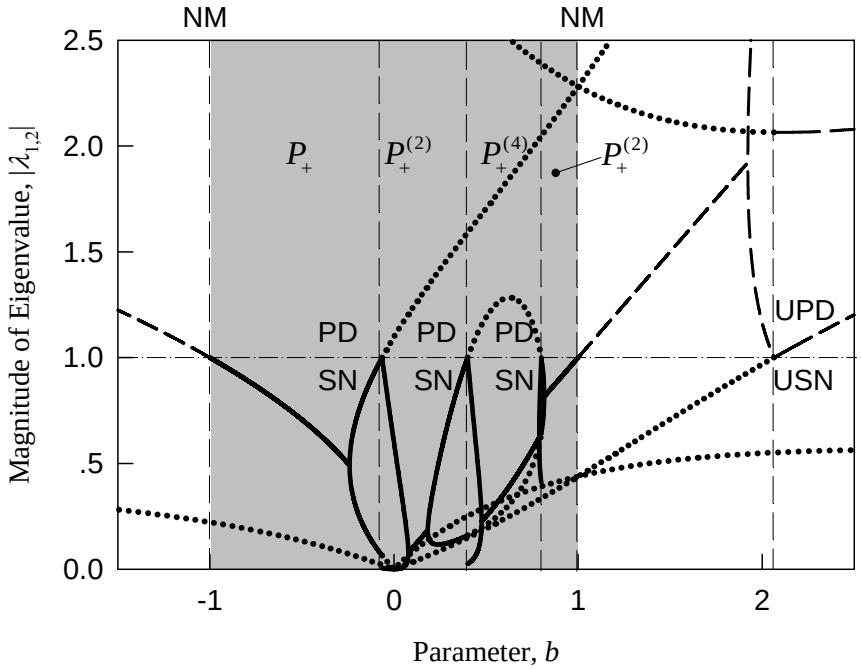

(d)

Figure 2.2 Continue

In a similar pattern, the analytical prediction of stable and unstable periodic solutions of negative mapping P_- for $a = 0.85$ and $b \in (-\infty, +\infty)$ is presented in Figure 2.3 (a)-(d). The periodic solutions of the negative mapping are plotted in Figure 2.3 (a). The real part, and imaginary part, and magnitude of the eigenvalues for such periodic solutions are presented in Figure 2.3 (b)-(d), respectively. The stable periodic solutions for negative mapping P_- lie in $b \in (-\infty, -1.0)$ and $b \in (1.0, +\infty)$. The stable period-1 solution $P_-^{(1)}$ is stable focuses in $b \in (-\infty, -1.0)$ and stable nodes in $b \in (2.07, +\infty)$. For $b \in (-1.0, -0.07),$ the unstable $P_-^{(1)}$ solution is from the unstable focus to unstable node, which can also be determined by the positive mapping P_+. At $b = -1$, the bifurcation between the stable and unstable $P_-^{(1)}$ solution is the Neimark bifurcation (NB). For $b \in (-0.07, +\infty),$ the unstable $P_-^{(1)}$ solution is saddle. Thus, the bifurcation between the $P_-^{(1)}$ solution related to the unstable node and saddle occurs at $b \approx -0.07,$ which is called the unstable period-doubling bifurcation (UPD). For $b \in (-\infty, 2.07),$ the unstable $P_-^{(1)}$ solution is also saddle. At $b \approx 2.07,$ the period-doubling bifurcation (PD) of the $P_-^{(1)}$ solution takes place. For $b \in (-0.07, 0.39)$ and $b \in (0.8, 1.0)$, the unstable period-2 solution $P_-^{(2)}$ exists. For $b \in (1.0, 2.07),$ the stable $P_-^{(2)}$ solution exists from the stable focus to the stable nodes. Thus, the point at $b \approx -0.07$ is the bifurcation of the unstable $P_-^{(2)}$ solution which is the unstable saddle-node bifurcation between the unstable node and saddle (i.e., USN). At $b \approx 0.39$ and $b \approx 0.8$, the period-doubling bifurcations of the unstable $P_-^{(2)}$ solution occur, where the unstable saddle $P_-^{(2)}$ solution exists in between the two points. The unstable $P_-^{(4)}$ solution is in $b \in (0.39, 0.8)$. Unstable saddle-node bifurcations for the unstable $P_-^{(4)}$ solution occurs at $b \approx 0.39$ and $b \approx 0.8$.

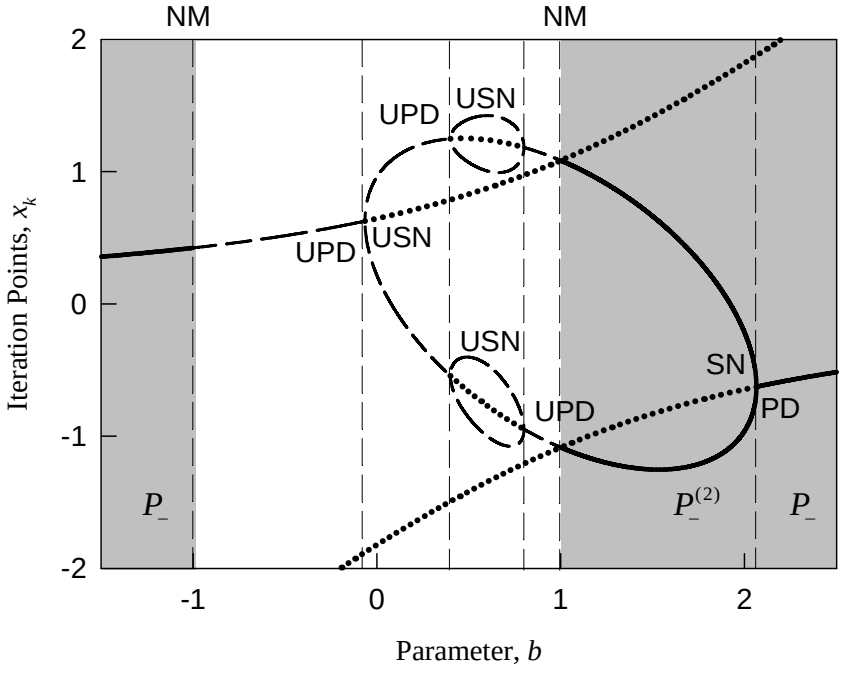

(a)

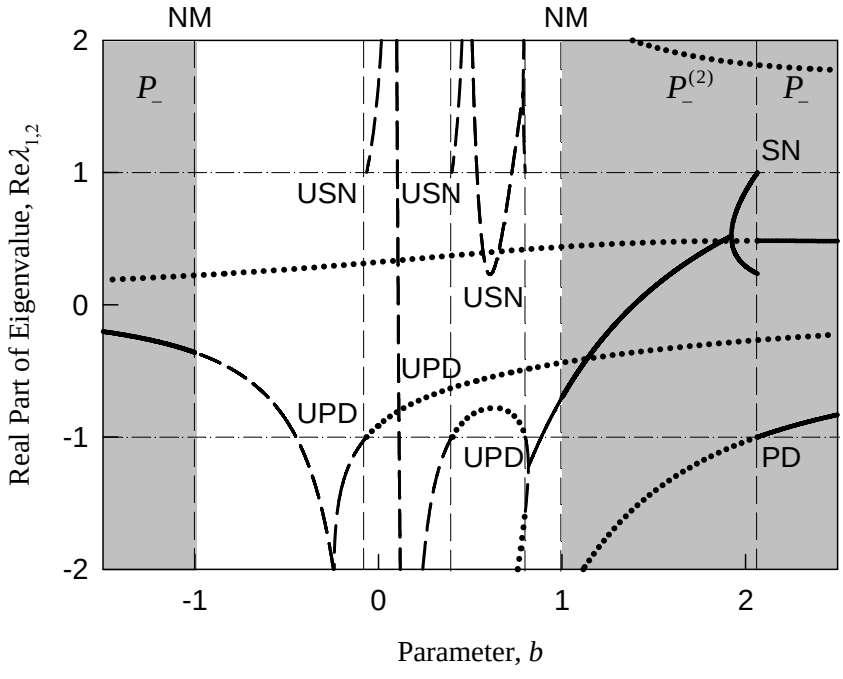

(b)

Figure 2.3: Analytical predictions of *stable* and *unstable* periodic solutions for negative mapping (P_-) of the Henon map: (a) periodic solutions, (b) Real part of eigenvalues, (c) Imaginary part of eigenvalues, (d) Magnitude of eigenvalues. ($a = 0.85$ and $b \in (-\infty, +\infty)$).

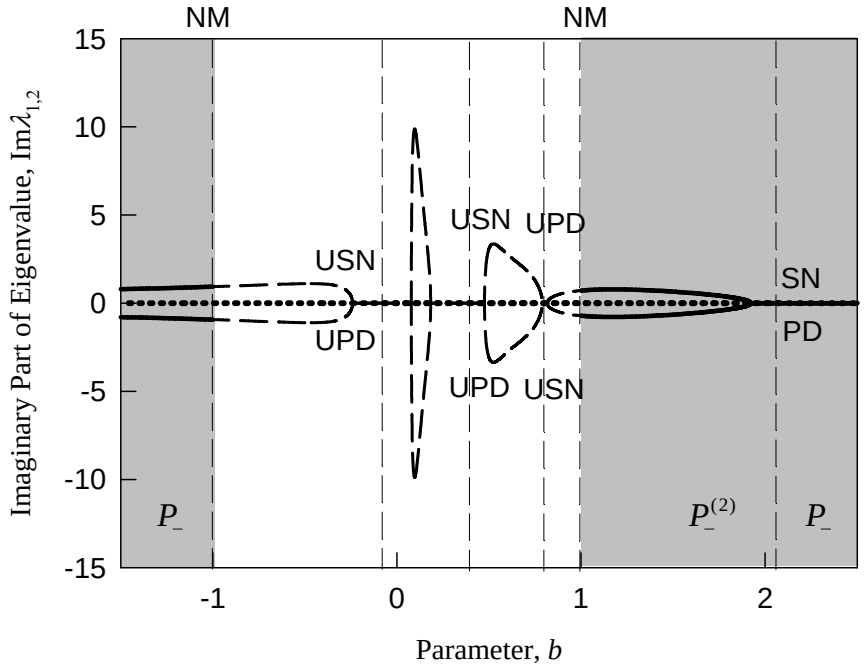

(c)

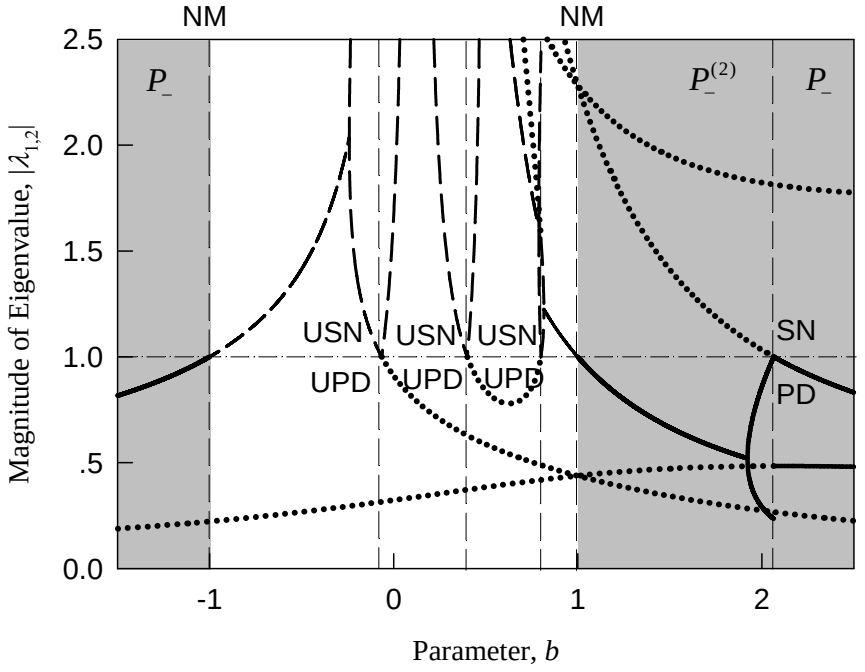

(d)

Figure 2.3 Continue

From the analytical prediction, the following statements are verified.

(i) The stable periodic solution of positive mapping P_+ is the unstable periodic solution of negative mapping P_- with all eigenvalues outside the unit cycle.

(ii) The stable periodic solution of negative mapping P_- is the unstable periodic solution of positive mapping P_+ with all eigenvalues outside the unit cycle.

(iii) The PD and SN bifurcations of the periodic solutions of positive mapping P_+ are the UPD and USN bifurcations of the periodic solutions of negative mapping P_-, vice versa.

(iv) The PD and SN bifurcations of the periodic solutions of negative mapping P_- are the UPD and USN bifurcations of the periodic solutions of positive mapping P_+, vice versa.

(v) If the unstable periodic solutions of positive mapping P_+ are saddle, the corresponding periodic solutions of negative mapping P_- are also saddle.

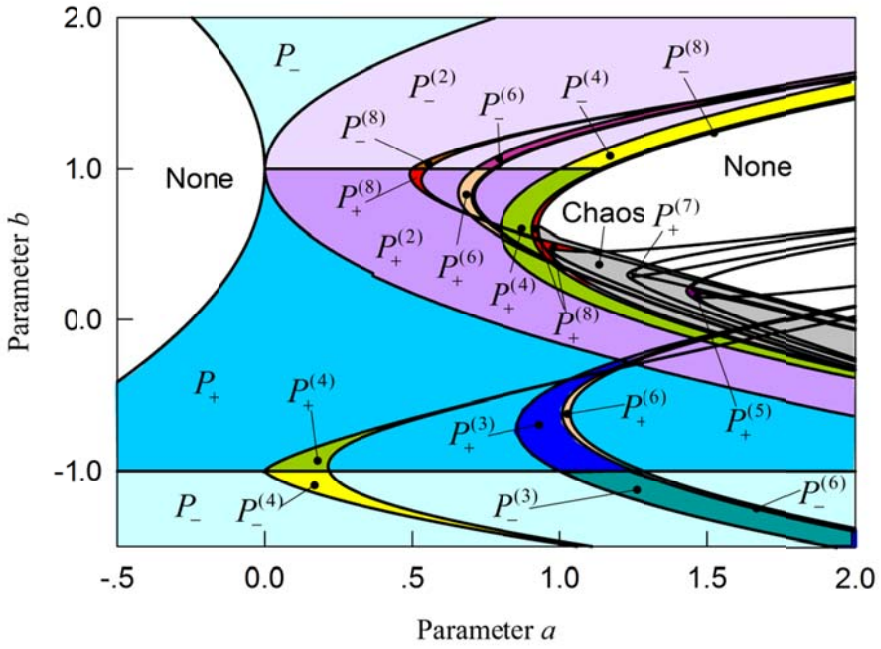

Figure 2.4: Parameter map of a and b.

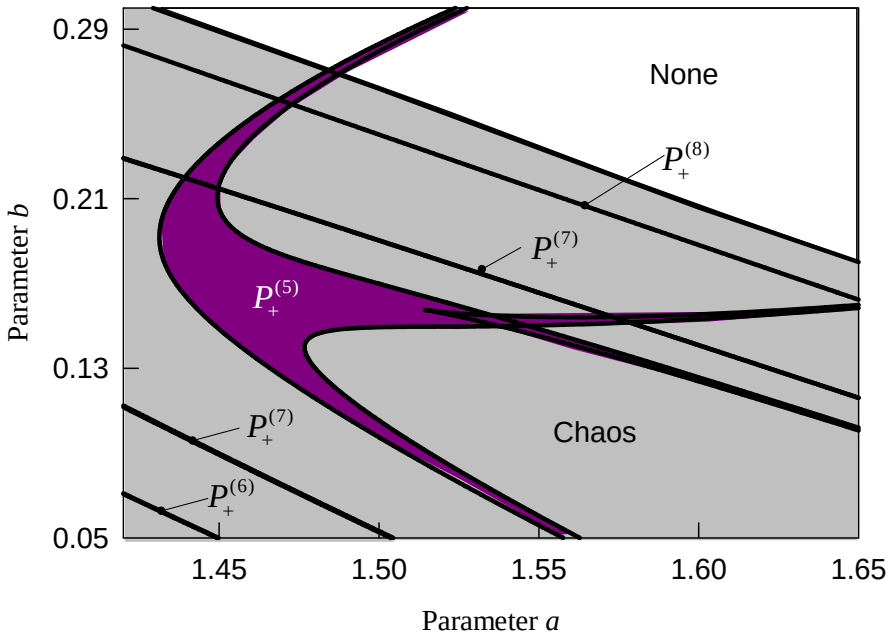

(a)

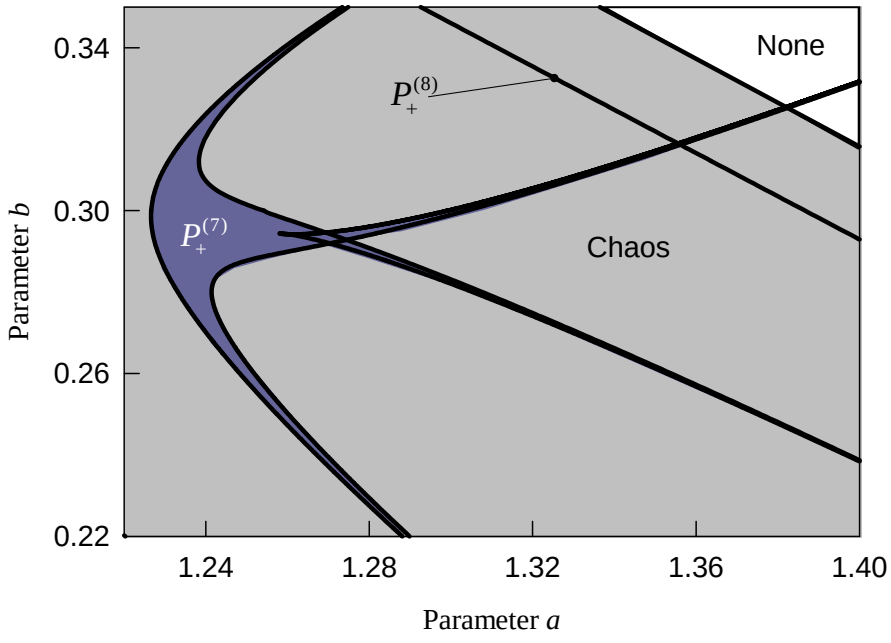

(b)

Figure 2.5: Zoomed view of the parameter maps a and b : (a) periodic solution of $P_+^{(5)}$ and (b) periodic solution of $P_+^{(7)}$.

From the analytical prediction, the parameter maps of both the positive and negative mappings are developed. An overall view of the parameter map is given in Figure 2.4. The positive and negative mappings are separated by the two Neimark bifurcations which are two straight lines at $b = \pm 1.0$. The zoomed views of the parameter map for periodic solutions of $P_{+}^{(5)}$ and $P_{+}^{(7)}$ are presented in Figure 2.5 (a) and (b) for a clear illustration. The corresponding periodic solutions are labeled by mapping structures. "None" represents no any periodic solutions exists in the area, which means the solution goes to infinity. "Chaotic" gives the regions for chaotic solutions. The existing theory can only provide the periodic solutions relative to the positive mapping. And the unstable periodic solutions with saddle cannot be expressed. However, by using the positive and negative mapping technique, the co-existing of the periodic solutions can also be observed.

Finally, the Neimark bifurcation between the periodic solution relative to the unstable and stable focuses is presented for a better understanding of the solution switching from positive to negative mappings. The Poincare mapping relative to the Neimark bifurcation of positive mapping (or negative mapping) at $a = 0.85$ and $b = \pm 1$ is presented in Figure 2.6. The Neimark bifurcation of period-1 solution at $b = -1.0$ is presented in Figure 2.6 (a), and the most inside point $(x_k^*, y_k^*) \approx (0.4237, -0.4237)$ is the point for the period-1 solution of P_{+} or P_{-} relative to the Neimark bifurcation. For the specific set of parameters, the initial values of (x_k, y_k) used for simulation are tabulated in Table 2.1. The most outside curve with the initial condition $(x_k^*, y_k^*) \approx (1.0597, -0.4237)$ is the separatrix for the strange attractors around the period-1 solutions with the Neimark bifurcation. The Neimark bifurcation of period-2 solution is presented in Figure 2.6 (b). For this case, there are two portions of the strange attractors. Similarly, the most inside points $(x_k^*, y_k^*) \approx (-1.0847, -1.0847)$ and $(1.0847, -1.0847)$ in the

two points of the two strange attractors are for the period-2 solution of P_+ and P_- relative to the Neimark bifurcation. The initial conditions are given in Table 2.2 for simulation. The corresponding initial condition for the two portion separatrices of the strange attractors is $(x_k^*, y_k^*) \approx (1.1728, -1.0847)$.

Table 2.1 Input data for Poincare mappings of period-1 at the Neimark bifurcation ($a = 0.85$ and $b = -1.0$).

(x_k, y_k)	(x_k, y_k)
(0.4737, –0.4737)	(0.8037, –0.4237)
(0.5537, –0.4237)	(0.9037, –0.4237)
(0.6237, –0.4237)	(1.0597, –0.4237)
(0.7037, –0.4237)	

Table 2.2 Input data for Poincare mappings of period-2 at the Neimark bifurcation ($a = 0.85$ and $b = 1.0$).

(x_k, y_k)	(x_k, y_k)
(1.0847, -1.0847)	(1.1328, -1.0847)
(1.0939, -1.0847)	(1.1542, -1.0847)
(1.1128, -1.0847)	(1.1728, -1.0847)

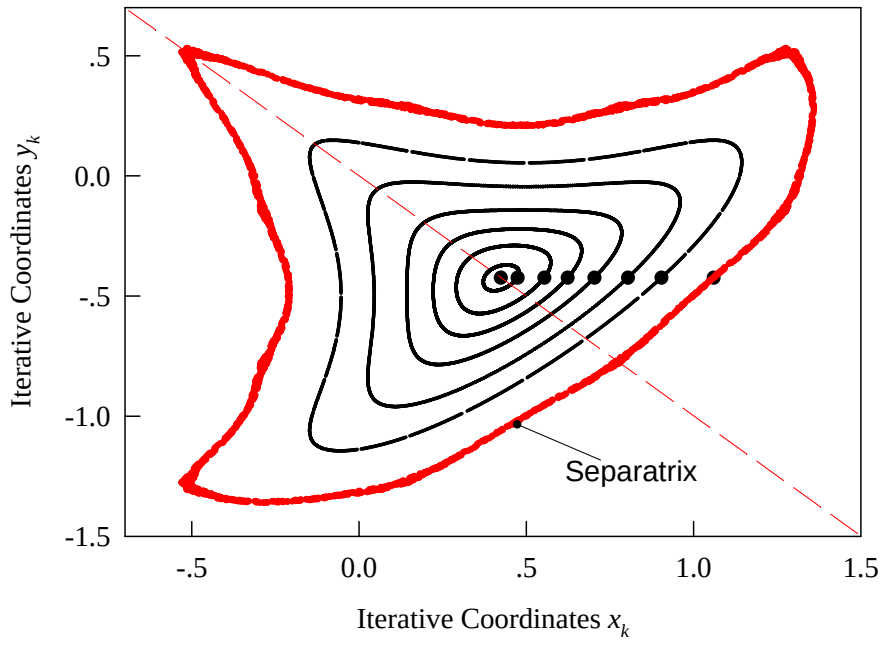

(a)

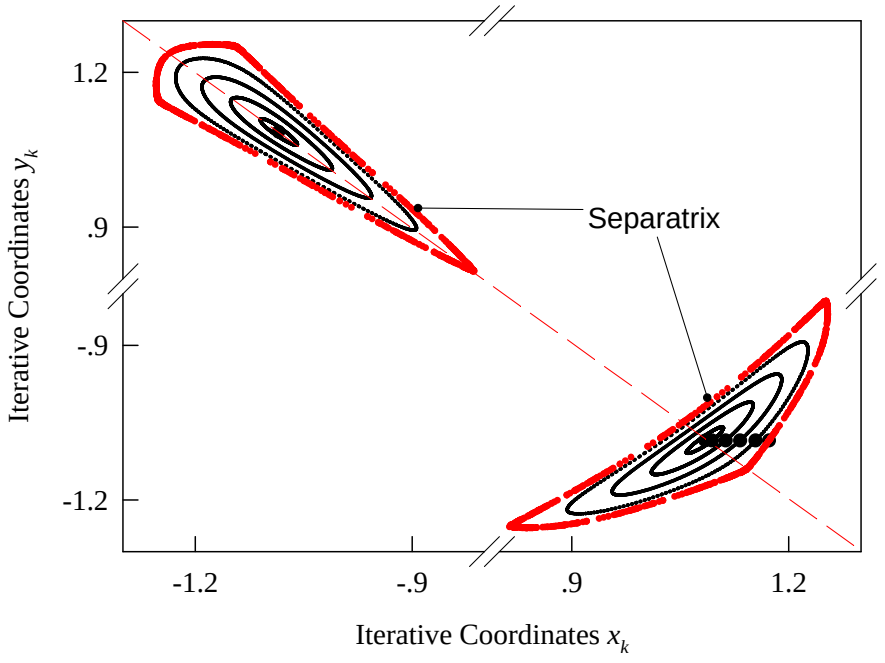

(b)

Figure 2.6: Poincare mappings at the Neimark bifurcation of period-1 solution at $b = -1.0$ and period-2 solution at $b = 1.0$ of the Henon map (a) Neimark bifurcation of period-1 solution, (b) Neimark bifurcation of period-2 solution. ($a = 0.85$).

2.3. Conclusions

In this chapter, the complete bifurcation and stability of the stable and unstable periodic solutions relative to the positive and negative mapping structures were analyzed. The positive and negative iterative mappings of discrete maps were used for mapping structures of the periodic solutions. The periodic solutions of positive and negative mappings give a complete picture of the periodic solution. Both of the positive and negative mappings are a pair. A comprehensive investigation on the Henon map is carried out for a better understanding of complexity in nonlinear discrete systems. The bifurcation scenario based on positive and negative mappings of the Henon map was presented, and the analytical predictions of the corresponding periodic solutions were achieved. The eigenvalue analysis of the periodic solutions based on the positive and negative mappings were carried out. The Poincare mapping sections relative to the Neimark bifurcations of periodic solutions are presented, and the chaotic layers for the discrete system with the Henon map are observed. A parameter map for different positive and negative mapping structures was presented. For the first time, the complete unstable and stable periodic solutions in nonlinear discrete systems were presented.

CHAPTER 3

BOUNCING BALL DYNAMICS

In this chapter, the theory of flow switchability for discontinuous dynamical systems is applied on the parametric analysis of a simple bouncing ball system. Domains and boundaries for such a discontinuous problem are defined and analytical conditions for motion switching are developed. These conditions explain the important role of switching phase on the motion switchability in such a system. In order to describe different motions in a simple and unified style, the generic mappings and mapping structures are introduced using a single discrete map. Bifurcation scenarios for periodic and chaotic motions are presented for a general understanding of different types of motion and the motion switchability. Analytical predictions of stable and unstable periodic motions are also presented with Eigenvalue stability analysis and switchability analysis. Furthermore, numerical simulation results are provided for a better image of periodic motions with only impacts and periodic motions with impact chatter to stick in the system. Finally, a detailed parameter map will be presented for a more comprehensive understanding of the system.

3.1. Physical Model Descriptions

As shown in Figure 3.1 the bouncing ball system consists of a ball impacting on a periodically moving table. The table of mass M is driven under a periodic displacement $X(t)$, and the ball of mass m is subjected to only gravity, as shown in Figure 3.1. The restitution coefficient for impacts between the ball and the table is given as e.

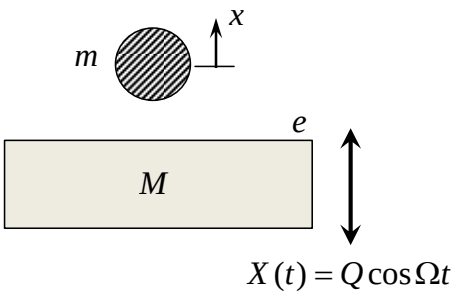

Figure 3.1: Physical model

Then motion of the table is controlled by the excitation displacement $X(t)$ as

$$\left.\begin{aligned} X &= Q\cos\Omega t, \\ \dot{X} &= -Q\Omega\sin\Omega t, \\ \ddot{X} &= -Q\Omega^2\cos\Omega t. \end{aligned}\right\} \tag{3.1}$$

If the particle does not stay on the table, the corresponding motion is called the *non-stick motion*. For this case, the equation of motion for the ball is given as

$$\ddot{x} = -g. \tag{3.2}$$

If the particle stays on the table and move together with it, this is called *the stick motion*. For this case, the equation of motion is

$$\ddot{x}_0 = \ddot{X} = -Q\Omega^2\cos\Omega t, \tag{3.3}$$

where $\ddot{x}_0$ is the acceleration for both the ball and the table. Assuming that the mass of the ball m is much smaller than the one of the table M, then the impact effect on the table from the ball can be ignored. Thus, the impact relation between the ball and the base can be described as

$$\begin{aligned} &x_+ = X_+ = x_- = X_-; \\ &\dot{X}_+ = \dot{X}_-, \\ &\dot{x}_+ = \frac{m\dot{x}_- + M\dot{X}_- - Me(\dot{x}_- - \dot{X}_-)}{m+M}. \end{aligned} \tag{3.4}$$

3.2. Discontinuous Modeling

In order to analyze the discontinuity caused by impacts in such a bouncing ball system, the domains and boundaries in absolute coordinate system are illustrated as in Figure 3.2, where Figure 3.2 (a) sketched the domain and boundary for non-stick motion, and Figure 3.2 (b) sketched the domains and boundaries definitions when stick motion exists. The origin of the absolute coordinate is set at the equilibrium position of the table. The shaded area represents the absolute domain Ω_1, which is defined as

$$\Omega_1 = \left\{(x, \dot{x}) \middle| x \geq X \right\}. \tag{3.5}$$

The grey area highlights the absolute domain for stick motion Ω_0, which is defined as

$$\Omega_0 = \left\{(x, \dot{x}) \middle| x \in (-\infty, X_{cr}), \dot{x} = \dot{X} \right\} \tag{3.6}$$

The corresponding absolute boundaries depicted by dashed curves are defined as

$$\left.\begin{aligned} \partial\Omega_{1(-\infty)} &= \left\{(x, \dot{x}) \middle| \varphi_{1(-\infty)} \equiv x - X = 0, \dot{x} \neq \dot{X} \right\}, \\ \partial\Omega_{10} = \partial\Omega_{01} &= \left\{(x, \dot{x}) \middle| \varphi_{10} \equiv x - X_{cr} = 0, \dot{x} = \dot{X}_{cr} \right\}, \end{aligned}\right\} \tag{3.7}$$

where in Figure 3.2 (a), the boundary of $\partial\Omega_{1(-\infty)}$ is represented by the dashed curve with $x = X$, and in Figure 3.2 (b) the stick boundary $\partial\Omega_{10}$ or $\partial\Omega_{01}$ is represented by the dashed curve with $x = X_{cr}$ and $\dot{x} = \dot{X}_{cr}$. Here X_{cr} and $\dot{X}_{cr}$ indicates the appearance and vanishing of stick motion.

From the domains and boundaries definitions, the following state vectors for absolute motions can be defined

$$\left.\begin{aligned} \mathbf{x}_\lambda &= (x_\lambda, \dot{x}_\lambda)^T, \\ \mathbf{f}_\lambda &= (\dot{x}_\lambda, F_\lambda)^T, \end{aligned}\right\} \text{ for } (\lambda = 0,1), \tag{3.8}$$

where $\lambda = 0,1$ stands for the stick or non-stick domain. Then the equation of absolute motion can be rewritten into state vector form

$$\dot{\mathbf{x}}_\lambda = \mathbf{f}_\lambda(\mathbf{x}_\lambda, t) \quad \text{for } \lambda = 0,1. \tag{3.9}$$

For the non-stick motion,

$$F_1(x_1, t) = -g, \tag{3.10}$$

while for the stick motion,

$$F_0(x_0, t) = -Q\Omega^2 \cos\Omega t. \tag{3.11}$$

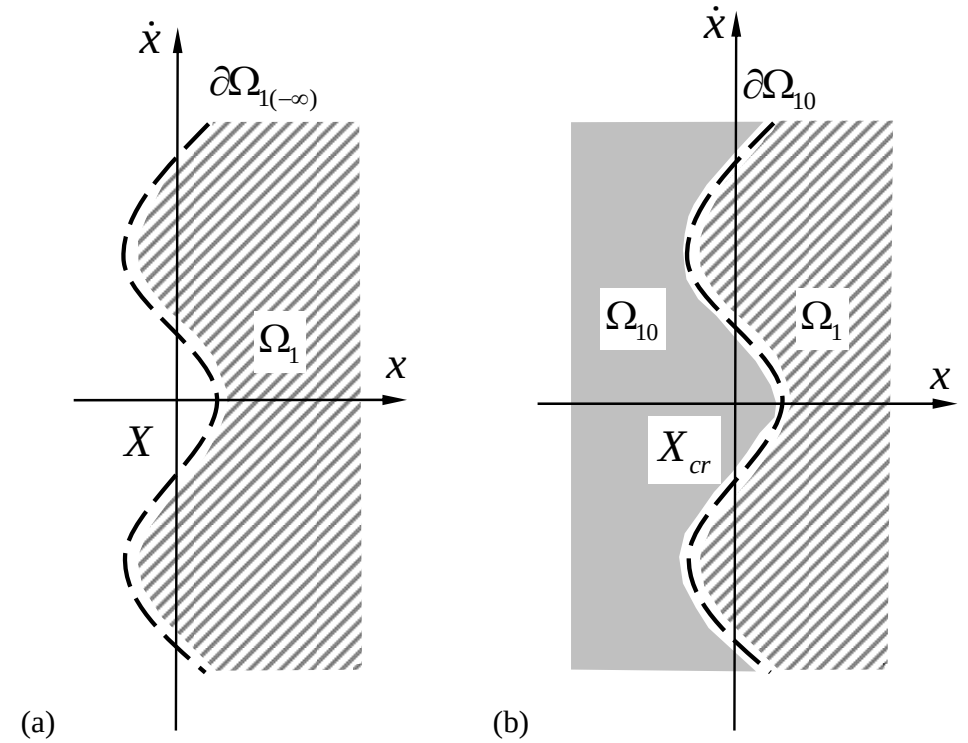

Figure 3.2: Absolute domains and boundaries. (a) Non-Stick motion. (b) Stick motion.

To simplify the time varying boundaries problem, relative coordinates are adopted for the system while the motion is close to the boundary. Considering the relative motion of the ball to the base, the relative displacement, velocity, and acceleration are given as $z = x - X$, $\dot{z} = \dot{x} - \dot{X}$,

and $\ddot{z} = \ddot{x} - \ddot{X}$. The relative domains and boundaries for the motion of the ball are then defined in Figure 3.3. The stick domain and boundaries in the relative phase space becomes points, as shown in Figure 3.3. The relative domains Ω_0 and Ω_1 are defined as

$$\left.\begin{aligned} \Omega_0 &= \left\{(z,\dot{z})\middle| z=0,\ \dot{z}=0\right\}, \\ \Omega_1 &= \left\{(z,\dot{z})\middle| z\in(-h,h)\right\}. \end{aligned}\right\} \tag{3.12}$$

The relative boundaries $\partial\Omega_{1(-\infty)}$, $\partial\Omega_{10}$, and $\partial\Omega_{01}$ are defined as follow

$$\left.\begin{aligned} \partial\Omega_{1(-\infty)} &= \left\{(z,\dot{z})\middle|\varphi_{1(-\infty)}\equiv z=0,\ \dot{z}\neq 0\right\}, \\ \partial\Omega_{10} = \partial\Omega_{01} &= \left\{(z,\dot{z})\middle|\varphi_{10}\equiv \dot{z}_{cr}=0,\ z_{cr}=0\right\}, \end{aligned}\right\} \tag{3.13}$$

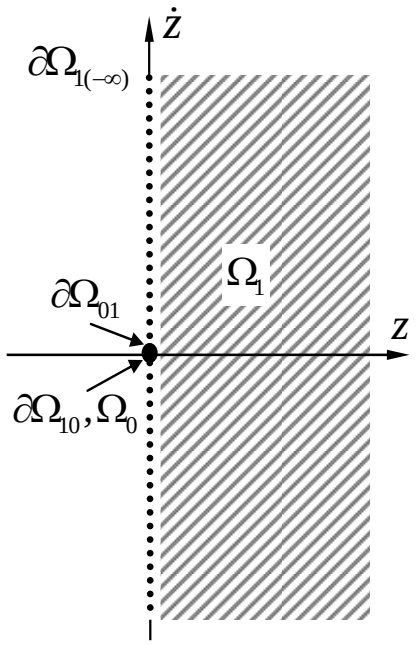

Figure 3.3: Relative domains and boundaries.

where $\partial\Omega_{1(-\infty)}$ is the relative impact-chatter boundaries without stick motion; $\partial\Omega_{10}, \partial\Omega_{01}$ are the relative stick motion boundaries. Using these definitions, the relative state vectors can be defined as

$$\mathbf{z}_\lambda = (z_\lambda, \dot{z}_\lambda)^T, \mathbf{g}_\lambda = \dot{\mathbf{z}}_\lambda = (\dot{z}_\lambda, g_\lambda)^T \tag{3.14}$$

where $\lambda = 0,1$ indicates the corresponding stick and non-stick domains. For $\lambda = 0,1$, the equations of relative motion is rewritten into the relative state vector form

$$\dot{\mathbf{z}}_\lambda = \mathbf{g}_\lambda(\mathbf{z}_\lambda, \mathbf{x}_\lambda, t) , \tag{3.15}$$

where $\dot{\mathbf{x}}_\lambda = \mathbf{f}_\lambda(\mathbf{x}_\lambda, t)$. For non-stick motion

$$g_1(\mathbf{z}_1, \mathbf{x}_1, t) = -g + Q\Omega^2 \cos\Omega t, \tag{3.16}$$

For stick motion

$$g_0(\mathbf{z}_0, \mathbf{x}_0, t) = 0. \tag{3.17}$$

3.3. Analytical Switching Conditions

The analytical switching conditions of stick and grazing motions will be developed in this section using the theory for switchability in discontinuous dynamical systems (Luo, A theory for flow switchability in discontinuous dynamical systems, 2008). First, the normal vector of the relative boundaries are given as

$$\mathbf{n}_{\partial\Omega_{\alpha\beta}} = \nabla\varphi_{\alpha\beta} = \left(\frac{\partial\varphi_{\alpha\beta}}{\partial z}, \frac{\partial\varphi_{\alpha\beta}}{\partial \dot{z}}\right)^T \tag{3.18}$$

where $\nabla = \left(\frac{\partial}{\partial z}, \frac{\partial}{\partial \dot{z}}\right)^T$. Thus, the normal vectors to the relative stick boundaries $\mathbf{n}_{\partial\Omega_{10}}, \mathbf{n}_{\partial\Omega_{01}}$ and relative impact-chatter boundaries $\mathbf{n}_{\partial\Omega_{1(-\infty)}}$ are given by

$$\left.\begin{aligned} \mathbf{n}_{\partial\Omega_{10}} &= \mathbf{n}_{\partial\Omega_{01}} = (0,1)^T, \\ \mathbf{n}_{\partial\Omega_{1(-\infty)}} &= (1,0)^T, \end{aligned}\right\} \tag{3.19}$$

The zero-order and first-order G-functions for the relative stick boundaries are

$$\left.\begin{aligned} G^{(0,0)}_{\partial\Omega_{01}}(\mathbf{z}_0, t_{m\pm}) &= \mathbf{n}^T_{\partial\Omega_{01}} \bullet \mathbf{g}(\mathbf{z}_0, \mathbf{x}_0, t_{m\pm}), \\ G^{(0,1)}_{\partial\Omega_{10}}(\mathbf{z}_1, t_{m\pm}) &= \mathbf{n}^T_{\partial\Omega_{10}} \bullet \mathbf{g}(\mathbf{z}_1, \mathbf{x}_1, t_{m\pm}), \\ G^{(1,0)}_{\partial\Omega_{01}}(\mathbf{z}_0, t_{m\pm}) &= \mathbf{n}^T_{\partial\Omega_{01}} \bullet D\mathbf{g}(\mathbf{z}_0, \mathbf{x}_0, t_{m\pm}), \\ G^{(1,1)}_{\partial\Omega_{10}}(\mathbf{z}_1, t_{m\pm}) &= \mathbf{n}^T_{\partial\Omega_{10}} \bullet D\mathbf{g}(\mathbf{z}_1, \mathbf{x}_1, t_{m\pm}), \end{aligned}\right\} \tag{3.20}$$

where t_m is the switching time of the motion on the corresponding boundary. $t_{m\pm} = t_m \pm 0$ represents the motion just off each side of the boundaries in different domains. The zero-order G-functions are the normal components of the vector fields for the stick boundaries and the first order G-functions are the change rate of the normal vector fields. The G-functions for the relative impact-chatter boundary $\partial\Omega_{1(-\infty)}$ are given

$$\left.\begin{aligned} G^{(0,1)}_{\partial\Omega_{1(-\infty)}}(\mathbf{z}_1, t_{m\pm}) &= \mathbf{n}^T_{\partial\Omega_{1(-\infty)}} \bullet \mathbf{g}(\mathbf{z}_1, \mathbf{x}_1, t_{m\pm}), \\ G^{(1,1)}_{\partial\Omega_{1(-\infty)}}(\mathbf{z}_1, t_{m\pm}) &= \mathbf{n}^T_{\partial\Omega_{1(-\infty)}} \bullet D\mathbf{g}(\mathbf{z}_1, \mathbf{x}_1, t_{m\pm}), \end{aligned}\right\} \tag{3.21}$$

With these G-functions define, the analytical switching conditions for stick motion can then be obtained from the passable flow condition from domain Ω_1 to Ω_0, i.e.,

$$G^{(0,1)}_{\partial\Omega_{10}}(\mathbf{z}_1, t_{m-}) < 0 \text{ and } G^{(0,0)}_{\partial\Omega_{10}}(\mathbf{z}_0, t_{m+}) < 0. \tag{3.22}$$

Therefore,

$$g_1(\mathbf{z}_1, \mathbf{x}_1, t_{m-}) < 0 \text{ and } g_0(\mathbf{z}_0, \mathbf{x}_0, t_{m+}) < 0. \tag{3.23}$$

Furthermore, with the relative force function per unit mass, the onset condition of stick motion is given by

$$\begin{aligned} &\text{If } |Q|\Omega^2 \le g, \text{ always stick.} \\ &\text{If } |Q|\Omega^2 > g, \\ &\left.\begin{aligned} &\mathrm{mod}(\Omega t_m, 2\pi) \in (\arccos\frac{g}{Q\Omega^2}, 2\pi - \arccos\frac{g}{Q\Omega^2}) \text{ for } Q > 0 \\ &\mathrm{mod}(\Omega t_m, 2\pi) \in (0, \arccos\frac{g}{Q\Omega^2}) \bigcup (2\pi - \arccos\frac{g}{Q\Omega^2}, 2\pi) \text{ for } Q < 0 \end{aligned}\right\} \end{aligned} \tag{3.24}$$

From Eqn.(3.24), if $|Q|\Omega^2 \le g$, the ball will always stick with the table once they come to same displacement and velocity; if $|Q|\Omega^2 > g$, in order for the ball to stick and move together with the table, the switching phase $\mathrm{mod}(\Omega t_m, 2\pi)$ of the system must be within the range of $(\arccos\frac{g}{Q\Omega^2}, 2\pi - \arccos\frac{g}{Q\Omega^2})$ for $Q > 0$, or for $Q < 0$ inside the ranges $(0, \arccos\frac{g}{Q\Omega^2})$ or $(2\pi - \arccos\frac{g}{Q\Omega^2}, 2\pi)$.

On the other hand, the criteria for vanishing of the stick motion are given for $\partial\Omega_{01}$ by

$$\left.\begin{aligned} &G^{(0,0)}_{\partial\Omega_{01}}(\mathbf{z}_0, t_{m-}) = 0 \text{ and } G^{(0,1)}_{\partial\Omega_{01}}(\mathbf{z}_1, t_{m+}) = 0, \\ &G^{(1,0)}_{\partial\Omega_{01}}(\mathbf{z}_0, t_{m-}) > 0 \text{ and } G^{(1,1)}_{\partial\Omega_{01}}(\mathbf{z}_1, t_{m+}) > 0. \end{aligned}\right\} \tag{3.25}$$

Simplifying the foregoing equations with the relative force relations for $\partial\Omega_{01}$, one can obtain

$$\left.\begin{aligned} &g_0(\mathbf{z}_0, \mathbf{x}_0, t_{m-}) = 0 \text{ and } g_1(\mathbf{z}_1, \mathbf{x}_1, t_{m+}) = 0, \\ &\tfrac{d}{dt} g_0(\mathbf{z}_0, \mathbf{x}_0, t_{m-}) > 0 \text{ and } \tfrac{d}{dt} g_1(\mathbf{z}_1, \mathbf{x}_1, t_{m+}) > 0. \end{aligned}\right\} \tag{3.26}$$

Further simplification of the above equation yields

$$\begin{aligned} &\text{If } |Q|\Omega^2 < g, \text{ no vanishing exists.} \\ &\text{If } |Q|\Omega^2 \ge g, \\ &\left.\begin{aligned} &\text{when } Q\Omega > 0, \mathrm{mod}(\Omega t_m, 2\pi) = 2\pi - \arccos\frac{g}{Q\Omega^2}, \\ &\text{when } Q\Omega < 0, \mathrm{mod}(\Omega t_m, 2\pi) = \arccos\frac{g}{Q\Omega^2}, \end{aligned}\right\} \end{aligned} \tag{3.27}$$

The above equation states: if $|Q|\Omega^2 < g$ the ball can never stop stick motion and have to move together with the table once the stick motion strats. Otherwise, when $Q\Omega > 0$, the stick motion can stop only when the switching phase $\mathrm{mod}(\Omega t_m, 2\pi)$ is equal to $2\pi - \arccos\frac{g}{Q\Omega^2}$. When $Q\Omega < 0$, the stick motion can only vanish when $\mathrm{mod}(\Omega t_m, 2\pi)$ equals to $\arccos\frac{g}{Q\Omega^2}$.

For grazing motion, the analytical condition can also be developed from the G-functions of the flow for the impact-chatter boundary $\partial\Omega_{1(-\infty)}$ as follow

$$G^{(0,1)}_{\partial\Omega_{1(-\infty)}}(\mathbf{z}_1, t_{m\pm}) = 0 \text{ and } G^{(1,1)}_{\partial\Omega_{1(-\infty)}}(\mathbf{z}_1, t_{m\pm}) > 0 \ , \tag{3.28}$$

Thus, the grazing motion condition of impact-chatter boundary is given as

$$\left.\begin{aligned} &\dot{x}_m + Q\Omega \sin\Omega t_m = 0, \\ &Q\Omega^2 \cos\Omega t_m > g \end{aligned}\right\} \text{for } \partial\Omega_{1(-\infty)} \tag{3.29}$$

Similarly, the grazing motion conditions for the stick boundaries are given as

$$\left.\begin{aligned} &G^{(0,1)}_{\partial\Omega_{10}}(\mathbf{z}_1, \mathbf{x}_1, t_{m\pm}) = 0 \text{ and } G^{(1,1)}_{\partial\Omega_{10}}(\mathbf{z}_1, \mathbf{x}_1, t_{m\pm}) > 0 \ \text{ for } \partial\Omega_{10}, \\ &G^{(0,0)}_{\partial\Omega_{01}}(\mathbf{z}_0, \mathbf{x}_0, t_{m\pm}) = 0 \text{ and } G^{(1,0)}_{\partial\Omega_{01}}(\mathbf{z}_0, \mathbf{x}_0, t_{m\pm}) < 0 \ \text{ for } \partial\Omega_{01}. \end{aligned}\right\} \tag{3.30}$$

Substitution of the relative motion relations into the above equations and simplify them yields

$$\left.\begin{aligned} &Q\Omega^2 \cos\Omega t = g \text{ and } Q\Omega^3 \sin\Omega t < 0, \text{ for } \partial\Omega_{10}, \\ &Q\Omega^2 \cos\Omega t = g \text{ and } Q\Omega^3 \sin\Omega t > 0, \text{ for } \partial\Omega_{01}, \end{aligned}\right\} \tag{3.31}$$

3.4. Discrete Mapping Structures

Based on the boundaries defined in Eqn.(3.7), the switching sets of bouncing ball system without stick can be defined as

$$\left.\begin{aligned} &\Sigma_{1(-\infty)} = \left\{ (x_k, \dot{x}_k, t_k) \middle| x_k = X, \ \dot{x}_k \neq \dot{X} \right\} \\ &\Sigma_{10} = \Sigma_{01} = \left\{ (x_k, \dot{x}_k, t_k) \middle| x_k = X, \ \dot{x}_k = \dot{X} \right\} \end{aligned}\right\} \tag{3.32}$$

where the switching set $\Sigma_{1(-\infty)}$ is defined on the impact chatter boundary $\partial\Omega_{1(-\infty)}$, Σ_{10} and Σ_{01} are defined on the stick boundaries $\partial\Omega_{10}$ and $\partial\Omega_{01}$, respectively. Thus, the generic mappings for such a bouncing ball system can be defined as

$$\left.\begin{aligned} &P_1 : \Sigma_{1(-\infty)} \to \Sigma_{1(-\infty)} \text{ or } \Sigma_{01} \to \Sigma_{1(-\infty)} \text{ or } \Sigma_{1(-\infty)} \to \Sigma_{10} \\ &P_0 : \Sigma_{10} \to \Sigma_{01}. \end{aligned}\right\} \tag{3.33}$$

where the mapping of P_1 represents an impact between the ball and the table, and the mapping of P_2 represents a stick motion of the ball on the table, as shown in Figure 3.4. From the above definitions, the governing equations for the generic mappings can be expressed by

$$\begin{aligned} P_1&:\begin{cases} f_1^{(1)}\left(x_k,\dot{x}_k,t_k,x_{k+1},\dot{x}_{k+1},t_{k+1}\right)=0,\\ f_2^{(1)}\left(x_k,\dot{x}_k,t_k,x_{k+1},\dot{x}_{k+1},t_{k+1}\right)=0,\end{cases}\\ P_0&:\begin{cases} f_1^{(0)}\left(x_k,\dot{x}_k,t_k,x_{k+1},\dot{x}_{k+1},t_{k+1}\right)=0,\\ f_2^{(0)}\left(x_{k+1},\dot{x}_{k+1},t_{k+1}\right)=g_1\left(0,\mathbf{x}_{k+1},t_{k+1}\right)=0,\end{cases}\end{aligned} \tag{3.34}$$

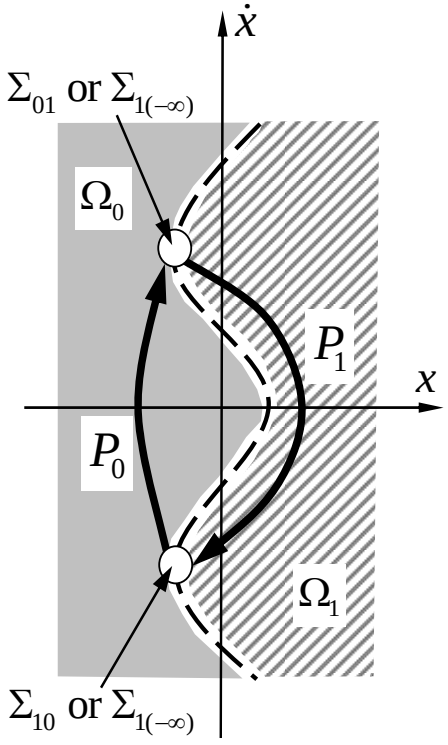

Figure 3.4: Illustration of switching sets and generic mappings.

with

$$\left.\begin{array}{l} x_k = X \ \text{ and } x_{k+1} = X \ \text{ for } P_1, \\ x_k = X \ \text{ and } \dot{x} = \dot{X} \text{ and} \\ \left.\begin{array}{l} \mathrm{mod}(\Omega t_m, 2\pi) \in (\arccos\dfrac{g}{Q\Omega^2}, \dfrac{\pi}{2}) \ \text{ and} \\ \mathrm{mod}(\Omega t_m, 2\pi) \in (\dfrac{3\pi}{2}, 2\pi - \arccos\dfrac{g}{Q\Omega^2}) \end{array}\right\} \text{ for } P_0. \end{array}\right\} \tag{3.35}$$

The notation for mapping action is introduced as

$$P_{j_k j_{k-1}\cdots j_1} = P_{j_k} \circ P_{j_{k-1}} \circ \cdots \circ P_{j_1}, \tag{3.36}$$

where $j_k \in \{1,0\}$. For a motion with m-time repeated mapping structure of $P_{j_1 j_2 \cdots j_k}$, the mapping structure can be expressed as

$$\begin{aligned} P^{(m)}_{j_k j_{k-1}\cdots j_1} &= \underbrace{\left(P_{j_k} \circ P_{j_{k-1}} \circ \cdots \circ P_{j_1}\right) \circ \cdots \circ \left(P_{j_k} \circ P_{j_{k-1}} \circ \cdots \circ P_{j_1}\right)}_{m} \\ &= P_{(j_k j_{k-1}\cdots j_1)^m}. \end{aligned} \tag{3.37}$$

Consider a motion with a generalized mapping structure

$$P = \underbrace{P_{1^{k_{2l}}0^{k_{1l}}} \circ \cdots \circ P_{1^{k_{11}}0^{k_{11}}}}_{l-terms} = P_{\underbrace{(1^{k_{2l}}0^{k_{1l}})\cdots(1^{k_{21}}0^{k_{11}})}_{l-terms}}, \tag{3.38}$$

where $k_{js} \in \{0,1\}$ and ($j = 1,2$; $s = 1,2,\cdots,l$). Define vectors $\mathbf{Y}_k \equiv (x_k, \dot{x}_k, t_k)^{\mathrm{T}}$. The motion pertaining to the mapping structure in Eqn. (3.38) can be determined by

$$\mathbf{Y}_{k+\Sigma_{s=1}^{l}(k_{1s}+n_s)} = P\mathbf{Y}_k = P_{\underbrace{(0^{k_{1l}}1^{n_l})\cdots(0^{k_{11}}1^{n_1})}_{l-terms}}\mathbf{Y}_k. \tag{3.39}$$

From the algebraic equations for generic mappings in Eqn. (3.34) and (3.35), one can obtain a set of nonlinear algebraic equations for such a mapping structure, i.e.,

$$\begin{array}{l} \mathbf{f}^{(0)}(\mathbf{Y}_k, \mathbf{Y}_{k+1}) = 0, \cdots, \mathbf{f}^{(1)}(\mathbf{Y}_{k+k_{11}}, \mathbf{Y}_{k+k_{11}+1}) = 0, \cdots, \\ \mathbf{f}^{(0)}(\mathbf{Y}_{k+k_{21}+k_{11}}, \mathbf{Y}_{k+k_{21}+k_{11}+1}) = 0, \cdots, \\ \mathbf{f}^{(1)}(\mathbf{Y}_{k+\Sigma_{s=1}^{l}(k_{2s}+k_{1s})-1}, \mathbf{Y}_{k+\Sigma_{s=1}^{l}(k_{2s}+k_{1s})}) = 0. \end{array} \tag{3.40}$$

The periodic motion pertaining to such a mapping requires

$$\mathbf{Y}_{k+\Sigma_{s=1}^{l}(k_{2s}+k_{1s})} = \mathbf{Y}_k \tag{3.41}$$

or

$$\left.\begin{aligned} x_{k+\Sigma_{s=1}^{l}(k_{2s}+k_{1s})} &= x_k, \\ \dot{x}_{k+\Sigma_{s=1}^{l}(k_{2s}+k_{1s})} &= \dot{x}_k \end{aligned}\right\} \\ \Omega t_{k+\Sigma_{s=1}^{l}(k_{2s}+k_{1s})} = \Omega t_k + 2N\pi. \tag{3.42}$$

Solving Eqn. (3.40) to (3.42) generates the switching sets of periodic motion with respect to the mapping structure in Eqn.(3.38). Once the switching points for a specific periodic motion is obtained, its local stability and bifurcation analysis can be achieved through the corresponding Jacobian matrix. For instance, the Jacobian matrix of the mapping structure in Eqn. (3.38) is given as

$$DP = DP_{\underbrace{(1^{k_{1l}}0^{k_{1l}})\cdots(1^{k_{21}}0^{k_{11}})}_{l-terms}} = \prod_{s=1}^{l} DP_1^{(k_{2s})} \cdot DP_0^{(k_{1s})}, \tag{3.43}$$

where

$$DP_\sigma = \left[\frac{\partial \mathbf{Y}_{\sigma+1}}{\partial \mathbf{Y}_\sigma}\right]_{2\times 2}. \tag{3.44}$$

for $\sigma = k, k+1, \cdots, k+\Sigma_{s=1}^{l}(k_{2s}+k_{1s})-1$ and all the Jacobian matrix components can be computed through Eqn. (3.44). The equations for a set of switching points $\{\mathbf{Y}_k^*, \mathbf{Y}_{k+1}^*, \cdots, \mathbf{Y}_{k+\Sigma_{s=1}^{l}(k_{2s}+k_{1s})}^*\}$ is

$$\Delta\mathbf{Y}_{k+\Sigma_{s=1}^{l}(k_{2s}+k_{1s})} = DP(\mathbf{Y}_k^*)\Delta\mathbf{Y}_k \tag{3.45}$$

If $\Delta\mathbf{Y}_{k+\Sigma_{s=1}^{l}(k_{2s}+k_{1s})} \equiv \lambda\Delta\mathbf{Y}_k$, then the Eigenvalues can be computed by

$$\left|DP(\mathbf{Y}_k^*) - \lambda\mathbf{I}\right| = 0 \tag{3.46}$$

For Eigenvalue stability:

If all $|\lambda_i| < 1$ for $(i = 1, 2)$, the periodic motion is stable.

If one of $|\lambda_i| > 1$ for $(i \in \{1, 2\})$, the periodic motion is unstable.

If one of $\lambda_i = -1$ and $|\lambda_j| < 1$ for $(i, j \in \{1, 2\}$ and $j \neq i)$, the period-doubling bifurcation of periodic motion occurs.

If one of $\lambda_i = 1$ and $|\lambda_j| < 1$ for $(i, j \in \{1, 2\}$ and $j \neq i)$, the saddle-node bifurcation of the periodic motion occurs.

If $|\lambda_{1,2}| = 1$ is a pair of complex Eigenvalues, the Neimark bifurcation of the periodic motion occurs.

However, the Eigenvalue analysis cannot be used to predict sticking and grazing motions. Both of them should be determined through the normal vector fields, where the onset and vanishing of stick motion is determined by Eqn. (3.24) and (3.27); the grazing motion is determined by Eqn. (3.29) or (3.31).

3.5. Illustrations

In this section bifurcation scenario will be presented for the bouncing ball system together with the analytical predictions and Eigenvalue stability. Simulations of periodic motions with only impacts and periodic motions with impact chatter to stick will also be illustrated for the system using the switching sets and generic mappings. Finally, a detailed parameter map will be presented for a better understanding of different motions in the system.

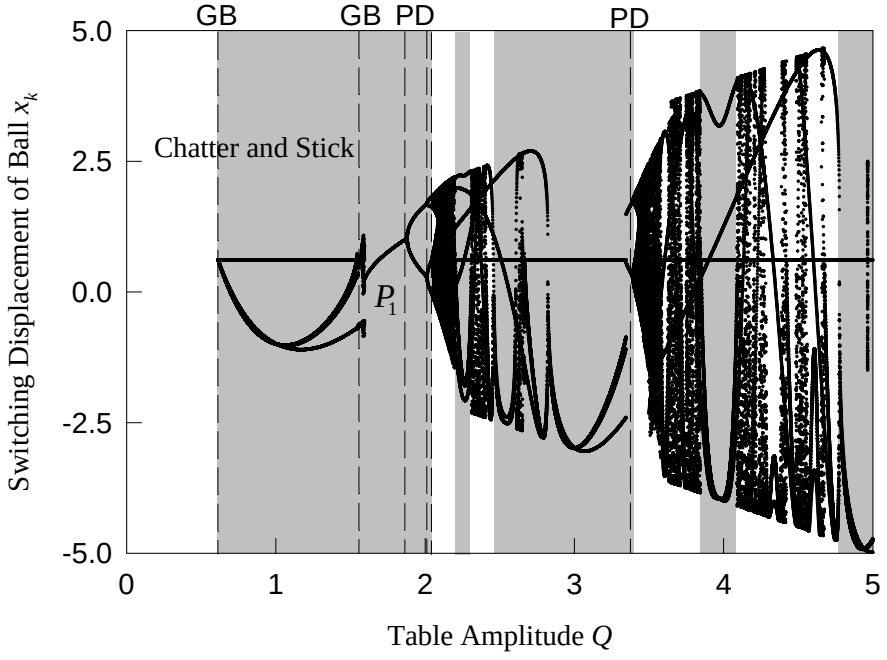

(a)

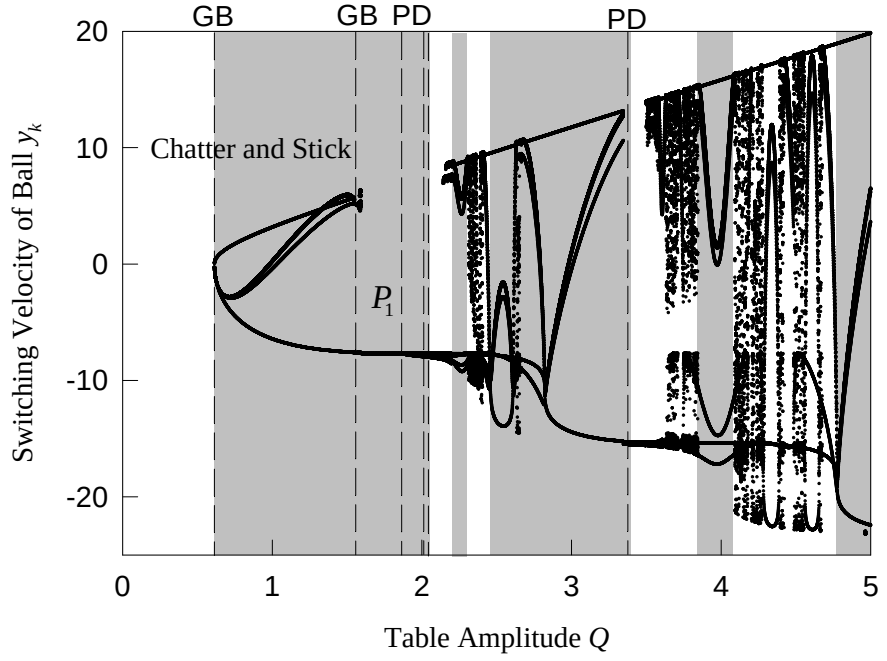

(b)

Figure 3.5: Bifurcation scenario of varying table displacement amplitude Q . (a) Switching displacement of the ball. (b) Switching velocity of the ball. (c) Switching phase $\mathrm{mod}(\Omega t, 2\pi)$. ($\Omega = 4.0, e = 0.1, M = 1.0, m = 0.00001.$)

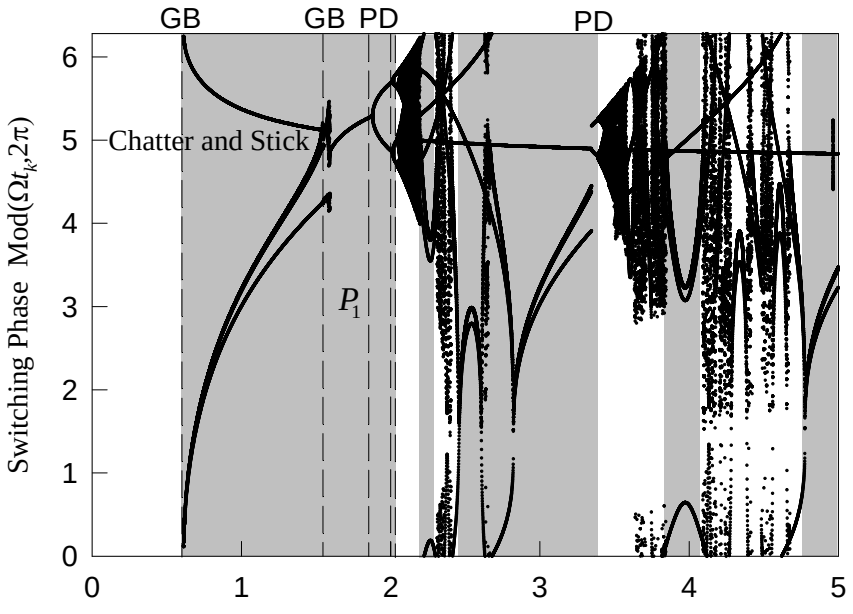

(c)

Figure 3.5 Continue

The bifurcation scenario of varying table displacement amplitude Q for the bouncing ball is presented in Figure 3.5. The parameters are $\Omega = 4.0,\ M = 1.0,\ m = 0.00001,\ e = 0.1$. The bifurcation of the ball's switching displacement versus the table displacement amplitude Q is shown in Figure 3.5 (a), while the bifurcation of the ball's switching velocity versus Q is given in Figure 3.5 (b). The bifurcation of the switching phase versus Q is also presented in Figure 3.5 (c). The acronyms "PD" and "GB" represent period-doubling bifurcation and grazing bifurcation, respectively. The shaded regions indicate the regions of periodic motion. This includes periodic motion with impact chatter and stick as well as periodic motions with only impacts

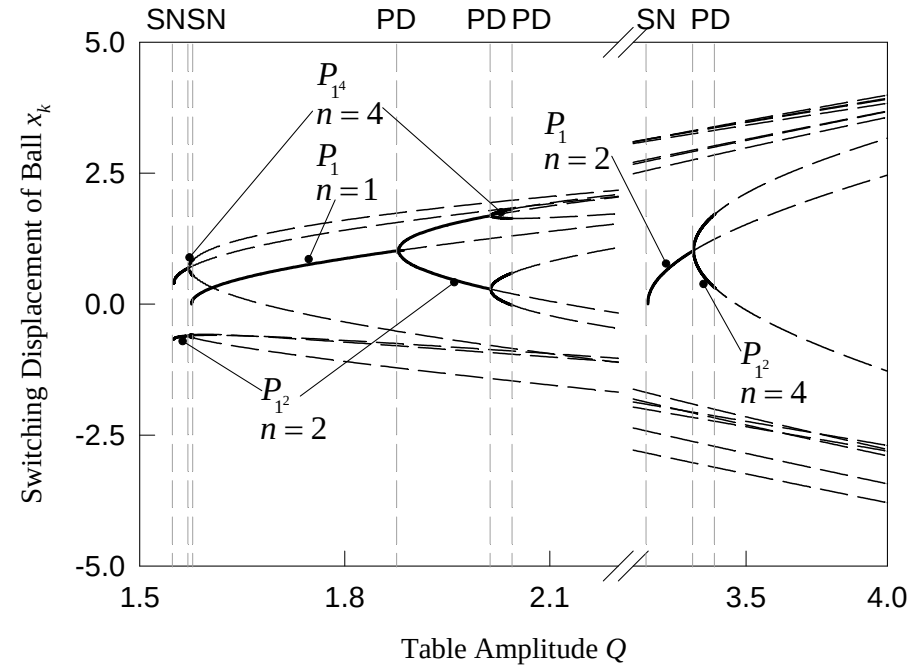

(a)

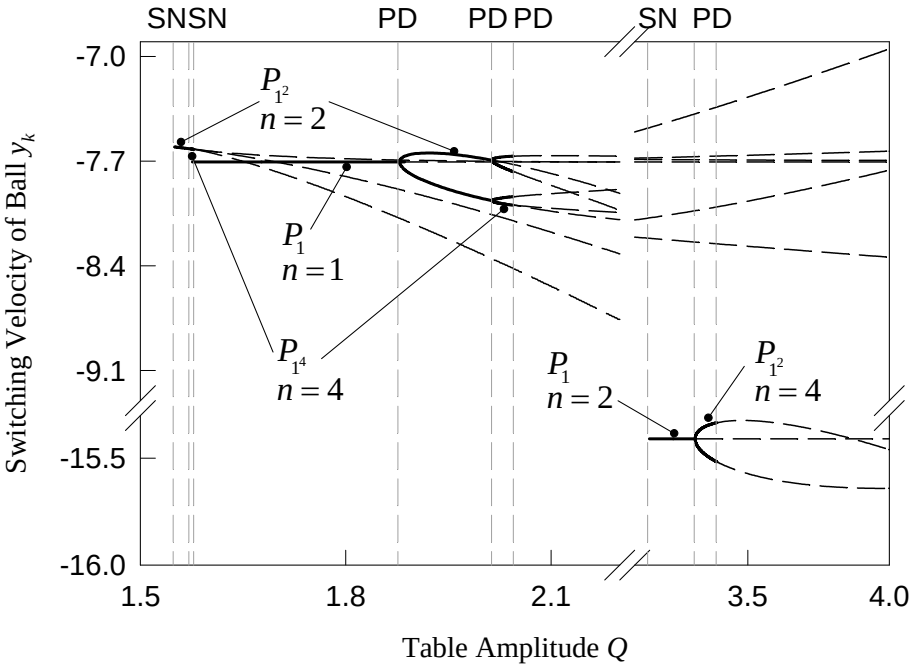

(b)

Figure 3.6: Analytical prediction of varying the table displacement amplitude Q. (a) Switching displacement of the ball. (b) Switching velocity of the ball. (c) Switching phase $\mathrm{mod}(\Omega t, 2\pi)$. (d) Real part of Eigenvalues. (e) Imaginary part of Eigenvalues. (f) Magnitude of Eigenvalues. ($\Omega = 4.0,\quad e = 0.1,\quad M = 1.0,\quad m = 0.00001.$)

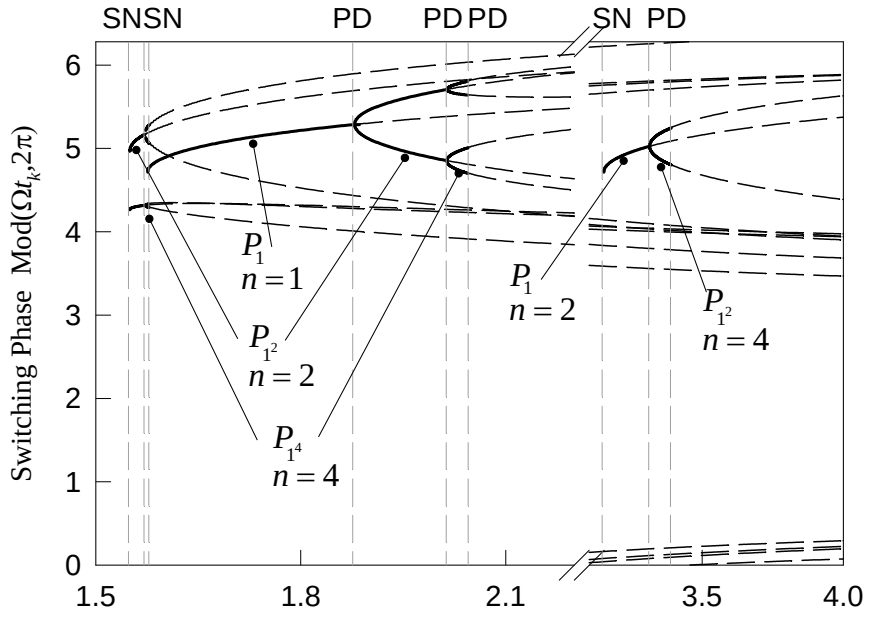

(c)

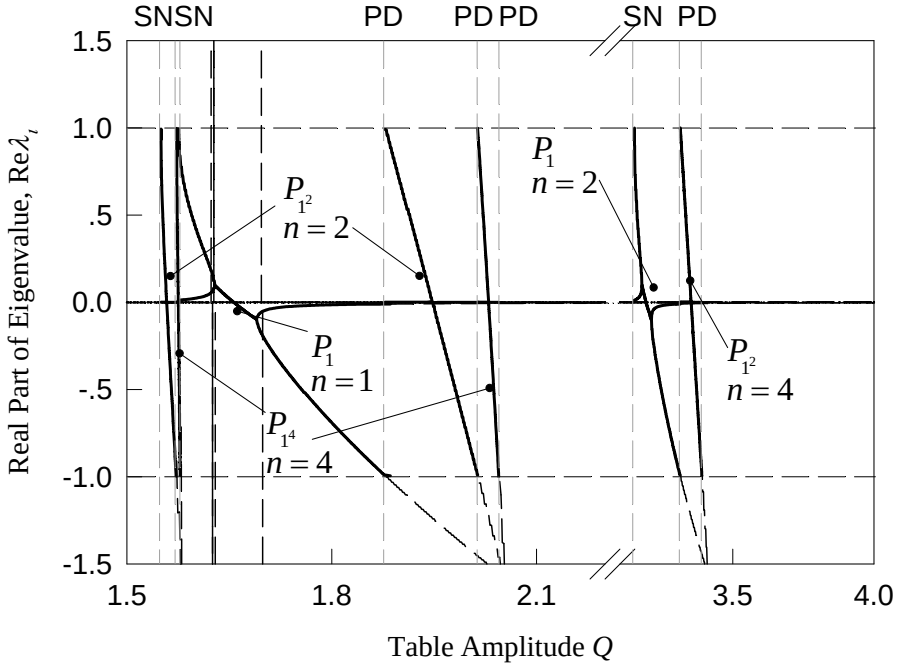

(d)

Figure 3.6 Continue

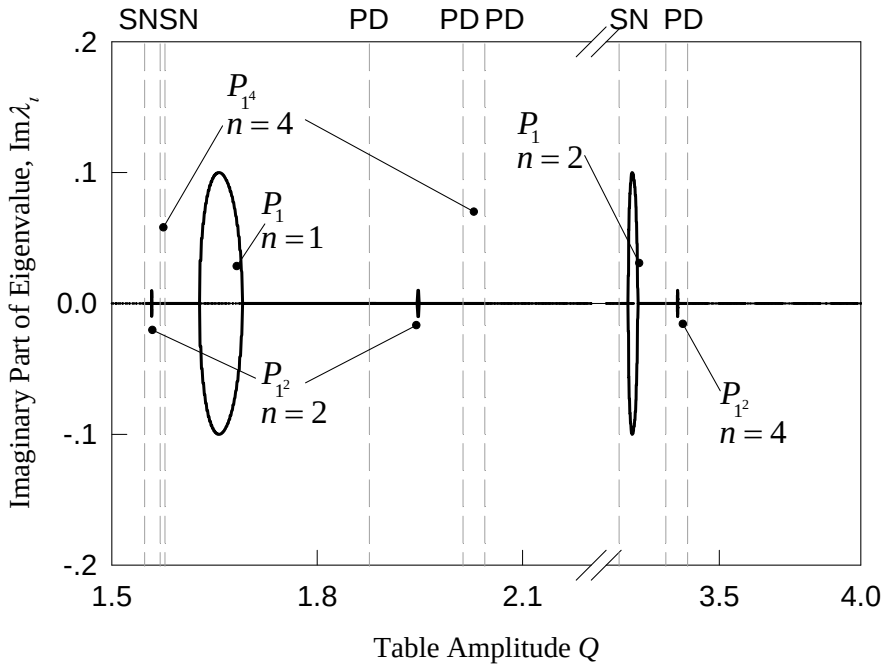

(e)

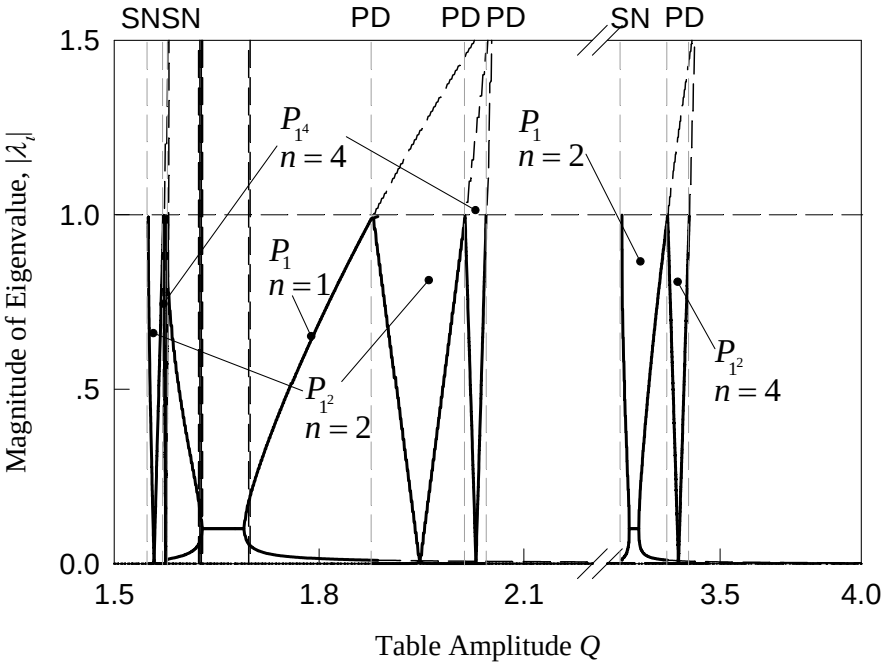

(f)

Figure 3.6 Continue

Using same parameters, the corresponding analytical predictions for impact only periodic motion are presented in Figure 3.6, where Figure 3.6 (a), (b), and (c) present the switching displacement, switching velocity, and switching phase of the ball versus the table displacement amplitude Q, respectively; Figure 3.6 (d), (e), and (f) illustrate the real part, imaginary part, and magnitude of Eigenvalues versus Q, respectively. Furthermore, the analytical predictions of periodic motions with impact chatter and stick are also provided in Figure 3.7, where Figure 3.7 (a), (b), and (c) are presenting the switching displacement, switching velocity, and switching phase of the ball versus Q, respectively. The symbols 'PD', 'SN', and 'GB' represent the period doubling bifurcation, saddle node bifurcation, and grazing bifurcation, correspondingly. In Figure 3.6, the solid curves indicate stable periodic motions while the dashed curves indicate the unstable periodic motions; and $n = 1, 2, ...$ indicate the order of the periodic motion according to table displacement period. As presented in Figure 3.6, for $Q \in (1.55, 1.57)$, the period-2 P_{1^2} motion with only impacts exists. To the left, this motion ends at the saddle node bifurcation where $Q \approx 1.55$; To the right, this motion becomes unstable at $Q \approx 1.57$ due to a period doubling bifurcation which corresponds to the saddle node bifurcation of the period-4 P_{1^4} motion. And the period-4 P_{1^4} motion exists in the range $Q \in (1.57, 1.58)$. This motion eventually becomes unstable at the period doubling bifurcation at $Q \approx 1.58$. For $Q \in (1.57, 1.87)$, there is another branch of periodic motion existing, the period-1 P_1 motion, similarly this motion ends at $Q \approx 1.57$ because of a saddle node bifurcation and becomes unstable after $Q \approx 1.87$ due to a period doubling bifurcation. After the period doubling another branch of period-2 P_{1^2} motion starts. This motion continues until $Q \approx 2.01$, where a period doubling bifurcation cause it to go unstable. The new started period-4 P_{1^4} motion continues

until it reaches the period doubling bifurcation at $Q \approx 2.04$. In a similar pattern, the period-2 P_1 motion with only impact runs from $Q \approx 3.15$ to $Q \approx 3.31$. To the left, this motion disappears at the saddle node bifurcation at $Q \approx 3.15$; to the right the motion becomes unstable after a period doubling bifurcation at $Q \approx 3.31$. After the period doubling, the period-4 P_{1^2} motion exist for $Q \in (3.31, 3.39)$. This motion becomes unstable at $Q \approx 3.39$ after the period doubling bifurcation. All these periodic motions consist of only impacts between the ball and the table. They are relatively simple comparing to the periodic motions consist of impact chatter and stick which will be presented latter.

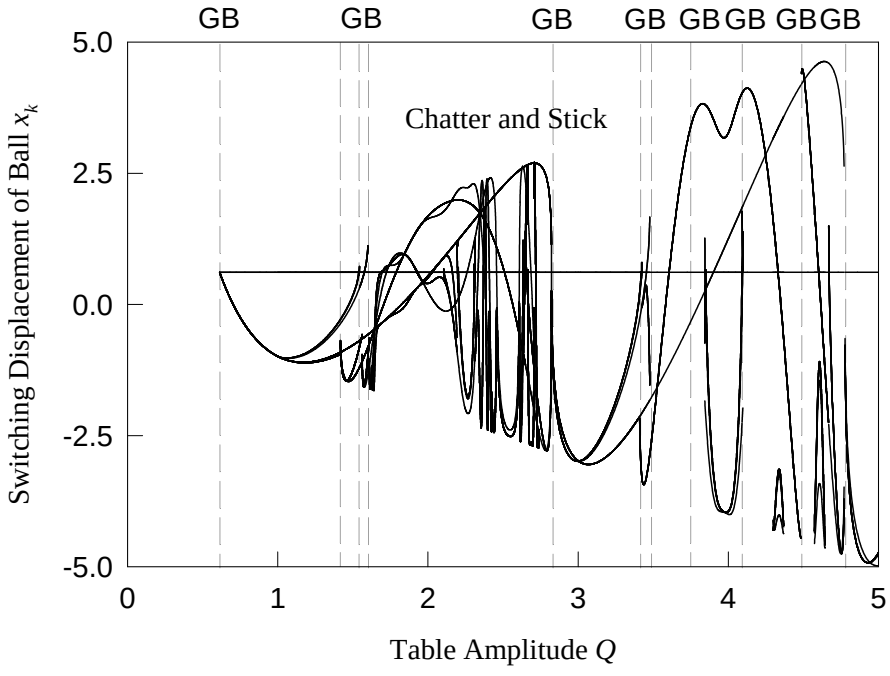

(a)

Figure 3.7: Analytical prediction for impact chatter and stick motion varying the table displacement amplitude Q. (a) Switching displacement of the ball. (b) Switching velocity of the ball. (c) Switching phase $\mathrm{mod}(\Omega t, 2\pi)$. (d) Real part of Eigenvalues. (e) Imaginary part of Eigenvalues. (f) Magnitude of Eigenvalues. ($\Omega = 4.0$, $e = 0.1$, $M = 1.0$, $m = 0.00001$.)

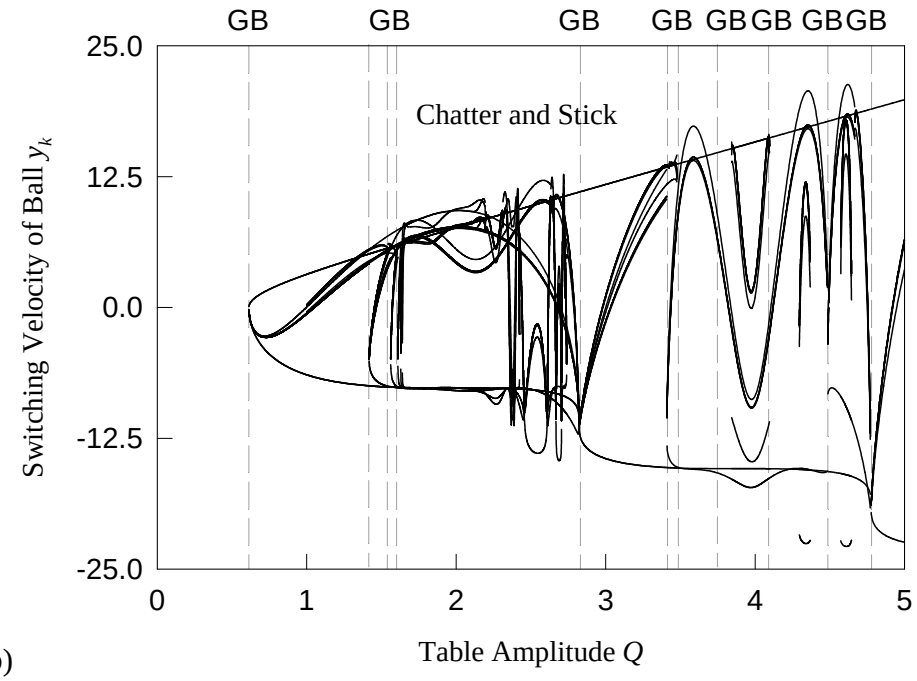

(b)

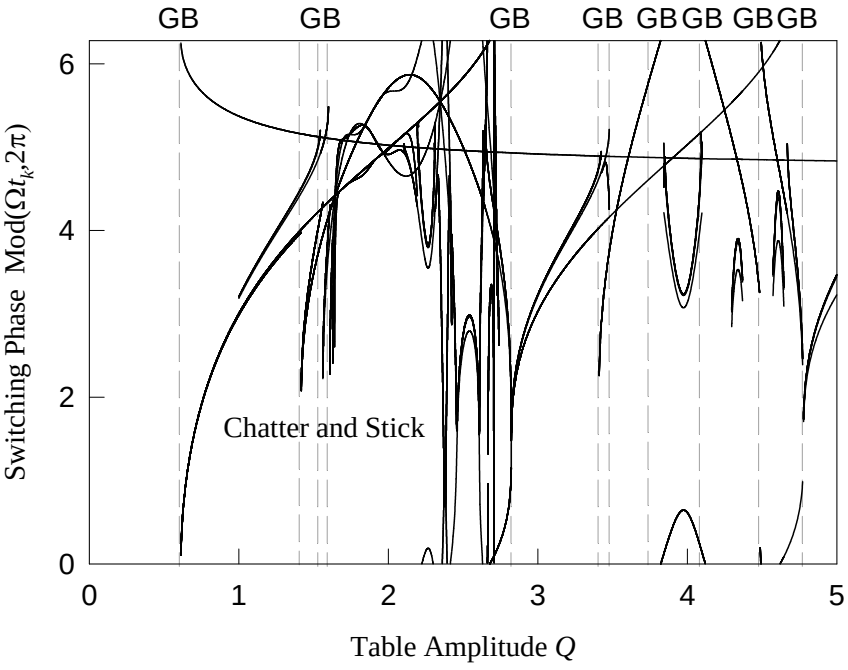

(c)

Figure 3.7 Continues

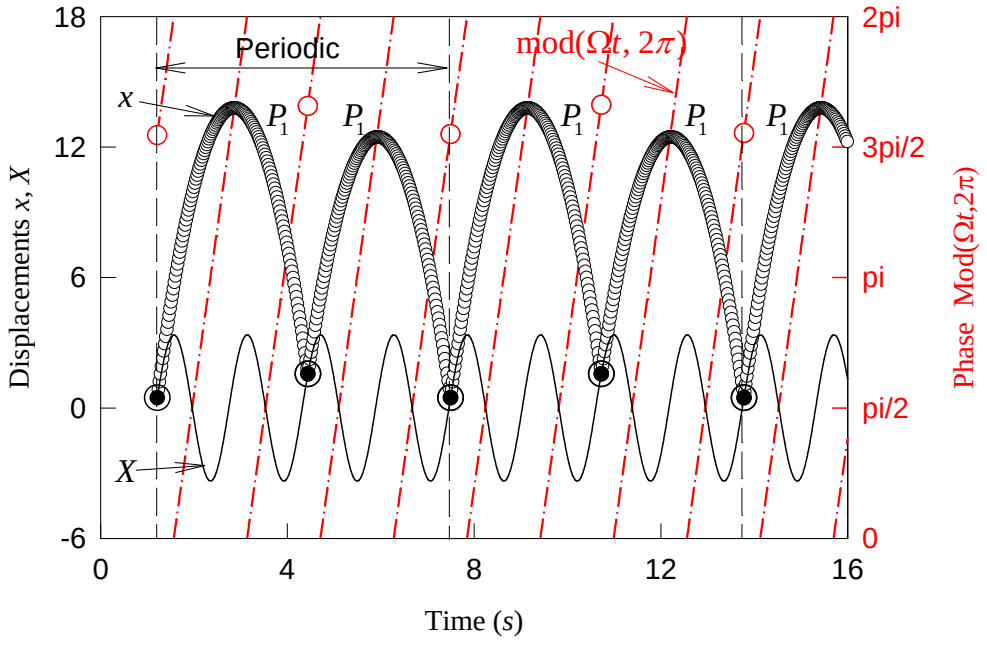

(a)

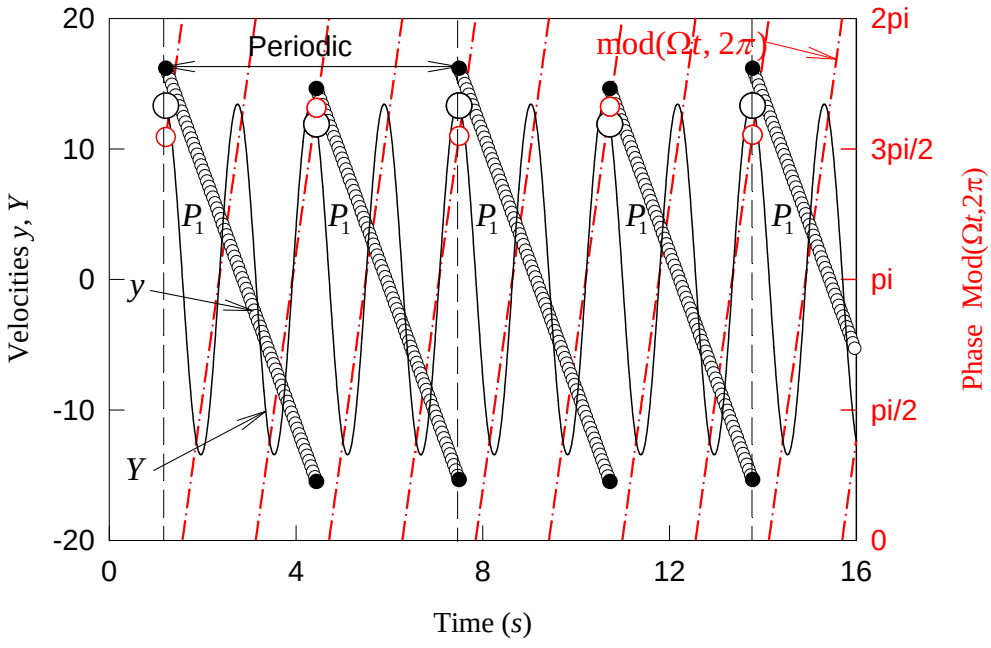

(b)

Figure 3.8: Simulation of period-4 motion with a mapping structure of P_{1^2}. ($Q = 3.36$, $\Omega = 4.0$, $e = 0.1$, $M = 1.0$, $m = 0.00001$). (a) Displacement time history. (b) Velocity time history. (c) Phase portrait of the ball with moving boundaries. The initial conditions are: $t_0 = 1.21297116$, $x_0 = 0.467186746$, $\dot{x}_0 = 16.1746312$.

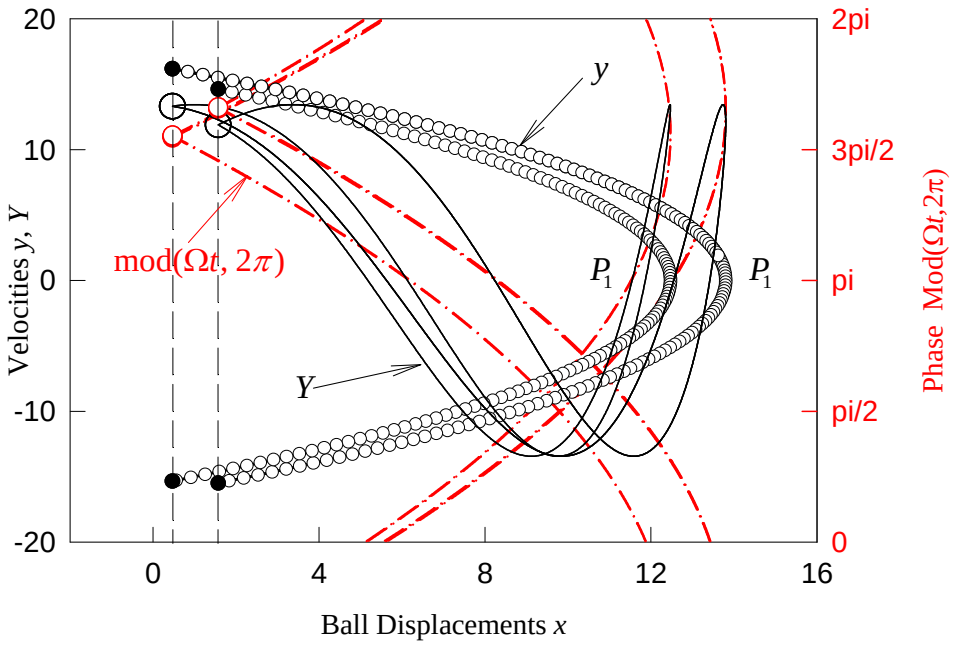

(c)

Figure 3.8 Continue

With the same set of parameters and same range for the excitation amplitude Q, the analytical prediction for impact chatter with stick periodic motions are presented in Figure 3.7. In a similar fashion with Figure 3.6, Figure 3.7(a), (b), and (c) presented the switching displacement, switching velocity, and switching phase, respectively. The symbol "GB" stands for grazing bifurcations, where one of the impact chatters disappears after the bifurcation. The grazing bifurcation cannot be seen from the Eigenvalue stability analysis, and can only be predicted by the analytical conditions presented in Eqn. (3.29) and (3.31). As can be observed from the figure, the impact chatter and stick motions can cause some very complex periodic motion. These motions were sometimes recognized as chaos by mistakes.

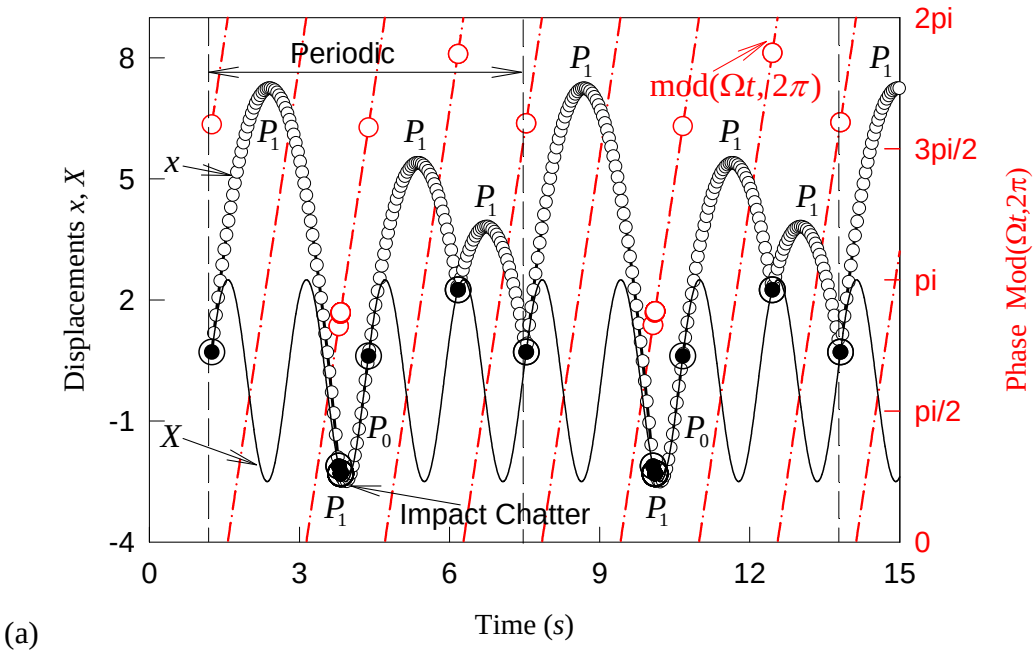

(a)

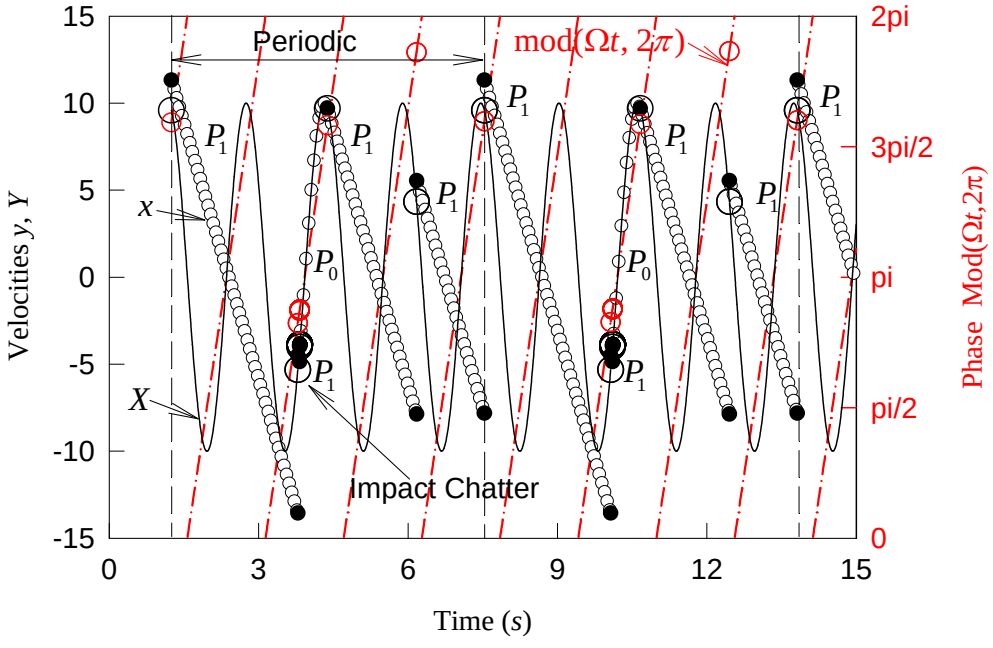

(b)

Figure 3.9: Simulation of impact chatter with stick periodic motion of mapping structure $P_{1^{10}0}$ **.** ($Q = 2.5,\ \Omega = 3.0,\ e = 0.1,\ M = 1.0,\ m = 0.00001$)**. (a) Displacement time history. (b) Velocity time history. (c) Phase portrait of the ball with moving boundaries. The initial conditions are:** $t_0 = 1.25019058,\ x_0 = 0.710982795,\ \dot{x}_0 = 11.3269665$**.**

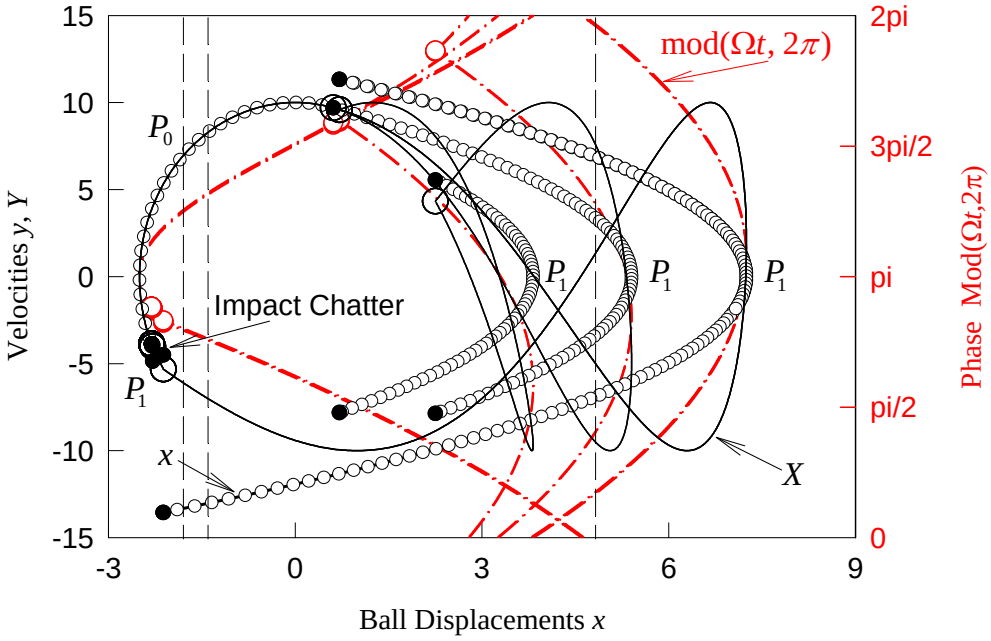

(c)

Figure 3.9 Continue

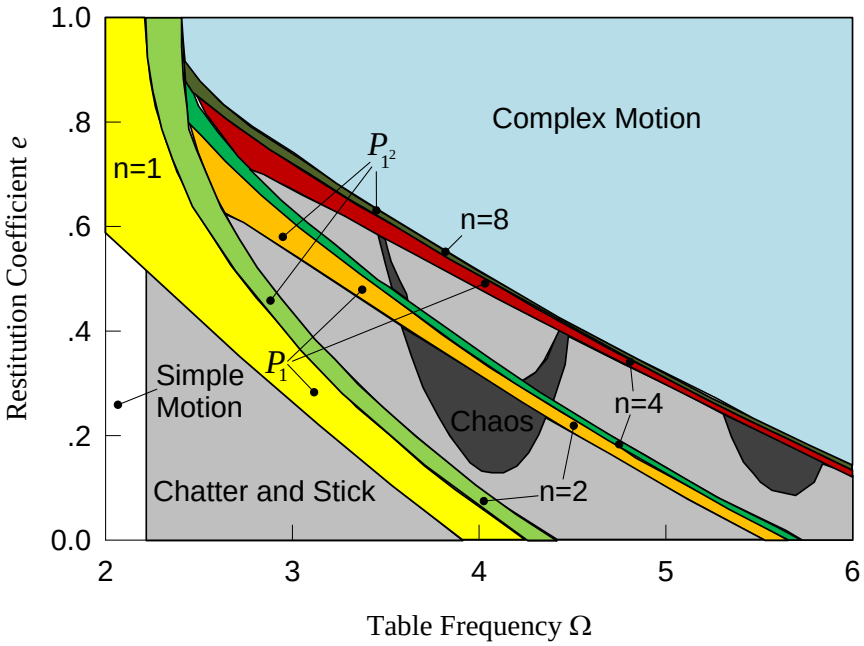

Figure 3.10: Parameter map of restitution coefficient e versus table displacement frequency Ω . ($Q = 2.0,\ M = 1.0,\ m = 0.00001$)

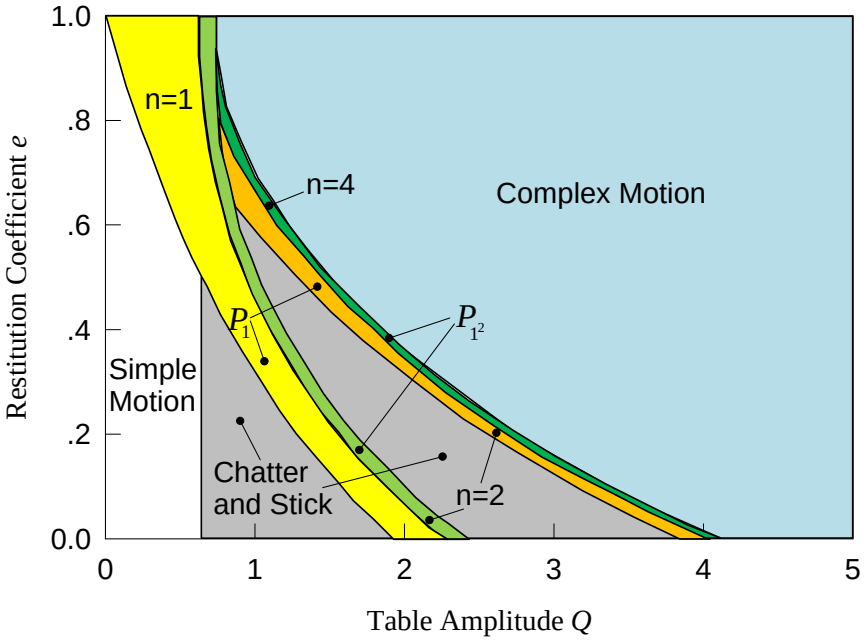

Figure 3.11: Parameter map of restitution coefficient e versus table displacement amplitude Q . ($\Omega = 4.0,\ M = 1.0,\ m = 0.00001$)

A simulation of a period-4 motion with only impacts is presented in Figure 3.8 under the same set of parameters with $Q = 3.36$. The mapping structure of this periodic motion is P_{1^2}, And the initial conditions are given as: $t_0 = 1.21297116,\ x_0 = 0.467186746,\ \dot{x}_0 = 16.1746312$. The time histories of displacement and velocity are presented in Figure 3.8 (a) and (b), respectively. The black solid curves represent the motion of the table, while the smaller black hollow circles represent the motion of the ball. The bigger black hollow circles shows the switching points of the table, while the smaller black solid circles represent the switching points of the ball. The red dashed curves indicate the change of phase with respect to time, which provides the analytical condition of motion switching such as stick and grazing. The corresponding phase portrait of the ball's motion with its moving boundaries is presented in Figure 3.8 (c), where the black solid curves indicate the moving boundaries and the small hollow

circles highlight the motion of the ball. Again, the red dashed curves present the change of switching phase, which is an indicator of analytical conditions.

Furthermore, simulation results of a relatively complex periodic motion with impact chatter and stick is also illustrated in Figure 3.9 under the same parameters with $Q = 2.5$. This is a period-4 motion and the mapping structure of this motion is given as $P_{1^{10}0}$. The initial conditions are chosen as: $t_0 = 1.25019058,\ x_0 = 0.710982795,\ \dot{x}_0 = 11.3269665$. In a similar pattern, the time histories of displacements, velocities, and the motion of the ball in phase portrait are presented in Figure 3.9 (a), (b), and (c), respectively. Since $\Omega = 4.0$ and $|Q|\Omega^2 > g$, the onset condition of stick motion is provided from Eqn. (3.24) as $\mathrm{mod}(\Omega t,\ 2\pi) \in (0.42\pi, 1.58\pi)$. On the other hand, the vanishing condition of stick motion is obtained from Eqn. (3.27) as $\mathrm{mod}(\Omega t,\ 2\pi)$ equal to about 1.58π. From Figure 3.9, the fulfillment of onset stick motion condition can be observed right after the impact chattering at $t \approx 3.84s$, where the switching phase $\mathrm{mod}(\Omega t,\ 2\pi) \approx 0.88\pi$. Thus, the stick motion starts until $t \approx 4.41s$. At this moment, the switching phase of the system $\mathrm{mod}(\Omega t,\ 2\pi) \approx 1.58\pi$ which predicts that the ball should separate with the table. And the stick motion must vanish. Thus the ball starts doing impacts with the table again.

For a more thorough understanding of the dynamics of this bouncing ball system, parameter maps are provided. The parameter map of restitution coefficient e versus the table displacement frequency Ω is presented in Figure 3.10, while the parameter map of restitution coefficient e versus the table displacement amplitude Q was presented in Figure 3.11. In these figures, the white area indicates the area of simple motions, where the ball will eventually stick together with the table and never separate; the light grey region indicates the identified

periodic motion with chatter and stick; the chaotic region is indicated by dark grey region; the region of complex motion consisting with complex periodic motion and chaos is presented in light blue. The periodic motions of only impacts with different orders are also presented in Figure 3.10 and Figure 3.11, using different color coded areas: the yellow, orange, and red areas represent the period-1, period-2, and period-4 P_1 motions, respectively. Similarly, the period-2, period-4, and period-8 P_{1^2} motions are also illustrated using different colors.

3.6. Conclusions

In this chapter, a simple bouncing ball system was investigated using the theory of flow switchability for discontinuous dynamical systems. Discontinuous model was constructed using domains and boundaries and analytical conditions for motion switching were developed. These conditions were closely related to the switching phase of the system. Different types of motions were described in a simple and unified style by introducing the generic mappings and mapping structures. Bifurcation scenarios for periodic and chaotic motions were presented. Analytical predictions of stable and unstable periodic motions were also presented with Eigenvalue stability. Furthermore, numerical simulation results are provided for a better image of periodic motions with only impacts and periodic motions with impact chatter to stick in the system. Finally, parameter maps were provided for a more comprehensive understanding of the motions affected by different parameters.

CHAPTER 4

HORIZONTAL IMPACT PAIR

In this chapter, complex motions of a ball in the horizontal impact pair with a periodic excitation is studied using the theory of discontinuous dynamical system. Analytical conditions for motion switching such as stick and grazing are developed, and generic mapping structures are introduced to describe different periodic and chaotic motion. Analytical prediction of complex periodic motion of the ball in the periodically shaken impact pair is completed and the corresponding stability and bifurcation analysis is also carried out. Parameter map and numerical illustrations of periodic and chaotic motions are also given.

4.1. Physical Model Descriptions

Consider a horizontal impact pair consisting of a ball moving inside a base with two vertical walls. The distance between the walls is d. The base of mass M possesses a periodic shaken displacement $X(t)$, and the ball of mass m is free to move between the two walls of the base, as shown in Figure 4.1. The restitution coefficient for impacts between the ball and the base is e.

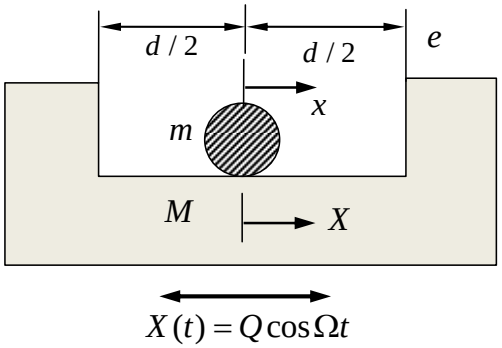

Figure 4.1: Mechanical model

The motion of the base possesses a sinusoidal displacement. Thus,

$$X = Q_0 \cos \Omega t,\ \dot{X} = -Q_0 \Omega \sin \Omega t, \ddot{X} = -Q_0 \Omega^2 \cos \Omega t \tag{4.1}$$

where $\dot{X} = dX / dt$. If the ball does not move together with the base, the corresponding motion is called the *non-stick motion or free-flight motion.* For this case, the equation of motion for the ball is given as

$$\ddot{x} = 0 \tag{4.2}$$

If the ball moves together with the base, such a motion is called *the stick motion*. The equation of motion is given as

$$(m + M)\ddot{x}^{(i)} = M\ddot{X} = -MQ_0 \Omega^2 \cos \Omega t, \tag{4.3}$$

where $\ddot{x}^{(i)}$ ($i = 2, 3$) is the acceleration for both the ball and the base. The impact relation between the ball and the base can be described as

$$x_+ = X_+ = x_- = X_-;\ \dot{X}_+ = \dot{X}_-, \dot{x}_+ = \frac{m\dot{x}_- + M\dot{X}_- - Me(\dot{x}_- - \dot{X}_-)}{m + M}. \tag{4.4}$$

If $M >> m$, the impact effect of base velocity can be ignored.

4.2. Discontinuous Modeling

Since the motion discontinuity of the ball is caused by impacts, the domains and boundaries in absolute coordinate system are sketched in Figure 4.2. The origin of the absolute coordinate is set at the equilibrium position of the base. The absolute domain Ω_1 for the ball without stick is defined as

$$\Omega_1 = \left\{(x, y) \middle| x \in (X - d, X + d)\right\} \tag{4.5}$$

where $y = \dot{x}$ .The corresponding boundaries are defined as

$$\left.\begin{aligned}\partial\Omega_{1(+\infty)} &= \left\{(x,y)\middle|\varphi_{1(+\infty)} \equiv x - X - d/2 = 0, \dot{x} \neq \dot{X}\right\},\\ \partial\Omega_{1(-\infty)} &= \left\{(x,y)\middle|\varphi_{1(-\infty)} \equiv x - X + d/2 = 0, \dot{x} \neq \dot{X}\right\}.\end{aligned}\right\} \tag{4.6}$$

The domain is represented by a hatched area, and the boundaries are depicted by dashed curves in Figure 4.2. The boundary of $\partial\Omega_{1(+\infty)}$ is given by a dashed curve with $x = X + d/2$ and the boundary of $\partial\Omega_{1(-\infty)}$ is depicted by a dashed curve with $x = X - d/2$. The absolute domains Ω_2, Ω_3 and Ω_1 with stick motion for the ball are defined as

$$\left.\begin{aligned}\Omega_2 &= \left\{(x,\dot{x})\middle|x \in (-\infty, X_{cr} - d/2), \dot{x} = \dot{X}\right\},\\ \Omega_3 &= \left\{(x,\dot{x})\middle|x \in (X_{cr} + d/2, +\infty), \dot{x} = \dot{X}\right\},\\ \Omega_1 &= \left\{(x,\dot{x})\middle|x \in \left(X_{cr} - d/2, X_{cr} + d/2\right), \dot{x} \neq \dot{X}\right\},\end{aligned}\right\} \tag{4.7}$$

where X_{cr} is for appearance and vanishing of stick motion. The domain of Ω_1 is represented by the hatched area. Domains Ω_2 and Ω_3 are represented by shaded regions in Figure 4.2 (b). The absolute boundaries are given by dashed curves. The stick boundaries are defined as

$$\begin{aligned}\partial\Omega_{12} &= \left\{(x,\dot{x})\middle|\varphi_{12} \equiv x - X_{cr} + d/2 = 0, \dot{x} = \dot{X}_{cr}\right\},\\ \partial\Omega_{13} &= \left\{(x,\dot{x})\middle|\varphi_{13} \equiv x - X_{cr} - d/2 = 0, \dot{x} = \dot{X}_{cr}\right\}.\end{aligned} \tag{4.8}$$

From the defined domains, the vectors for absolute motions can be introduced by

$$\mathbf{x}^{(\lambda)} = (x^{(\lambda)}, y^{(\lambda)})^{\mathrm{T}}, \mathbf{F}^{(\lambda)} = (y^{(\lambda)}, F^{(\lambda)})^{\mathrm{T}} \quad \text{for } \lambda = 1,2,3 \tag{4.9}$$

where $\lambda = 1$ gives non-stick domain and $\lambda = 2,3$ give the stick motions at the left and right walls of the base, respectively. The equation of absolute motion is rewritten in the vector form of

$$\dot{\mathbf{x}}^{(\lambda)} = \mathbf{F}^{(\lambda)}(\mathbf{x}^{(\lambda)}, t) \quad \text{for } \lambda = 1,2,3 \tag{4.10}$$

For the non-stick motion,

$$F^{(1)}(\mathbf{x}^{(1)}, t) = 0, \tag{4.11}$$

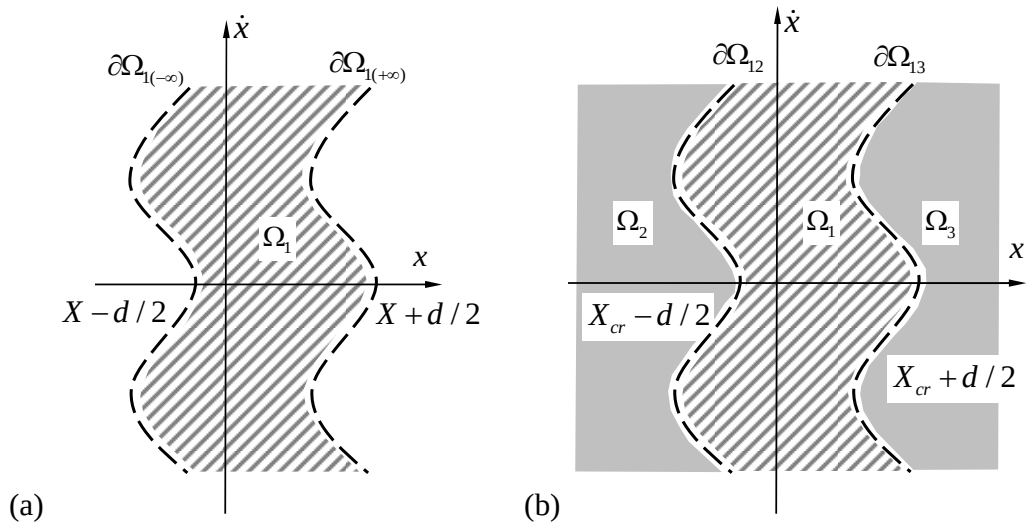

Figure 4.2: Absolute domain and boundaries. (a) Absolute domain and boundaries without stick. (b) Absolute domains and boundaries with stick.

while for the stick motion,

$$F^{(\lambda)}(\mathbf{x}^{(\lambda)},t) = -\frac{M}{m+M} Q_0 \Omega^2 \cos\Omega t \quad \text{for} \quad \lambda = 2,3. \tag{4.12}$$

For simplicity, analytical conditions based on the time varying boundaries can be obtained through the relative coordinates for such a horizontal impact pair. The relative displacement, velocity, and acceleration of the ball to the periodically shaken base are

$$z = x - X\,,\ \dot{z} = \dot{x} - \dot{X}\,,\ \text{ and } \ddot{z} = \ddot{x} - \ddot{X}\ . \tag{4.13}$$

The relative domains and boundaries for the motion of the ball are sketched in Figure 4.3. The stick domain and boundaries in relative phase space becomes points. The relative domains Ω_1, Ω_2, and Ω_3 for the ball are defined as

$$\left.\begin{aligned} \Omega_2 &= \left\{(z,\dot{z})\middle|\dot{z} = -d/2,\ z = 0\right\}, \\ \Omega_3 &= \left\{(z,\dot{z})\middle|\dot{z} = d/2,\ z = 0\right\}, \\ \Omega_1 &= \left\{(z,\dot{z})\middle|z \in (-d/2, d/2)\right\}. \end{aligned}\right\} \tag{4.14}$$

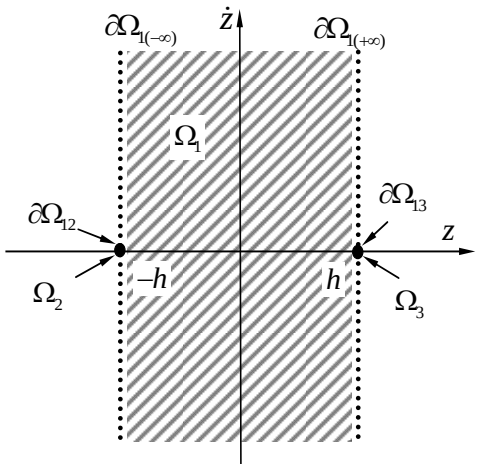

Figure 4.3: Relative domains and boundaries.

The relative boundaries $\partial\Omega_{1(+\infty)}, \partial\Omega_{1(-\infty)}$, $\partial\Omega_{12}$ and $\partial\Omega_{13}$ for the ball are defined as

$$\left.\begin{aligned}
&\partial\Omega_{1(-\infty)} = \left\{(z,\dot{z})\middle|\varphi_{1(-\infty)} \equiv z = 0,\ \dot{z} \neq 0\right\},\\
&\partial\Omega_{1(+\infty)} = \left\{(z,\dot{z})\middle|\varphi_{1(+\infty)} \equiv z = 0,\ \dot{z} \neq 0\right\},\\
&\partial\Omega_{12} = \partial\Omega_{21} = \left\{(z,\dot{z})\middle|\varphi_{12} \equiv \dot{z}_{cr} = 0,\ z_{cr} = -d/2\right\},\\
&\partial\Omega_{13} = \partial\Omega_{31} = \left\{(z,\dot{z})\middle|\varphi_{13} \equiv \dot{z}_{cr} = 0,\ z_{cr} = d/2\right\},
\end{aligned}\right\} \tag{4.15}$$

where $\partial\Omega_{1(-\infty)}, \partial\Omega_{1(+\infty)}$ are the relative impact-chatter boundaries for the ball. $\partial\Omega_{12}$ and $\partial\Omega_{13}$ are the relative stick motion boundaries for the ball. The relative vectors in the relative coordinate are defined as

$$\mathbf{z}^{(\lambda)} = (z^{(\lambda)}, \dot{z}^{(\lambda)})^{\mathrm{T}},\ \mathbf{g}^{(\lambda)} = \dot{\mathbf{z}}^{(\lambda)} = (\dot{z}^{(\lambda)}, g^{(\lambda)})^{\mathrm{T}} \tag{4.16}$$

where $\lambda = 1,2,3$ give the corresponding stick and non-stick domains. For $\lambda = 1,2,3$, equations of relative motion is rewritten in the vector form of

$$\dot{\mathbf{z}}^{(\lambda)} = \mathbf{g}^{(\lambda)}(\mathbf{z}^{(\lambda)}, \mathbf{X}^{(\lambda)}, t) \text{ and } \dot{\mathbf{X}}^{(\lambda)} = \mathbf{F}^{(\lambda)}(\mathbf{X}^{(\lambda)}, t) \tag{4.17}$$

For non-stick motion

$$g^{(1)}(\mathbf{z}^{(1)}, \mathbf{X}^{(1)}, t) = Q_0\Omega^2 \cos\Omega t. \tag{4.18}$$

For stick motion

$$g^{(i)}(\mathbf{z}^{(i)}, \mathbf{X}^{(i)}, t) = 0 \text{ for } i = 2, 3. \tag{4.19}$$

4.3. Analytical Switching Conditions

The switching conditions of stick and grazing motions will be developed using the theory of flow switchability for discontinuous dynamical systems (Luo, A theory for flow switchability in discontinuous dynamical systems, 2008). First, the normal vector of the relative boundary is defined

$$\mathbf{n}_{\partial\Omega_{\alpha\beta}} = \nabla\varphi_{\alpha\beta} = \left(\frac{\partial\varphi_{\alpha\beta}}{\partial \mathrm{z}}, \frac{\partial\varphi_{\alpha\beta}}{\partial \dot{z}}\right)^{\mathrm{T}} \tag{4.20}$$

where $\nabla = \left(\partial / \partial z, \partial / \partial \dot{z}\right)^{\mathrm{T}}$. The normal vectors to the relative stick boundaries $\mathbf{n}_{\partial\Omega_{12}}, \mathbf{n}_{\partial\Omega_{13}}$ and relative impact-chatter boundaries $\mathbf{n}_{\partial\Omega_{1(-\infty)}}, \mathbf{n}_{\partial\Omega_{1(+\infty)}}$ are given by

$$\mathbf{n}_{\partial\Omega_{12}} = \mathbf{n}_{\partial\Omega_{13}} = (0,1)^{\mathrm{T}} \text{ and } \mathbf{n}_{\partial\Omega_{1(-\infty)}} = \mathbf{n}_{\partial\Omega_{1(+\infty)}} = (1,0)^{\mathrm{T}}. \tag{4.21}$$

The zero-order and first-order G-functions for the relative stick boundaries are then defined as

$$\left.\begin{aligned}
G^{(0,i)}_{\partial\Omega_{1i}}(\mathbf{z}^{(i)}_m, \mathbf{X}^{(i)}_m, t_{m\pm}) &= \mathbf{n}^{\mathrm{T}}_{\partial\Omega_{1i}} \cdot \mathbf{g}^{(i)}(\mathbf{z}^{(i)}_m, \mathbf{X}^{(i)}_m, t_{m\pm}),\\
G^{(0,1)}_{\partial\Omega_{1i}}(\mathbf{z}^{(1)}_m, \mathbf{X}^{(1)}_m, t_{m\pm}) &= \mathbf{n}^{\mathrm{T}}_{\partial\Omega_{1i}} \cdot \mathbf{g}^{(1)}(\mathbf{z}^{(1)}_m, \mathbf{X}^{(1)}_m, t_{m\pm}),\\
G^{(1,i)}_{\partial\Omega_{1i}}(\mathbf{z}^{(i)}_m, \mathbf{X}^{(i)}_m, t_{m\pm}) &= \mathbf{n}^{\mathrm{T}}_{\partial\Omega_{1i}} \cdot D\mathbf{g}^{(i)}(\mathbf{z}^{(i)}, \mathbf{X}^{(i)}, t_{m\pm}),\\
G^{(1,1)}_{\partial\Omega_{1i}}(\mathbf{z}^{(1)}_m, \mathbf{X}^{(1)}_m, t_{m\pm}) &= \mathbf{n}^{\mathrm{T}}_{\partial\Omega_{1i}} \cdot D\mathbf{g}^{(1)}(\mathbf{z}^{(1)}_m, \mathbf{X}^{(1)}_m, t_{m\pm}),
\end{aligned}\right\} \tag{4.22}$$

where t_m is the switching time of the motion on the corresponding boundary and $t_{m\pm} = t_m \pm 0$ represents the motion in domains instead of the boundary. The G-functions for the relative impact-chatter boundaries are given as

$$\left.\begin{aligned}
G^{(0,1)}_{\partial\Omega_{1(+\infty)}}(\mathbf{z}^{(1)}_m,\mathbf{X}^{(1)}_m,t_{m\pm}) &= \mathbf{n}^{\mathrm{T}}_{\partial\Omega_{1(+\infty)}}\cdot\mathbf{g}^{(1)}(\mathbf{z}^{(1)}_m,\mathbf{X}^{(1)}_m,t_{m\pm}),\\
G^{(1,1)}_{\partial\Omega_{1(+\infty)}}(\mathbf{z}^{(1)}_m,\mathbf{X}^{(1)}_m,t_{m\pm}) &= \mathbf{n}^{\mathrm{T}}_{\partial\Omega_{1(+\infty)}}\cdot D\mathbf{g}^{(1)}(\mathbf{z}^{(1)}_m,\mathbf{X}^{(1)}_m,t_{m\pm}),\\
G^{(0,1)}_{\partial\Omega_{1(-\infty)}}(\mathbf{z}^{(1)}_m,\mathbf{X}^{(1)}_m,t_{m\pm}) &= \mathbf{n}^{\mathrm{T}}_{\partial\Omega_{1(-\infty)}}\cdot\mathbf{g}^{(1)}(\mathbf{z}^{(1)}_m,\mathbf{X}^{(1)}_m,t_{m\pm}),\\
G^{(1,1)}_{\partial\Omega_{1(-\infty)}}(\mathbf{z}^{(1)}_m,\mathbf{X}^{(1)}_m,t_{m\pm}) &= \mathbf{n}^{\mathrm{T}}_{\partial\Omega_{1(-\infty)}}\cdot D\mathbf{g}^{(1)}(\mathbf{z}^{(1)}_m,\mathbf{X}^{(1)}_m,t_{m\pm}).
\end{aligned}\right\} \tag{4.23}$$

Using these G-functions, the switching conditions for stick motion can be obtained from the passable flow condition (Luo, Discontinuous Dynamical Systems on Time-varying Domains, 2009) from domain Ω_1 to Ω_i ($i=2,3$), i.e.,

$$(-1)^i G^{(0,1)}_{\partial\Omega_{1i}}(\mathbf{z}^{(1)}_m,\mathbf{X}^{(1)}_m,t_{m-})<0 \text{ and } (-1)^i G^{(0,i)}_{\partial\Omega_{1i}}(\mathbf{z}^{(1)}_m,\mathbf{X}^{(1)}_m,t_{m+})<0. \tag{4.24}$$

Thus,

$$(-1)^i g^{(1)}(\mathbf{z}^{(1)}_m,\mathbf{X}^{(1)}_m,t_{m-})<0 \text{ and } (-1)^i g^{(i)}(\mathbf{z}^{(i)}_m,\mathbf{X}^{(i)}_m,t_{m+})<0. \tag{4.25}$$

where $i=2,3$ indicates when the ball stick with the base on the left or right walls of the base, respectively. With the relative force function per unit mass, the onset conditions of stick motion on the left or right walls is given by

$$\left.\begin{aligned}
&\mathrm{mod}(\Omega t_m,2\pi)\in(\frac{\pi}{2},\frac{3\pi}{2}) \text{ for } \partial\Omega_{12},\\
&\mathrm{mod}(\Omega t_m,2\pi)\in(\frac{3\pi}{2},2\pi)\cup(0,\frac{\pi}{2}) \text{ for } \partial\Omega_{13},
\end{aligned}\right\} \tag{4.26}$$

From Eq.(4.26), the phase angle $\mathrm{mod}(\Omega t_m,2\pi)$ lies in the second or third quadrant for the ball sticking with the base at the left wall. For the ball sticking at the right wall, the phase angle $\mathrm{mod}(\Omega t_m,2\pi)$ should be in first or fourth quadrant.

Similarly, the criteria for vanishing of the stick motion can be given for $\partial\Omega_{1i}$ by

$$\left.\begin{aligned}
&G^{(0,0)}_{\partial\Omega^{(i)}_{01}}(\mathbf{z}^{(i)}_m,\mathbf{X}^{(i)}_m,t_{m-})=0 \text{ and } G^{(0,1)}_{\partial\Omega^{(i)}_{01}}(\mathbf{z}^{(1)}_m,\mathbf{X}^{(1)}_m,t_{m+})=0,\\
&(-1)^i G^{(1,i)}_{\partial\Omega^{(i)}_{01}}(\mathbf{z}^{(i)}_m,\mathbf{X}^{(i)}_m,t_{m-})>0 \text{ and } (-1)^i G^{(1,1)}_{\partial\Omega^{(i)}_{01}}(\mathbf{z}^{(1)}_m,\mathbf{X}^{(1)}_m,t_{m+})>0,
\end{aligned}\right\} \tag{4.27}$$

From the foregoing equations, the relative force relations for $\partial\Omega_{1i}$ are obtained, i.e.,

$$\left.\begin{array}{l} g^{(i)}(\mathbf{z}_m^{(i)}, \mathbf{X}_m^{(i)}, t_{m-}) = 0 \text{ and } g^{(1)}(\mathbf{z}_m^{(1)}, \mathbf{X}_m^{(1)}, t_{m+}) = 0, \\ (-1)^i \frac{d}{dt} g^{(i)}(\mathbf{z}_m^{(i)}, \mathbf{X}_m^{(i)}, t_{m-}) > 0 \\ \text{and } (-1)^i g^{(1)}(\mathbf{z}_m^{(1)}, \mathbf{X}_m^{(1)}, t_{m+}) > 0. \end{array}\right\} \tag{4.28}$$

Further simplify the above equation yields

$$\text{mod}(\Omega t_m, 2\pi) = \frac{3\pi}{2} \text{ for } \partial\Omega_{12}, \ \text{mod}(\Omega t_m, 2\pi) = \frac{\pi}{2} \text{ for } \partial\Omega_{13}. \tag{4.29}$$

From the above equation, the ball leaves from the left wall of the base at $\text{mod}(\Omega t_m, 2\pi) = 3\pi / 2$ and from the right wall at $\text{mod}(\Omega t_m, 2\pi) = \pi / 2$.

From the G-functions of the flow to each boundary, the grazing motion conditions can also be developed, i.e.,

$$\left.\begin{array}{l} G_{\partial\Omega_{1(-\infty)}}^{(0,1)}(\mathbf{z}_m^{(1)}, \mathbf{X}_m^{(1)}, t_{m\pm}) = 0 \ \text{ and } G_{\partial\Omega_{1(-\infty)}}^{(1,1)}(\mathbf{z}_m^{(1)}, \mathbf{X}_m^{(1)}, t_{m\pm}) > 0 \ \text{ for } \partial\Omega_{1(-\infty)}, \\ G_{\partial\Omega_{1(+\infty)}}^{(0,1)}(\mathbf{z}_m^{(1)}, \mathbf{X}_m^{(1)}, t_{m\pm}) = 0 \ \text{ and } G_{\partial\Omega_{1(+\infty)}}^{(1,1)}(\mathbf{z}_m^{(1)}, \mathbf{X}_m^{(1)}, t_{m\pm}) < 0 \ \text{ for } \partial\Omega_{1(+\infty)}. \end{array}\right\} \tag{4.30}$$

So the grazing motion conditions at the left or right impact-chatter boundaries are

$$\left.\begin{array}{l} \dot{x}_m + Q\Omega \sin \Omega t_m = 0 \text{ and} \\ \text{mod}(\Omega t_m, 2\pi) \in (\frac{3\pi}{2}, 2\pi) \cup (0, \frac{\pi}{2}) \text{ for } \partial\Omega_{1(-\infty)}, \\ \text{mod}(\Omega t_m, 2\pi) \in (\frac{\pi}{2}, \frac{3\pi}{2}) \text{ for } \partial\Omega_{1(+\infty)}. \end{array}\right\} \tag{4.31}$$

From the above equations, when the velocity of ball equals to the velocity of base, $\text{mod}(\Omega t_m, 2\pi)$ should be in the first or fourth quadrant for the ball to graze on the left impact-chatter boundary. If $\text{mod}(\Omega t_m, 2\pi)$ is in the second or third quadrant, then the ball will graze to the right impact-chatter boundary.

Similarly, the grazing motion conditions for the stick boundaries are provided as

$$\begin{aligned} &G^{(0,1)}_{\partial\Omega_{1i}}(\mathbf{z}^{(1)}_m, \mathbf{X}^{(1)}_m, t_{m\pm}) = 0 \text{ and } (-1)^i G^{(1,1)}_{\partial\Omega_{1i}}(\mathbf{z}^{(1)}_m, \mathbf{X}^{(1)}_m, t_{m\pm}) > 0 \text{ for } \partial\Omega_{1i}, \\ &G^{(0,i)}_{\partial\Omega_{1i}}(\mathbf{z}^{(i)}_m, \mathbf{X}^{(i)}_m, t_{m\pm}) = 0 \text{ and } (-1)^i G^{(1,i)}_{\partial\Omega_{1i}}(\mathbf{z}^{(i)}_m, \mathbf{X}^{(i)}_m, t_{m\pm}) < 0 \text{ for } \partial\Omega_{1i}. \end{aligned} \tag{4.32}$$

Substitution of the relative motion relations into the above equations and simplification of the above equations gives

$$\begin{aligned} &\text{mod}(\Omega t_m, 2\pi) = \frac{3\pi}{2} \text{ for } \partial\Omega_{12} \text{ in } \Omega_1, \\ &\text{mod}(\Omega t_m, 2\pi) \in (0, \pi) \text{ for } \partial\Omega_{12} \text{ in } \Omega_2; \\ &\text{mod}(\Omega t_m, 2\pi) = \frac{\pi}{2} \text{ for } \partial\Omega_{13} \text{ in } \Omega_1, \\ &\text{mod}(\Omega t_m, 2\pi) \in (\pi, 2\pi) \text{ for } \partial\Omega_{13} \text{ in } \Omega_3. \end{aligned} \tag{4.33}$$

From the forgoing equations, when the ball reaches the stick boundaries from Ω_1, the condition of $\text{mod}(\Omega t_m, 2\pi) = 3\pi/2$ is for the ball to graze on the left stick boundary. The condition of $\text{mod}(\Omega t_m, 2\pi) = \pi/2$ is for the ball to graze on the right stick boundary. When the ball reaches the stick boundaries from domain Ω_2, if $\text{mod}(\Omega t_m, 2\pi)$ is in first or second quadrant, then the ball will graze to the left stick boundary. If $\text{mod}(\Omega t_m, 2\pi)$ is in the third or fourth quadrant, then the ball will graze to the right stick boundary. And the stick motion will continue.

4.4. Discrete Mapping Structures

Using the boundaries in Eq.(4.6), the switching sets of the horizontal impact pair without stick can be defined as

$$\left.\begin{aligned} \Xi_{1(-\infty)} &= \left\{(x_k, \dot{x}_k, t_k) \middle| x_k = X_k - d/2, \dot{x}_k \neq \dot{X}_k\right\} \\ \Xi_{1(+\infty)} &= \left\{(x_k, \dot{x}_k, t_k) \middle| x_k = X_k + d/2, \dot{x}_k \neq \dot{X}_k\right\} \end{aligned}\right\} \tag{4.34}$$

where the switching sets $\Xi_{1(-\infty)}$ and $\Xi_{1(+\infty)}$ are defined on the boundary $\partial\Omega_{1(-\infty)}$ and $\partial\Omega_{1(+\infty)}$, respectively. Thus, the generic mappings for motions without stick are defined as

$$\begin{aligned} &P_1:\Xi_{1(-\infty)}\to\Xi_{1(+\infty)},\ P_2:\Xi_{1(+\infty)}\to\Xi_{1(-\infty)},\\ &P_3:\Xi_{1(-\infty)}\to\Xi_{1(-\infty)},\ P_4:\Xi_{1(+\infty)}\to\Xi_{1(+\infty)}. \end{aligned} \tag{4.35}$$

From the above definitions, the switching sets and mappings are sketched in Figure 4.4 (a) for the ball. Based on the boundaries in Eq.(4.6) and (4.8), the switching sets of the horizontal impact pair with stick motion are also defined as

$$\left.\begin{aligned} \Xi_{12}&=\left\{(x_k,\dot{x}_k,t_k)\middle|x_k=X_k-d/2,\dot{x}_k=\dot{X}_k\right\},\\ \Xi_{13}&=\left\{(x_k,\dot{x}_k,t_k)\middle|x_k=X_k+d/2,\dot{x}_k=\dot{X}_k\right\},\\ \Xi_{1(-\infty)}&=\left\{(x_k,\dot{x}_k,t_k)\middle|x_k=X_k-d/2,\dot{x}_k\neq\dot{X}_k\right\},\\ \Xi_{1(+\infty)}&=\left\{(x_k,\dot{x}_k,t_k)\middle|x_k=X_k+d/2,\dot{x}_k\neq\dot{X}_k\right\} \end{aligned}\right\} \tag{4.36}$$

where the switching sets Ξ_{1i} ($i=2,3$) are defined on the boundaries $\partial\Omega_{1i}$. Thus, the generic mappings for the stick motion are defined as

$$\begin{aligned} &P_1:\Xi_{12}\to\Xi_{1(+\infty)},\text{ or }\Xi_{1(-\infty)}\to\Xi_{13},\\ &P_2:\Xi_{1(+\infty)}\to\Xi_{12},\text{ or }\Xi_{13}\to\Xi_{1(-\infty)},\\ &P_3:\Xi_{1(-\infty)}\to\Sigma_{12},\ P_4:\Xi_{13}\to\Xi_{1(+\infty)},\\ &P_5:\Xi_{12}\to\Xi_{12},\ \Xi_6:\Sigma_{13}\to\Xi_{13}. \end{aligned} \tag{4.37}$$

where the global mappings of P_1 and P_2 will map from one switching set to another, and the local mappings of P_3, P_4, P_5 and P_6 map from one switching set to itself, as shown in Figure 4.4 (b). From the above definitions, the governing equations for generic mapping P_j ($j=1,2,3,4$) can be expressed by

$$P_j:\begin{cases} f_1^{(j)}\left(x_k,\dot{x}_k,t_k,x_{k+1},\dot{x}_{k+1},t_{k+1}\right)=0,\\ f_2^{(j)}\left(x_k,\dot{x}_k,t_k,x_{k+1},\dot{x}_{k+1},t_{k+1}\right)=0, \end{cases} \tag{4.38}$$

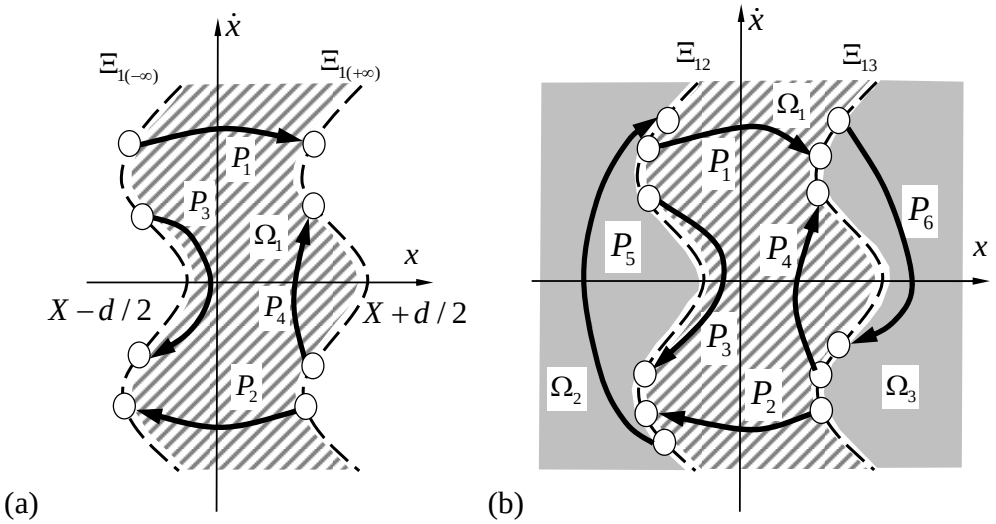

Figure 4.4: Switching sets and generic mappings in absolute coordinates. (a) Non-stick motion. (b) stick motion.

with

$$\left.\begin{aligned} &x_k = X_k - d/2 \ \text{ and } x_{k+1} = X_{k+1} + d/2 \ \text{ for } P_1,\\ &x_k = X_k + d/2 \ \text{ and } x_{k+1} = X_{k+1} - d/2 \ \text{ for } P_2,\\ &x_k = X_k - d/2 \ \text{ and } x_{k+1} = X_{k+1} - d/2 \ \text{ for } P_3,\\ &x_k = X_k + d/2 \ \text{ and } x_{k+1} = X_{k+1} + d/2 \ \text{ for } P_4. \end{aligned}\right\} \tag{4.39}$$

The governing equations of stick motion mappings P_5 and P_6 can be expressed as

$$P_\alpha : \begin{cases} f_1^{(\alpha)}(x_k, \dot{x}_k, t_k, x_{k+1}, \dot{x}_{k+1}, t_{k+1}) = 0, \\ f_2^{(\alpha)}(x_{k+1}, \dot{x}_{k+1}, t_{k+1}) = g^{(1)}(\mathbf{0}, \mathbf{X}_{k+1}, t_{k+1}) = 0, \end{cases} \tag{4.40}$$

with $\alpha = 5, 6$, where

$$\left.\begin{aligned} &x_k = X_k - d/2 \text{ and } \dot{x}_k = \dot{X}_k, \\ &x_{k+1} = X_k - h \text{ and } \dot{x}_{k+1} = \dot{X}_{k+1}, \\ &\mathrm{mod}(\Omega t_k, 2\pi) \in (\frac{\pi}{2}, \frac{3\pi}{2}), \\ &\text{and } \ \mathrm{mod}(\Omega t_{k+1}, 2\pi) \in (\pi, 2\pi), \end{aligned}\right\} \text{ for mapping } P_5, \tag{4.41}$$

and

$$\left.\begin{aligned} &x_k = X + h \text{ and } \dot{x}_k = \dot{X}, \\ &x_{k+1} = X + h \text{ and } \dot{x}_{k+1} = \dot{X}, \\ &\mathrm{mod}(\Omega t_k, 2\pi) \in (\frac{3\pi}{2}, 2\pi) \bigcup (0, \frac{\pi}{2}), \\ &\text{and } \mathrm{mod}(\Omega t_{k+1}, 2\pi) \in (0, \pi), \end{aligned}\right\} \text{ for mapping } P_6. \tag{4.42}$$

The notation for mapping action is introduced as

$$P_{j_k j_{k-1} \cdots j_1} = P_{j_k} \circ P_{j_{k-1}} \circ \cdots \circ P_{j_1}, \tag{4.43}$$

where $j_k \in \{1,2,3,4,5,6\}$ is a positive integer. For a motion with m-time repeated mapping structure of $P_{j_1 j_2 \cdots j_k}$, the mapping structure can be expressed as

$$\begin{aligned} P^{(m)}_{j_k j_{k-1} \cdots j_1} &= \underbrace{(P_{j_k} \circ P_{j_{k-1}} \circ \cdots \circ P_{j_1}) \circ \cdots \circ (P_{j_k} \circ P_{j_{k-1}} \circ \cdots \circ P_{j_1})}_{m} \\ &= P_{(j_k j_{k-1} \cdots j_1)^m}. \end{aligned} \tag{4.44}$$

Consider a motion with a generalized mapping structure

$$\begin{aligned} P &= \underbrace{P_{2^{k_{4l}}6^{k_{3l}}4^{m_l}1^{k_{2l}}5^{k_{1l}}3^{n_l}} \circ \cdots \circ P_{2^{k_{41}}6^{k_{31}}4^{m_1}1^{k_{21}}5^{k_{11}}3^{n_1}}}_{l-terms} \\ &= P_{\underbrace{(2^{k_{4l}}6^{k_{3l}}4^{m_l}1^{k_{2l}}5^{k_{1l}}3^{n_l}) \cdots (2^{k_{41}}6^{k_{31}}4^{m_1}1^{k_{21}}5^{k_{11}}3^{n_1})}_{l-terms}}, \end{aligned} \tag{4.45}$$

where $k_{js} \in \{0,1\}$ and $m_s, n_s \in \mathbb{N}$ ($s = 1,2,\cdots,l$). Define vectors $\mathbf{Y}_k \equiv (\dot{x}_k, t_k)^{\mathrm{T}}$. The motion pertaining to the mapping structure in Eq.(45) can be determined by

$$\mathbf{Y}_{k+\Sigma_{s=1}^{l}(k_{4s}+k_{3s}+m_s+k_{2s}+k_{1s}+n_s)} = P\mathbf{Y}_k = P_{\underbrace{(2^{k_{4l}}6^{k_{3l}}4^{m_l}1^{k_{2l}}5^{k_{1l}}3^{n_l}) \cdots (2^{k_{41}}6^{k_{31}}4^{m_1}1^{k_{21}}5^{k_{11}}3^{n_1})}_{l-terms}} \mathbf{Y}_k. \tag{4.46}$$

From the algebraic equations of generic mappings in Eqs.(4.38)-(4.42), one can obtain a set of nonlinear algebraic equations as follow

$$\left.\begin{aligned} &\mathbf{f}^{(3)}(\mathbf{Y}_k, \mathbf{Y}_{k+1}) = 0, \cdots, \mathbf{f}^{(5)}(\mathbf{Y}_{k+n_1}, \mathbf{Y}_{k+n_1+1}) = 0, \cdots, \\ &\mathbf{f}^{(1)}(\mathbf{Y}_{k+k_{11}+n_1}, \mathbf{Y}_{k+k_{11}+n_1+1}) = 0, \cdots, \\ &\mathbf{f}^{(2)}(\mathbf{Y}_{k+\Sigma_{s=1}^{l}(k_{4s}+k_{3s}+m_s+k_{2s}+k_{1s}+n_s)-1}, \mathbf{Y}_{k+\Sigma_{s=1}^{l}(k_{4s}+k_{3s}+m_s+k_{2s}+k_{1s}+n_s)}) = 0. \end{aligned}\right\} \tag{4.47}$$

The periodic motion pertaining to such a mapping requires

$$\mathbf{Y}_{k+\Sigma_{s=1}^{l}(k_{4s}+k_{3s}+m_s+k_{2s}+k_{1s}+n_s)} = \mathbf{Y}_k \tag{4.48}$$

or

$$\left.\begin{aligned} x_{k+\Sigma_{s=1}^{l}(k_{4s}+k_{3s}+m_s+k_{2s}+k_{1s}+n_s)} &= x_k, \\ \dot{x}_{k+\Sigma_{s=1}^{l}(k_{4s}+k_{3s}+m_s+k_{2s}+k_{1s}+n_s)} &= \dot{x}_k \end{aligned}\right\} \\ \Omega t_{k+\Sigma_{s=1}^{l}(k_{4s}+k_{3s}+m_s+k_{2s}+k_{1s}+n_s)} = \Omega t_k + 2N\pi. \tag{4.49}$$

Solving Eqs.(4.47)-(4.49) generates the switching sets of periodic motion with respect to the mapping structure in Eq.(4.45). Once the switching points for a specific periodic motion is obtained, its local stability and bifurcation analysis can be achieved through the corresponding Jacobian matrix. For instance, the Jacobian matrix of the mapping structure in Eq.(4.45) is given as

$$\begin{aligned} DP &= DP_{\underbrace{(2^{k_{4l}}6^{k_{3l}}4^{m_l}1^{k_{2l}}5^{k_{1l}}3^{n_l})\cdots(2^{k_{41}}6^{k_{31}}4^{m_1}1^{k_{21}}5^{k_{11}}3^{n_1})}_{l-terms}} \\ &= \prod_{s=1}^{l} DP_2^{(k_{4s})} \cdot DP_6^{(k_{3s})} \cdot DP_4^{(m_s)} \cdot DP_1^{(k_{2s})} \cdot DP_5^{(k_{1s})} \cdot DP_3^{(n_s)}, \end{aligned} \tag{4.50}$$

where

$$DP_\sigma = \left[\frac{\partial \mathbf{Y}_{\sigma+1}}{\partial \mathbf{X}_\sigma}\right]_{2\times 2} = \left[\frac{\partial Y_{(\sigma+1)i}}{\partial X_{\sigma j}}\right]_{2\times 2}. \tag{4.51}$$

for $\sigma = k, k+1, \cdots, k+\Sigma_{s=1}^{l}(m_s + k_{3s} + k_{2s} + n_s + k_{1s}) - 1$ and all the Jacobian matrix components can be computed through Eq.(4.49). The variational equation for a set of switching points $\{\mathbf{Y}_k^*, \cdots, \mathrm{Y}^*_{k+\Sigma_{s=1}^{l}(m_s+k_{3s}+k_{2s}+n_s+k_{1s})}\}$ is

$$\Delta \mathbf{Y}_{k+\Sigma_{s=1}^{l}(m_s+k_{3s}+k_{2s}+n_s+k_{1s})} = DP(\mathbf{Y}_k^*)\Delta \mathbf{Y}_k \tag{4.52}$$

If $\Delta \mathbf{Y}_{k+\Sigma_{s=1}^{l}(m_s+k_{3s}+k_{2s}+n_s+k_{1s})} \equiv \lambda \Delta \mathbf{Y}_k$, then the eigenvalues is computed by

$$\left|DP(\mathbf{Y}_k^*) - \lambda \mathbf{I}\right| = 0 \tag{4.53}$$

If all $|\lambda_i| < 1$ for $(i = 1, 2)$, the periodic motion is stable. If one of $|\lambda_i| > 1$ for $(i \in \{1, 2\})$, the periodic motion is unstable.

If one of $\lambda_i = -1$ and $|\lambda_j| < 1$ for $(i, j \in \{1, 2\}$ and $j \neq i)$, the period-doubling bifurcation of periodic motion occurs.

If one of $\lambda_i = 1$ and $|\lambda_j| < 1$ for $(i, j \in \{1, 2\}$ and $j \neq i)$, the saddle-node bifurcation of the periodic motion occurs.

If $|\lambda_{1,2}| = 1$ is a pair of complex eigenvalues, the Neimark bifurcation of the periodic motion occurs.

However, the eigenvalue analysis cannot be used to predict sticking and grazing motions. Both of them should be determined through the G-functions, where the stick motion is determined by Eq.(4.25) or (4.26) and the grazing bifurcation is determined by Eq.(4.32) or (4.33).

4.5. Illustrations

Consider the system parameters as $Q_0 = 0.4$, $\Omega = 0.5$, $M = 1.0$, $m = 0.001$, and $d = 0.15$. The bifurcation scenario of varying the coefficient of restitution e is presented in Figure 4.5 for the horizontal impact pair. The bifurcation scenario of the ball's switching displacement versus the coefficient of restitution e is shown in Figure 4.5 (a), while the bifurcation of the ball's switching velocity versus the restitution coefficient e is given in Figure 4.5 (b). The bifurcation of the switching phase versus e is also presented in Figure 4.5 (c). The symbol 'PD' and 'GB' indicate period-doubling bifurcation and grazing bifurcation,

respectively; the shaded regions indicate the regions of periodic motion (includes periodic motions with impact only and periodic motion with impact chatter to stick). Furthermore, for $e \in (0.514, 0.597)$, the yellow colored region indicates the region of complex periodic motion with four different branches of periodic solutions coexisting, which belong to two different pairs of asymmetric coexisting solutions. This will be further discussed in detail later using the analytical prediction and eigenvalue stability. Toward the end, for $e = 1.0$, there is a Neimark bifurcation existing. However, it could not be obtained through simulation. Thus, this Neimark bifurcation will be illustrated through analytical predictions later.

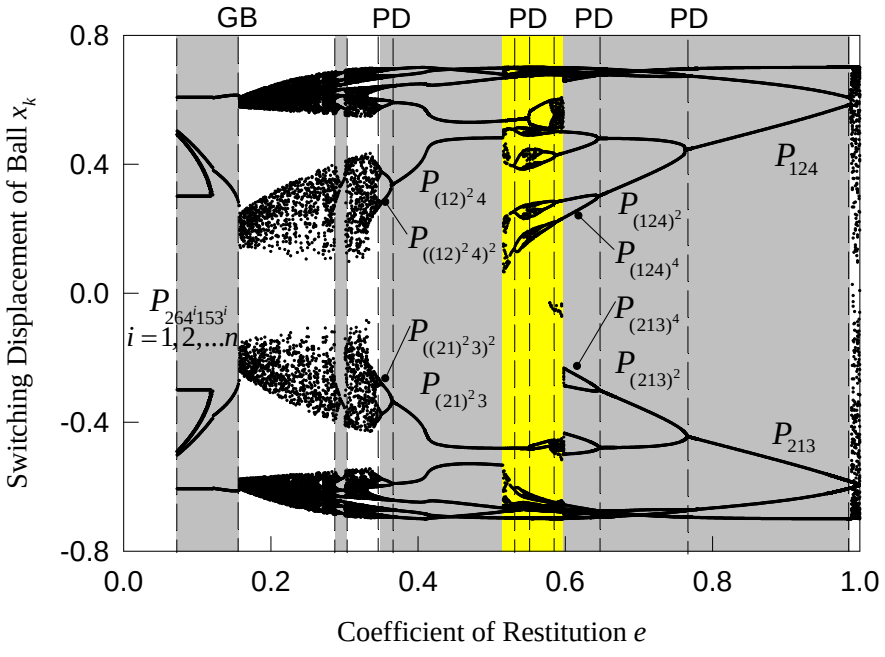

(a)

Figure 4.5: Bifurcation scenario of varying the restitution coefficient e. (a) Switching displacement of the ball. (b) Switching velocity of the ball. (c) Switching phase $\mathrm{mod}(\Omega t, 2\pi)$**.** ($Q_0 = 0.4$, $\Omega = 0.5$, $M = 1.0$, $m = 0.001$, $d = 0.15$.)

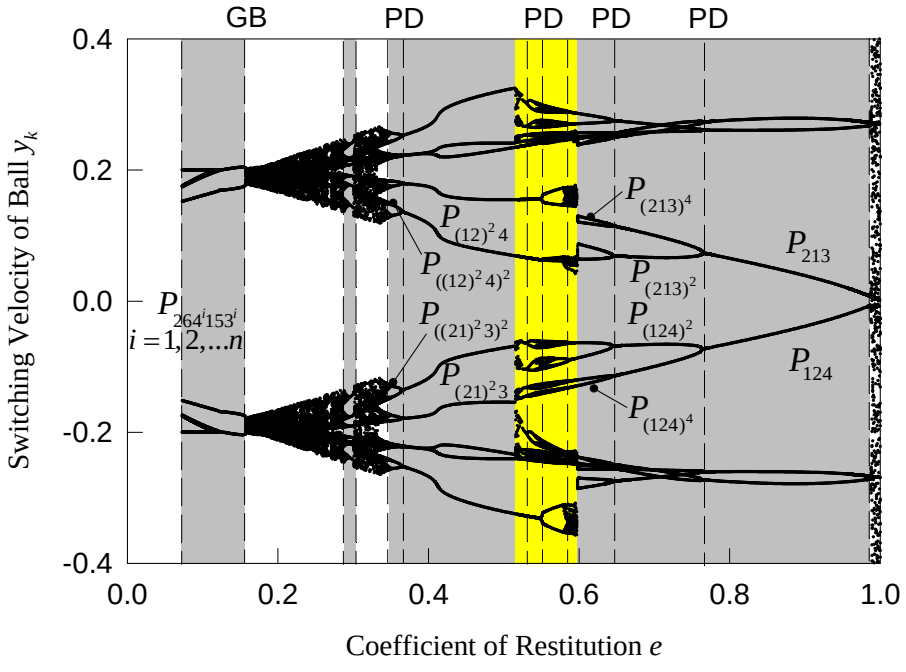

(b)

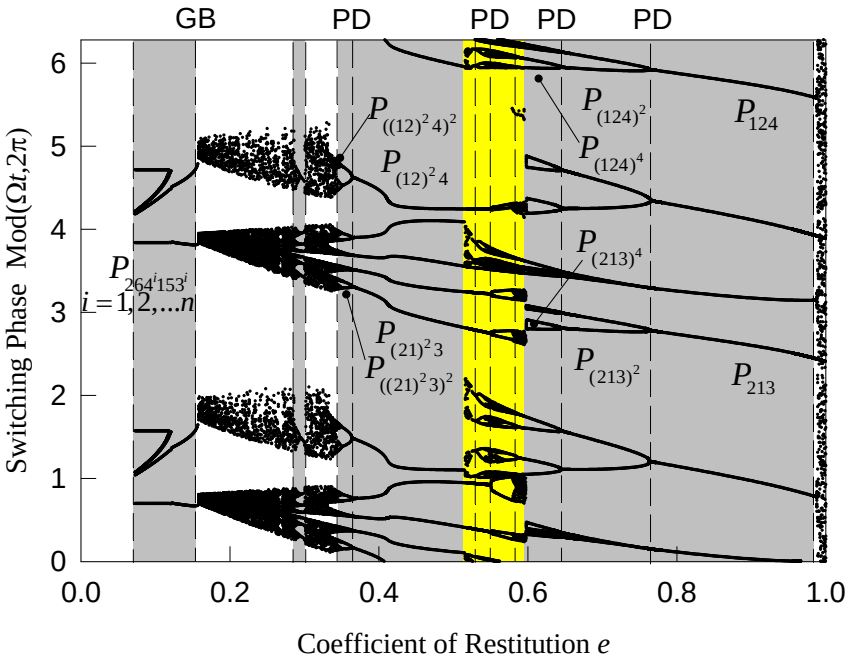

(c)

Figure 4.5 Continue

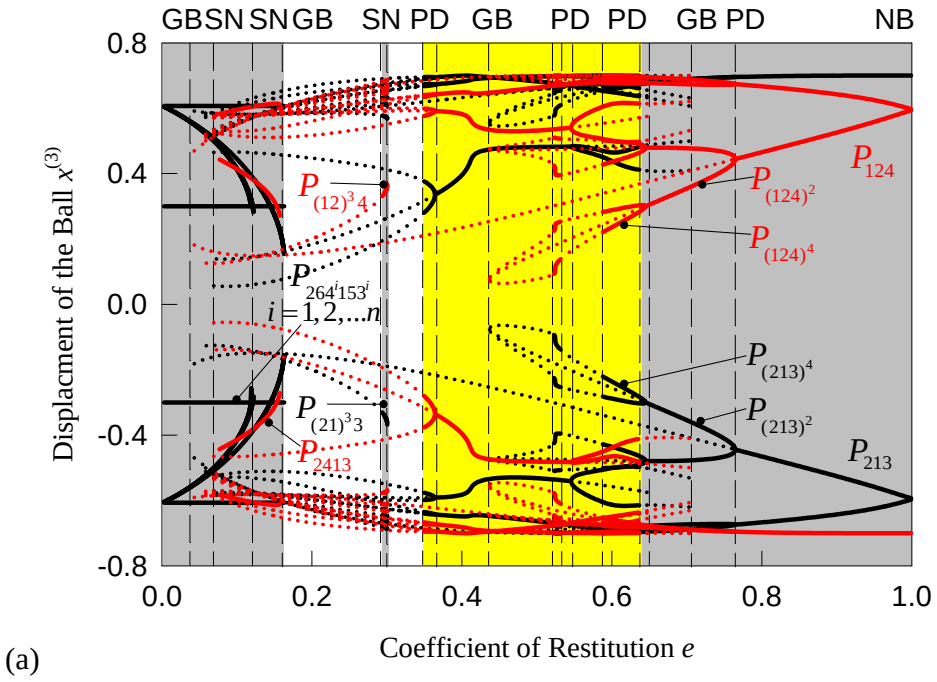

(a)

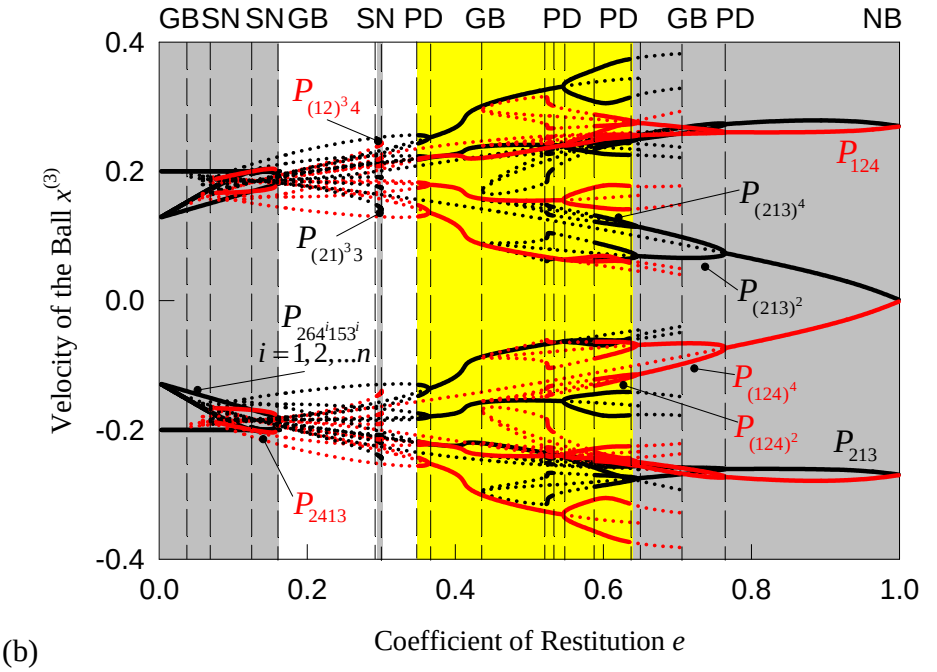

(b)

Figure 4.6: Analytical prediction of varying the coefficient of restitution e. (a) Switching displacement of the ball. (b) Switching velocity of the ball. (c) Switching phase $\mathrm{mod}(\Omega t, 2\pi)$. (d) Real parts of eignevalues. (e) Imaginary parts of eigenvalues. (f) Magnitudes of eigenvalues. ($Q_0 = 0.4$, $\Omega = 0.5$, $M = 1.0$, $m = 0.001$, $d = 0.15$.)

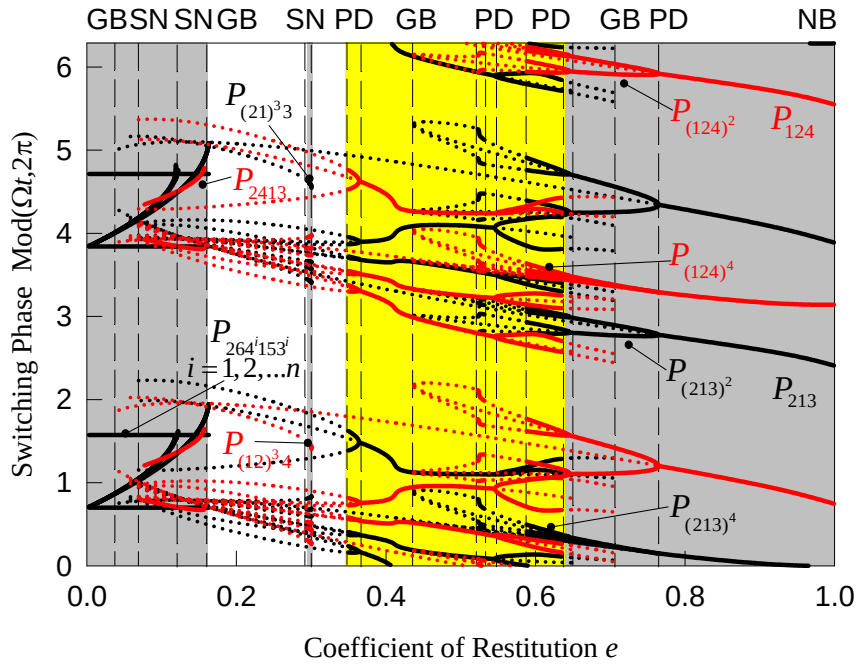

(c)

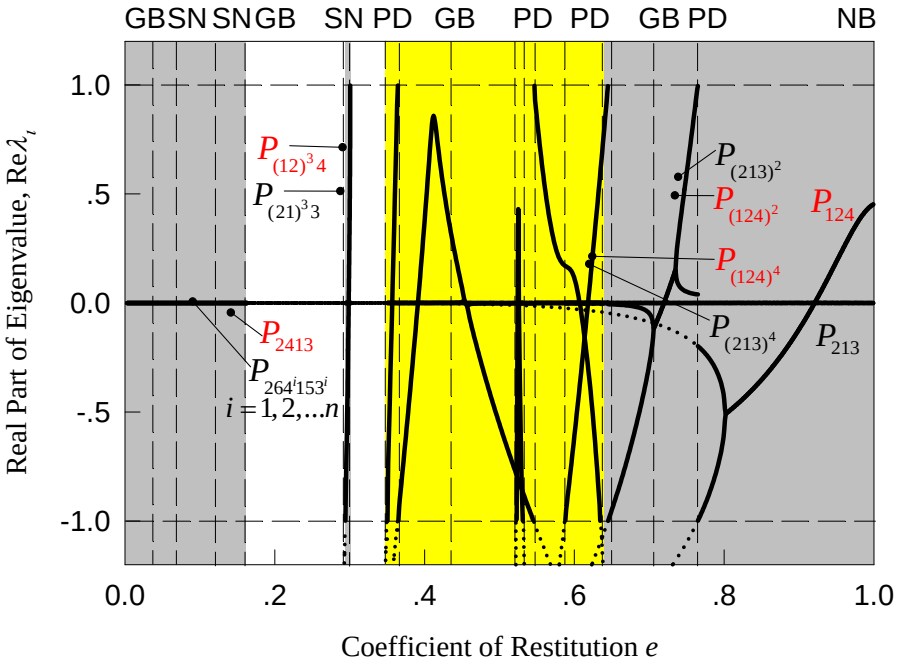

(d)

Figure 4.6 Continue

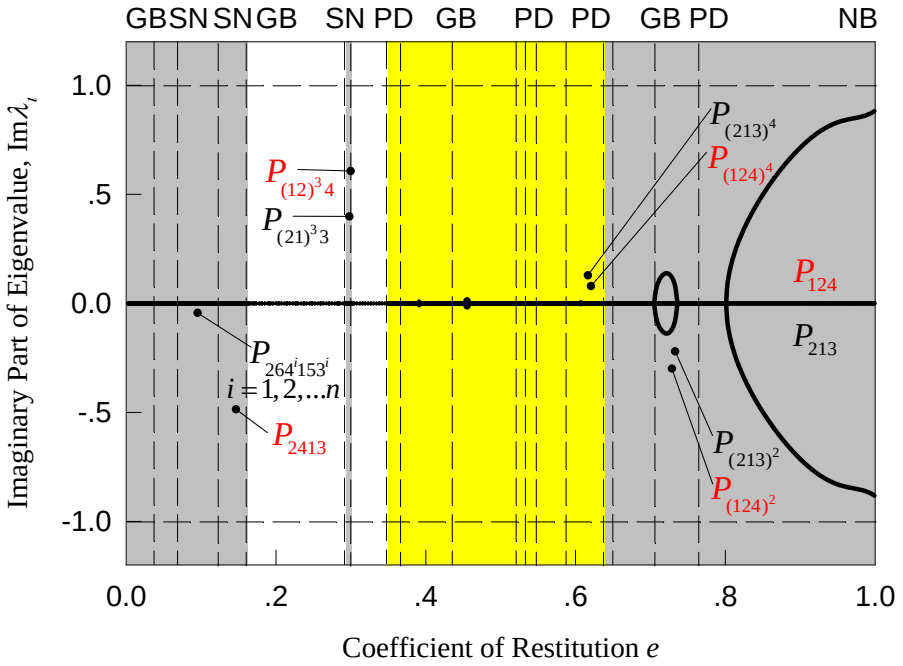

(e)

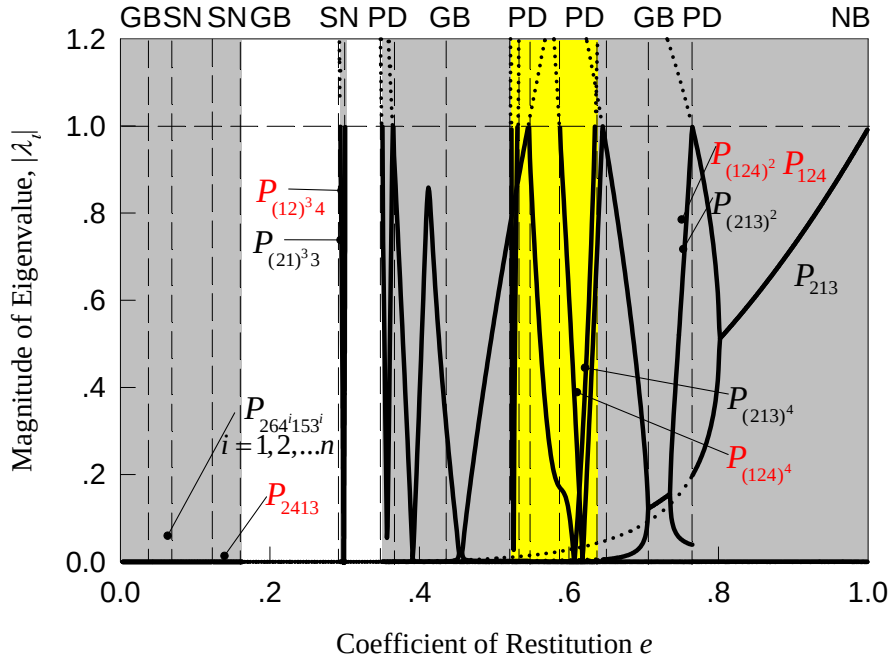

(f)

Figure 4.6 Continue

Using the mapping structure and analytical conditions, the switching displacement, switching velocity, and switching phase of the ball versus restitution coefficient e are predicted analytically, as presented in Figure 4.6 (a)-(c), respectively. The acronyms 'PD', 'SN', 'GB', and 'NB' represent the period doubling bifurcation, saddle node bifurcation, grazing bifurcation, and Neimark bifurcation, respectively. The solid and dotted curves indicate stable and unstable solutions, respectively. The red and black color indicate different branches of periodic motion coexisting. For $e \in (0.0, 0.162)$, the periodic motion of impact chattering with stick exists, the mapping structure is given as $P_{264^i153^i}$ $(i = 1, 2, ..., n)$. For $e \in (0.073, 0.162)$, there is a coexisting motion of P_{2413}. The periodic motion of $P_{(21)^3 3}$ and its asymmetric coexisting solution of $P_{(12)^3 4}$ occur for $e \in (0.292, 0.302)$. The two solutions are symmetric to each other, with same eigenvalues and same stability properties. The period doubling bifurcation for both $P_{(21)^3 3}$ and $P_{(12)^3 4}$ periodic motion takes place at $e = 0.292$, and the saddle node bifurcation occurs at $e = 0.302$. The periodic motion of $P_{((21)^2 3)^2}$ occurs in the range of $e \in (0.349, 0.364)$ and $e \in (0.545, 0.636)$, and its asymmetric solution of $P_{((12)^2 4)^2}$ coexists in the same regions. At $e = 0.349$ and $e = 0.636$, the period doubling bifurcations of $P_{((21)^2 3)^2}$ and $P_{((12)^2 4)^2}$ motions occur, and the corresponding saddle node bifurcations take place at $e = 0.364$ and $e = 0.545$ which are also corresponding to the period doubling bifurcations of the $P_{(21)^2 3}$ and $P_{(12)^2 4}$ motions. The motion of $P_{(21)^2 3}$ and its asymmetric coexisting motion of $P_{(12)^2 4}$ lay in the region of $e \in (0.364, 0.545)$. For $e \in (0.522, 0.532)$ and $e \in (0.587, 0.646)$, The motion of $P_{(213)^4}$ coexists asymmetrically with the motion of $P_{(124)^4}$. These periodic motions in two different regions with

same mapping structure are connected to each other through the unstable solutions after period doubling bifurcations at $e = 0.532$ and $e = 0.587$. At $e = 0.522$, there is a period doubling bifurcation, and the original stable motion becomes unstable. At $e = 0.646$, the saddle node bifurcations of the motions of $P_{(213)^4}$ and $P_{(124)^4}$ exist, which correspond to the period doubling bifurcations of $P_{(213)^2}$ and $P_{(124)^2}$ motions. The $P_{(213)^2}$ and $P_{(124)^2}$ motions coexist in the range of $e \in (0.646, 0.764)$, and the saddle node bifurcations occur at $e = 0.764$, which correspond to the period doubling bifurcation of P_{213} and P_{124} motions, respectively. Finally, the P_{213} and P_{124} motions coexist in the region of $e \in (0.764, 1.0)$ with Neimark bifurcations existing at $e = 1.0$. Similarly, other complicated periodic motions can be predicted analytically.

Using the same set of parameters, choose $e = 0.08$ to demonstrate a periodic motion with the mapping structure of $P_{264^5153^5}$ in Figure 4.7. The initial conditions are $t_0 = 8.44183604$, $x_0 = -0.488769302$, $\dot{x}_0 = 0.178074511$. The time histories of displacement and velocity are presented in Figure 4.7 (a) and (b), respectively. The thin black curves represent the motion of the base. The thick red curves indicate the motion of the ball, and the shaded area gives one period of the motion. The black circles represent the switching points of the motion. Discontinuity of the velocities can be observed from Figure 4.7 (b). The corresponding phase portrait of the ball's motion with its moving boundaries is presented in Figure 4.7 (c). Also, the switching phase $\mathrm{mod}(\Omega t, 2\pi)$ which is closely related to the analytical conditions is presented in Figure 4.7 (d). At $t \approx 8.5$, the ball is at boundary $\partial\Omega_{12}$ and the switching phase $\mathrm{mod}(\Omega t, 2\pi) \approx 4.3$, which satisfy the stick motion condition. Thus the ball starts to move together with the base on the left wall. At $t \approx 9.4$, the ball is at boundary $\partial\Omega_{21}$ and the switching phase $\mathrm{mod}(\Omega t, 2\pi) = \frac{3\pi}{2}$, which satisfy the vanishing condition of stick motion. Thus,

the ball separates from the left wall and start moving freely in the base. Similarly, the analytical conditions for onset and vanishing of stick motion satisfy at $t \approx 14.8$ and $t \approx 15.7$, respectively for the right wall. As a result, the stick motion on the right wall occurs and stops within this time span. The thin black curves give the moving boundaries and the thick red curves represent the motion of the ball. Again discontinuity of velocity caused by impacts can be observed in Figure 4.7 (c).

Furthermore, the simulation of a chaotic motion is also illustrated in Figure 4.8 under the same parameters with $e = 0.2$. The initial conditions are chosen to be $t_0 = 1.33468433$, $x_0 = 0.61418775$, $\dot{x}_0 = 0.204449281$. Similarly, the time histories of displacements and velocities are presented in Figure 4.8 (a) and (b), respectively. The thin black curves indicate the motion of the left and right walls of the base and thick red curves represent the motion of the ball. Also the Poincare section mappings of switching displacement and velocity are presented in Figure 4.8 (c) and (d), respectively.

Finally, a parameter map of different types of motions was presented in Figure 4.9. In this figure, the regions with different color indicate different types of motion as the parameters change. The grey regions represent the chaotic motion and the cyan region indicates the periodic region with impact chatter and stick. All other regions depict the different periodic motions with impacts. As predicted before, it can be observed that most of these periodic regions with impacts contain a pair of asymmetric coexisting solutions.

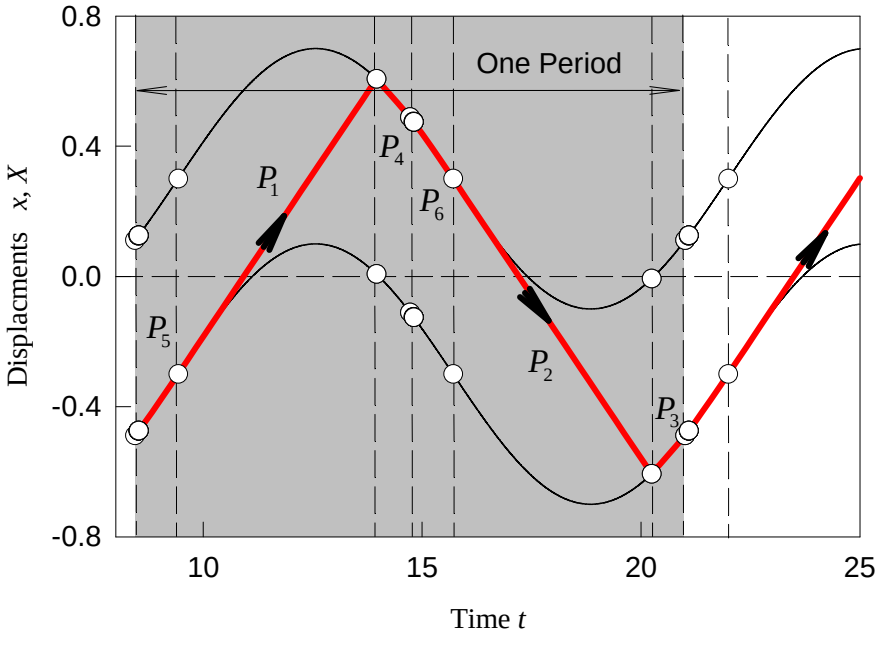

(a)

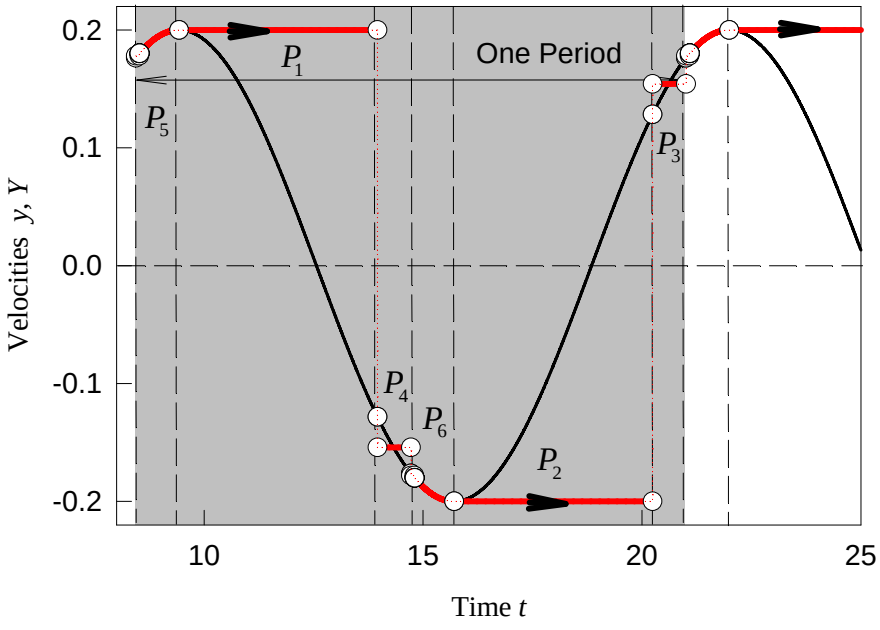

(b)

Figure 4.7: Periodic motion with a mapping structure of $P_{264^5153^5}$: (a) Displacement time history. (b) Velocity time history. (c) Phase portrait of the ball with moving boundaries. (d) Corresponding change of switching phase $\mathrm{mod}(\Omega t, 2\pi)$. ($Q_0 = 0.4,\ \Omega = 0.5,\ M = 1.0,$ $m = 0.001,\ e = 0.08,\ d = 0.15$) The initial conditions are $t_0 = 8.44183604$, $x_0 = -0.488769302$, $\dot{x}_0 = 0.178074511$.

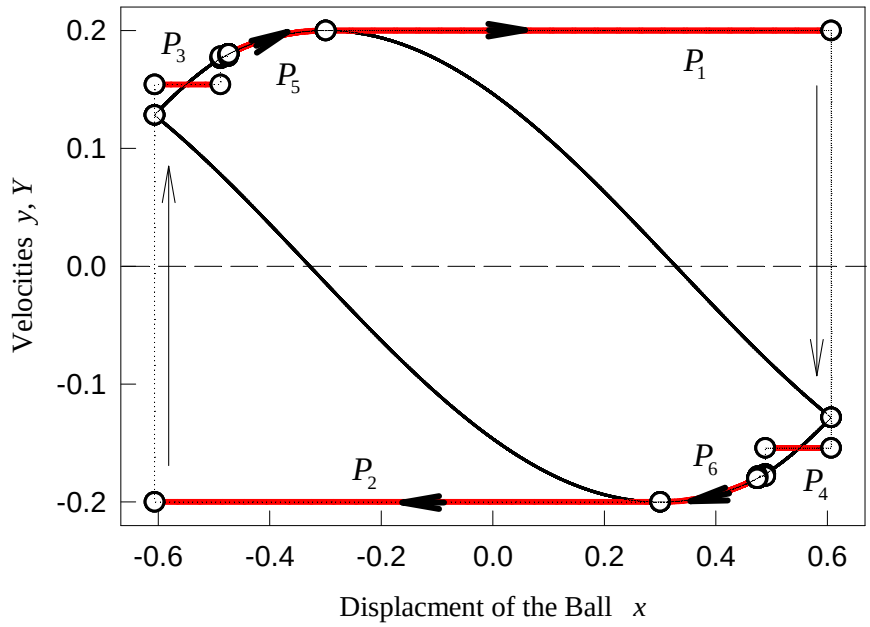

(c)

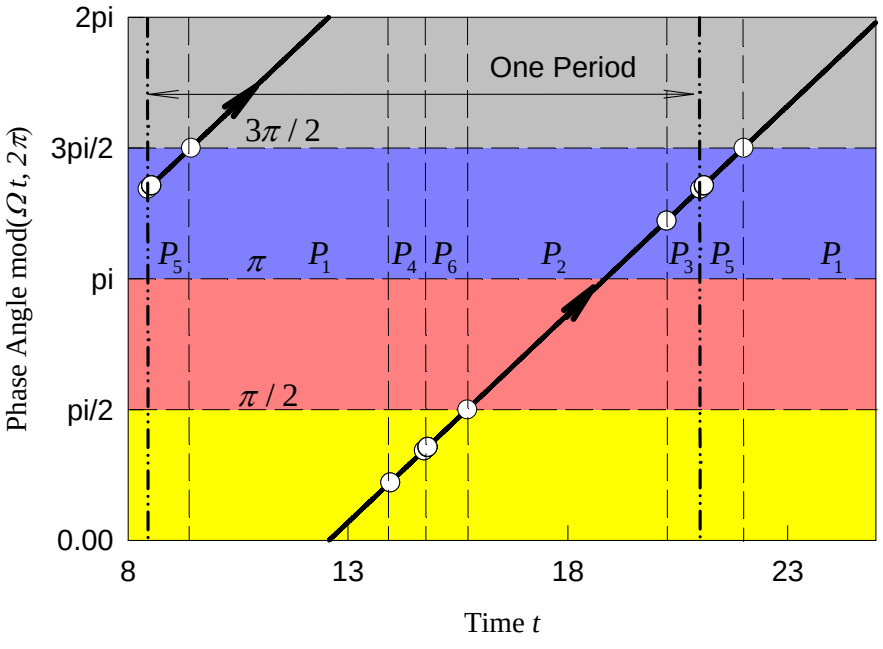

(d)

Figure 4.7 Continue

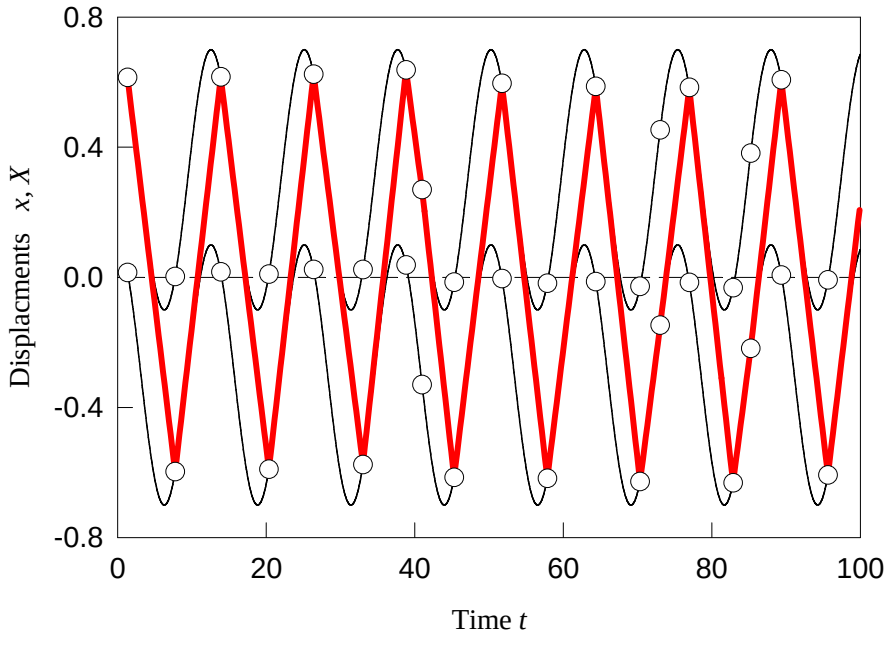

(a)

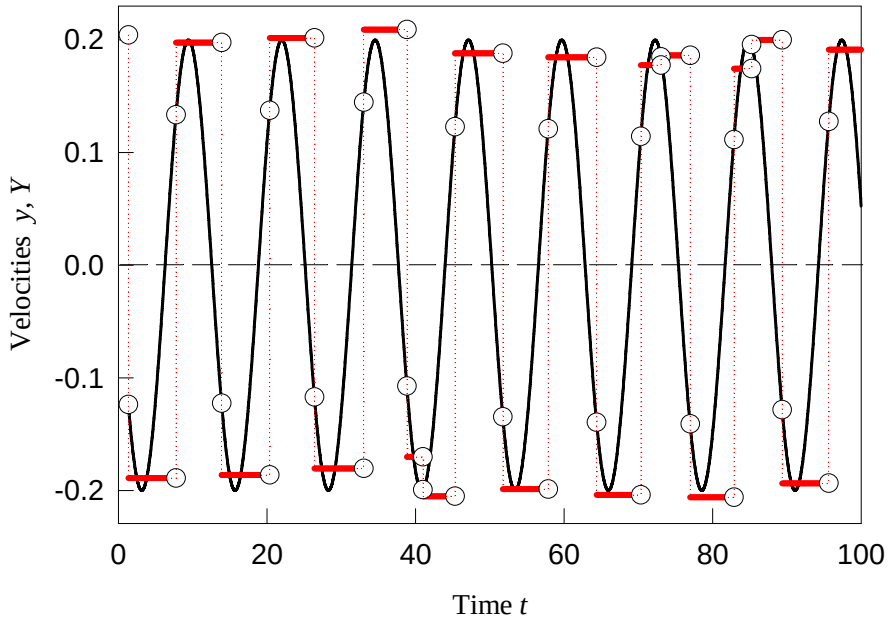

(b)

Figure 4.8: Chaotic motion: (a) displacement time history, (b) velocity time history, (c) Poincare map of switching displacement, (d) Poincare map of switching velocity. ($Q_0 = 0.4,$ $\Omega = 0.5,$ $M = 1.0,$ $m = 0.001,$ $e = 0.2,$ $d = 0.15$ **). The initial conditions are** $t_0 = 1.33468433,$ $x_0 = 0.61418775,$ $\dot{x}_0 = 0.204449281.$

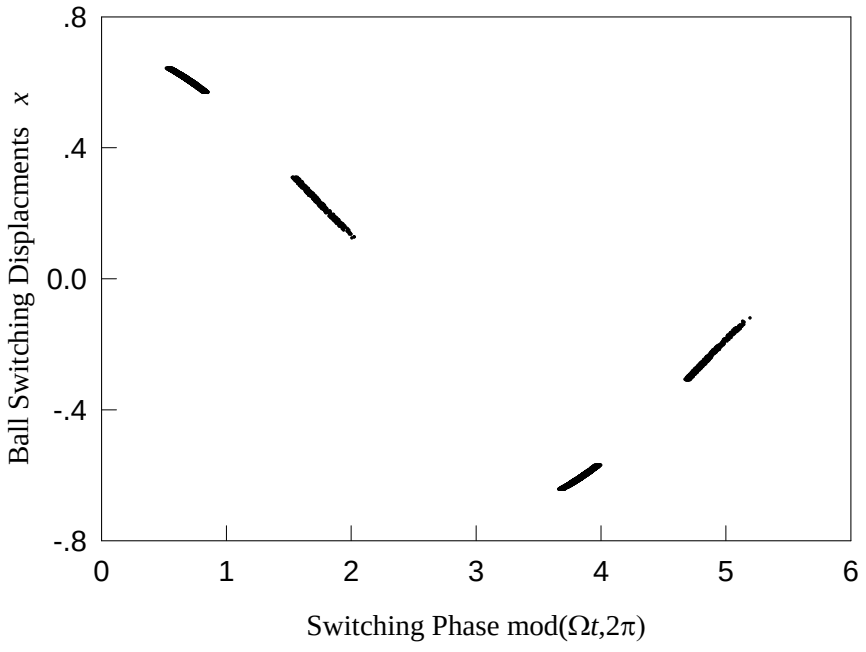

(c)

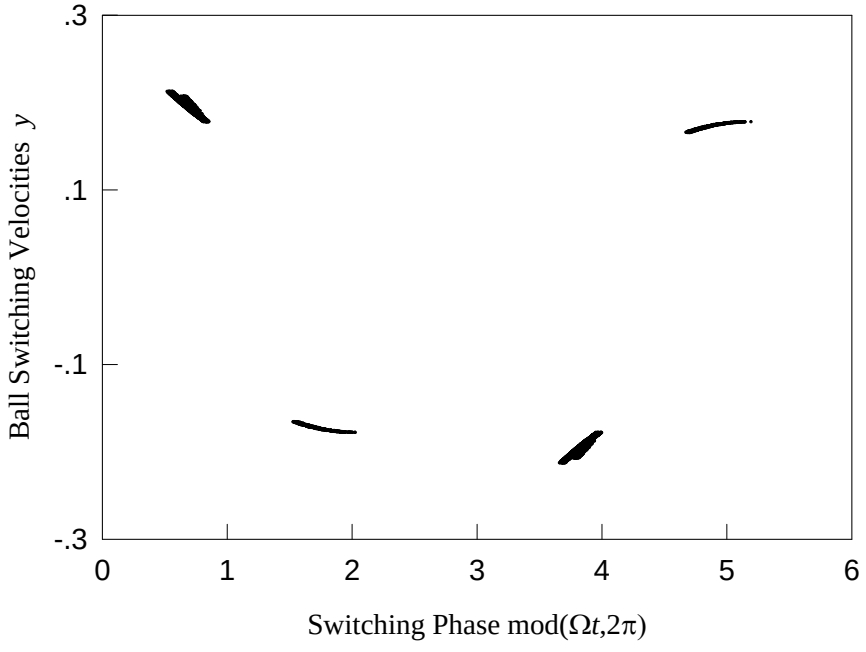

(d)

Figure 4.8 Continue

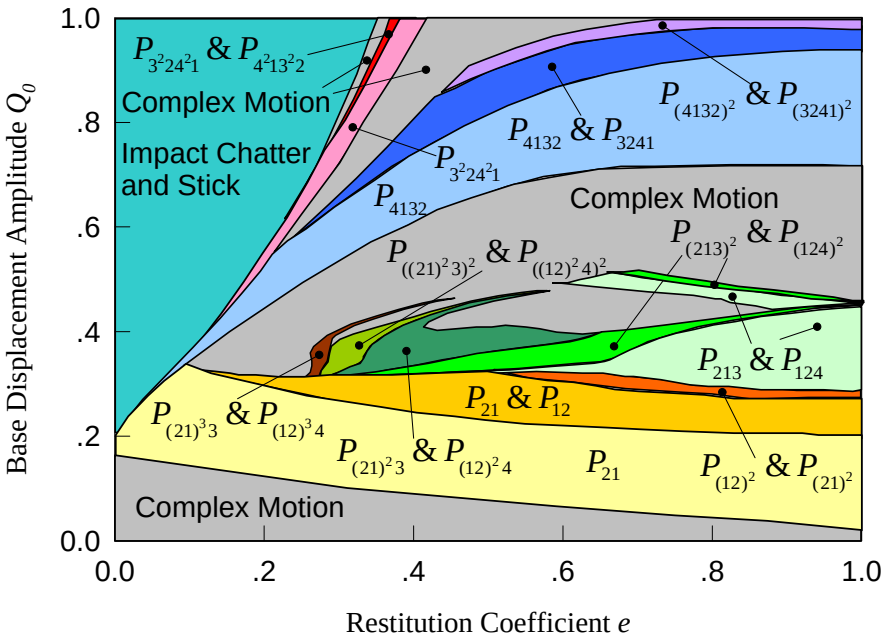

Figure 4.9: Parameter map of base displacement amplitude Q_0 vs. restitution coefficient e.

4.6. Conclusions

In this chapter, complex periodic motions and bifurcation in a horizontal impact pair with periodic excitation were investigated using the theory of flow switchability for discontinuous dynamical systems. Analytical conditions for stick and grazing motions to the corresponding boundaries were developed to explain motion complexity. The analytical predictions of complex motions were completed through the mapping structure. Periodic and chaotic motions in such a system were illustrated. The parameter maps for all possible complex motions were also presented in detail using color maps.

CHAPTER 5

DUAL EXCITED FERMI ACCELERATOR

In this chapter, the stability and bifurcation of motions in a Fermi oscillator under dual excitations are presented using the theory of discontinuous dynamical systems. The analytical conditions for motion switching in such a Fermi-oscillator are obtained, and the generic mappings are introduced to describe the periodic and chaotic motions for such oscillator. Considering the case when the two excitations are same with each other, the bifurcation scenarios for periodic and chaotic motions are presented, and analytical predictions of periodic motions are also presented. In addition, numerical illustrations of periodic and chaotic motions in such an oscillator are given. The flutter oscillations of such an oscillator are presented through the switching section of Neimark bifurcation. Finally, a detailed parameter map for such an oscillator will be presented for the case when the same excitations are applied. Similarly, investigations on bifurcation, prediction, and simulation are presented considering different excitations. More complexity can be observed from this case.

5.1. Physical Model Descriptions

The investigated Fermi accelerator with dual excitations consists of a particle moving vertically between two periodically excited oscillators (Luo & Guo, Switchability and bifurcation of motions in a double-excited Fermi-acceleration oscillator, 2010). The mass in each oscillator $m^{(\alpha)}$ ($\alpha \in \{1, 2\}$) is connected with a spring of constant $k^{(\alpha)}$ and a damper of coefficient $c^{(\alpha)}$ to the fixed wall. Both oscillators are driven with periodic excitation force $F^{(\alpha)}(t)$, as shown in Figure 5.1. The mass of particle is $m^{(3)}$ and the restitution coefficients of impact for the bottom and top oscillators are $e^{(1)}$ and $e^{(2)}$, respectively. The gap between the equilibrium positions of

the two oscillators is h. If the particle does not move together with any of the oscillators, the corresponding motion is called the non-stick motion. For this case, the equations of motion are given by the Newton's law, i.e.,

$$\left.\begin{aligned} &\ddot{x}^{(3)} = -g, \\ &\ddot{x}^{(\alpha)} + 2\xi^{(\alpha)}\dot{x}^{(\alpha)} + (\omega^{(\alpha)})^2 x^{(\alpha)} = \frac{Q^{(\alpha)}}{m^{(\alpha)}}\cos\Omega^{(\alpha)}t, \end{aligned}\right\} \tag{5.1}$$

where $\xi^{(\alpha)} = c^{(\alpha)}/2m^{(\alpha)}$, $\omega^{(\alpha)} = \sqrt{k^{(\alpha)}/m^{(\alpha)}}$. $\ddot{x}^{(i)}$ is the acceleration, $\dot{x}^{(i)}$ is the velocity, and $x^{(i)}$ is the displacement ($i = 1, 2, 3$).

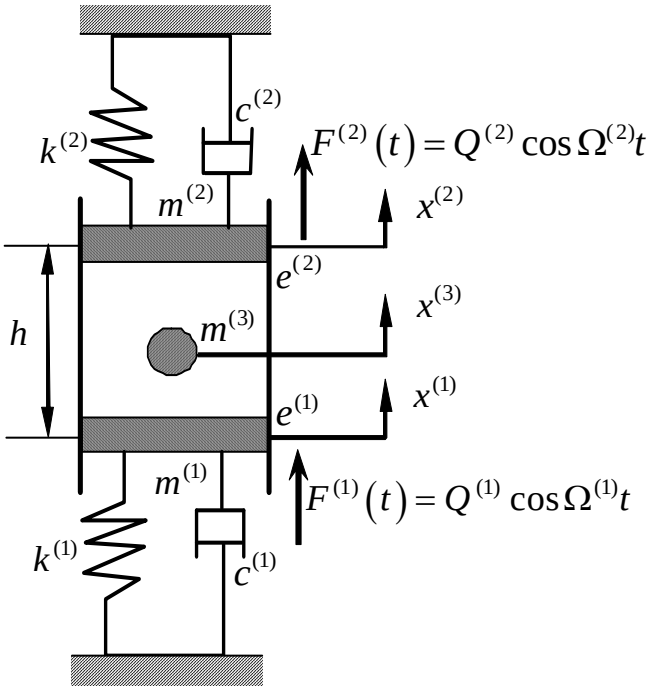

Figure 5.1: Mechanical model

If the particle stays on one of the two oscillators and moves together, this motion is called a stick motion. For this case, the equations of motion are given as

$$\left.\begin{aligned}\ddot{x}^{(\alpha)}+2\xi^{(\alpha)}\dot{x}^{(\alpha)}+(\omega^{(\alpha)})^2x^{(\alpha)}&=\frac{Q^{(\alpha)}}{m^{(\alpha)}}\cos\Omega^{(\alpha)}t,\\ \ddot{x}^{(0)}+2d^{(0)}\dot{x}^{(0)}+(\omega^{(0)})^2x^{(0)}&=\frac{Q^{(\bar{\alpha})}}{m^{(3)}+m^{(\bar{\alpha})}}\cos\Omega^{(\bar{\alpha})}t,\end{aligned}\right\} \tag{5.2}$$

where $\ddot{x}^{(0)}$ is the acceleration, $\dot{x}^{(0)}$ is the velocity, and $x^{(0)}$ is the displacement for both the ball and oscillator. Also $d^{(0)}=c^{(\bar{\alpha})}/2(m^{(3)}+m^{(\bar{\alpha})})$, $\omega^{(0)}=\sqrt{k^{(\bar{\alpha})}/m^{(3)}+m^{(\bar{\alpha})}}$ where

$$\bar{\alpha}=\begin{cases}2, \text{ if } \alpha=1;\\ 1, \text{ if } \alpha=2.\end{cases} \tag{5.3}$$

The impact relation among the particle and the oscillators are

$$\begin{aligned}&x_+^{(3)}=x_+^{(\alpha)}=x_-^{(3)}=x_-^{(\alpha)};\\ &\dot{x}_+^{(3)}=\frac{m^{(3)}\dot{x}_-^{(3)}+m^{(\alpha)}\dot{x}_-^{(\alpha)}-m^{(\alpha)}e^{(\alpha)}\left(\dot{x}_-^{(3)}-\dot{x}_-^{(\alpha)}\right)}{m^{(3)}+m^{(\alpha)}},\\ &\dot{x}_+^{(\alpha)}=\frac{m^{(3)}\dot{x}_-^{(3)}+m_2\dot{x}_-^{(\alpha)}+m^{(3)}e^{(\alpha)}\left(\dot{x}_-^{(3)}-\dot{x}_-^{(\alpha)}\right)}{m^{(3)}+m^{(\alpha)}}.\end{aligned} \tag{5.4}$$

5.2. Discontinuous Modeling

Due to the discontinuity of the system, the domains and boundaries in absolute coordinate system are introduced as sketched in Figure 5.2. The origin of the absolute coordinate is set at the equilibrium position of the bottom oscillator. The absolute domains $\Omega_1^{(1)}$ and $\Omega_1^{(2)}$ for the bottom and top oscillators and domain $\Omega_1^{(3)}$ for the particle without stick are defined as

$$\left.\begin{aligned}\Omega_1^{(1)}&=\left\{(x^{(1)},\dot{x}^{(1)})\middle|x^{(1)}\in(-\infty,x^{(3)})\right\},\\ \Omega_1^{(2)}&=\left\{(x^{(2)},\dot{x}^{(2)})\middle|x^{(2)}\in(x^{(3)},+\infty)\right\},\\ \Omega_1^{(3)}&=\left\{(x^{(3)},\dot{x}^{(3)})\middle|x^{(3)}\in(x^{(1)},x^{(2)})\right\}.\end{aligned}\right\} \tag{5.5}$$

The corresponding absolute boundaries are defined as

$$\left.\begin{aligned}\partial\Omega_{1(+\infty)}^{(i)} &= \left\{(x^{(i)},\dot{x}^{(i)})\middle|\varphi_{1(+\infty)}^{(i)} \equiv x^{(i)} - x^{(\bar{i})} = 0, \dot{x}^{(i)} \neq \dot{x}^{(\bar{i})}\right\},\\ \partial\Omega_{1(-\infty)}^{(j)} &= \left\{(x^{(j)},\dot{x}^{(j)})\middle|\varphi_{1(-\infty)}^{(j)} \equiv x^{(j)} - x^{(\bar{j})} = 0, \dot{x}^{(j)} \neq \dot{x}^{(\bar{j})}\right\},\end{aligned}\right\} \tag{5.6}$$

where $i = 2,3$ and $\bar{i} = 3,2$ with ($j = 1,3$ and $\bar{j} = 3,1$). The domains are represented by a shaded area and the boundaries are depicted by dashed and solid curves in Figure 5.2. The boundaries of $\partial\Omega_{1(+\infty)}^{(2)}$ and $\partial\Omega_{1(+\infty)}^{(3)}$ are the curves at $x^{(2)} = x^{(3)}$ and the boundaries of $\partial\Omega_{1(-\infty)}^{(1)}$ and $\partial\Omega_{1(-\infty)}^{(3)}$ are the curves at $x^{(1)} = x^{(2)}$. For stick motion, the absolute domains $\Omega_0^{(i)}$ and $\Omega_1^{(i)}$ ($i = 1,2,3$) for the two oscillators and particle are defined as

$$\left.\begin{aligned}\Omega_0^{(1)} &= \left\{(x^{(1)},\dot{x}^{(1)})\middle|x^{(1)} \in (x_{cr}^{(3)}, x^{(2)}), \dot{x}^{(1)} = \dot{x}^{(3)}\right\},\\ \Omega_0^{(2)} &= \left\{(x^{(2)},\dot{x}^{(2)})\middle|x^{(2)} \in (x^{(1)}, x_{cr}^{(3)}), \dot{x}^{(2)} = \dot{x}^{(3)}\right\},\\ \Omega_0^{(3)} &= \left\{(x^{(3)},\dot{x}^{(3)})\middle|\begin{matrix}x^{(3)} \in (-\infty, x_{cr}^{(1)}), \dot{x}^{(3)} = \dot{x}^{(1)}\\ \text{or } x^{(3)} \in (x_{cr}^{(2)}, +\infty), \dot{x}^{(3)} = \dot{x}^{(2)}\end{matrix}\right\},\\ \Omega_1^{(1)} &= \left\{(x^{(1)},\dot{x}^{(1)})\middle|x^{(1)} \in \left(-\infty, x_{cr}^{(3)}\right), \dot{x}^{(3)} \neq \dot{x}^{(1)}\right\},\\ \Omega_1^{(2)} &= \left\{(x^{(2)},\dot{x}^{(2)})\middle|x^{(2)} \in \left(x_{cr}^{(3)}, +\infty\right), \dot{x}^{(3)} \neq \dot{x}^{(2)}\right\},\\ \Omega_1^{(3)} &= \left\{(x^{(3)},\dot{x}^{(3)})\middle|\begin{matrix}x^{(3)} \in \left(x_{cr}^{(1)}, x^{(2)}\right), \dot{x}^{(3)} \neq \dot{x}^{(1)}\\ \text{or } x^{(3)} \in \left(x^{(1)}, x_{cr}^{(2)}\right), \dot{x}^{(3)} \neq \dot{x}^{(2)}\end{matrix}\right\},\end{aligned}\right\} \tag{5.7}$$

where $x_{cr}^{(i)}$ is for appearance and vanishing of stick motion with $\dot{x}_{cr}^{(3)} = \dot{x}_{cr}^{(\alpha)}$ and $x_{cr}^{(3)} = x_{cr}^{(a)}$, and $\alpha = 1,2$ are for stick on the bottom and top, respectively. The domains of $\Omega_1^{(i)}$ and $\Omega_0^{(i)}$ are presented by shaded and filled regions in Figure 5.1. The corresponding absolute boundaries are given by dashed curves, and the stick boundaries are defined as

$$\left.\begin{aligned}\partial\Omega_{10}^{(1)} &= \left\{(x^{(1)},\dot{x}^{(1)})\middle|\varphi_{10}^{(1)} \equiv x^{(1)} - x_{cr}^{(3)} = 0, \dot{x}^{(1)} = \dot{x}_{cr}^{(3)}\right\},\\ \partial\Omega_{10}^{(2)} &= \left\{(x^{(2)},\dot{x}^{(2)})\middle|\varphi_{10}^{(2)} \equiv x^{(2)} - x_{cr}^{(3)} = 0, \dot{x}^{(2)} = \dot{x}_{cr}^{(3)}\right\},\\ \partial\Omega_{10}^{(3)} &= \left\{(x^{(3)},\dot{x}^{(3)})\middle|\begin{matrix}\varphi_{10}^{(3)} \equiv x^{(3)} - x_{cr}^{(1)} = 0, \dot{x}^{(3)} = \dot{x}_{cr}^{(1)}\\ \text{or } \varphi_{10}^{(3)} \equiv x^{(3)} - x_{cr}^{(2)} = 0, \dot{x}^{(3)} = \dot{x}_{cr}^{(2)}\end{matrix}\right\}.\end{aligned}\right\} \tag{5.8}$$

The vectors for absolute motions can be defined as follow

$$\left.\begin{aligned}\mathbf{x}_{\lambda}^{(i)} &= (x_{\lambda}^{(i)}, \dot{x}_{\lambda}^{(i)})^{\mathrm{T}},\\ \mathbf{f}_{\lambda}^{(i)} &= (\dot{x}_{\lambda}^{(i)}, F_{\lambda}^{(i)})^{\mathrm{T}},\end{aligned}\right\} \text{ for } (i = 1,2,3 \text{ and } \lambda = 0,1), \tag{5.9}$$

where $i = 1,2,3$ represents the bottom, top oscillators, and the particle, respectively; $\lambda = 0,1$ stands for the stick or non-stick domains. Then equation of absolute motion is

$$\dot{\mathbf{x}}_{\lambda}^{(i)} = \mathbf{f}_{\lambda}^{(i)}(\mathbf{x}_{\lambda}^{(i)}, t) \quad \text{for } i = 1,2,3 \text{ and } \lambda = 0,1. \tag{5.10}$$

For non-stick motion,

$$\left.\begin{aligned}F_1^{(i)}(x_1^{(i)}, t) &= -2\xi^{(i)}\dot{x}^{(i)} - (\omega^{(i)})^2 x^{(i)} + \frac{Q^{(i)}}{m^{(i)}}\cos\Omega^{(i)}t, (i = 1,2),\\ F_1^{(3)}(x_1^{(3)}, t) &= -g.\end{aligned}\right\} \tag{5.11}$$

For the stick motion,

$$\left.\begin{aligned}F_1^{(\bar{\alpha})}(x_1^{(\bar{\alpha})}, t) &= -2\xi^{(\bar{\alpha})}\dot{x}^{(\bar{\alpha})} - (\omega^{(\bar{\alpha})})^2 x^{(\bar{\alpha})} + \frac{Q^{(\bar{\alpha})}}{m^{(\bar{\alpha})}}\cos\Omega^{(\bar{\alpha})}t\\ F_0^{(i)}(x_0^{(i)}, t) &= -2d^{(0)}\dot{x}^{(0)} - (\omega^{(0)})^2 x^{(0)} + \frac{Q^{(\alpha)}}{m^{(3)} + m^{(\alpha)}}\cos\Omega^{(\alpha)}t\end{aligned}\right\} (i = \alpha, 3). \tag{5.12}$$

For simplicity, the relative displacement, velocity, and acceleration between the particle and the bottom or top oscillators are defined as $z^{(i)} = x^{(i)} - x^{(\bar{i})}$, $\dot{z}^{(i)} = \dot{x}^{(i)} - \dot{x}^{(\bar{i})}$, and $\ddot{z}^{(i)} = \ddot{x}^{(i)} - \ddot{x}^{(\bar{i})}$, where $i = \alpha, 3$ and $\bar{i} = 3, \alpha$ represent the particle and one of the two oscillators, accordingly. The relative domains and boundaries for the particle and oscillators are then defined as sketched in Figure 5.2 and Figure 5.3 for the motion relative to bottom or top oscillators. The stick domain and boundaries in the relative phase space becomes a point in Figure 5.4 and Figure 5.5 (a) and (c). The stick domains and boundaries in the relative velocity and acceleration (i.e., $(\dot{z}^{(i)}, \ddot{z}^{(i)})$) plane is illustrated in Figure 5.4 and Figure 5.5 (b) and (d). The filled regions indicate the stick domains while the shaded regions indicate the non-stick domains.

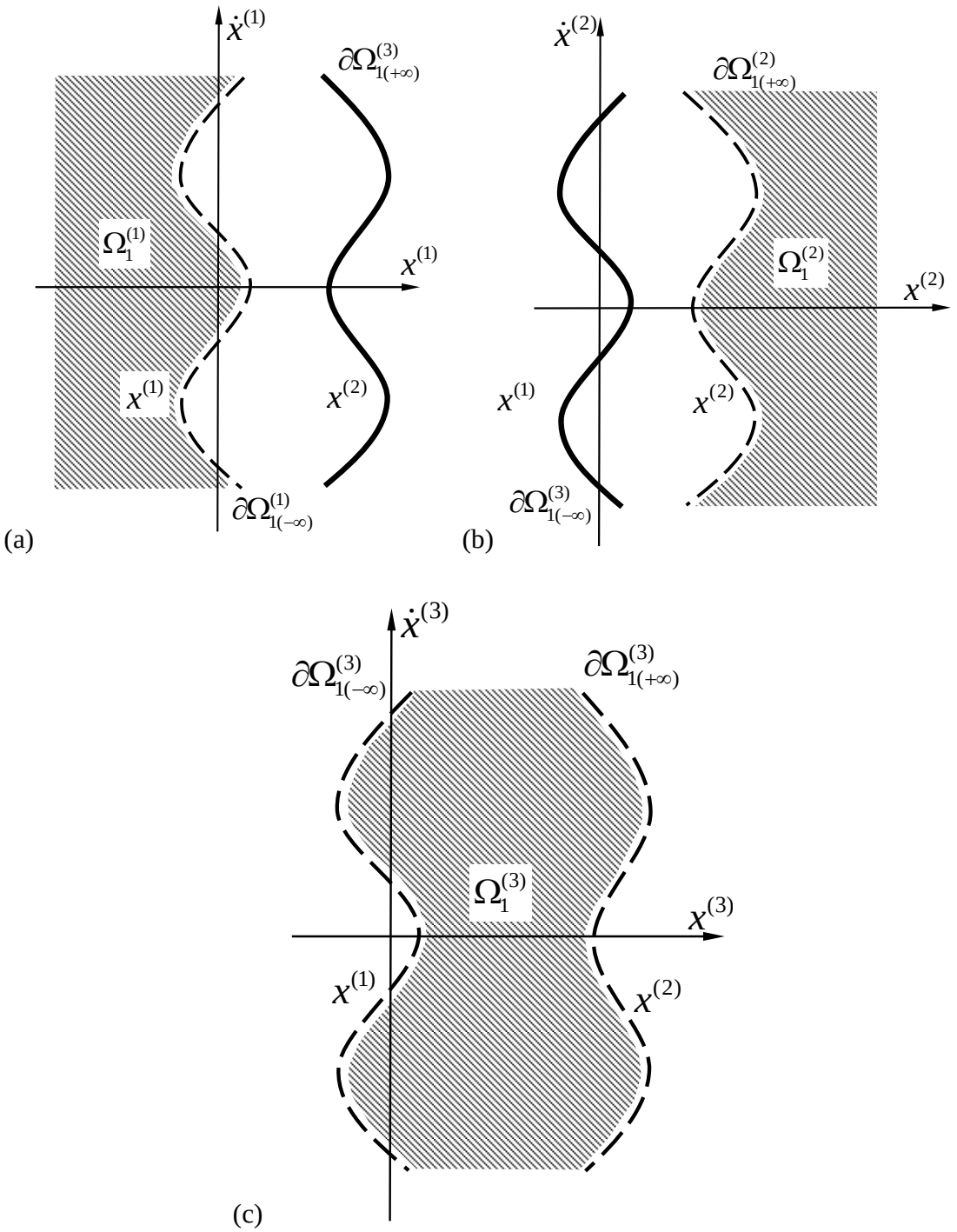

Figure 5.2: Absolute domains and boundaries without stick: (a) Bottom oscillator, (b) top oscillator, and (c) particle.

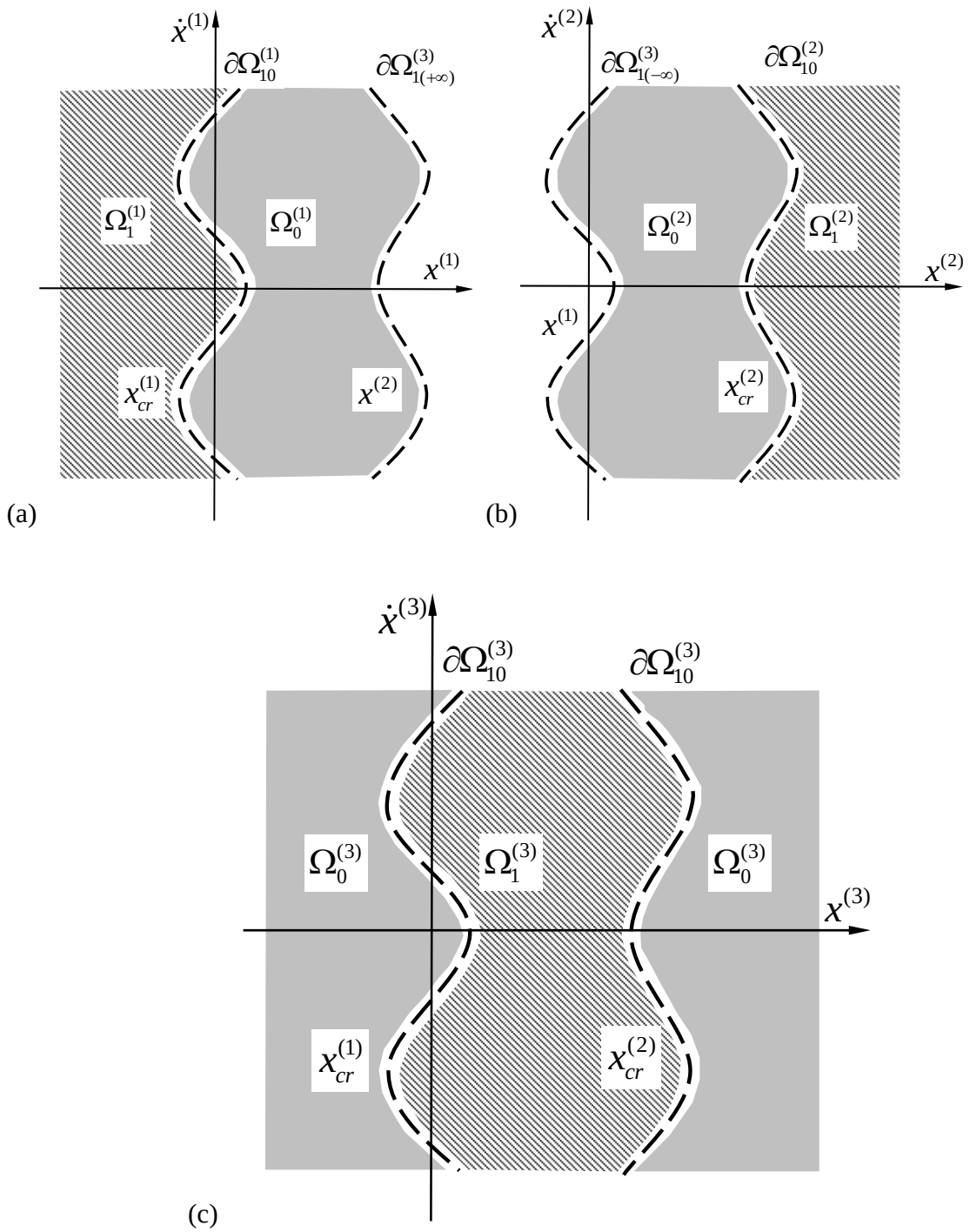

Figure 5.3: Absolute domains and boundaries with stick: (a) bottom oscillator, (b) top oscillator, and (c) particle.

The domains $\Omega_0^{(i)}$ and $\Omega_1^{(i)}$ for the relative motions for the particle and the two oscillators are

$$\left.\begin{aligned}
\Omega_0^{(i)} &= \left\{(z^{(i)}, \dot{z}^{(i)}) \middle| \dot{z}^{(i)} = 0, z^{(i)} = 0\right\}, \\
\Omega_1^{(1)} &= \left\{(z^{(1)}, \dot{z}^{(1)}) \middle| z^{(1)} \in (-\infty, 0)\right\}, \\
\Omega_1^{(2)} &= \left\{(z^{(2)}, \dot{z}^{(2)}) \middle| z^{(2)} \in (0, +\infty)\right\}, \\
\Omega_1^{(3)} &= \left\{(z^{(3)}, \dot{z}^{(3)}) \middle| \begin{matrix} z^{(3)} \in (x^{(1)} - x^{(3)}, 0), \\ \text{or } z^{(3)} \in (0, x^{(2)} - x^{(3)}) \end{matrix} \right\}.
\end{aligned}\right\} \tag{5.13}$$

The boundaries $\partial\Omega_{1(+\infty)}^{(i)}$, $\partial\Omega_{1(-\infty)}^{(i)}$, $\partial\Omega_{10}^{(i)}$, and $\partial\Omega_{01}^{(i)}$ for the particle associated with the bottom or top oscillators are

$$\left.\begin{aligned}
\partial\Omega_{1(-\infty)}^{(i)} &= \left\{(z^{(i)}, \dot{z}^{(i)}) \middle| \varphi_{1(-\infty)}^{(i)} \equiv z^{(i)} = 0, \dot{z}^{(i)} \neq 0\right\}, \\
\partial\Omega_{1(+\infty)}^{(j)} &= \left\{(z^{(j)}, \dot{z}^{(j)}) \middle| \varphi_{1(+\infty)}^{(j)} \equiv z^{(j)} = 0, \dot{z}^{(j)} \neq 0\right\}, \\
\partial\Omega_{10}^{(l)} &= \partial\Omega_{01}^{(l)} = \left\{(z^{(l)}, \dot{z}^{(l)}) \middle| \varphi_{10}^{(l)} \equiv \dot{z}_{cr}^{(l)} = 0, z_{cr}^{(l)} = 0\right\},
\end{aligned}\right\} \tag{5.14}$$

where $i = 1, 3$, $j = 2, 3$, $l = 1, 2, 3$. $\partial\Omega_{1(-\infty)}^{(3)}$ and $\partial\Omega_{1(+\infty)}^{(3)}$ are the impact chatter boundaries for the particle relative to the bottom or top oscillators, respectively. $\partial\Omega_{10}^{(3)}$ and $\partial\Omega_{01}^{(3)}$ are the stick motion boundaries for the particle. $\partial\Omega_{1(-\infty)}^{(1)}$ and $\partial\Omega_{1(+\infty)}^{(2)}$ are the impact-chatter boundaries for the bottom or top oscillators, respectively. $\partial\Omega_{10}^{(1)}$ and $\partial\Omega_{01}^{(1)}$ are the stick motion boundaries for the bottom oscillator. $\partial\Omega_{10}^{(2)}$ and $\partial\Omega_{01}^{(2)}$ are the stick motion boundaries for the top oscillator. The relative vectors in the relative coordinates are

$$\mathbf{z}_\lambda^{(i)} = (z_\lambda^{(i)}, \dot{z}_\lambda^{(i)})^{\mathrm{T}}, \mathbf{g}_\lambda^{(i)} = \dot{\mathbf{z}}_\lambda^{(i)} = (\dot{z}_\lambda^{(i)}, g_\lambda^{(i)})^{\mathrm{T}} \tag{5.15}$$

where $i = 1, 2$ are the bottom and top oscillators, respectively; $i = 3$ are for the particle. $\lambda = 0, 1$ gives the corresponding stick and non-stick domains. For $i = 1, 2, 3$ and $\lambda = 0, 1$, the equations of relative motion are in the relative vector form of

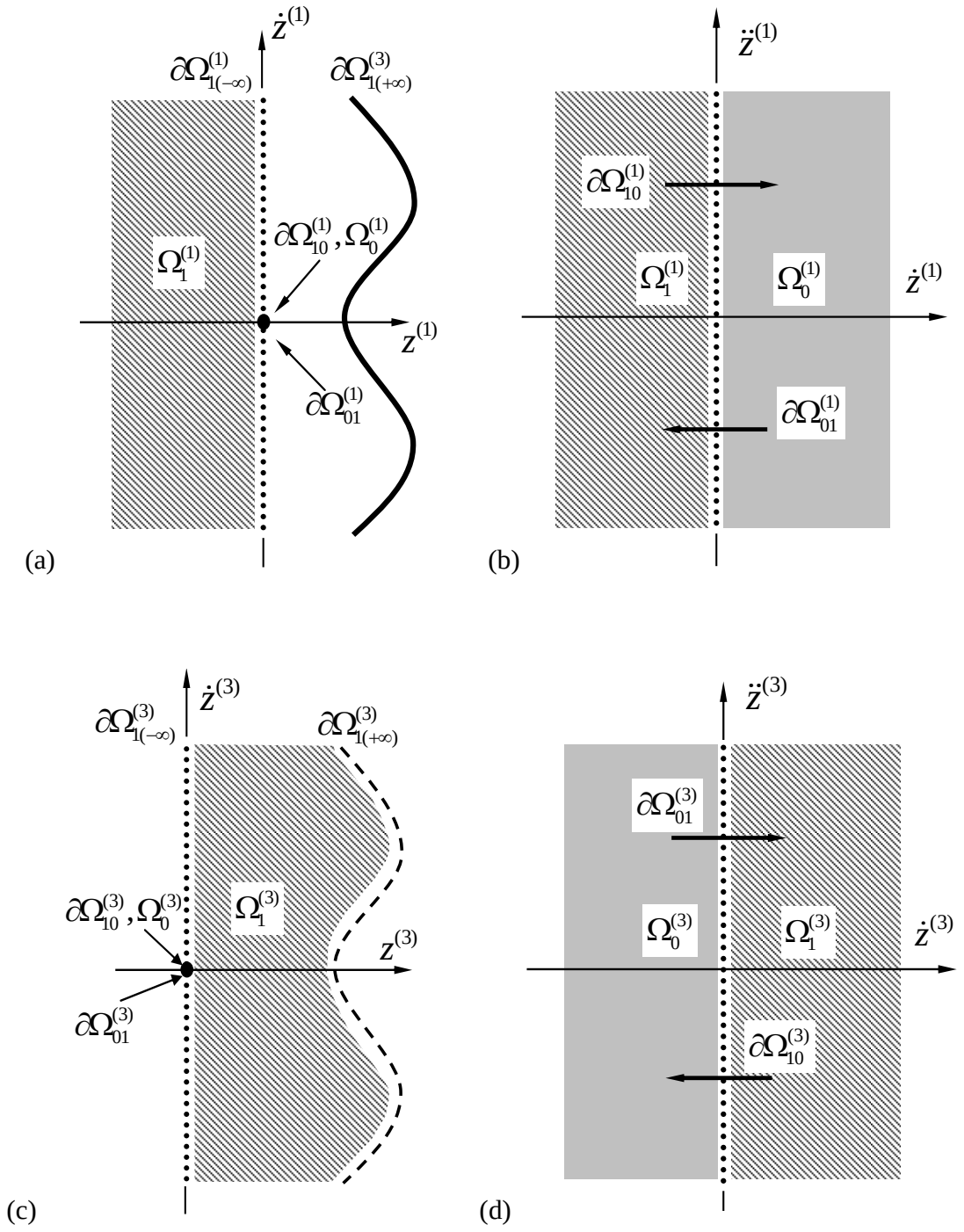

Figure 5.4: Domains and boundaries definition relative to the bottom oscillator: (a) $(z, \dot{z})$-plane for bottom oscillator, (b) $(\dot{z}, \ddot{z})$-plane for bottom oscillator, (c) $(z, \dot{z})$-plane for particle, and (d) $(\dot{z}, \ddot{z})$-plane for particle.

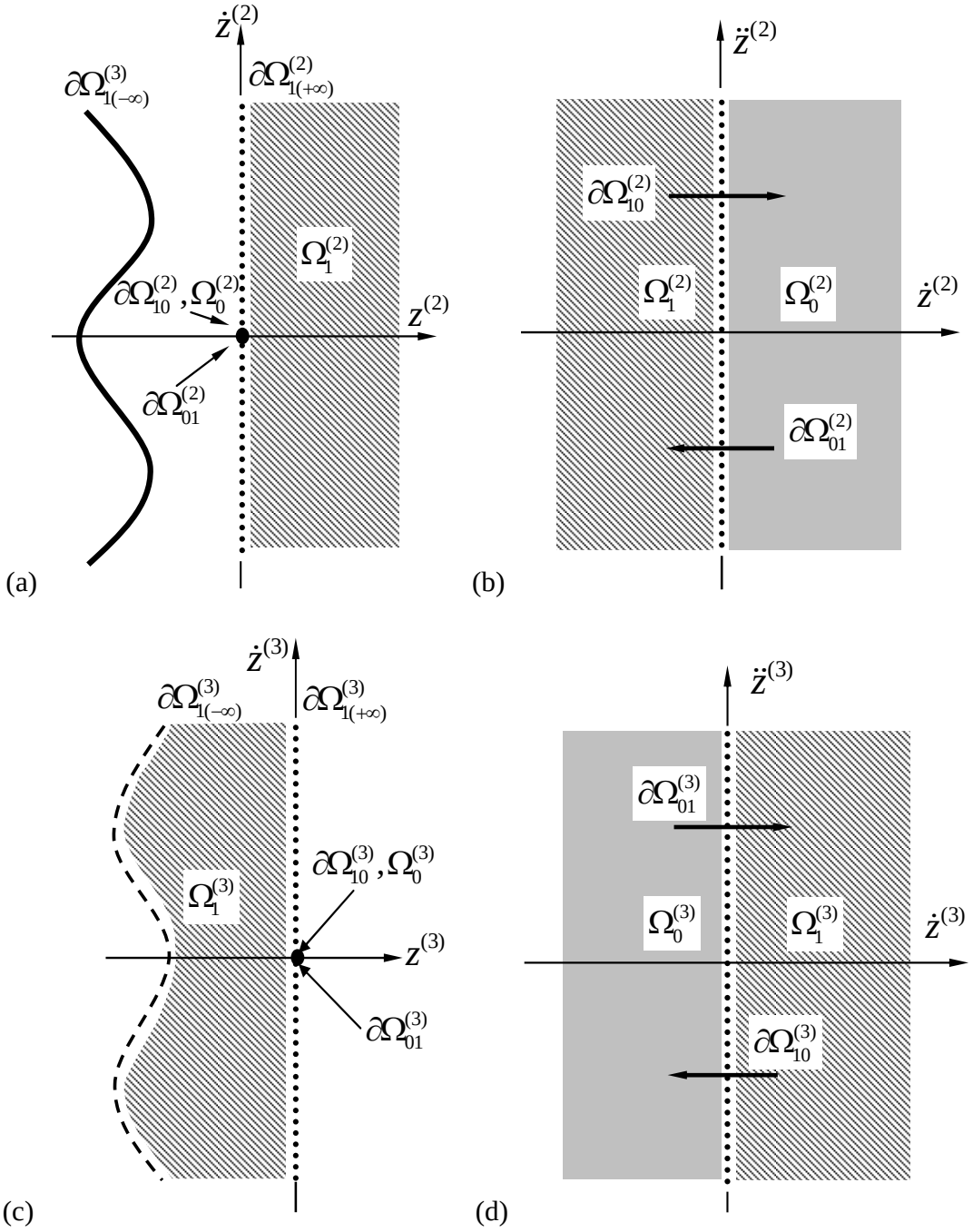

Figure 5.5: Domains and boundaries definition relative to the top oscillator: (a) $(z, \dot{z})$ **-plane for top oscillator, (b)** $(\dot{z}, \ddot{z})$ **-plane for top oscillator, (c)** $(z, \dot{z})$ **-plane for particle, and (d)** $(\dot{z}, \ddot{z})$ **-plane for particle.**

$$\left.\begin{aligned}\dot{\mathbf{z}}_\lambda^{(\bar{\alpha})} &= \mathbf{g}_\lambda^{(\bar{\alpha})}(\mathbf{x}_\lambda^{(\bar{\alpha})}, t)\ , \\ \dot{\mathbf{z}}_\lambda^{(\alpha)} &= \mathbf{g}_\lambda^{(\alpha)}(\mathbf{z}_\lambda^{(\alpha)}, \mathbf{x}_\lambda^{(3)}, t)\ , \\ \dot{\mathbf{z}}_\lambda^{(3)} &= \mathbf{g}_\lambda^{(3)}(\mathbf{z}_\lambda^{(3)}, \mathbf{x}_\lambda^{(\alpha)}, t)\ ,\end{aligned}\right\} \tag{5.16}$$

where $\dot{\mathbf{x}}_\lambda^{(i)} = \mathbf{f}_\lambda^{(i)}(\mathbf{x}_\lambda^{(i)}, t)$.

(i) For non-stick motion, the relative forces per unit mass are

$$\left.\begin{aligned} g_1^{(\bar{\alpha})}(\mathbf{z}_1^{(\bar{\alpha})}, \mathbf{x}_1^{(\bar{\alpha})}, t) &= -2\xi^{(\bar{\alpha})}\dot{x}_1^{(\bar{\alpha})} - (\omega^{(\bar{\alpha})})^2 x_1^{(\bar{\alpha})} + \frac{Q^{(\bar{\alpha})}}{m^{(\bar{\alpha})}}\cos\Omega^{(\bar{\alpha})}t, \\ g_1^{(\alpha)}(\mathbf{z}_1^{(\alpha)}, \mathbf{x}_1^{(\alpha)}, t) &= -2\xi^{(\alpha)}\dot{x}_1^{(\alpha)} - (\omega^{(\alpha)})^2 x_1^{(\alpha)} + \frac{Q^{(\alpha)}}{m^{(\alpha)}}\cos\Omega^{(\alpha)}t + g, \\ g_1^{(3)}\left(\mathbf{z}_1^{(3)}, \mathbf{x}_1^{(\alpha)}, t\right) &= -g + 2\xi^{(\alpha)}\dot{x}_1^{(\alpha)} + (\omega^{(\alpha)})^2 x_1^{(\alpha)} - \frac{Q^{(\alpha)}}{m^{(\alpha)}}\cos\Omega^{(\alpha)}t, \end{aligned}\right\} \tag{5.17}$$

(ii) For stick motion, the relative velocities and the relative forces per unit mass are

$$\left.\begin{aligned} \dot{z}_0^{(3)} &= \dot{z}_0^{(\alpha)} = 0 \\ g_1^{(\bar{\alpha})}(\mathbf{z}_1^{(\bar{\alpha})}, \mathbf{x}_1^{(\bar{\alpha})}, t) &= -2\xi^{(\bar{\alpha})}\dot{x}_1^{(\bar{\alpha})} - (\omega^{(\bar{\alpha})})^2 x_1^{(\bar{\alpha})} + \frac{Q^{(\bar{\alpha})}}{m^{(\bar{\alpha})}}\cos\Omega^{(\bar{\alpha})}t, \\ g_0^{(\alpha)}(\mathbf{z}_1^{(\alpha)}, \mathbf{x}_1^{(\alpha)}, t) &= g_0^{(3)}(\mathbf{z}_1^{(3)}, \mathbf{x}_1^{(\alpha)}, t) = 0, \end{aligned}\right\} \tag{5.18}$$

5.3. Analytical Switching Conditions

To develop the analytical conditions for stick and grazing motions of the Fermi oscillator, the normal vector of the boundary relative to the bottom or top oscillator is

$$\mathbf{n}_{\partial\Omega_{\alpha\beta}} = \nabla\varphi_{\alpha\beta} = \left(\frac{\partial\varphi_{\alpha\beta}}{\partial z}, \frac{\partial\varphi_{\alpha\beta}}{\partial\dot{z}}\right)^{\mathrm{T}} \tag{5.19}$$

where $\nabla = \left(\partial/\partial z\,, \partial/\partial\dot{z}\right)^{\mathrm{T}}$. $\mathbf{n}_{\partial\Omega_{10}^{(3)}}$ and $\mathbf{n}_{\partial\Omega_{01}^{(3)}}$ are the normal vectors of the stick boundaries, and the normal vectors of $\mathbf{n}_{\partial\Omega_{1(-\infty)}^{(3)}}$ and $\mathbf{n}_{\partial\Omega_{1(+\infty)}^{(3)}}$ are for impact chatter boundaries. Thus,

$$\left.\begin{aligned}\mathbf{n}_{\partial\Omega_{10}^{(3)}} &= \mathbf{n}_{\partial\Omega_{01}^{(3)}} = (0,1)^{\mathrm{T}},\\ \mathbf{n}_{\partial\Omega_{1(-\infty)}^{(3)}} &= \mathbf{n}_{\partial\Omega_{1(+\infty)}^{(3)}} = (1,0)^{\mathrm{T}}.\end{aligned}\right\} \tag{5.20}$$

The zero-order and first-order G-functions for the stick boundaries relative to the bottom or top oscillators are introduced by Luo (Luo, Discontinuous Dynamical Systems on Time-varying Domains, 2009; Luo, A theory for flow switchability in discontinuous dynamical systems, 2008),

$$\left.\begin{aligned}
&G^{(0,0)}_{\partial\Omega^{(\alpha)}_{01}}(\mathbf{z}^{(\alpha)}_0,\mathbf{x}^{(3)}_0,t_{m\pm}) = \mathbf{n}^T_{\partial\Omega^{(\alpha)}_{01}}\cdot\mathbf{g}^{(\alpha)}(\mathbf{z}^{(\alpha)}_0,\mathbf{x}^{(3)}_0,t_{m\pm}),\\
&G^{(1,0)}_{\partial\Omega^{(\alpha)}_{10}}(\mathbf{z}^{(\alpha)}_1,\mathbf{x}^{(3)}_1,t_{m\pm}) = \mathbf{n}^T_{\partial\Omega^{(\alpha)}_{10}}\cdot\mathbf{g}^{(\alpha)}(\mathbf{z}^{(\alpha)}_1,\mathbf{x}^{(3)}_1,t_{m\pm}),\\
&G^{(0,1)}_{\partial\Omega^{(\alpha)}_{01}}(\mathbf{z}^{(\alpha)}_0,\mathbf{x}^{(3)}_0,t_{m\pm}) = \mathbf{n}^T_{\partial\Omega^{(\alpha)}_{01}}\cdot D\mathbf{g}^{(\alpha)}(\mathbf{z}^{(\alpha)}_0,\mathbf{x}^{(3)}_0,t_{m\pm}),\\
&G^{(1,1)}_{\partial\Omega^{(\alpha)}_{10}}(\mathbf{z}^{(\alpha)}_1,\mathbf{x}^{(3)}_1,t_{m\pm}) = \mathbf{n}^T_{\partial\Omega^{(\alpha)}_{10}}\cdot D\mathbf{g}^{(\alpha)}(\mathbf{z}^{(\alpha)}_1,\mathbf{x}^{(3)}_1,t_{m\pm}),\\
&G^{(0,0)}_{\partial\Omega^{(3)}_{01}}(\mathbf{z}^{(3)}_0,\mathbf{x}^{(\alpha)}_0,t_{m\pm}) = \mathbf{n}^T_{\partial\Omega^{(3)}_{01}}\cdot\mathbf{g}^{(3)}(\mathbf{z}^{(3)}_0,\mathbf{x}^{(\alpha)}_0,t_{m\pm}),\\
&G^{(1,0)}_{\partial\Omega^{(3)}_{10}}(\mathbf{z}^{(3)}_1,\mathbf{x}^{(\alpha)}_1,t_{m\pm}) = \mathbf{n}^T_{\partial\Omega^{(3)}_{10}}\cdot\mathbf{g}^{(3)}(\mathbf{z}^{(3)}_1,\mathbf{x}^{(\alpha)}_1,t_{m\pm}),\\
&G^{(0,1)}_{\partial\Omega^{(3)}_{01}}(\mathbf{z}^{(3)}_0,\mathbf{x}^{(\alpha)}_0,t_{m\pm}) = \mathbf{n}^T_{\partial\Omega^{(3)}_{01}}\cdot D\mathbf{g}^{(3)}(\mathbf{z}^{(3)}_0,\mathbf{x}^{(\alpha)}_0,t_{m\pm}),\\
&G^{(1,0)}_{\partial\Omega^{(3)}_{10}}(\mathbf{z}^{(3)}_1,\mathbf{x}^{(\alpha)}_1,t_{m\pm}) = \mathbf{n}^T_{\partial\Omega^{(3)}_{10}}\cdot D\mathbf{g}^{(3)}(\mathbf{z}^{(3)}_1,\mathbf{x}^{(\alpha)}_1,t_{m\pm}).
\end{aligned}\right\} \tag{5.21}$$

Notice that t_m is the switching time of the motion on the corresponding boundary and $t_{m\pm} = t_m \pm 0$ which represents the motion on each side of the boundary in different domains. The G-functions for the impact chatter boundaries are

$$\left.\begin{aligned}
&G^{(0,1)}_{\partial\Omega^{(3)}_{1(+\infty)}}(\mathbf{z}^{(3)}_1,\mathbf{x}^{(2)}_1,t_{m\pm}) = \mathbf{n}^T_{\partial\Omega^{(3)}_{1(+\infty)}}\cdot\mathbf{g}^{(3)}(\mathbf{z}^{(3)}_1,\mathbf{x}^{(2)}_1,t_{m\pm}),\\
&G^{(1,1)}_{\partial\Omega^{(3)}_{1(+\infty)}}(\mathbf{z}^{(3)}_1,\mathbf{x}^{(2)}_1,t_{m\pm}) = \mathbf{n}^T_{\partial\Omega^{(3)}_{1(+\infty)}}\cdot D\mathbf{g}^{(3)}(\mathbf{z}^{(3)}_1,\mathbf{x}^{(2)}_1,t_{m\pm}),\\
&G^{(0,1)}_{\partial\Omega^{(3)}_{1(-\infty)}}(\mathbf{z}^{(3)}_1,\mathbf{x}^{(1)}_1,t_{m\pm}) = \mathbf{n}^T_{\partial\Omega^{(3)}_{1(-\infty)}}\cdot\mathbf{g}^{(3)}(\mathbf{z}^{(3)}_1,\mathbf{x}^{(1)}_1,t_{m\pm}),\\
&G^{(1,1)}_{\partial\Omega^{(3)}_{1(-\infty)}}(\mathbf{z}^{(3)}_1,\mathbf{x}^{(1)}_1,t_{m\pm}) = \mathbf{n}^T_{\partial\Omega^{(3)}_{1(-\infty)}}\cdot D\mathbf{g}^{(3)}(\mathbf{z}^{(3)}_1,\mathbf{x}^{(1)}_1,t_{m\pm}).
\end{aligned}\right\} \tag{5.22}$$

Using the G-functions, the analytical conditions for stick motion on bottom or top oscillators can be obtained for the passable flow condition from domain $\Omega_1^{(i)}$ to $\Omega_0^{(i)}$ (Luo, A

theory for flow switchability in discontinuous dynamical systems, 2008; Luo, Discontinuous Dynamical Systems on Time-varying Domains, 2009),

$$\left.\begin{aligned}(-1)^{\alpha} G^{(0,1)}_{\partial\Omega^{(\alpha)}_{10}}(\mathbf{z}^{(\alpha)}_1, \mathbf{x}^{(3)}_1, t_{m-}) < 0,\\ (-1)^{\alpha} G^{(0,0)}_{\partial\Omega^{(\alpha)}_{01}}(\mathbf{z}^{(\alpha)}_0, \mathbf{x}^{(3)}_0 t_{m+}) < 0.\end{aligned}\right\}$$
$$\left.\begin{aligned}(-1)^{\alpha} G^{(0,1)}_{\partial\Omega^{(3)}_{10}}(\mathbf{z}^{(3)}_1, \mathbf{x}^{(\alpha)}_1, t_{m-}) > 0,\\ (-1)^{\alpha} G^{(0,0)}_{\partial\Omega^{(3)}_{01}}(\mathbf{z}^{(3)}_0, \mathbf{x}^{(\alpha)}_0, t_{m+}) > 0.\end{aligned}\right\} \tag{5.23}$$

Therefore,

$$\left.\begin{aligned}(-1)^{\alpha} g^{(\alpha)}_1(\mathbf{z}^{(\alpha)}_1, \mathbf{x}^{(3)}_1, t_{m-}) < 0,\\ (-1)^{\alpha} g^{(\alpha)}_0(\mathbf{z}^{(\alpha)}_0, \mathbf{x}^{(3)}_0, t_{m+}) < 0.\end{aligned}\right\}$$
$$\left.\begin{aligned}(-1)^{\alpha} g^{(3)}_1(\mathbf{z}^{(3)}_1, \mathbf{x}^{(\alpha)}_1, t_{m-}) > 0,\\ (-1)^{\alpha} g^{(3)}_0(\mathbf{z}^{(3)}_0, \mathbf{x}^{(\alpha)}_0, t_{m+}) > 0.\end{aligned}\right\} \tag{5.24}$$

Simplification of the foregoing conditions gives the onset conditions of stick motion on bottom or top oscillators, i.e.,

$$\left.\begin{aligned}\ddot{x}^{(1)}(t_{m\pm}) > \ddot{x}^{(3)}(t_{m\pm}) = -g, \text{ for the bottom}\\ \ddot{x}^{(2)}(t_{m\pm}) < \ddot{x}^{(3)}(t_{m\pm}) = -g, \text{ for the top}\end{aligned}\right\} \tag{5.25}$$

which means that the acceleration of the bottom oscillator $\ddot{x}^{(1)}(t_{m\pm})$ should be larger than the particle's acceleration of $\ddot{x}^{(3)}(t_{m\pm}) = -g$ in order for the particle to stick on the bottom oscillator. However, the acceleration of the top oscillator $\ddot{x}^{(2)}(t_{m\pm})$ should be less than the particle acceleration in order for the particle to stick on the top oscillator. Similarly, the criteria for vanishing of the stick motion (Luo, A theory for flow switchability in discontinuous dynamical systems, 2008; Luo, Discontinuous Dynamical Systems on Time-varying Domains, 2009) from the bottom or top oscillator at $\partial\Omega^{(\alpha)}_{01}$ are,

$$\left.\begin{aligned} &G^{(0,0)}_{\partial\Omega^{(\alpha)}_{01}}(\mathbf{z}^{(\alpha)}_0,\mathbf{x}^{(3)}_0,t_{m-})=0,\ (-1)^{\alpha}G^{(0,1)}_{\partial\Omega^{(\alpha)}_{01}}(\mathbf{z}^{(\alpha)}_0,\mathbf{x}^{(3)}_0,t_{m-})>0;\\ &G^{(1,0)}_{\partial\Omega^{(\alpha)}_{01}}(\mathbf{z}^{(\alpha)}_1,\mathbf{x}^{(3)}_1,t_{m+})=0,\ (-1)^{\alpha}G^{(1,1)}_{\partial\Omega^{(\alpha)}_{01}}(\mathbf{z}^{(3)}_1,\mathbf{x}^{(\alpha)}_1,t_{m+})>0. \end{aligned}\right\}$$
$$\left.\begin{aligned} &G^{(0,0)}_{\partial\Omega^{(3)}_{01}}(\mathbf{z}^{(3)}_0,\mathbf{x}^{(\alpha)}_0,t_{m-})=0,\ (-1)^{\alpha}G^{(0,1)}_{\partial\Omega^{(\alpha)}_{01}}(\mathbf{z}^{(3)}_0,\mathbf{x}^{(\alpha)}_0,t_{m-})<0;\\ &G^{(1,0)}_{\partial\Omega^{(3)}_{01}}(\mathbf{z}^{(3)}_1,\mathbf{x}^{(\alpha)}_1,t_{m+})=0,\ (-1)^{\alpha}G^{(1,1)}_{\partial\Omega^{(3)}_{01}}(\mathbf{z}^{(3)}_1,\mathbf{x}^{(\alpha)}_1,t_{m+})<0. \end{aligned}\right\} \tag{5.26}$$

From the foregoing equations, the relative force relations for $\partial\Omega^{(\alpha)}_{01}$ are

$$\left.\begin{aligned} &g^{(\alpha)}_0(\mathbf{z}^{(\alpha)}_0,\mathbf{x}^{(3)}_0,t_{m-})=0,(-1)^{\alpha}\frac{d}{dt}g^{(\alpha)}_0(\mathbf{z}^{(\alpha)}_0,\mathbf{x}^{(3)}_0,t_{m-})>0;\\ &g^{(\alpha)}_1(\mathbf{z}^{(\alpha)}_1,\mathbf{x}^{(3)}_1,t_{m+})=0,(-1)^{\alpha}\frac{d}{dt}g^{(\alpha)}_1(\mathbf{z}^{(\alpha)}_1,\mathbf{x}^{(3)}_1,t_{m+})<0. \end{aligned}\right\}$$
$$\left.\begin{aligned} &g^{(3)}_0(\mathbf{z}^{(3)}_0,\mathbf{x}^{(\alpha)}_0,t_{m-})=0,(-1)^{\alpha}\frac{d}{dt}g^{(3)}_0(\mathbf{z}^{(3)}_0,\mathbf{x}^{(\alpha)}_0,t_{m-})<0;\\ &g^{(3)}_1(\mathbf{z}^{(3)}_1,\mathbf{x}^{(\alpha)}_1,t_{m+})=0,(-1)^{\alpha}\frac{d}{dt}g^{(3)}_1(\mathbf{z}^{(3)}_1,\mathbf{x}^{(\alpha)}_1,t_{m+})>0. \end{aligned}\right\} \tag{5.27}$$

With the relative acceleration and jerk, one gets

$$\left.\begin{aligned} &\left.\begin{aligned} &\ddot{x}^{(1)}(t_{m\pm})=\ddot{x}^{(3)}(t_{m\pm})=-g,\\ &\dddot{x}^{(1)}_{m\pm}<\dddot{x}^{(3)}_{m\pm}=0, \end{aligned}\right\}\ \text{for the bottom,}\\ &\left.\begin{aligned} &\ddot{x}^{(2)}(t_{m\pm})=\ddot{x}^{(3)}(t_{m\pm})=-g,\\ &\dddot{x}^{(2)}_{m\pm}>\dddot{x}^{(3)}_{m\pm}=0, \end{aligned}\right\}\ \text{for the top.} \end{aligned}\right\} \tag{5.28}$$

Using the G-functions of the flow to each boundary, the conditions of grazing motions are as follows,

$$\left.\begin{aligned} &(-1)^{\alpha}G^{(1,0)}_{\partial\Omega^{(\alpha)}_{1(-\infty)}}(\mathbf{z}^{(\alpha)}_1,\mathbf{x}^{(3)}_1,t_{m\pm})=0,\ \text{and}(-1)^{\alpha}G^{(1,1)}_{\partial\Omega^{(\alpha)}_{1(-\infty)}}(\mathbf{z}^{(\alpha)}_1,\mathbf{x}^{(3)}_1,t_{m\pm})>0\quad\text{for }\partial\Omega^{(\alpha)}_{1(-\infty)};\\ &(-1)^{\alpha}G^{(1,0)}_{\partial\Omega^{(\alpha)}_{1(+\infty)}}(\mathbf{z}^{(\alpha)}_1,\mathbf{x}^{(3)}_1,t_{m\pm})=0,\ \text{and}\ (-1)^{\alpha}G^{(1,1)}_{\partial\Omega^{(\alpha)}_{1(+\infty)}}(\mathbf{z}^{(\alpha)}_1,\mathbf{x}^{(3)}_1,t_{m\pm})>0\quad\text{for }\partial\Omega^{(\alpha)}_{1(+\infty)}.\\ &(-1)^{\alpha}G^{(1,0)}_{\partial\Omega^{(3)}_{1(-\infty)}}(\mathbf{z}^{(3)}_1,\mathbf{x}^{(\alpha)}_1,t_{m\pm})=0,\ \text{and}\ (-1)^{\alpha}G^{(1,1)}_{\partial\Omega^{(3)}_{1(-\infty)}}(\mathbf{z}^{(\alpha)}_1,\mathbf{x}^{(\alpha)}_1,t_{m\pm})<0\quad\text{for }\partial\Omega^{(\alpha)}_{1(-\infty)},\\ &(-1)^{\alpha}G^{(1,0)}_{\partial\Omega^{(3)}_{1(+\infty)}}(\mathbf{z}^{(3)}_1,\mathbf{x}^{(\alpha)}_1,t_{m\pm})=0,\ \text{and}\ (-1)^{\alpha}G^{(1,1)}_{\partial\Omega^{(3)}_{1(+\infty)}}(\mathbf{z}^{(3)}_1,\mathbf{x}^{(\alpha)}_1t_{m\pm})<0\quad\text{for }\partial\Omega^{(\alpha)}_{1(+\infty)}. \end{aligned}\right\} \tag{5.29}$$

So the grazing motion conditions on the bottom and top for the non-stick motion boundaries are

$$\left.\begin{aligned}&\dot{x}^{(3)}=\dot{x}^{(1)}\ \text{and}\ \ddot{x}^{(1)}<\ddot{x}^{(3)}=-g\ \ \text{for}\ \partial\Omega^{(1)}_{1(-\infty)},\partial\Omega^{(3)}_{1(-\infty)};\\&\dot{x}^{(3)}=\dot{x}^{(2)}\ \text{and}\ \ddot{x}^{(2)}>\ddot{x}^{(3)}=-g\ \ \text{for}\ \partial\Omega^{(2)}_{1(+\infty)},\partial\Omega^{(3)}_{1(+\infty)}.\end{aligned}\right\}\tag{5.30}$$

Similarly, the grazing conditions for stick motion boundaries are given as

$$\left.\begin{aligned}&G^{(1,0)}_{\partial\Omega^{(\alpha)}_{10}}(\mathbf{z}^{(\alpha)}_1,\mathbf{x}^{(3)}_1,t_{m\pm})=0,\text{ and }(-1)^{\alpha}G^{(1,1)}_{\partial\Omega^{(i)}_{10}}(\mathbf{z}^{(\alpha)}_1,\mathbf{x}^{(3)}_1,t_{m\pm})>0\ \ \text{for}\ \partial\Omega^{(\alpha)}_{10},\\&G^{(0,0)}_{\partial\Omega^{(\alpha)}_{01}}(\mathbf{z}^{(\alpha)}_0,\mathbf{x}^{(3)}_0,t_{m\pm})=0,\text{ and }(-1)^{\alpha}G^{(0,1)}_{\partial\Omega^{(\alpha)}_{01}}(\mathbf{z}^{(\alpha)}_0,\mathbf{x}^{(3)}_0,t_{m\pm})<0\ \ \text{for}\ \partial\Omega^{(\alpha)}_{01}.\\&G^{(1,0)}_{\partial\Omega^{(3)}_{10}}(\mathbf{z}^{(3)}_1,\mathbf{x}^{(\alpha)}_1,t_{m\pm})=0,\text{ and }(-1)^{\alpha}G^{(1,1)}_{\partial\Omega^{(i)}_{10}}(\mathbf{z}^{(3)}_1,\mathbf{x}^{(\alpha)}_1,t_{m\pm})<0\ \ \text{for}\ \partial\Omega^{(\alpha)}_{10},\\&G^{(0,0)}_{\partial\Omega^{(\alpha)}_{01}}(\mathbf{z}^{(3)}_0,\mathbf{x}^{(\alpha)}_0,t_{m\pm})=0,\text{ and }(-1)^{\alpha}G^{(0,1)}_{\partial\Omega^{(\alpha)}_{01}}(\mathbf{z}^{(3)}_0,\mathbf{x}^{(\alpha)}_0,t_{m\pm})>0\ \ \text{for}\ \partial\Omega^{(\alpha)}_{01}.\end{aligned}\right\}\tag{5.31}$$

The corresponding accelerations and jerks should satisfy the following relations.

$$\left.\begin{aligned}&\left.\begin{aligned}&\ddot{x}^{(1)}=\ddot{x}^{(3)}=-g\ \text{and}\ \dddot{x}^{(1)}<\dddot{x}^{(3)}=0\ \text{for}\ \partial\Omega^{(1)}_{10},\ \partial\Omega^{(3)}_{10},\\&\ddot{x}^{(1)}=\ddot{x}^{(3)}=-g\ \text{and}\ \dddot{x}^{(1)}>\dddot{x}^{(3)}=0\ \text{for}\ \partial\Omega^{(1)}_{01},\partial\Omega^{(3)}_{01},\end{aligned}\right\}\text{for bottom;}\\&\left.\begin{aligned}&\ddot{x}^{(2)}=\ddot{x}^{(3)}=-g\ \text{and}\ \dddot{x}^{(2)}>\dddot{x}^{(3)}=0\ \text{for}\ \partial\Omega^{(2)}_{10},\partial\Omega^{(3)}_{10},\\&\ddot{x}^{(2)}=\ddot{x}^{(3)}=-g\ \text{and}\ \dddot{x}^{(2)}<\dddot{x}^{(3)}=0\ \text{for}\ \partial\Omega^{(2)}_{01},\partial\Omega^{(3)}_{10},\end{aligned}\right\}\text{for top.}\end{aligned}\right\}\tag{5.32}$$

5.4. Discrete Mapping Structures

Using the previously defined discontinuous domains and boundaries, the switching sets of the Fermi oscillator without stick are introduced as

$$\left.\begin{aligned}\Sigma_{1(-\infty)}&=\Sigma^{(1)}_{1(-\infty)}\otimes\Sigma^{(2)}_{1(-\infty)}\otimes\Sigma^{(3)}_{1(-\infty)}\\&=\left\{(x^{(1)}_k,\dot{x}^{(1)}_k,x^{(2)}_k,\dot{x}^{(2)}_k,x^{(3)}_k,\dot{x}^{(3)}_k,t_k)\,\middle|\,x^{(3)}_k=x^{(1)}_{k+},\dot{x}^{(3)}_k\neq\dot{x}^{(1)}_k\right\}\\\Sigma_{1(+\infty)}&=\Sigma^{(1)}_{1(+\infty)}\otimes\Sigma^{(2)}_{1(+\infty)}\otimes\Sigma^{(3)}_{1(+\infty)}\\&=\left\{(x^{(1)}_k,\dot{x}^{(1)}_k,x^{(2)}_k,\dot{x}^{(2)}_k,x^{(3)}_k,\dot{x}^{(3)}_k,t_k)\,\middle|\,x^{(3)}_k=x^{(2)}_{k+},\dot{x}^{(3)}_k\neq\dot{x}^{(2)}_k\right\}\end{aligned}\right\}\tag{5.33}$$

where the switching sets $\Sigma^{(i)}_{1(-\infty)}$ and $\Sigma^{(i)}_{1(+\infty)}$ are defined on boundary $\partial\Omega^{(i)}_{1(-\infty)}$ and $\partial\Omega^{(i)}_{1(+\infty)}$, respectively. The corresponding definitions for the top and bottom oscillators plus the particle are given as

$$\left.\begin{aligned}\Sigma_{1(-\infty)}^{(i)} &= \left\{\left(x_k^{(i)}, \dot{x}_k^{(i)}, t_k\right)\middle| x_k^{(\alpha)} = x_k^{(\bar{\alpha})},\ \dot{x}_k^{(\alpha)} \neq \dot{x}_k^{(\bar{\alpha})}\right\} \subset \partial\Omega_{1(-\infty)}^{(i)}, \alpha = 1,3,\\ \Sigma_{1(+\infty)}^{(i)} &= \left\{\left(x_k^{(i)}, \dot{x}_k^{(i)}, t_k\right)\middle| x_k^{(\alpha)} = x_k^{(\bar{\alpha})},\ \dot{x}_k^{(\alpha)} \neq \dot{x}_k^{(\bar{\alpha})}\right\} \subset \partial\Omega_{1(+\infty)}^{(i)}, \alpha = 2,3.\end{aligned}\right\} \tag{5.34}$$

Thus, the generic mappings for motions without stick motion are

$$\begin{aligned}&P_1 : \Sigma_{1(-\infty)} \to \Sigma_{1(+\infty)},\ P_2 : \Sigma_{1(+\infty)} \to \Sigma_{1(-\infty)},\\ &P_3 : \Sigma_{1(-\infty)} \to \Sigma_{1(-\infty)}, P_4 : \Sigma_{1(+\infty)} \to \Sigma_{1(+\infty)}.\end{aligned} \tag{5.35}$$

From the above definitions, the switching subsets and the sub-mappings without stick motion are sketched in Figure 5.6 (a) and (b) for the bottom and top oscillators, respectively. In Figure 5.6 (c), the sub-mappings without stick motion for the particle are presented.

$$\begin{aligned}&P_1 = ({}^{(1)}P_1, {}^{(2)}P_1, {}^{(3)}P_1),\ P_2 = ({}^{(1)}P_2, {}^{(2)}P_2, {}^{(3)}P_2),\\ &P_3 = ({}^{(1)}P_3, {}^{(2)}P_3, {}^{(3)}P_3),\ P_4 = ({}^{(1)}P_4, {}^{(2)}P_4, {}^{(3)}P_4),\end{aligned} \tag{5.36}$$

$$\begin{aligned}&{}^{(i)}P_1 : \Sigma_{1(-\infty)}^{(i)} \to \Sigma_{1(+\infty)}^{(i)},\ {}^{(i)}P_2 : \Sigma_{1(+\infty)}^{(i)} \to \Sigma_{1(-\infty)}^{(i)},\\ &{}^{(i)}P_3 : \Sigma_{1(-\infty)}^{(i)} \to \Sigma_{1(-\infty)}^{(i)},\ {}^{(i)}P_4 : \Sigma_{1(+\infty)}^{(i)} \to \Sigma_{1(+\infty)}^{(i)}.\end{aligned} \tag{5.37}$$

motion for the particle are sketched in Figure 5.7 (c). Base on the previously defined boundaries, the switching sets of the Fermi oscillator with stick motion are defined as

$$\left.\begin{aligned}{}_{\alpha}\Sigma_{10} &= {}_{\alpha}\Sigma_{10}^{(1)} \otimes_{\alpha} \Sigma_{10}^{(2)} \otimes_{\alpha} \Sigma_{10}^{(3)}\\ &= \left\{\left(x_k^{(\bar{\alpha})}, \dot{x}_k^{(\bar{\alpha})}, x_k^{(\alpha)}, \dot{x}_k^{(\alpha)}, x_k^{(3)}, \dot{x}_k^{(3)}, t_k\right)\middle| x_k^{(3)} = x_k^{(\alpha)},\ \dot{x}_k^{(3)} = \dot{x}_k^{(\alpha)}\right\},\\ \Sigma_{1(-\infty)} &= \Sigma_{1(-\infty)}^{(1)} \otimes \Sigma_{1(-\infty)}^{(2)} \otimes \Sigma_{1(-\infty)}^{(3)}\\ &= \left\{\left(x_k^{(1)}, \dot{x}_k^{(1)}, x_k^{(2)}, \dot{x}_k^{(2)}, x_k^{(3)}, \dot{x}_k^{(3)}, t_k\right)\middle| x_k^{(3)} = x_k^{(1)},\ \dot{x}_k^{(3)} \neq \dot{x}_k^{(1)}\right\},\\ \Sigma_{1(+\infty)} &= \Sigma_{1(+\infty)}^{(1)} \otimes \Sigma_{1(+\infty)}^{(2)} \otimes \Sigma_{1(+\infty)}^{(3)}\\ &= \left\{\left(x_k^{(1)}, \dot{x}_k^{(1)}, x_k^{(2)}, \dot{x}_k^{(2)}, x_k^{(3)}, \dot{x}_k^{(3)}, t_k\right)\middle| x_k^{(3)} = x_k^{(2)},\ \dot{x}_k^{(3)} \neq \dot{x}_k^{(2)}\right\},\end{aligned}\right\} \tag{5.38}$$

where $\alpha = 1,2$ with $\bar{\alpha} = 2,1$. The switching set ${}_{\alpha}\Sigma_{10}$ is defined on the boundary $\partial\Omega_{10}$.

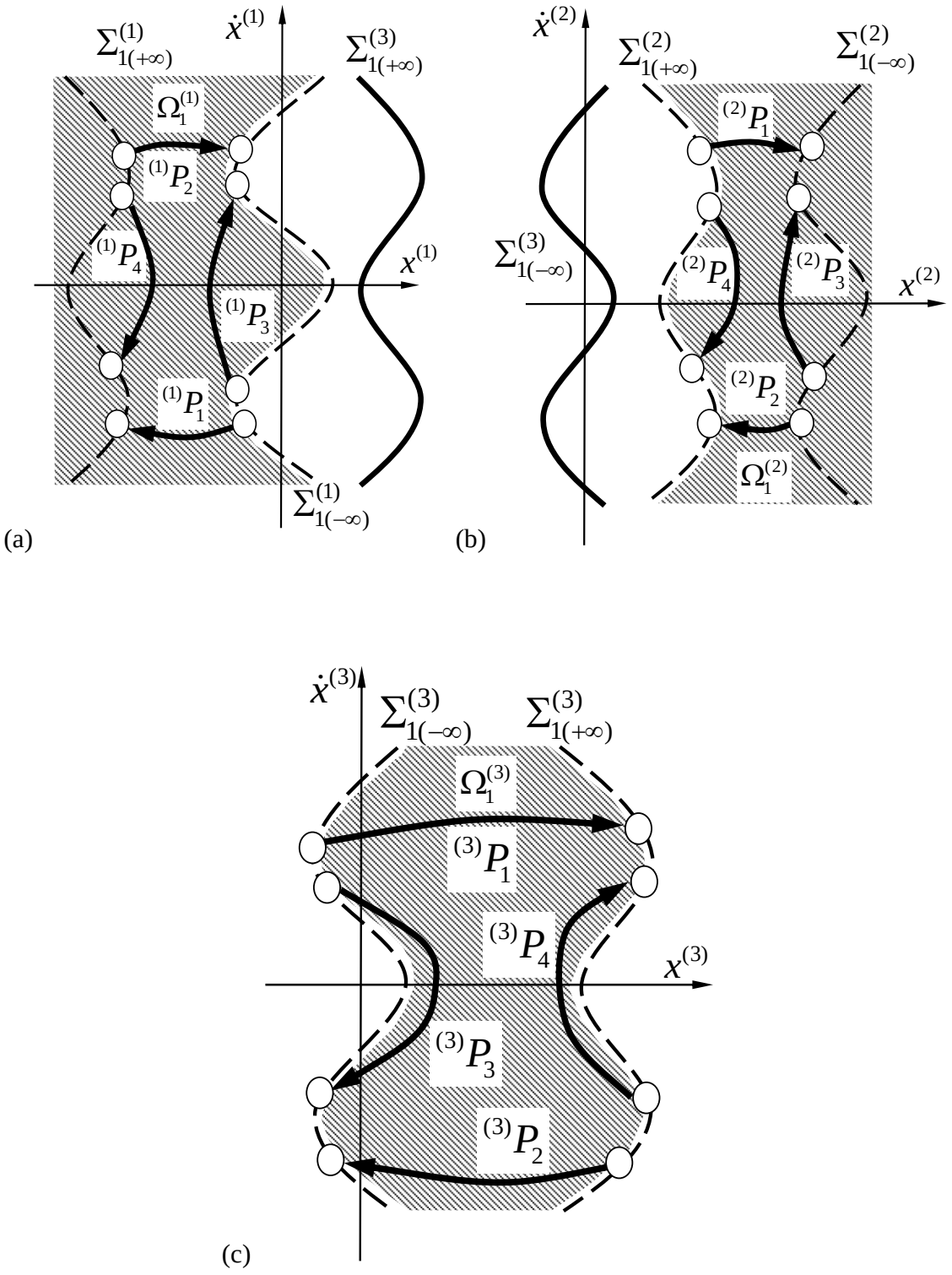

Figure 5.6: Switching sets and generic mappings for non-stick motion in absolute coordinates: (a) bottom oscillator, (b) top oscillator, and (c) particle.

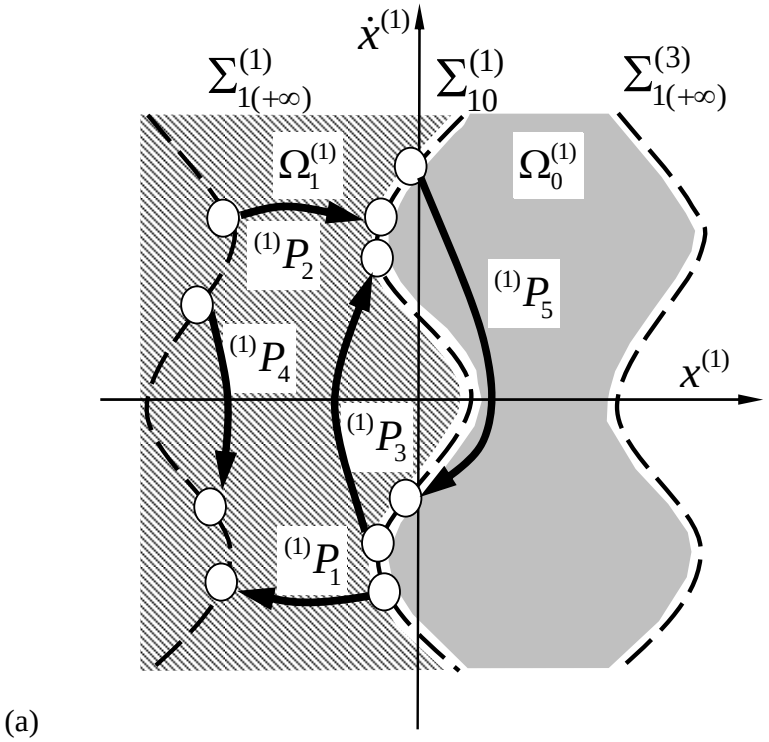

(a)

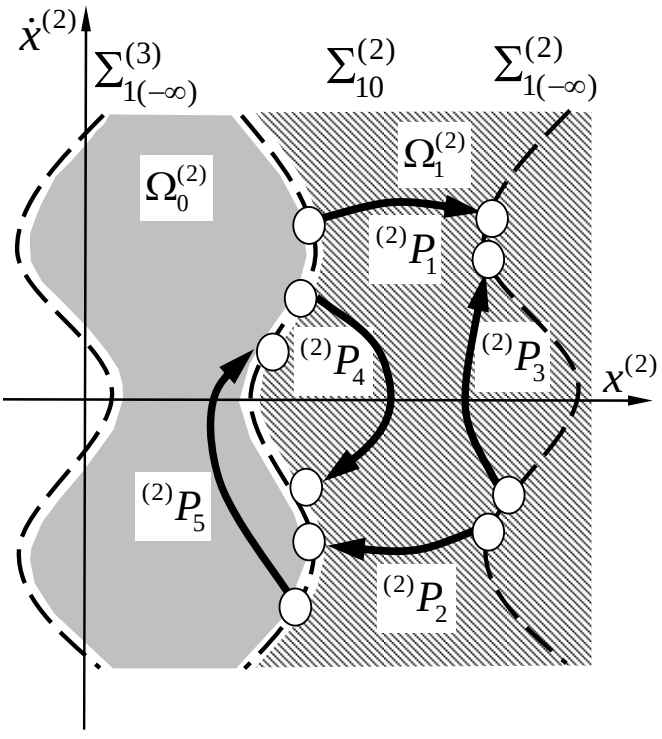

(b)

Figure 5.7: Switching sets and generic mappings for stick motion in absolute coordinates: (a) bottom oscillator, (b) top oscillator, and (c) particle.

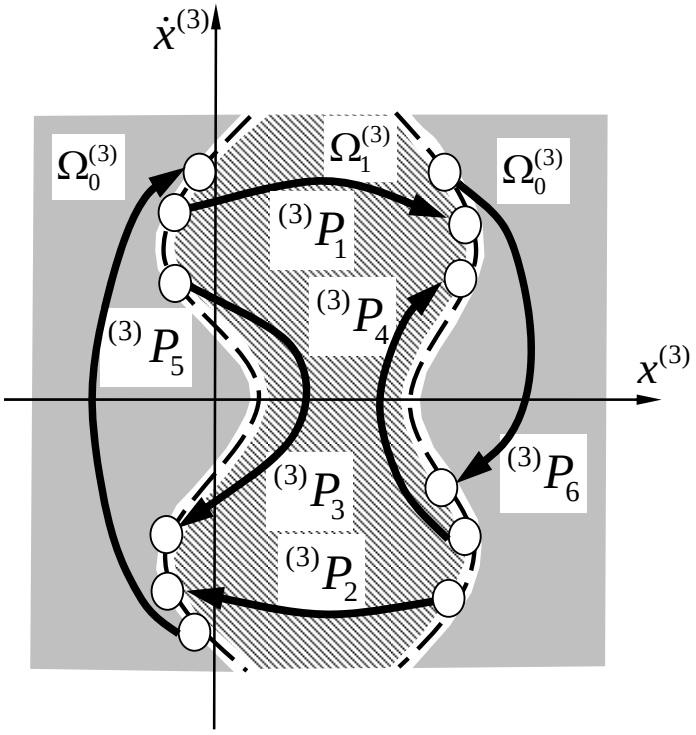

(c)

Figure 5.7: Continue

Similarly, the switching subsets and the sub-mappings with stick motion are presented in Figure 5.7 (a) and (b) for the bottom and top oscillators, respectively. The sub-mappings with stick are

$$
\begin{aligned}
{}_{\alpha}\Sigma_{10}^{(i)} &= \left\{ (x_k^{(i)}, \dot{x}_k^{(i)}, t_k) \middle| \begin{matrix} x_k^{(3)} = x_k^{(\alpha)}, \\ \dot{x}_k^{(3)} = \dot{x}_k^{(\alpha)}, \end{matrix} \right\} \subset \partial\Omega_{10}^{(i)}, \text{ for } \alpha = 1,2;\ i = 1,2,3; \\
\Sigma_{1(-\infty)}^{(i)} &= \left\{ (x_k^{(i)}, \dot{x}_k^{(i)}, t_i) \middle| \begin{matrix} x_k^{(3)} = x_k^{(1)}, \\ \dot{x}_k^{(3)} \neq \dot{x}_k^{(1)}, \end{matrix} \right\} \subset \partial\Omega_{1(-\infty)}^{(i)}, \text{ for } i = 1,3; \\
\Sigma_{1(+\infty)}^{(i)} &= \left\{ (x_k^{(i)}, \dot{x}_k^{(i)}, t_i) \middle| \begin{matrix} x_k^{(3)} = x_k^{(2)}, \\ \dot{x}_k^{(3)} \neq \dot{x}_k^{(2)}, \end{matrix} \right\} \subset \partial\Omega_{1(+\infty)}^{(i)}, \text{ for } i = 2,3.
\end{aligned}
\tag{5.39}
$$

Thus, the generic mappings for the stick motion are defined as

$$
\begin{aligned}
&P_1 : \Sigma_{10}^{(1)} \to \Sigma_{1(+\infty)}, \text{ or } \Sigma_{1(-\infty)} \to \Sigma_{10}^{(2)}, \\
&P_2 : \Sigma_{1(+\infty)} \to \Sigma_{10}^{(1)}, \text{ or } \Sigma_{10}^{(2)} \to \Sigma_{1(-\infty)}, \\
&P_3 : \Sigma_{1(-\infty)} \to \Sigma_{10}^{(1)}, \; P_4 : \Sigma_{10}^{(2)} \to \Sigma_{1(+\infty)}, \\
&P_5 : \Sigma_{10}^{(1)} \to \Sigma_{10}^{(1)}, \text{ and } P_6 : \Sigma_{10}^{(2)} \to \Sigma_{10}^{(2)}.
\end{aligned} \tag{5.40}
$$

where the global mappings of P_1 and P_2 will map from one switching set to another. The local mappings of (P_3, P_4, P_5, and P_6) map from one switching set to itself, as shown in Figure 5.6 and Figure 5.7. From the above definitions, the governing equations for a given generic mapping P_j ($j = 1, 2, 3, 4$) can be expressed by

$$
\mathbf{f}^{(j)}\left(\mathbf{Y}_k, \mathbf{Y}_{k+1}\right) = 0 \text{ for } P_j. \tag{5.41}
$$

with

$$
\left.
\begin{aligned}
&\mathbf{f}^{(j)} = \left(f_1^{(j)}, f_2^{(j)}, f_3^{(j)}, f_4^{(j)}, f_5^{(j)}, f_6^{(j)} \right)^{\mathrm{T}}, \\
&\mathbf{Y}_k = \left(x_k^{(1)}, \dot{x}_k^{(1)}, x_k^{(2)}, \dot{x}_k^{(2)}, x_k^{(3)}, \dot{x}_k^{(3)}, t_k \right)^{\mathrm{T}}, \\
&\mathbf{Y}_{k+1} = \left(x_{k+1}^{(1)}, \dot{x}_{k+1}^{(1)}, x_{k+1}^{(2)}, \dot{x}_{k+1}^{(2)}, x_{k+1}^{(3)}, \dot{x}_{k+1}^{(3)}, t_{k+1} \right)^{\mathrm{T}};
\end{aligned}
\right\},
\left\{
\begin{aligned}
&x_k^{(3)} = x_k^{(1)} \text{ and } x_{k+1}^{(3)} = x_{k+1}^{(2)} \text{ for } P_1, \\
&x_k^{(3)} = x_k^{(2)} \text{ and } x_{k+1}^{(3)} = x_{k+1}^{(1)} \text{ for } P_2, \\
&x_k^{(3)} = x_k^{(1)} \text{ and } x_{k+1}^{(3)} = x_{k+1}^{(1)} \text{ for } P_3, \\
&x_k^{(3)} = x_k^{(2)} \text{ and } x_{k+1}^{(3)} = x_{k+1}^{(2)} \text{ for } P_4.
\end{aligned}
\right\} \tag{5.42}
$$

The governing equations for the stick mapping $P_5^{(\alpha)}$ and $P_6^{(\alpha)}$ can be expressed as

$$
\mathbf{f}^{(j)}(\mathbf{Z}_k^{(j)}, \mathbf{Z}_{k+1}^{(j)}) = 0 \text{ for } P_j^{(\alpha)} \; (j = 5, 6) \tag{5.43}
$$

and

$$
\begin{aligned}
&\mathbf{Z}_k^{(j)} = \left(x_k^{(\bar{\alpha})}, \dot{x}_k^{(\bar{\alpha})}, x_k^{(3)}, \dot{x}_k^{(3)}, t_k \right)^{\mathrm{T}} \\
&\mathbf{Z}_{k+1}^{(j)} = \left(x_{k+1}^{(\bar{\alpha})}, \dot{x}_{k+1}^{(\bar{\alpha})}, x_{k+1}^{(3)}, \dot{x}_{k+1}^{(3)}, t_{k+1} \right)^{\mathrm{T}} \\
&\mathbf{f}^{(j)} = \left({}_{(\bar{\alpha})} f_1^{(0)}, {}_{(\bar{\alpha})} f_2^{(0)}, {}_{(3)} f_1^{(0)}, {}_{(3)} f_2^{(0)}, {}_{(\alpha)} f_5^{(0)} \right)^{T} \\
&{}_{(\alpha)} f_5^{(0)} = g_1^{(\alpha)}(0, \mathbf{x}_{k+1}^{(\alpha)}, t_{k+1}). \\
&\left.
\begin{aligned}
&x_k^{(3)} = x_k^{(\alpha)} \text{ and } \dot{x}_k^{(3)} = \dot{x}_k^{(\alpha)}, \; x_{k+1}^{(3)} = x_{k+1}^{(\alpha)} \text{ and } \dot{x}_{k+1}^{(3)} = \dot{x}_{k+1}^{(\alpha)}, \\
&(-1)^{\alpha} \ddot{x}_k^{(\alpha)} < (-1)^{\alpha+1} g, \text{ and } (-1)^{\alpha} \ddot{x}_{k+1}^{(\alpha)} > (-1)^{\alpha+1} g,
\end{aligned}
\right\} \\
&\text{with } j = 5, 6 \text{ for } (\alpha, \bar{\alpha}) = (1, 2) \text{ and } (2, 1).
\end{aligned} \tag{5.44}
$$

The notation for mapping action is introduced as

$$P_{j_k j_{k-1}\cdots j_1} = P_{j_k} \circ P_{j_{k-1}} \circ \cdots \circ P_{j_1}, \tag{5.45}$$

where $j_k \in \{1,2,3,4,5,6\}$ is a positive integer. For a motion with m -time repeated mapping structure of $P_{j_1 j_2 \cdots j_k}$, the total mapping structure can be expressed as

$$P^{(m)}_{j_k j_{k-1}\cdots j_1} = \underbrace{\left(P_{j_k} \circ P_{j_{k-1}} \circ \cdots \circ P_{j_1}\right) \circ \cdots \circ \left(P_{j_k} \circ P_{j_{k-1}} \circ \cdots \circ P_{j_1}\right)}_{m} = P_{(j_k j_{k-1}\cdots j_1)^m}. \tag{5.46}$$

Consider a motion with a generalized map,

$$P = \underbrace{P_{4^{m_l}0^{k_{3l}}2^{k_{2l}}3^{n_l}1^{k_{1l}}} \circ \cdots \circ P_{4^{m_1}0^{k_{31}}2^{k_{21}}3^{n_1}1^{k_{11}}}}_{l-terms} = \underbrace{P_{(4^{m_l}0^{k_{3l}}2^{k_{2l}}3^{n_l}1^{k_{1l}})\cdots(4^{m_1}0^{k_{31}}2^{k_{21}}3^{n_1}1^{k_{11}})}}_{l-terms}, \tag{5.47}$$

where $k_{js} \in \{0,1\}$ and $m_s, n_s \in \mathbb{N}$ ($s = 1,2,\cdots,l$). Define vectors $\mathbf{X}_k \equiv (X_{k1}, X_{k2}, X_{k3}, X_{k4}, X_{k5}, X_{k6})^T$ ($X_{kr} \in \{x_k^{(1)}, \dot{x}_k^{(1)}, x_k^{(2)}, \dot{x}_k^{(2)}, x_k^{(3)}, \dot{x}_k^{(3)}, t_k\}$) and $\mathbf{Y}_k \equiv (Y_{k1}, Y_{k2}, Y_{k3}, Y_{k4}, Y_{k5}, Y_{k6})^T$ ($Y_{kr} \in \{x_k^{(1)}, \dot{x}_k^{(1)}, x_k^{(2)}, \dot{x}_k^{(2)}, x_k^{(3)}, \dot{x}_k^{(3)}, t_k\}$). The motion pertaining to the mapping structure in Eq.(5.47) can be determined by

$$\mathbf{Y}_{k+\Sigma_{s=1}^{l}(m_s+k_{3s}+k_{2s}+n_s+k_{1s})} = P\mathbf{X}_k = \underbrace{P_{(4^{m_l}0^{k_{3l}}2^{k_{2l}}3^{n_l}1^{k_{1l}})\cdots(4^{m_1}0^{k_{31}}2^{k_{21}}3^{n_1}1^{k_{11}})}}_{l-terms}\mathbf{X}_k. \tag{5.48}$$

From the algebraic equations for generic mappings in Eqs. (5.41) - (5.44), one can obtain a set of nonlinear algebraic equations for such a mapping structure, i.e.,

$$\left.\begin{aligned} &\mathbf{f}^{(1)}(\mathbf{X}_k, \mathbf{Y}_{k+1}) = 0, \cdots, \mathbf{f}^{(3)}(\mathbf{X}_{k+k_{1l}}, \mathbf{Y}_{k+k_{1l}+1}) = 0, \cdots, \\ &\mathbf{f}^{(2)}(\mathbf{X}_{k+k_{1l}+n_l}, \mathbf{Y}_{k+k_{1l}+n_l+1}) = 0, \cdots, \\ &\mathbf{f}^{(4)}(\mathbf{X}_{k+\Sigma_{s=1}^{l}(m_s+k_{3s}+k_{2s}+n_s+k_{1s})-1}, \mathbf{Y}_{k+\Sigma_{s=1}^{l}(m_s+k_{3s}+k_{2s}+n_s+k_{1s})}) = 0 \\ &\mathbf{Y}_{k+\sigma} = \mathbf{X}_{k+\sigma}. \end{aligned}\right\} \tag{5.49}$$

where $\sigma = 1,\cdots,\Sigma_{s=1}^{l}(m_s + k_{3s} + k_{2s} + n_s + k_{1s}) - 1$. The periodic motion pertaining to such a mapping requires

$$\mathbf{Y}_{k+\Sigma_{s=1}^{l}(n_s+k_{3s}+m_s+k_{2s}+k_{1s})} = \mathbf{X}_k \tag{5.50}$$

or

$$\left.\begin{aligned} x^{(i)}_{k+\Sigma_{s=1}^{l}(m_s+k_{3s}+k_{2s}+n_s+k_{1s})} &= x^{(i)}_k, \\ \dot{x}^{(i)}_{k+\Sigma_{s=1}^{l}(m_s+k_{3s}+k_{2s}+n_s+k_{1s})} &= \dot{x}^{(i)}_k \end{aligned}\right\} \text{ for } i = 1,2,3$$
$$\Omega t^{(i)}_{k+\Sigma_{s=1}^{l}(m_s+k_{3s}+k_{2s}+n_s+k_{1s})} = \Omega t^{(i)}_k + 2N\pi. \tag{5.51}$$

Solving Eqs. (5.49) - (5.51) generates the switching sets of periodic motion relative to the mapping structure in Eq. (5.47). Once the switching points for a specific periodic motion is obtained, its local stability and bifurcation analysis can be completed through the corresponding Jacobian matrix. For instance, the Jacobian matrix of the mapping structure in Eq. (5.47) is computed, i.e.,

$$\begin{aligned} DP &= DP_{\underbrace{(4^{m_l}0^{k_{3l}}2^{k_{2l}}3^{n_l}1^{k_{1l}})\cdots(4^{m_1}0^{k_{31}}2^{k_{21}}3^{n_1}1^{k_{11}})}_{l-terms}} \\ &= \prod_{s=1}^{l} DP_4^{(m_s)} \cdot DP_0^{(k_{3s})} \cdot DP_2^{(k_{2s})} \cdot DP_3^{(m_s)} \cdot DP_1^{(k_{1s})}, \end{aligned} \tag{5.52}$$

where

$$DP_\sigma = \left[\frac{\partial \mathbf{Y}_{\sigma+1}}{\partial \mathbf{X}_\sigma}\right]_{6\times 6} = \left[\frac{\partial Y_{(\sigma+1)i}}{\partial X_{\sigma j}}\right]_{6\times 6}. \tag{5.53}$$

for $\sigma = k, k+1, \cdots, k+\Sigma_{s=1}^{l}(m_s+k_{3s}+k_{2s}+n_s+k_{1s})-1$ and all the Jacobian matrix components can be computed through Eq. (5.53). The variational equation for a set of switching points $\{\mathbf{X}_k^*, \mathbf{Y}_{k+1}^*, \cdots, \mathbf{X}^*_{k+\Sigma_{s=1}^{l}(m_s+k_{3s}+k_{2s}+n_s+k_{1s})}\}$ is

$$\Delta \mathbf{Y}_{k+\Sigma_{s=1}^{l}(m_s+k_{3s}+k_{2s}+n_s+k_{1s})} = DP(\mathbf{X}_k^*)\Delta \mathbf{X}_k \tag{5.54}$$

If $\Delta \mathbf{Y}_{k+\Sigma_{s=1}^{l}(m_s+k_{3s}+k_{2s}+n_s+k_{1s})} \equiv \lambda \Delta \mathbf{X}_k$, the Eigenvalues are computed by

$$\left|DP(\mathbf{X}_k^*) - \lambda \mathbf{I}\right| = 0 \tag{5.55}$$

If all $|\lambda_i|<1$ for $(i=1,2,\cdots,6)$, the periodic motion is stable. If one of $|\lambda_i|>1$ for ($i\in\{1,2,\cdots,6\}$), the periodic motion is unstable. If one of $\lambda_i=-1$ and $|\lambda_j|<1$ for ($i,\ j\in\{1,2,3,4,5,6\}$ and $j\neq i$), the period-doubling bifurcation of periodic motion occurs. If one of $\lambda_i=1$ and $|\lambda_j|<1$ for ($i,\ j\in\{1,2,3,4,5,6\}$ and $j\neq i$), the saddle-node bifurcation of the periodic motion occurs. If $|\lambda_{1,2,3,4}|<1$ with the complex Eigenvalues of $|\lambda_{5,6}|=1$, the Neimark bifurcation of the periodic motion occurs. However, the Eigenvalue analysis cannot be used to predict sticking and grazing motions. Both of them should be determined through the normal vector fields, the stick motion is determined by Eq. (5.25) and the grazing bifurcation is determined by Eq. (5.30) or (5.32).

5.5. Illustrations of Same Excitations

Setting $e^{(1)}=e^{(2)}=e$, the bifurcation scenario of varying e for the Fermi oscillator is presented in Figure 5.8. The parameters are $Q^{(1)}=Q^{(2)}=20.0,\quad \Omega^{(1)}=\Omega^{(2)}=10.0,$ $m^{(1)}=m^{(2)}=1.0,\quad m^{(3)}=0.01,\quad h=0.5,\quad k^{(1)}=k^{(2)}=80.0,\quad c^{(1)}=c^{(2)}=0.1$. The switching displacement, velocity, and phase of the particle versus the restitution coefficient e are shown in Figure 5.8 (a)-(c), respectively. The acronyms ‘PD’ and ‘GB’ indicate the period-doubling bifurcation and grazing bifurcation respectively. The shaded areas are for regions of periodic motion. For $e\in(0,0.5)$, the impact charter with stick motion exists. In other words, the particle is undergoing the periodic motion where stick motion with top or bottom oscillator occurs after impact chattering. At $e=0.323, 0.336, 0.371,$ and 0.5, grazing bifurcations occur and the current periodic motion disappears, and another different periodic motion starts.

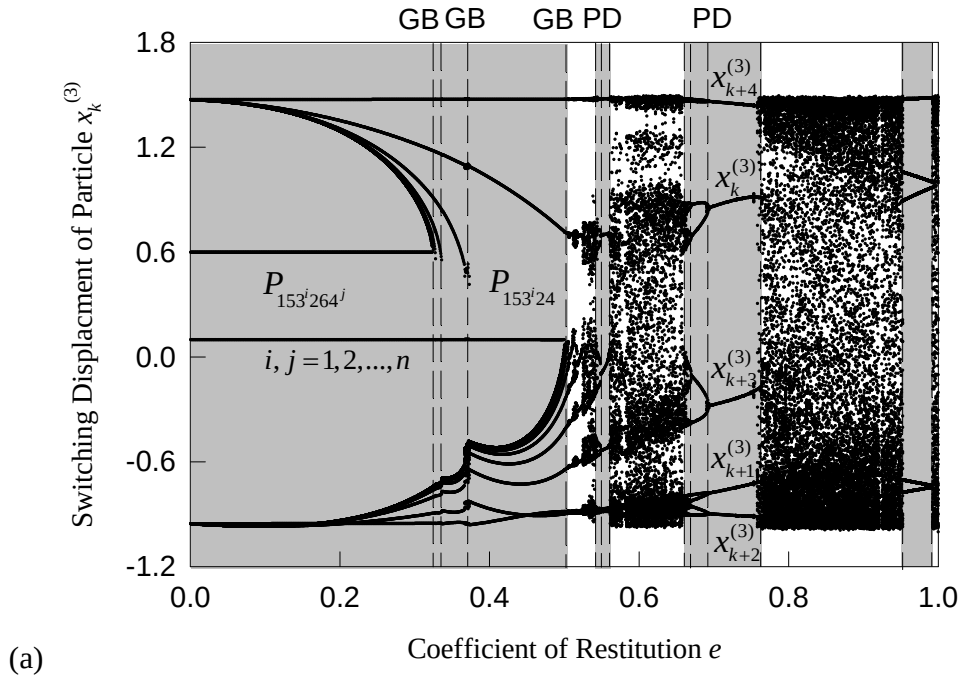

(a)

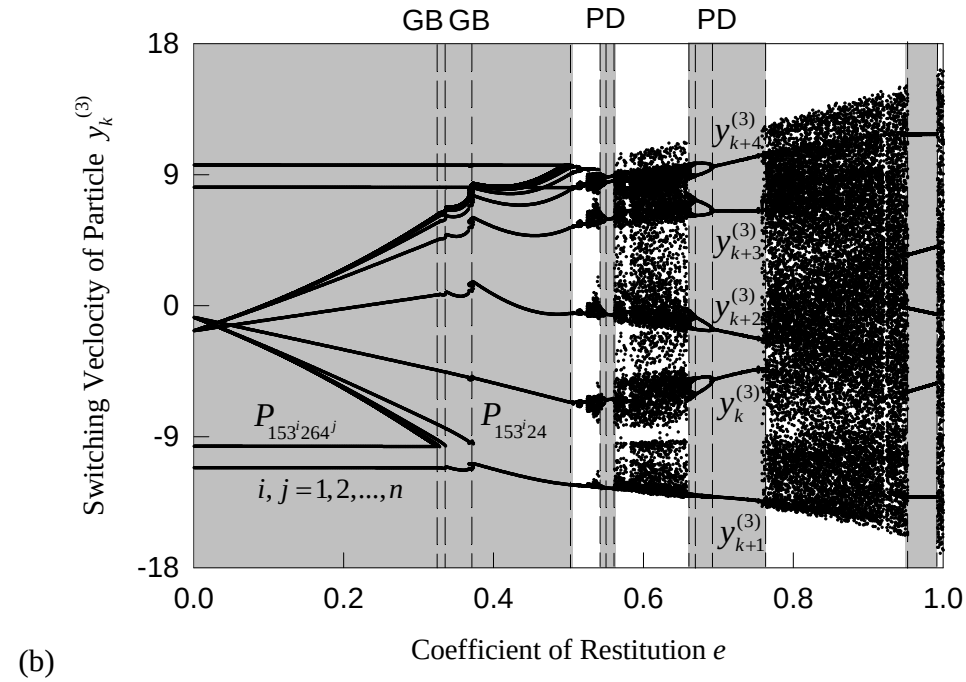

(b)

Figure 5.8: Bifurcation scenario of varying restitution coefficient e: (a) displacement of particle, (b) velocity of particle, and (c) switching phase. ($Q^{(1)} = Q^{(2)} = 20.0$, $\Omega^{(1)} = \Omega^{(2)} = 10.0$, $m^{(1)} = m^{(2)} = 1.0$, $m^{(3)} = 0.01$, $h = 0.5$, $k^{(1)} = k^{(2)} = 80.0$, $c^{(1)} = c^{(2)} = 0.1$).

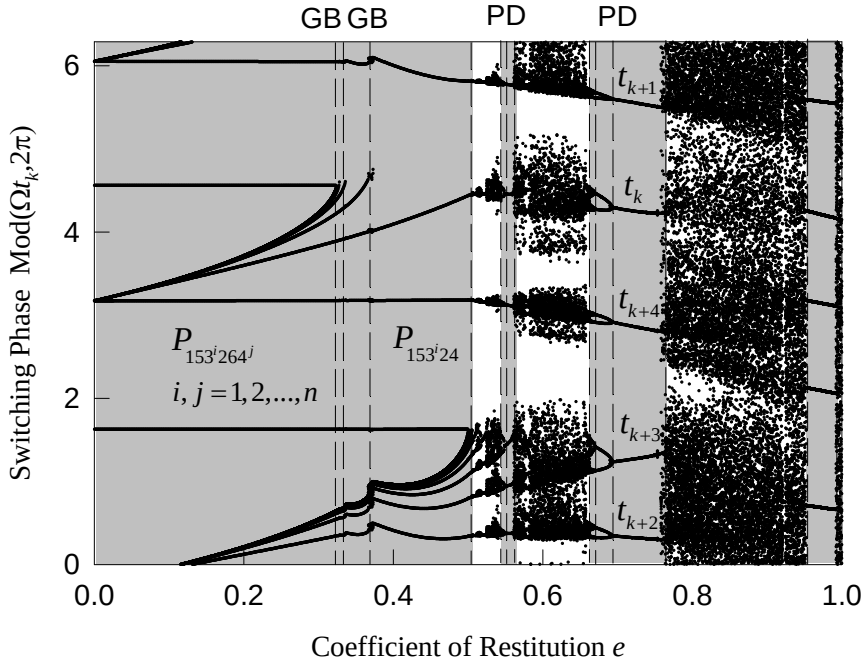

(c)

Figure 5.8 Continue

With the same parameters the analytical prediction of periodic motions with varying the restitution coefficient e is presented in Figure 5.9. The displacement, velocity, and switching phase of the particle versus the coefficient of restitution e are shown in Figure 5.9 (a), (b), and (c), respectively. The solid and dotted curves represent the stable and unstable solutions, respectively. The acronyms 'PD', 'SN', 'NB', and 'GB' represent the period doubling bifurcation, saddle node bifurcation, Neimark bifurcation, and grazing bifurcation, respectively. For $e \in (0.0, 0.5)$, the periodic motion of impact chatter with stick exists. At $e = 0.323, 0.336, 0.371, \text{and } 0.5$, the grazing bifurcations occur. For $e \in (0.5396, 0.5522)$, the stable periodic motion of $P_{(3^3241)^2}$ exists. At $e = 0.5396$, a period doubling bifurcation occurs. At $e = 0.5522$, a saddle-node bifurcation of periodic motion of $P_{(3^3241)^2}$ occurs and this periodic motion disappears. Such a value of $e = 0.5522$ is also for period-doubling of periodic motion of

P_{3^3241}. The stable periodic motion of P_{3^3241} exists in the region of $e \in (0.5522, 0.5626)$. At $e = 0.5626$, the saddle-node bifurcation of periodic motion of P_{3^3241} occurs, and such a periodic motion disappears. For $e \in (0.6688, 0.6960)$, the stable periodic motion of $P_{(413^22)^2}$ exists. At $e = 0.6688$, a period doubling bifurcation occurs, and the periodic motion of $P_{(413^22)^2}$ becomes unstable. At $e = 0.6960$, a saddle node bifurcation of periodic motion of $P_{(413^22)^2}$ takes place, and the periodic motion of $P_{(413^22)^2}$ vanishes. However, the periodic motion of P_{413^22} starts; this corresponds to the period doubling bifurcation of P_{413^22} motion, where the motion becomes unstable. The stable periodic motion of P_{413^22} lies in $e \in (0.6960, 0.7668)$. At $e = 0.7668$ the stable periodic motion of P_{413^22} disappears because of the saddle-node bifurcation. Finally, for $e \in (0.9042, 1.0)$, the stable periodic motion of P_{1324^2} is observed. At $e = 0.9042$ and 1, the Neimark bifurcation of the periodic motion of P_{1324^2} takes place. The prediction stops at $e = 1.0$ because the restitution coefficient cannot be greater than one. The real parts, imaginary parts, and magnitudes of the Eigenvalues are also illustrated in Figure 5.9 (d)-(f), respectively.

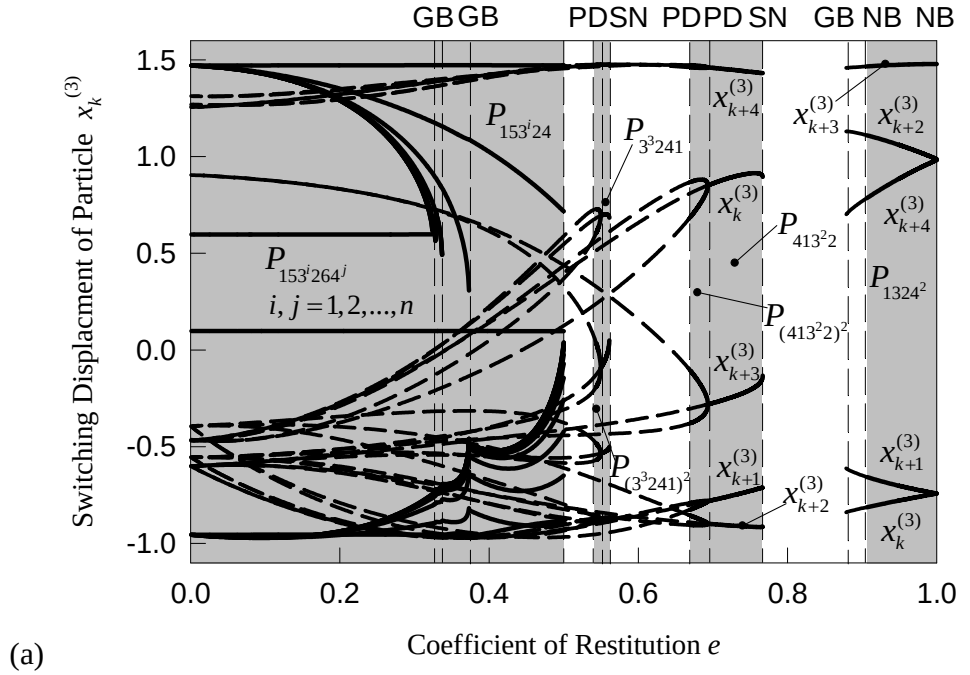

(a)

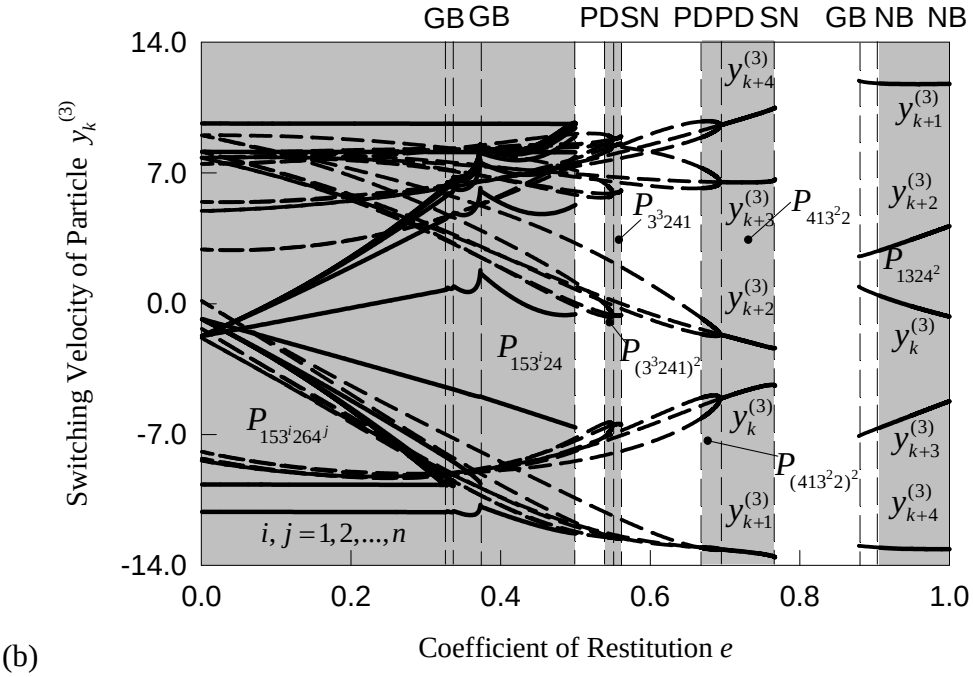

(b)

Figure 5.9: Analytical prediction of varying the excitation amplitude Q : (a) switching displacement of particle, (b) switching velocity of particle; (c) switching phase; (d) real part of eigenvalues, (e) imaginary part of eigenvalues, and (f) magnitude of eigenvalues.
($e^{(1)} = e^{(2)} = 0.6$, $\Omega^{(1)} = \Omega^{(2)} = 10.0$, $m^{(1)} = m^{(2)} = 1.0$, $m^{(3)} = 0.01$, $h = 0.5$, $k^{(1)} = k^{(2)} = 80.0$, $c^{(1)} = c^{(2)} = 0.1$ **).**

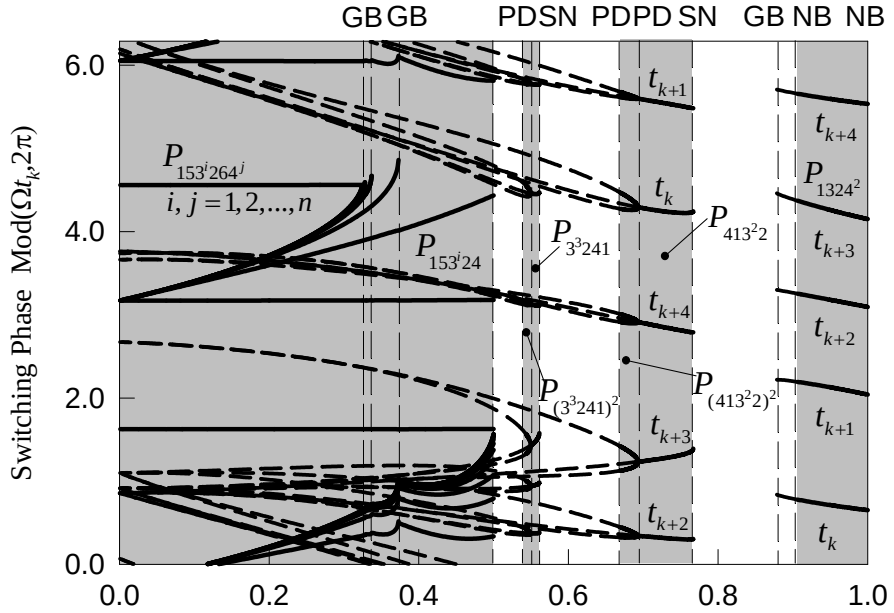

(c)

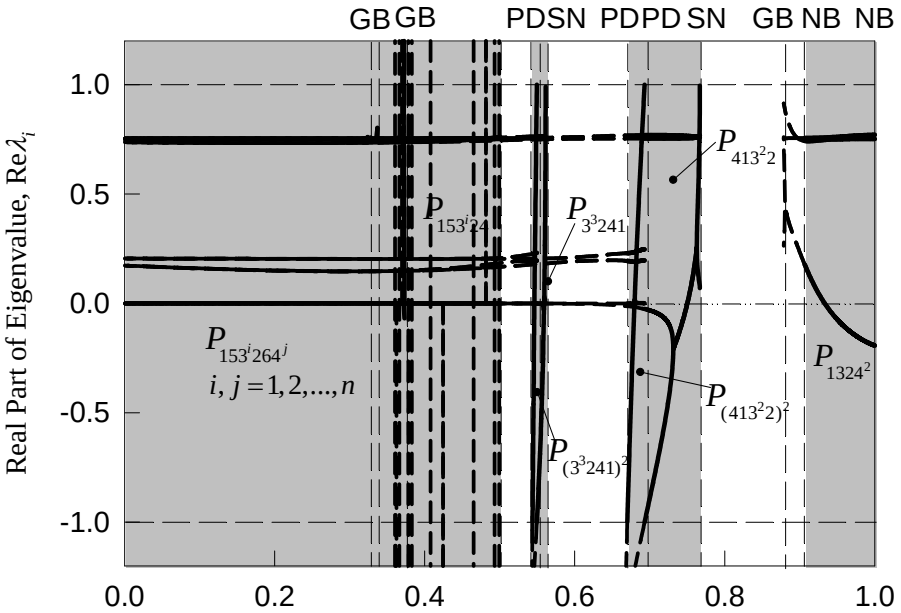

(d)

Figure 5.9 Continue

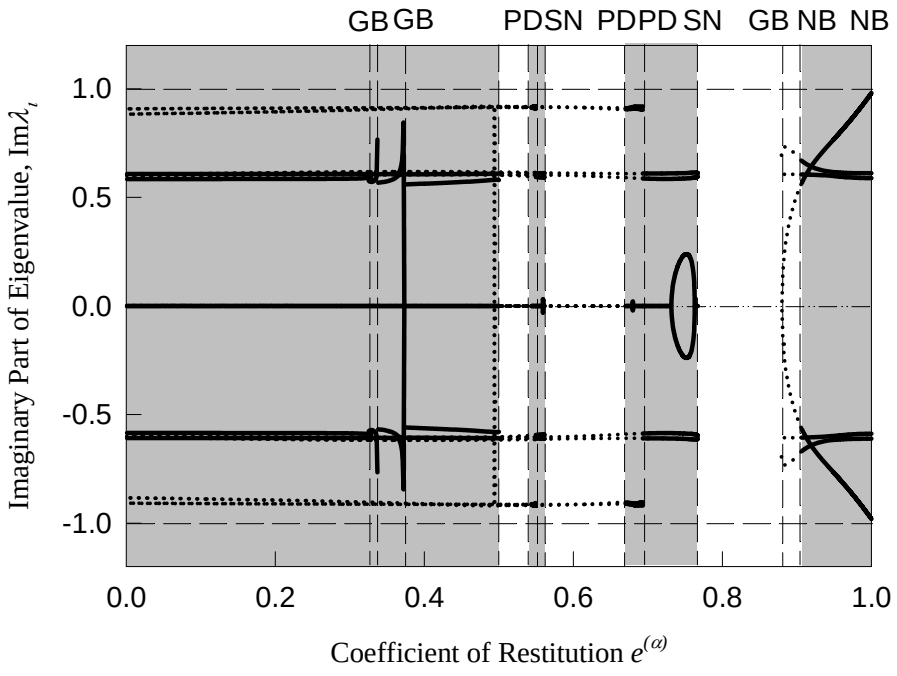

(e)

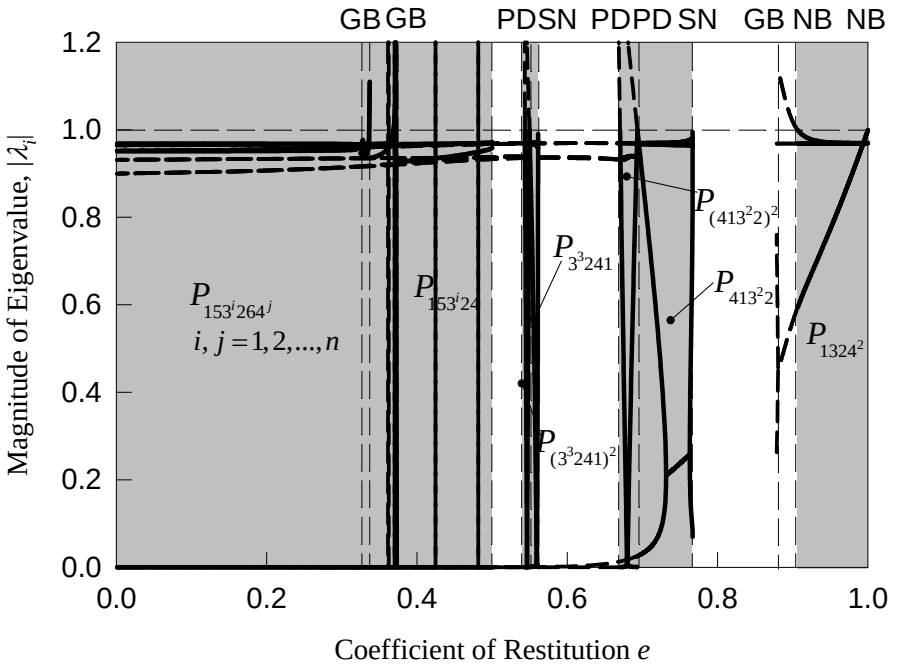

(f)

Figure 5.9 Continue

Using the same parameters, a periodic motion of $P_{153^7264^7}$ is illustrated with $e = 0.2$ in Figure 5.10. The initial conditions are $x_0^{(1)} = 0.79534917$, $\dot{x}_0^{(1)} = -5.49025226$, $x_0^{(2)} = 1.30373854$, $\dot{x}_0^{(2)} = -5.51085936$, $x_0^{(3)} = 1.30373854$, $\dot{x}_0^{(3)} = -5.57828916$ for $t_0 = 0.368919034$. The time histories of displacement and velocity are presented in Figure 5.10 (a) and (b), respectively. The thin solid curves give the motion of the bottom and top oscillators. The thick solid curve depicts the motion of the particle. The shaded area indicates the region of stick motion, and the black circles represent the switching points of the motion. The particle with the top oscillator impact seven times (P_4^7), and then the stick motion is formed with the top oscillator (P_6). After that, the particle will free flight. The particle with the bottom oscillator impacts seven times (P_3^7). After that, the stick motion with the bottom oscillator (P_5) is formed. This forms a complete periodic motion. Discontinuity of the velocities can be observed from Figure 5.10 (b). The velocities of the bottom and top oscillators are very close to each other, and they do not change much after impact because the mass of the particle is chosen to be much smaller than the two oscillators. The corresponding phase portrait of the particle with moving boundaries is presented in Figure 5.10 (c), where the thin solid curves indicates the moving boundaries, and the thick solid curve represents the motion of the particle. The discontinuity due to impacts is also observed from Figure 5.10 (c) for both of the moving boundaries and the motion of the particle. For illustration of the onset and vanishing condition of stick motion, the time histories of acceleration and jerk are presented in Figure 5.10 (d) and (e), respectively. After impacting seven times with the top oscillator, the velocities of particle and top oscillator becomes equal, and the acceleration of the top oscillator is less than the acceleration of the particle ($-g$), thus the onset condition of stick motion with the top oscillator (P_6) are satisfied. Thus, the particle starts to

move together with the top oscillator. This motion will continue until the forces per unit mass (or acceleration) equal to $-g$ again. At the same time, the jerks of the two become greater than zero, which satisfies the vanishing condition of stick motion on top. Thus, the motion relative to P_6 switches into the motion relative to P_2. And then the particle impacts seven times with the bottom oscillator, until the velocity of the particle equal to that of the bottom oscillator, while at the same time, the acceleration of the bottom oscillator is greater than the one of the particle ($-g$); the onset condition of the stick motion on the bottom (P_5) satisfies. Thus, the particle starts moving together with the bottom oscillator until their acceleration equals to $-g$ again; meanwhile, their jerk is less than zero, which satisfies the vanishing condition of the stick motion on bottom. Thus the particle separates with the bottom oscillator and switches into the free flight motion in domain Ω_1 until the particle impacts with the top oscillator again.

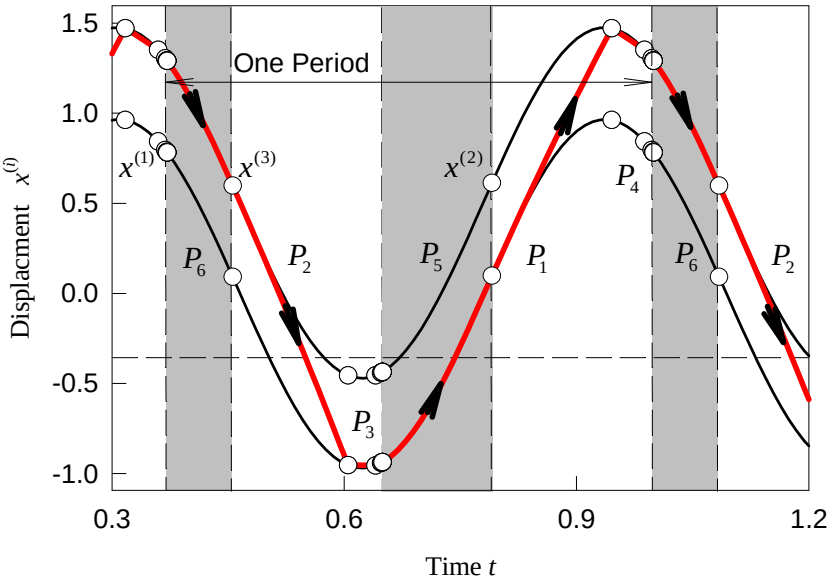

(a)

Figure 5.10: Periodic motion $P_{253^7164^7}$: (a) displacement time history, (b) velocity time history, (c) trajectory of particle with moving boundaries. ($Q^{(1)} = Q^{(2)} = 20.0$, $h = 0.5$, $\Omega^{(1)} = \Omega^{(2)} = 10.0$, $m^{(1)} = m^{(2)} = 1.0$, $m^{(3)} = 0.01$, $e^{(1)} = e^{(2)} = 0.2$, $k^{(1)} = k^{(2)} = 80.0$, $c^{(1)} = c^{(2)} = 0.1$). Initial conditions $x_0^{(1)} = 0.79534917$, $\dot{x}_0^{(1)} = -5.49025226$, $x_0^{(2)} = 1.30373854$, $\dot{x}_0^{(2)} = -5.51085936$, $x_0^{(3)} = 1.30373854$, $\dot{x}_0^{(3)} = -5.57828916$, $t_0 = 0.368919034$.

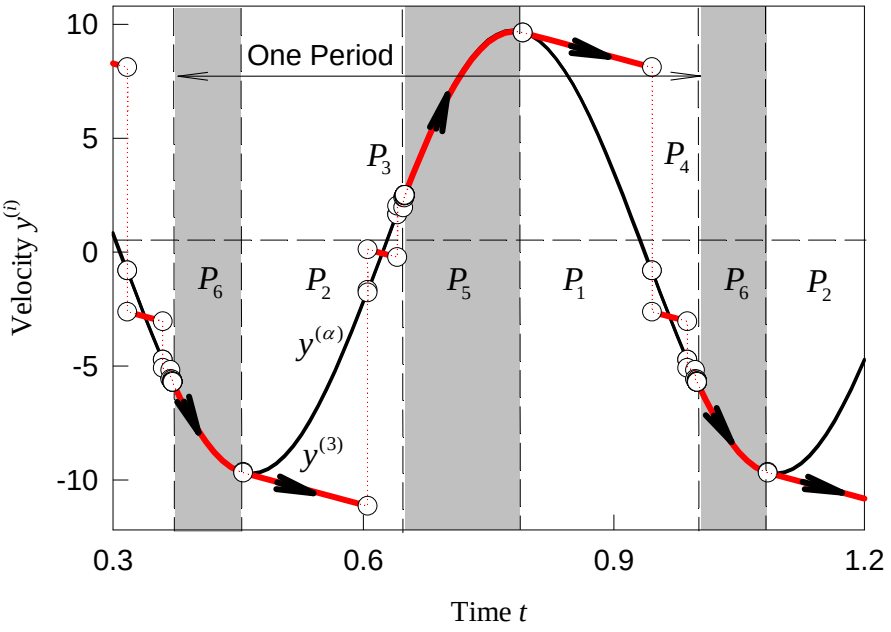

(b)

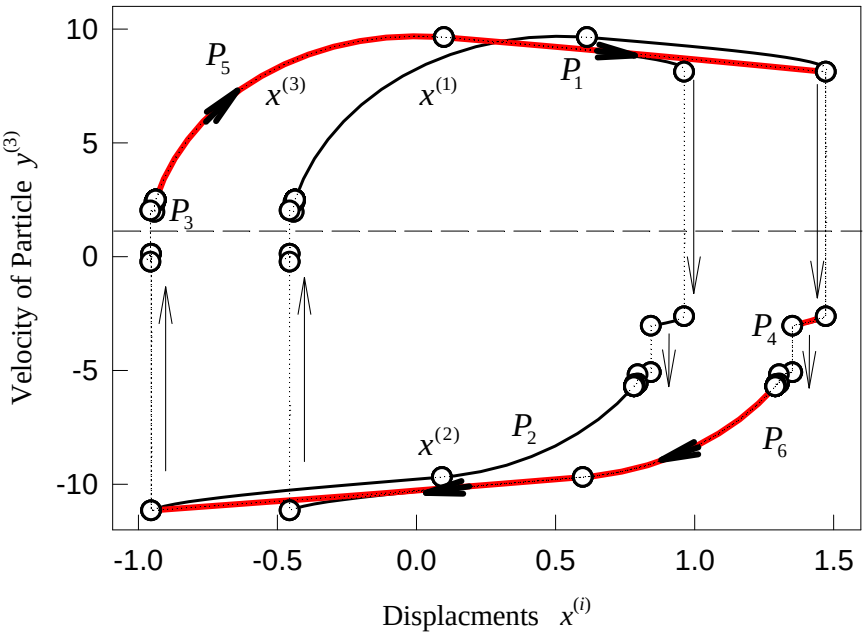

(c)

Figure 5.10 Continue

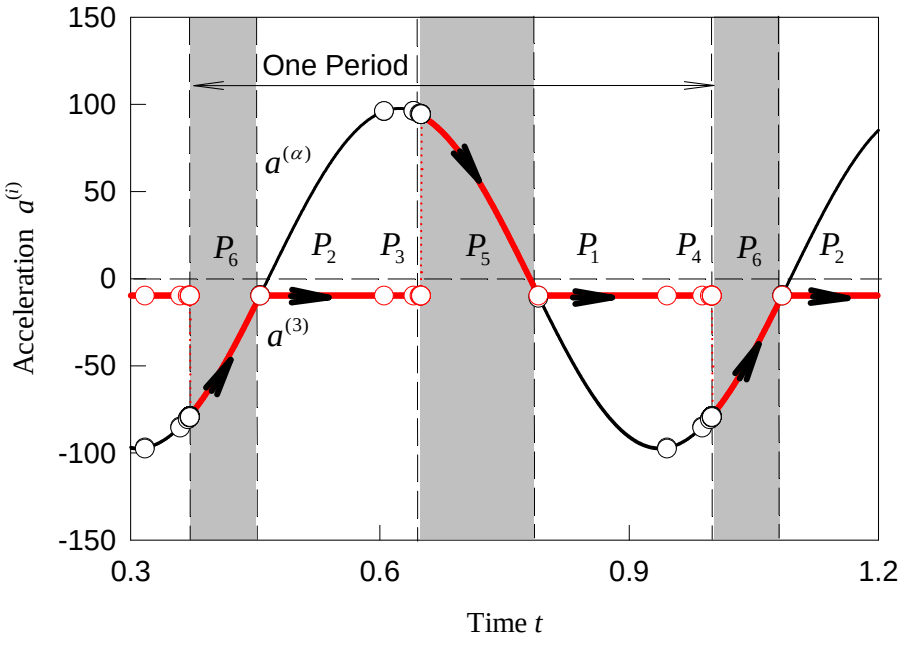

(d)

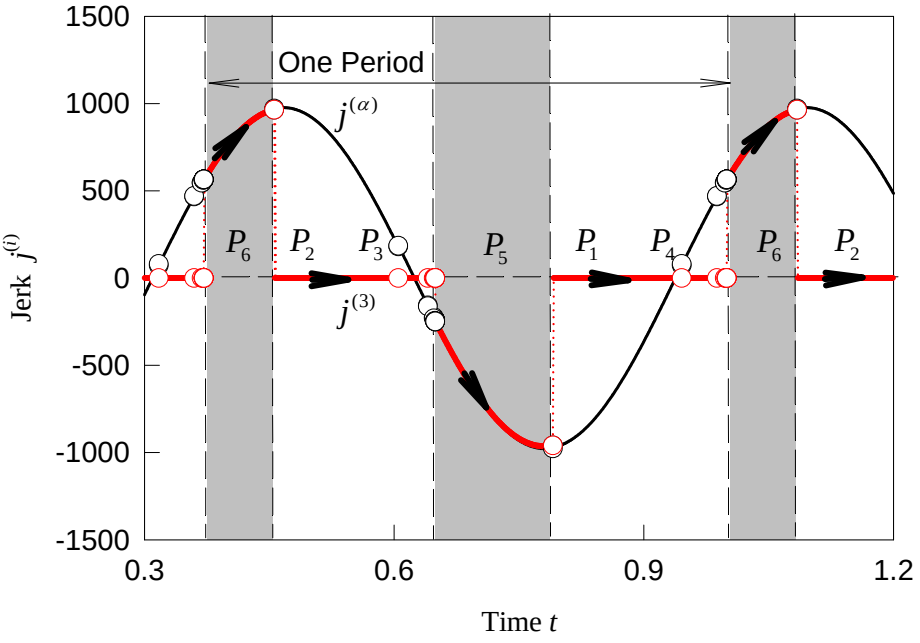

(e)

Figure 5.10 Continue

The simulation of a chaotic motion is given in Figure 5.11 under the same parameters with $e = 0.9$. The initial conditions are $x_0^{(1)} = 0.941968193$, $\dot{x}_0^{(1)} = 1.86109613$, $x_0^{(2)} = 1.45709118$, $\dot{x}_0^{(2)} = 1.82722043$, $x_0^{(3)} = 1.45709118$, and $\dot{x}_0^{(3)} = 10.7134817$ for $t_0 = 0.289711605$. The time histories of displacements and velocities are presented in Figure 5.11 (a) and (b), respectively. The thin solid curves depict the motions of the bottom and top oscillators, and the thick solid curve represents the motion of particle. The switching sections for the particle, bottom and top oscillators in phase plane are also shown in Figure 5.11 (c) and (d), respectively. Furthermore, the switching sections for particle's displacement and velocity versus switching phase are presented in Figure 5.11 (e) and (f), respectively. The invariant set of such a chaotic motion is presented.

Two Neimark bifurcations with $e = 0.9067$ and $e = 1.0$ coexist with chaotic motions. The two Neimark bifurcations have five strange attractors with a very small scale of 10^{-3}. To illustrate the Neimark bifurcations, a switching sections of the Neimark bifurcation with $e = 0.9067$ is carried out as shown in Figure 5.12. The input data for initial conditions of the simulation are listed in Table 5.1, and the center location of each of the five strange attractors are listed in Table 5.2. The overall view of the five strange attractors of the Neimark bifurcation is presented in Figure 5.12 (a). The acronyms SA_i indicates the ith strange attractor with $i = 1, 2..., 5$. A zoomed view of each strange attractor in Poincare mapping sections is then presented in Figure 5.12 (b)-(f), respectively. The flutter oscillation zone can be observed from each of the zoomed plots.

Table 5.1: Input data for switching sections of the Neimark bifurcation

(x_k, y_k)	(x_k, y_k)
$(-0.812857, -13.0542)$	$(-0.813146, -13.0542)$
$(-0.812946, -13.0542)$	$(-0.813217, -13.0542)$
$(-0.813038, -13.0542)$	

Table 5.2: Center location of each strange attractor

Strange Attractors	Center Locations (x_k, y_k)
SA_1	$(1.1098, 11.7877)$
SA_2	$(1.4663, 2.8409)$
SA_3	$(0.7860, -6.6410)$
SA_4	$(-0.6566, 0.4242)$
SA_5	$(-0.8129, -13.0542)$

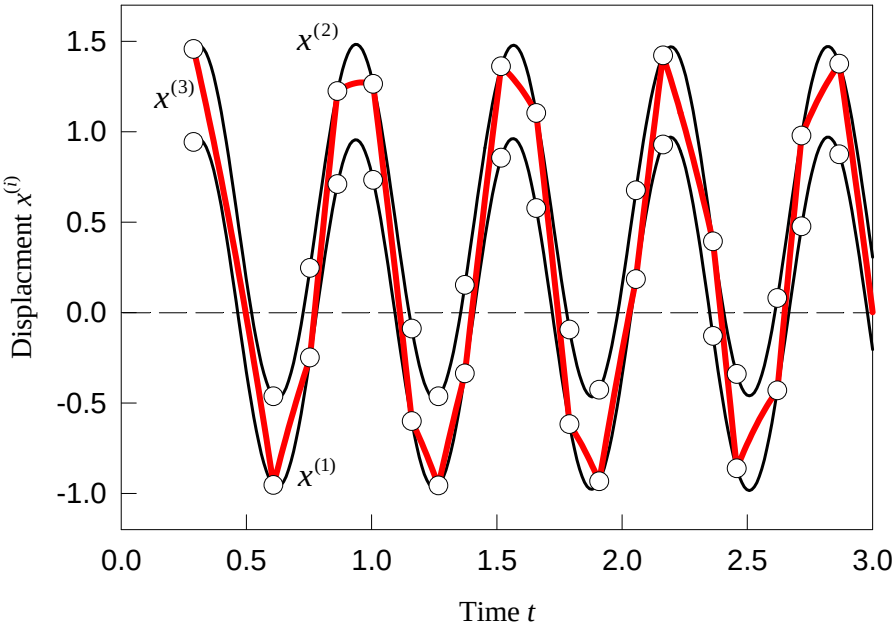

(a)

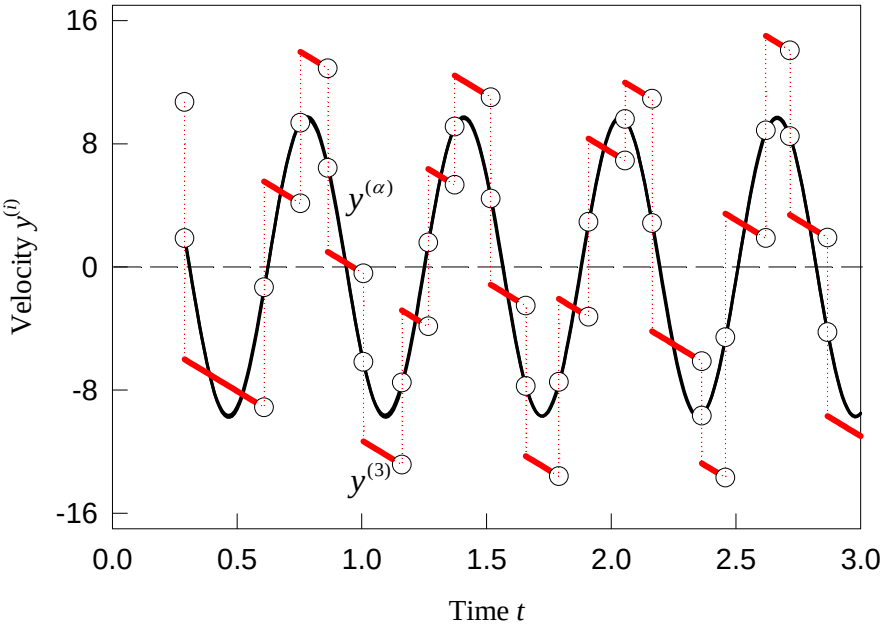

(b)

Figure 5.11: Chaotic motion: (a) time history of displacement, (b) time history of velocity, (c) switching sections of $(x_k^{(3)}, y_k^{(3)})$**, (d) switching sections of** $(x_k^{(\alpha)}, y_k^{(\alpha)})$**, (e) switching section of** $(x_k^{(3)}, \mathrm{mod}(\Omega t_k, 2\pi))$**, and (f) switching section of** $(y_k^{(3)}, \mathrm{mod}(\Omega t_k, 2\pi))$**.** ($Q^{(1)} = Q^{(2)} = 20.0$, $\Omega^{(1)} = \Omega^{(2)} = 10.0$, $m^{(1)} = m^{(2)} = 1.0$, $m^{(3)} = 0.01$, $e = 0.9$, $h = 0.5$, $k^{(1)} = k^{(2)} = 80.0$, $c^{(1)} = c^{(2)} = 0.1$)**. The initial conditions are** $x_0^{(1)} = 0.941968193$, $\dot{x}_0^{(1)} = 1.86109613$, $x_0^{(2)} = 1.45709118$, $\dot{x}_0^{(2)} = 1.82722043$, $x_0^{(3)} = 1.45709118$, **and** $\dot{x}_0^{(3)} = 10.7134817$ **for** $t_0 = 0.289711605$**.**

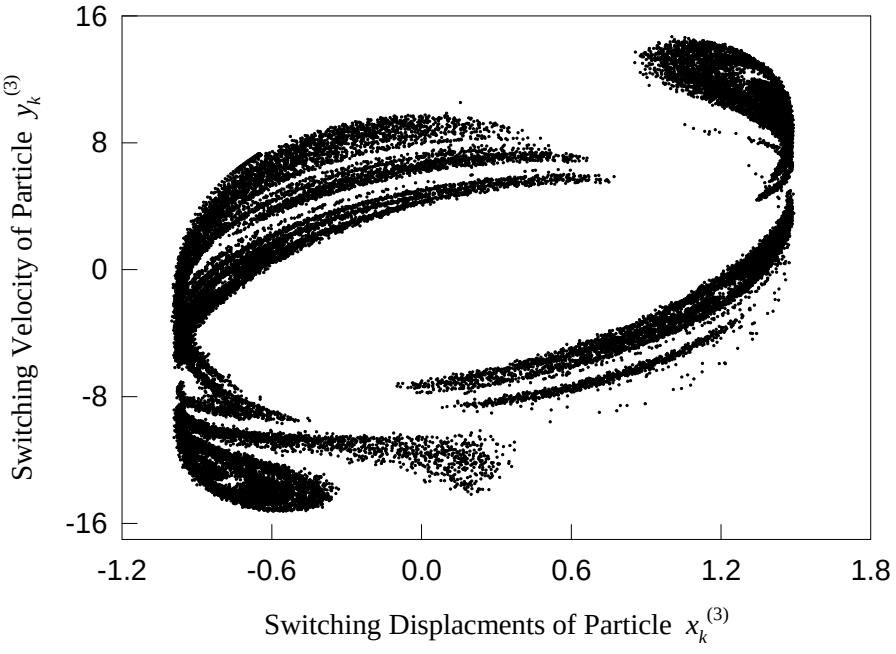

(c)

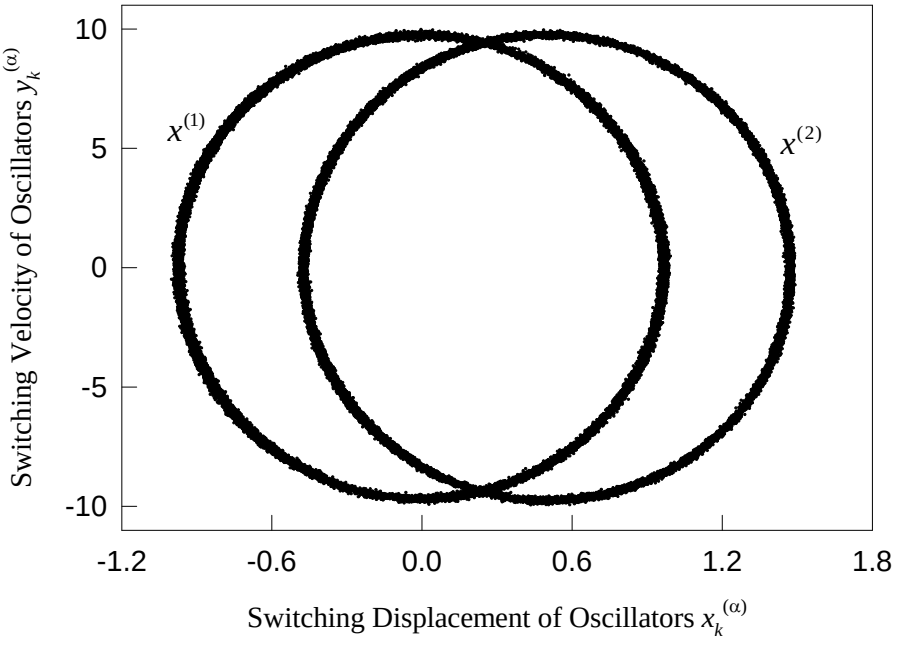

(d)

Figure 5.11 Continue

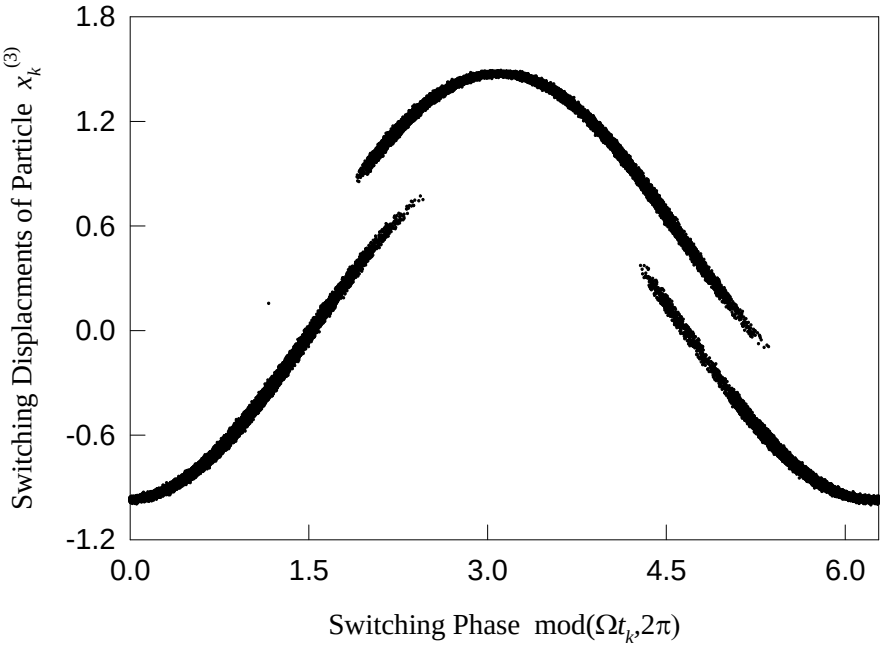

(e)

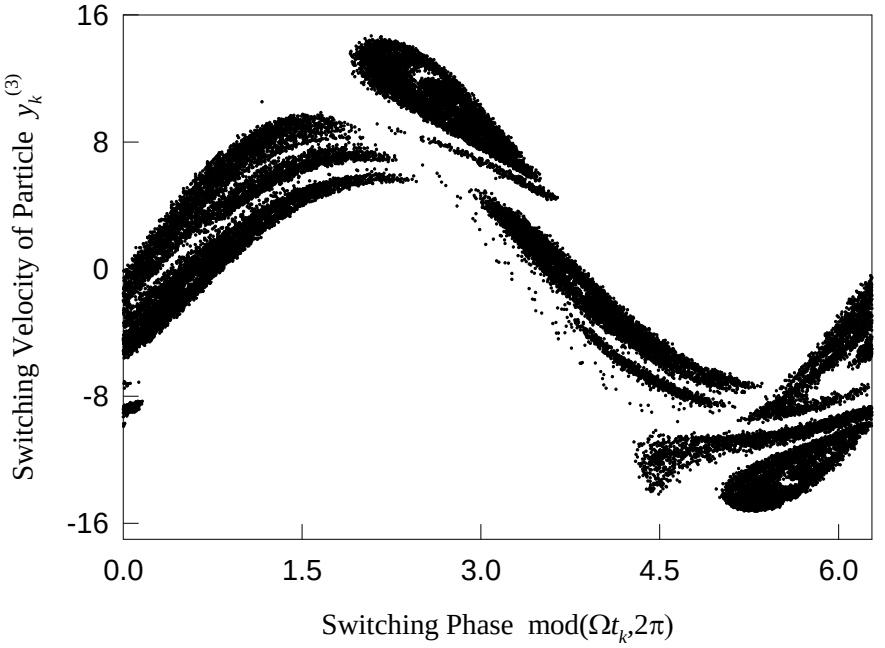

(f)

Figure 5.11 Continue

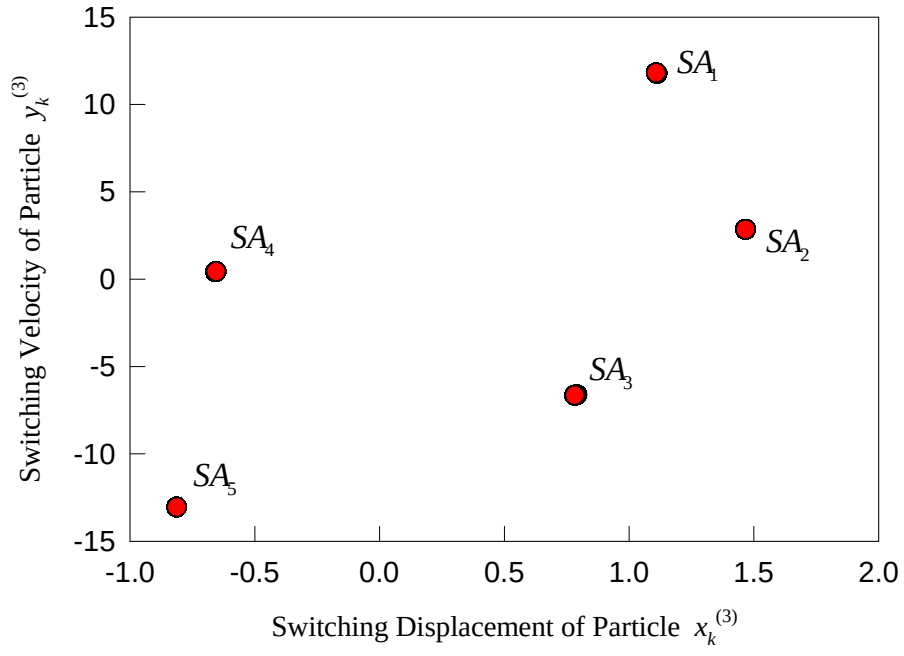

(a)

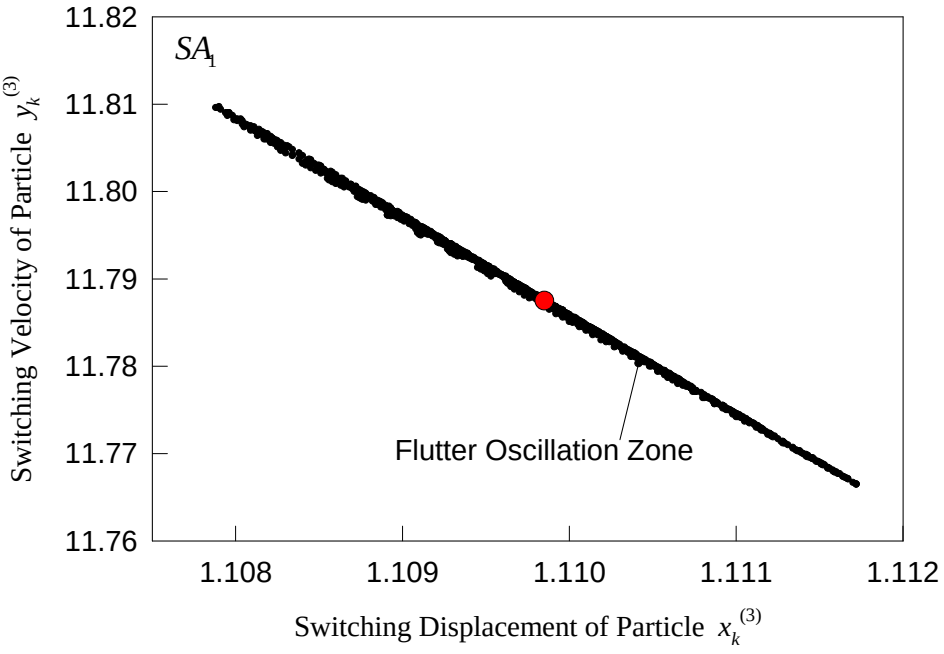

(b)

Figure 5.12: Switching sections for the Neimark bifurcation of particle at $e = 0.9067$: (a) global view and (b)-(f) local view (SA_1 , SA_2 , SA_3 , SA_4 , and SA_5) ($Q^{(1)} = Q^{(2)} = 20.0$, $\Omega^{(1)} = \Omega^{(2)} = 10.0$, $m^{(1)} = m^{(2)} = 1.0$, $m^{(3)} = 0.01$, $h = 0.5$, $k^{(1)} = k^{(2)} = 80.0$, $c^{(1)} = c^{(2)} = 0.1$).

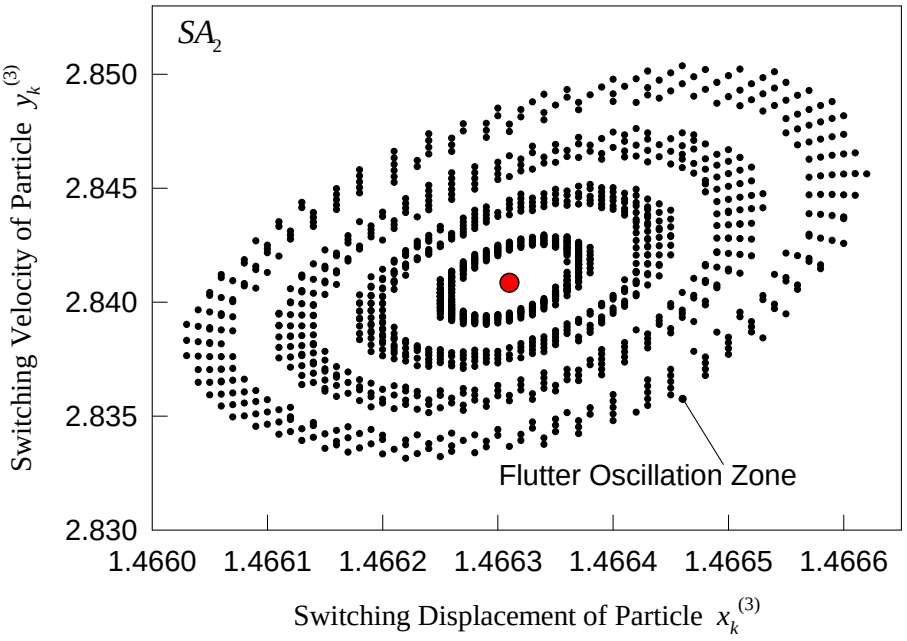

(c)

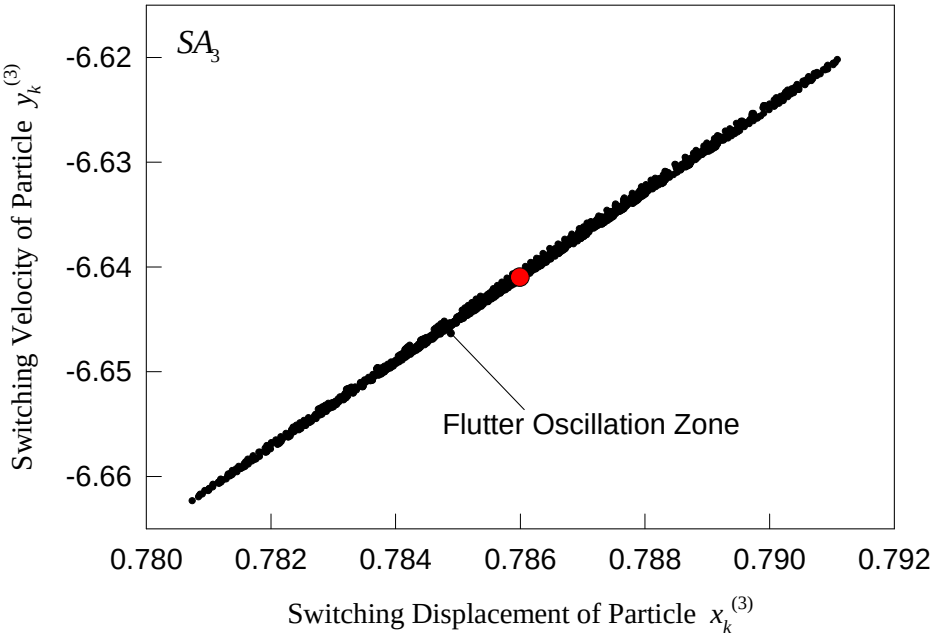

(d)

Figure 5.12 Continue

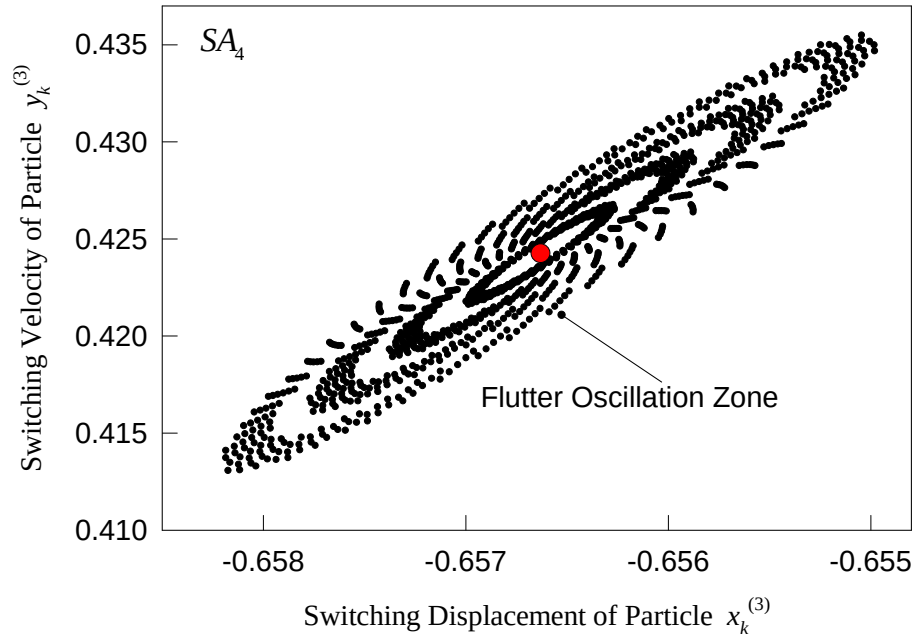

(e)

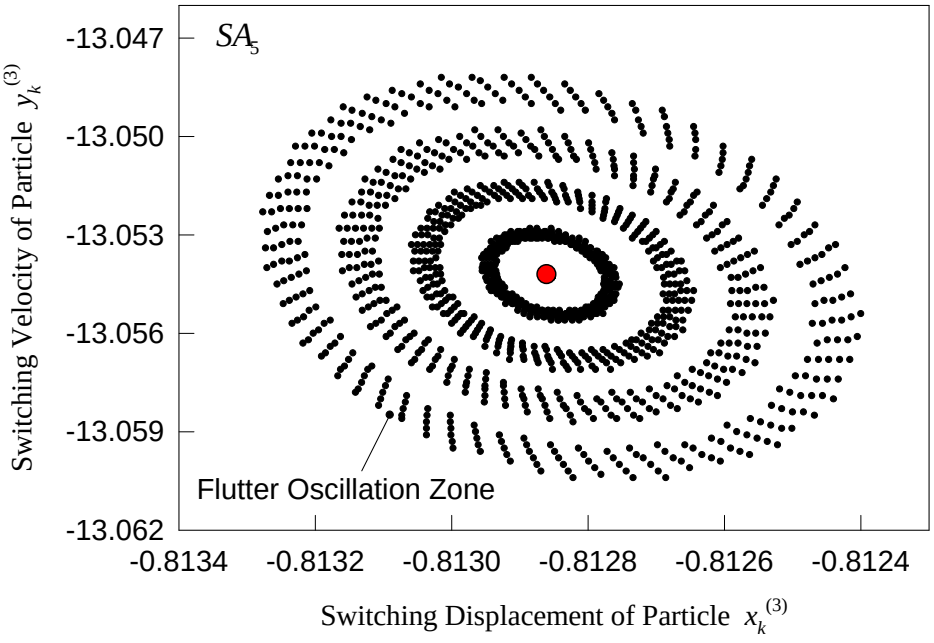

(f)

Figure 5.12 Continue

5.6. Illustration of Different Excitations

When the two excitations of the Fermi Oscillator are different with each other, the behavior of such system will become more complicated comparing to when the excitations are the same. Consider a relatively simpler case, where the two excitations are proportional to each other. Illustrations of the motions in such a system are presented in this section.

With e representing the value of both $e^{(1)}$ and $e^{(2)}$, the bifurcation scenario of varying restitution coefficient e is presented in Fig.2. The parameters are given as $Q^{(1)} = Q^{(2)} = 20.0$, $\Omega^{(1)} = 28.0$, $\Omega^{(2)} = 14.0$, $m^{(1)} = 1.0$, $m^{(2)} = 2.0$, $m^{(3)} = 0.01$, $h = 0.5$, $k^{(1)} = k^{(2)} = 20.0$, $c^{(1)} = 0.8$, $c^{(2)} = 1.2$. The switching displacement, velocity, and phase of the particle versus restitution coefficient e are shown in Fig.2 (a)-(c), respectively. The switching phase is calculated base on $\Omega = \min(\Omega^{(1)}, \Omega^{(2)})$. The symbol 'PD', 'SN', and 'GB' means period-doubling bifurcation, saddle node bifurcation, and grazing bifurcation, respectively. The shaded areas indicate the regions of periodic motion. For $e \in (0, 0.25)$, the complex periodic motion with impact chatter and stick exists. Also for $e \in (0, 0.75)$, there are no interactions between the particle and the top oscillator, which means that the particle only impact or stick with the bottom oscillator. Thus for $e \in (0.32, 0.36)$, the periodic motion of P_{3^2} exists, where the particle only impact with the bottom oscillator. And when $e > 0.9$ the periodic motion where the particle interacts with both top and bottom oscillators exists. Mapping structure is observed as $P_{(21)^2}$ for $e \in (0.9, 0.94)$, and $P_{(21)^4}$ for $e \in (0.94, 1.0)$.

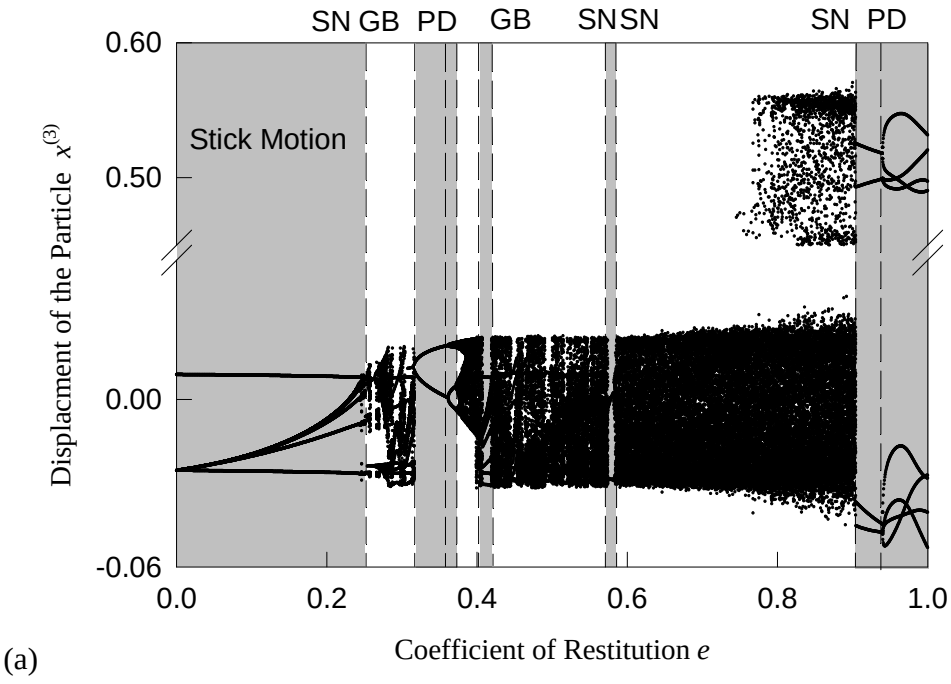

(a)

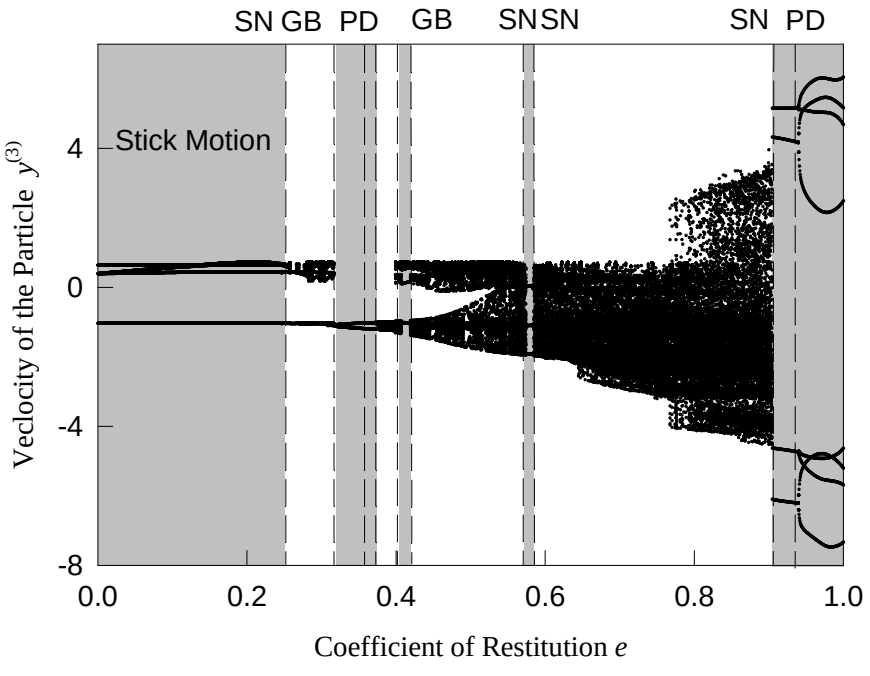

(b)

Figure 5.13: Bifurcation scenario of varying the restitution coefficient e : (a) Displacement of the particle. (b) Velocity of the particle. (c) Switching phase. ($Q^{(1)} = Q^{(2)} = 20.0$, $\Omega^{(1)} = 28.0$, $\Omega^{(2)} = 14.0$, $m^{(1)} = 1.0$, $m^{(2)} = 2.0$, $m^{(3)} = 0.01$, $h = 0.5$, $k^{(1)} = k^{(2)} = 20.0$, $c^{(1)} = 0.8, c^{(2)} = 1.2$).

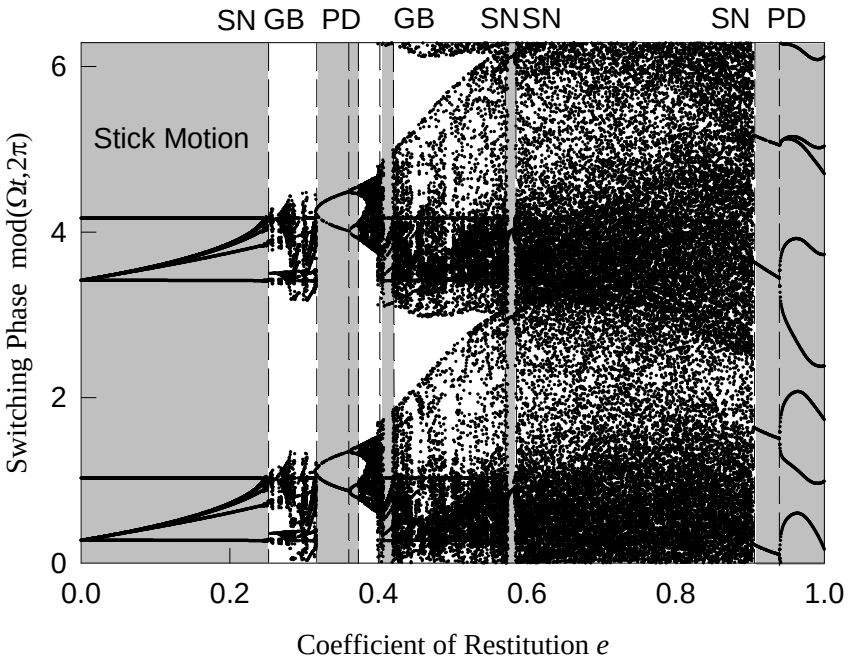

(c)

Figure 5.13 Continue

Using the same parameters, the corresponding analytical predictions are presented in Figure 5.14 with eigenvalue stability analysis. The switching displacement of the particle, switching velocity of the particle, and switching phase are presented in Figure 5.14 (a)-(c), respectively. For stability analysis, the real part, imaginary part, and magnitude of the eigenvalues are presented in Figure 5.14 (d)-(f), respectively. The solid curves indicate stable periodic motions, while the dotted curves represent the unstable ones. The symbols 'PD', 'SN', 'GB', and 'NB', represent period doubling bifurcation, saddle node bifurcation, grazing bifurcation, and Neimark bifurcation, respectively. For $e \in (0, 0.271)$, the periodic motion with impact chatter and stick exist with mapping structure $P_{(3^i5)^2}$ ($i = 1, 2, ..., n$), which disappears at $e = 0.271$. The symmetric periodic motion of mapping structure P_{3^2} exist in the range of $e \in (0.202, 0.312)$. This motion disappears at the saddle node bifurcation at $e = 0.202$, and become unstable after the saddle node bifurcation at $e = 0.312$. After the saddle node

bifurcation the asymmetric P_{3^2} periodic motion exists for $e \in (0.312, 0.358)$, which becomes unstable after the period doubling bifurcation at $e = 0.358$. Furthermore, the P_{3^4} periodic motion exits in the range of $e \in (0.358, 0.373)$, and it becomes unstable after the period doubling bifurcation at $e = 0.373$. The asymmetric coexisting motions of P_{3^2} and P_{3^4} are cause by the motion of the top oscillator, and can be observed only from the switching phase presented in Figure 5.14 (c), where the asymmetric coexisting motion is highlighted by red color. For $e \in (0.329, 0.421)$, more complex periodic motion with impact chatters and stick exists; this motion disappears with Neimark bifurcations at both $e = 0.329$ and $e = 0.421$. The symmetric P_{3^6} periodic motion exists for $e \in (0.571, 0.583)$, which disappears at the saddle node bifurcation at $e = 0.571$ and becomes unstable after the saddle node bifurcation at $e = 0.583$. Furthermore, The periodic motion of mapping structure $P_{(21)^2}$ exists in the range $e \in (0.86, 0.94)$. This motion stops at the saddle node bifurcation at $e = 0.86$, and becomes unstable at the period doubling bifurcation at $e = 0.94$. After the period doubling, the $P_{(21)^4}$ starts and continue existing until $e = 1.0$.

Choosing $e = 0.2$ from the prediction above, a periodic motion with impact chatter and stick is simulated. The mapping structure is $P_{(3^85)^2}$ as shown in Fig. 4. The initial conditions are $t_0 = 0.267608808$, $x_0^{(1)} = -0.0127506415$, $\dot{x}_0^{(1)} = 0.684250836$, $x_0^{(2)} = 0.542754638$, $\dot{x}_0^{(2)} = -0.455089481$, $x_0^{(3)} = -0.0127506415$, $\dot{x}_0^{(3)} = 0.733437531$. The time histories of displacement and velocity are presented in Fig. 4 (a) and (b), respectively. The thin solid black curves represent the motion of the bottom and top oscillators, and the thick solid red curve indicates the motion of the particle. The shaded area indicates the stick motion, and the black

circles represent the switching points. For this periodic motion, the particle is not interacting with the top oscillator, and the particle has formed a local periodic motion with the bottom oscillator before $t = 0.5$. However, since the periodicity of the whole system is considered, the global periodic motion goes until $t \approx 0.716$ to form a complete period. Discontinuity of the velocities can be observed from Fig. 4 (b). The corresponding phase portrait of the particle with moving boundaries is presented in Fig. 4 (c), where the dashed curves indicates the moving boundaries and the solid curve represents the motion of the particle. The discontinuity due to impacts is observed from Fig. 4 (c) for both of the moving boundaries and the motion of the particle.

Furthermore, with $e = 0.95$ from the analytical prediction, the simulation of another periodic motion without stick is given in Fig. 5 similarly. The initial conditions are given as $t_0 = 0.0870359397$, $x_0^{(1)} = \text{-}3.65132893\text{e-}3$, $\dot{x}_0^{(1)} = 0.400570796$, $x_0^{(2)} = 0.50227033$, $\dot{x}_0^{(2)} = 0.760171041$, $x_0^{(3)} = 0.50227033$, $\dot{x}_0^{(3)} = \text{-}4.03349807$. The time histories of displacements and velocities are presented in Fig. 5 (a) and (b), respectively, where the dashed curves indicate the motion of the bottom and top oscillators and solid curve represents the motion of the particles. The mapping structure of this periodic motion is given as $P_{(21)^4}$. This time, the particle is interacting with both the top and bottom oscillators. Furthermore, the phase portrait for the motion of the particle and moving boundaries are also illustrated in Fig. 5 (c), where again discontinuity of the system caused by impacts can be observed.

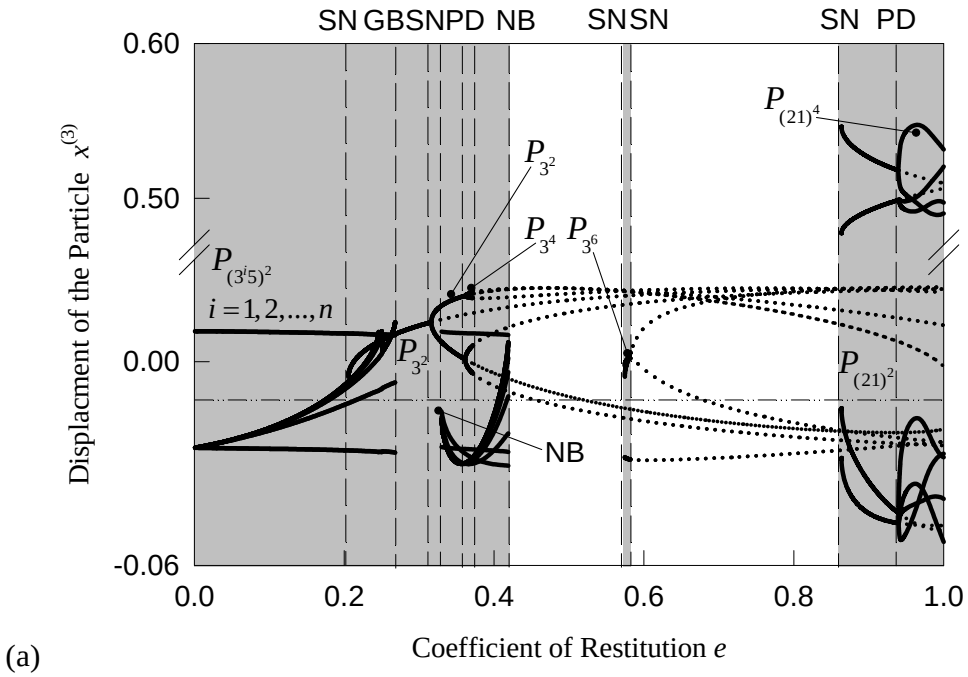

(a)

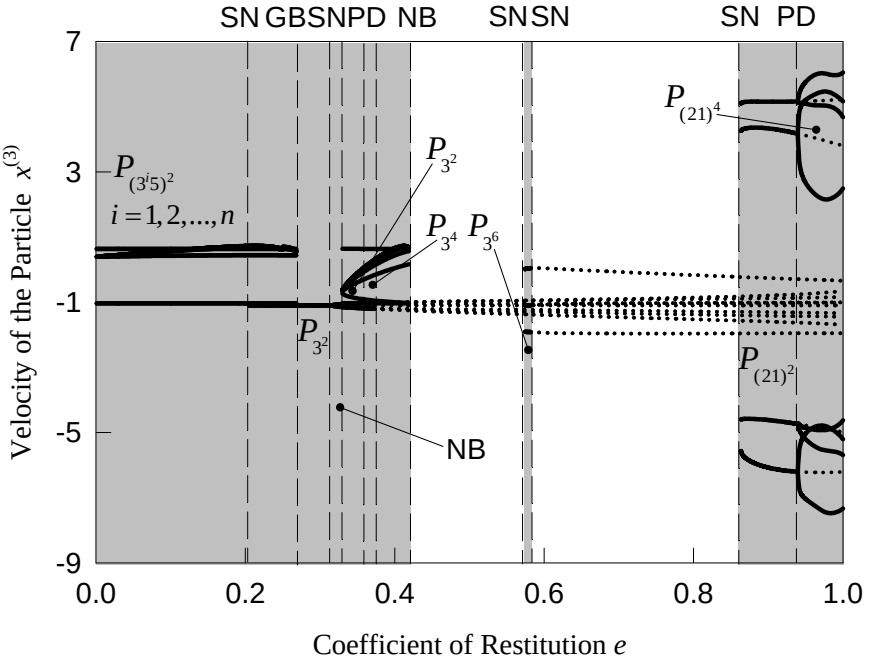

(b)

Figure 5.14: Analytical prediction of varying the restitution coefficient e: (a) Displacement of the particle. (b) Velocity of the particle. (c) Switching phase. (d) Real part of eigenvalues. (e) Imaginary part of eigenvalues. (f) Magnitude of eigenvalues. ($Q^{(1)} = Q^{(2)} = 20.0$, $\Omega^{(1)} = 28.0$, $\Omega^{(2)} = 14.0$, $m^{(1)} = 1.0$, $m^{(2)} = 2.0$, $m^{(3)} = 0.01$, $h = 0.5$, $k^{(1)} = k^{(2)} = 20.0$, $c^{(1)} = 0.8$, $c^{(2)} = 1.2$).

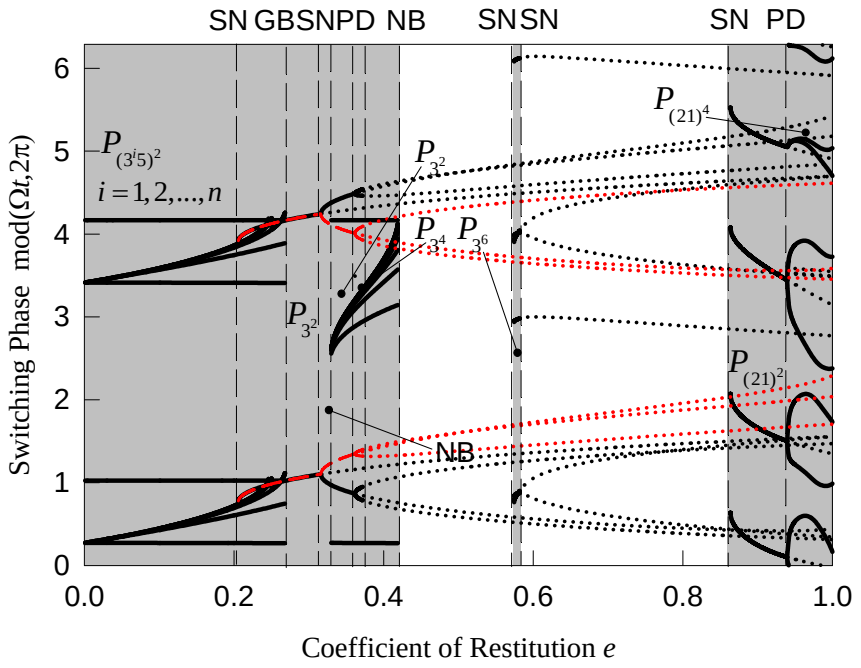

(c)

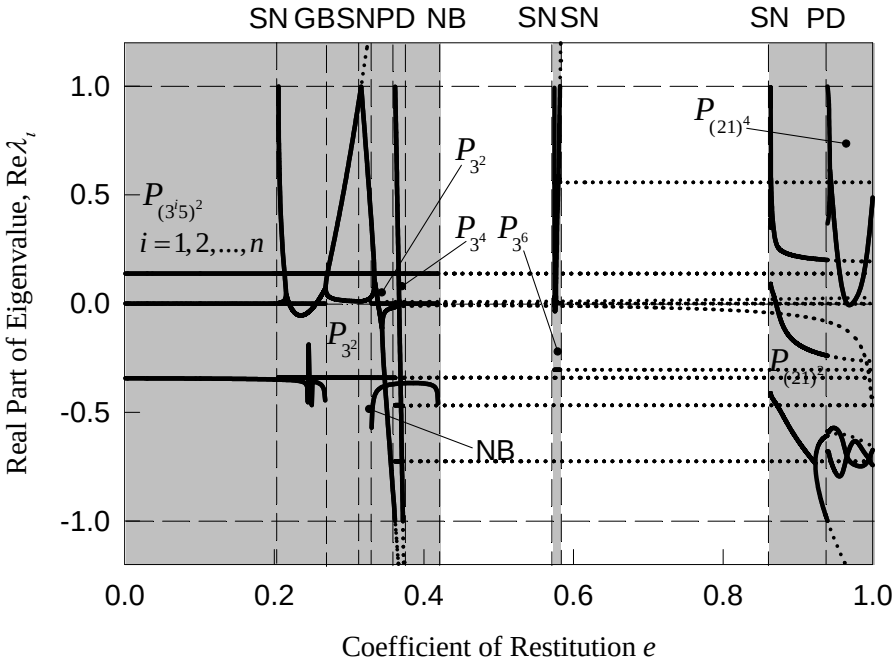

(d)

Figure 5.14 Continue

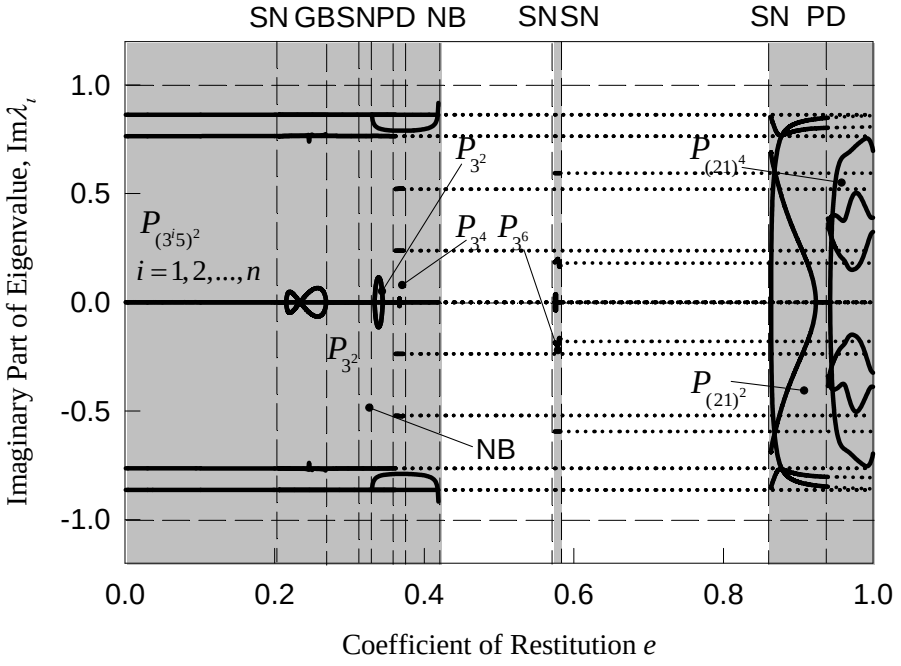

(e)

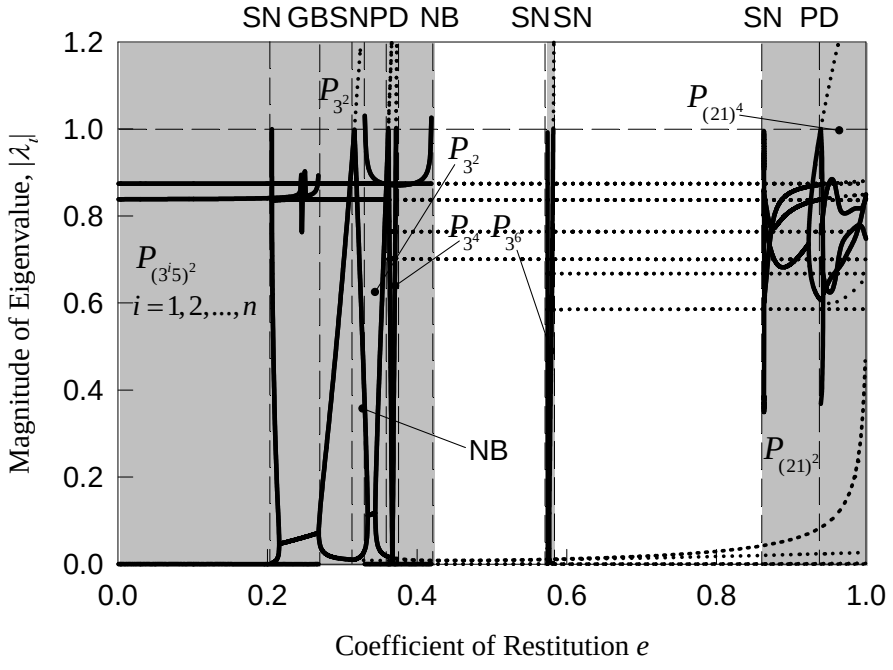

(f)

Figure 5.14 Continue

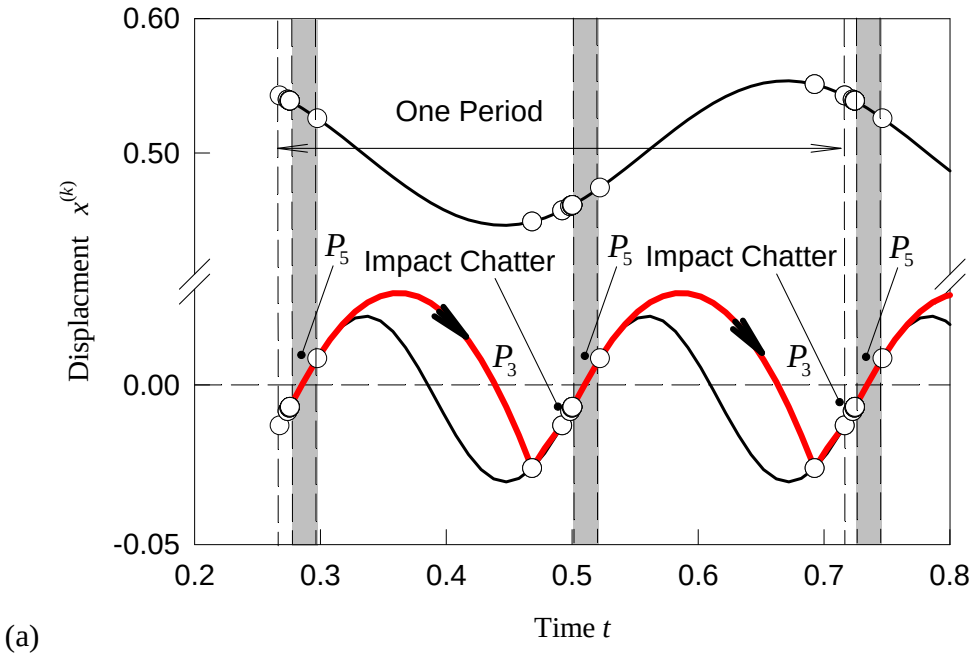

(a)

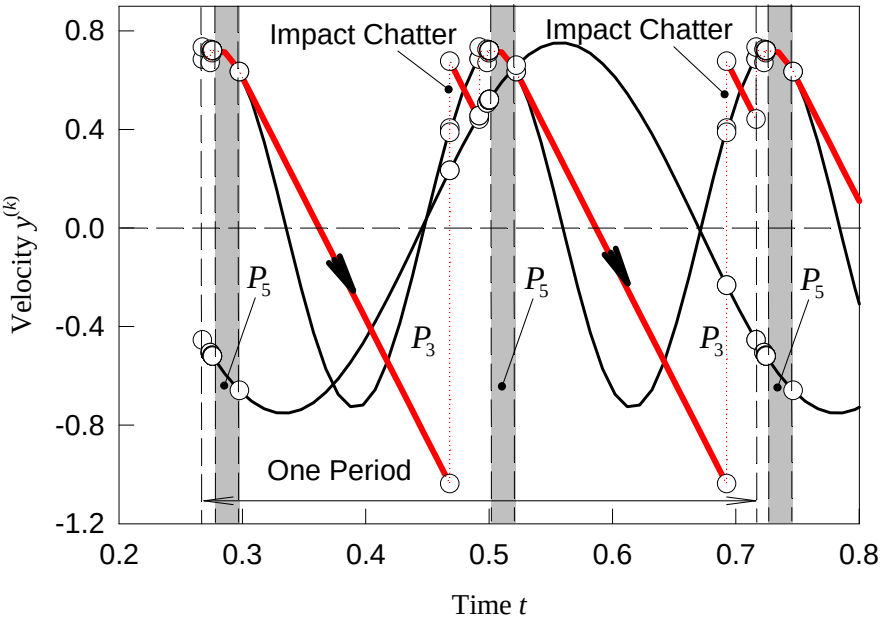

(b)

Figure 5.15: Periodic motion with a mapping structure of $P_{(3^8 5)^2}$: (a) displacement time history. (b) Velocity time history. (c) Phase portrait of the motion of the particle with moving boundaries. ($Q^{(1)} = Q^{(2)} = 20.0,\ h = 0.5,\ m^{(1)} = 1.0, m^{(2)} = 2.0,\ m^{(3)} = 0.01,$ $e^{(1)} = e^{(2)} = 0.2,\ k^{(1)} = k^{(2)} = 20.0, c^{(1)} = 0.8, c^{(2)} = 1.2, \Omega^{(1)} = 28.0, \Omega^{(2)} = 14.0$). The initial conditions are: $t_0 = 0.267608808, x_0^{(1)} = -0.0127506415, \dot{x}_0^{(1)} = 0.684250836,$ $x_0^{(2)} = 0.542754638, \dot{x}_0^{(2)} = -0.455089481,\ \ x_0^{(3)} = -0.0127506415,\ \ \dot{x}_0^{(3)} = 0.733437531.$

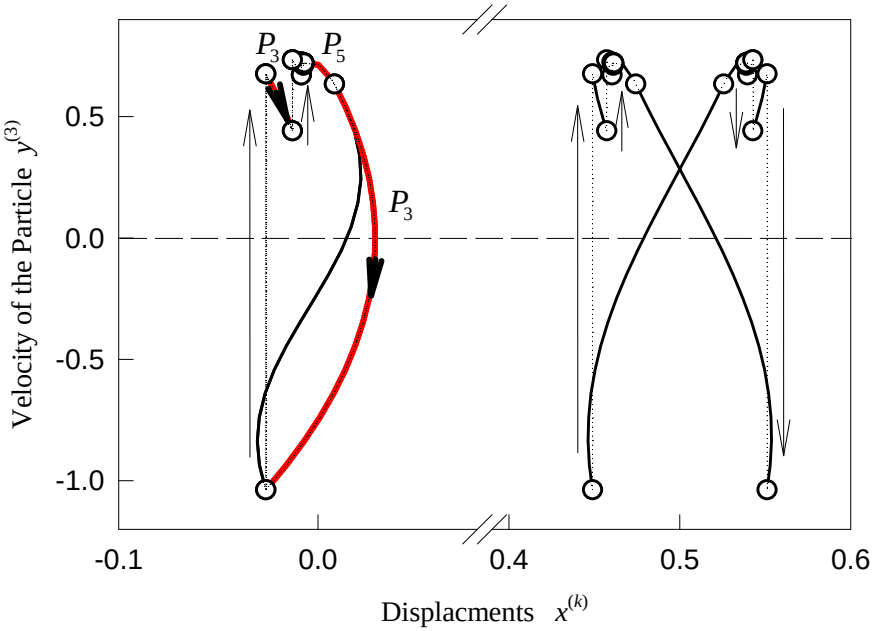

(c)

Figure 5.15 Continue

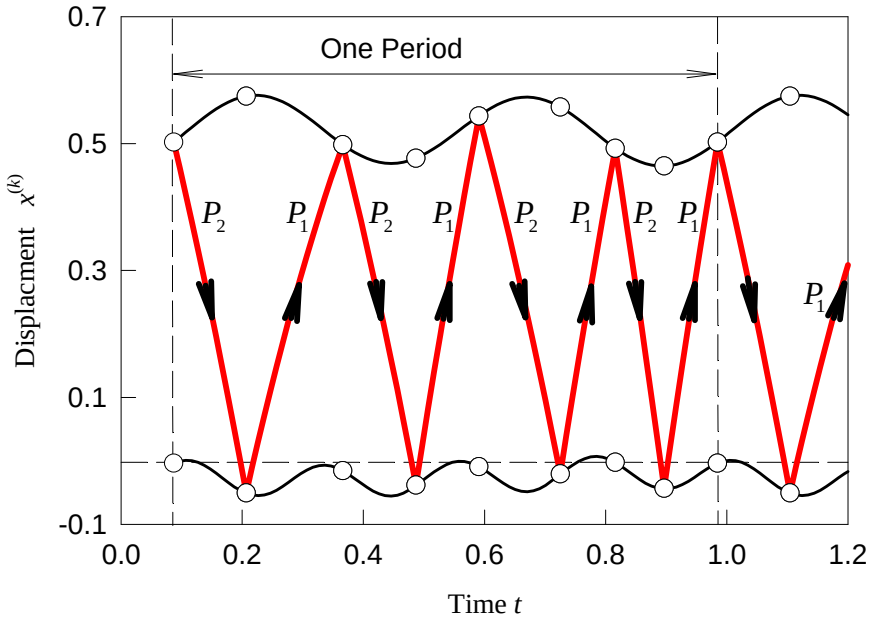

(a)

Figure 5.16: Periodic motion of the mapping structure $P_{(21)^4}$: (a) Displacement time history. (b) Velocity time history. (c) Phase portrait of the motion of the particle and the moving boundaries. ($Q^{(1)} = Q^{(2)} = 20.0,\quad m^{(1)} = 1.0,\quad m^{(2)} = 2.0,\quad m^{(3)} = 0.01,$ $e^{(1)} = e^{(2)} = 0.95, h = 0.5, k^{(1)} = k^{(2)} = 20.0, c^{(1)} = 0.8, c^{(2)} = 1.2, \Omega^{(1)} = 28.0, \Omega^{(2)} = 14.0$ **). The initial conditions are** $t_0 = 0.0870359397$, $x_0^{(1)} =$ -3.65132893e-3, $\dot{x}_0^{(1)} = 0.400570796$, $x_0^{(2)} = 0.50227033$, $\dot{x}_0^{(2)} = 0.760171041$, $x_0^{(3)} = 0.50227033$, $\dot{x}_0^{(3)} =$ -4.03349807.

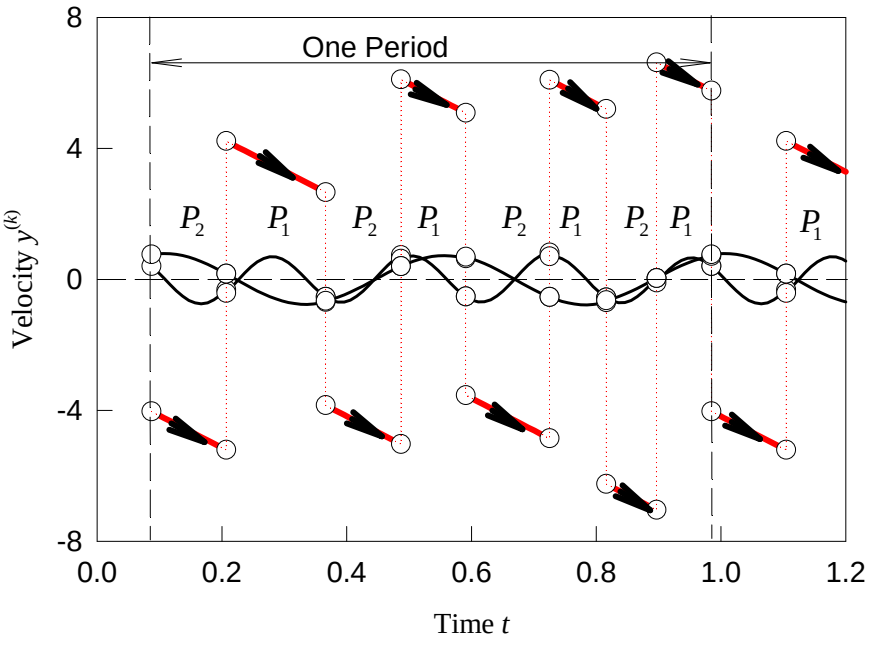

(b)

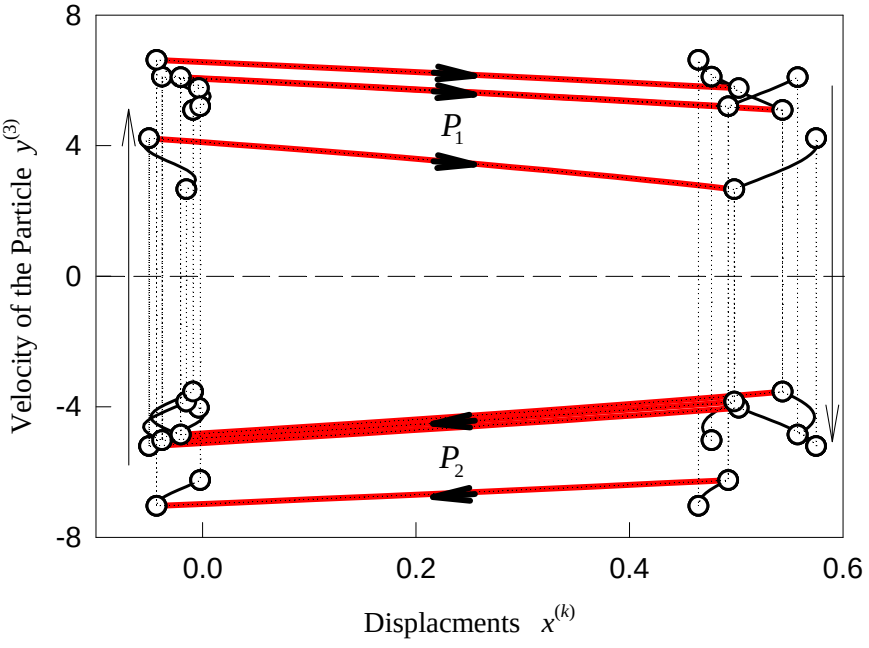

(c)

Figure 5.16 Continue

5.7. Conclusions

In this chapter, the switchability and bifurcation of motions in a dual-excited Fermi acceleration oscillator with same and different oscillation was investigated. Bifurcation scenarios are presented numerically for both same and different excitations. Corresponding analytical predictions of the stable and unstable periodic motions with a given mapping structures were provided with eigenvalues stability analysis. Then, simulations of periodic and chaotic motions in such oscillators were illustrated for both same and different excitations. For same excitations, the switching sections of existing Neimark bifurcations were illustrated; and a detailed parameter map was presented to demonstrate the effect of parameter change on different types of motions.

REFERENCES

Bapat, C. (1988). Impact-pair under periodic excitation. *Journal of Sound and Vibration, 120,* 53-61.

Bapat, C. (1995). The general motion of an inclined impact damper with friction. *Journal of Sound and Vibration, 184*, 417-427.

Bapat, C., & Popplewell, N. (1983). Stable periodic motions of an impact-pair. *Journal of Sound and Vibration, 87*, 19-40.

Barroso, J., Carneiro, M., & Macau, E. (2009). Bouncing ball problem: stability of the periodic modes. *Physical Review E, 79*(5), 026206/1-026206/10.

Bouchet, F. (2004). Minimal stochastic model for Fermi's acceleration. *Physical Review Letters, 92*(4), 040601(1-4).

Curry, J. (1979). On the Henon Transformation. *Communications in Mathematical Physics, 68*, 129-140.

Cvitanovic, P., Gunaratne, G., & Procaccia, I. (1988). Topological and metric properties of Henon-type strange attractors. *Physical Review A, 38*(3), 1503-1520.

Everson, R. (1986). Chaotic dynamics of a bouncing ball. *Physica D: Nonlinear Phenomena, 19*(3), 355-383.

Fermi, E. (1949). On the origin of the cosmic radiation. *Physical review, 75*(8), 1169-1174.

Gallas, J. (1993). Structure of the Parameter Space of the Henon Map. *Physical Review Letters, 70*(18), 2714-2717.

Giusepponi, S., Marchesoni, F., & and Borromeio, M. (2005). Randomness in the bouncing ball dynamics. *Physica A, 351*, 143-158.

Gonchenko, S., Gonchenko, V., & Tatjer, J. (2007). Bifurcations of Three-Dimensional Diffeomorphisms with Non-Simple Quadratic Homoclinic Tangencies and Generalized Henon Maps. *Regular and Chaotic Dynamics, 12*(2), 233-266.

Gonchenko, S., Meiss, J., & Ovsyannikov, I. (2006). Chaotic Dynamics of Three-Dimensional Henon Maps that Originate from a Homoclinic Bifurcation. *Regular and Chaotic Dynamics, 11*(2), 191-212.

Guo, Y., & Luo, A. (2011). Complex motions in a horizontal impact pair with periodic excitation. *Proceeding of the 2011 ASME International Design Engineering Technical Conference & Computers and Information in Engineering Conference, IDETC/CIE2011-47385*.

Han, R., Luo, A., & Deng, W. (1995). Chaotic Motion of a Horizontal Impact Pair. *Journal of Sound and Vibration, 181*(2), 231-250.

Heiman, M., Bajaj, A., & Sherman, P. (1988). Periodic motions and bifurcations in dynamics of an inclined impact pair. *Journal of Sound and Vibration, 124*(1), 55-78.

Heiman, M., Sherman, P., & Bajaj, A. (1987). On the dynamics and stability of an inclined impact pair. *Journal of Sound and Vibration, 114*(3), 535-547.

Henon, M. (1976). A Two-dimensional mapping with a strange attractor. *Communications in Mathematical Physics, 50*, 69-77.

Holmes, P. (1982). The dynamics of repeated impacts with a sinusoidally vibrating table. *Journal of Sound and Vibration , 84*, 173-189.

Joseph, S., Marino, I., & Sanjuan, A. (2012). Effect of the phase on the dynamics of a perturbed bouncing ball system. *Communications in Nonlinear Science and Numerical Simulation, 17*(8), 3279-3286.

Leine, R., & Heimsch, T. (2012). Global uniform symptotic attractive stability of the non-autonomous bouncing ball system. *Physica D, 241*(22), 2029-2041.

Leonel, E., & de Carvalho, R. (2006). A family of crisis in a dissipative Fermi accelerator model. *Physics Letters A, 364*, 475-479.

Leonel, E., & McClintock, P. (2005). A hybrid Fermi-Ulam-bouncer model. *Journal of Physics A: Mathematical and General, 38*, 823-839.

Leonel, E., & Silva, M. (2008). A bouncing ball model with two nonlinearities: a prototype for Fermi acceleration. *Journal of Physics A: Mathematical and Theoretical, 41*, Article ID 015104.

Leonel, E., da Silva, J., & Kamphorst, S. (2004). On the dynamical properties of a Fermi accelerator model. *Physica A, 331*, 435-447.

Lopac, V., & Dananic, V. (1998). Energy conservation and chaos in the gravitationally driven Fermi oscillator. *American Association of Physics Teachers, 66*, 892-902.

Lorenz, E. (2008). Compound Windows of the Henon-Map. *Physica D, 237*, 1689-1704.

Luna-Acosta, G. (1989). Regular and chaotic dynamics of the damped Fermi accelerator. *Physical Review A, 42*, 7155-7162.

Luo, A. (2002). An unsymmetrical motion in a horizontal impact oscillator. *Journal of Vibration and Acoustics, 124*, 420-426.

Luo, A. (2005). A theory for non-smooth dynamic systems on the connectable domains. *Communications in Nonlinear Science and Numerical Simulation, 10*, 1-55.

Luo, A. (2005). The mapping dynamics of periodic motions for a three-piecewise linear system under a periodic excitation. *Journal of Sound and Vibration, 283*, 723-748.

Luo, A. (2006). *Singularity and Dynamics on Discontinuous Vector Fields.* Amsterdam: Elsevier.

Luo, A. (2008). A theory for flow switchability in discontinuous dynamical systems. *Nonlinear Analysis: Hybrid Systems, 2*(4), 1030-1061.

Luo, A. (2009). *Discontinuous Dynamical Systems on Time-varying Domains.* Dordrecht: HEP-Springer.

Luo, A. (2010). A Ying-Yang theory in Nonlinear Discrete Dynamical Systems. *International Journal of Bifurcation and Chaos, 20*(4), 1085-1098.

Luo, A., & Chen, L. (2005). Grazing bifurcation and periodic motion switching in a piecewise linear, impacting oscillator under a periodical excitation. *ASME 2005 International Mechanical Engineering Congress and Exposition (IMECE2005) Design Engineering, Parts A and B*, 913-924.

Luo, A., & Gegg, B. (2006). Stick and non-stick periodic motions in periodically forced oscillators with dry friction. *Journal of Sound and Vibration, 291*, 132-168.

Luo, A., & Guo, Y. (2009). Motion switching and chaos of a particle in a generalized Fermi-acceleration oscillator. *Mathematical Problems in Engineering, Article ID 298906*.

Luo, A., & Guo, Y. (2010). Parameter characteristics for stable and unstable solutions in nonlinear discrete dynamical systems. *International Journal of Bifurcation and Chaos, 20*(10), 3173-3191.

Luo, A., & Guo, Y. (2010). Switchability and bifurcation of motions in a double-excited Fermi-acceleration oscillator. *Proceedings of the 2010 ASME International Mechanical Engineering Congress and Exposition*, IMECE2010-39165.

Luo, A., & Guo, Y. (2010). Switching mechanism and complex motions in an extended Fermi-acceleration oscillator. *Journal of Computational and Nonlinear Dynamics, 5*(4), 1-14.

Luo, A., & Guo, Y. (2011). Bifurcation analysis of a fermi-acceleration oscillator under different excitations. *ASME 2011 International Mechanical Engineering Congress and Exposition, IMECE 2011*(7 (PARTS A AND B)), 45-53.

Luo, A., & Han, R. (1992). Period Doubling and Multifractals in 1-D Iterative Maps. *Chaos, Solitons & Fractals, 2*(3), 335-348.

Luo, A., & Han, R. (1996). The dynamics of a bouncing ball with a sinusoidally vibrating table revisited. *Nonlinear Dynamics, 10*, 1-18.

Luo, A., & O'Connor, D. (2007). Mechanism of impacting chatter with stick in a gear transmission system. *International Journal of Bifurcation, 19*(6), 2093-2105.

Luo, A., & O'Connor, D. (2007). Nonlinear dynamics of a gear transmission system part I: mechanism of impacting chatter with stick. *Proceedings of the ASME 2007 International Design Engineering Technical Conference & Computers and Information in Engineering Conference*, DETC2007-34881.

Luo, A., & O'Connor, D. (2007). Nonlinear dynamics of a gear transmission system part II: periodic impacting chatter and stick. *Proceedings of the ASME 2007 International Design Engineering Technical Conference & Computers and Information in Engineering Conference*, DETC2007-43192.

Luo, A., & O'Connor, D. (2007). Periodic motion and chaos with impacting chatter and stick in a gear transmission system. *International Journal of Bifurcation, 19*(6), 1975-1994.

LuoA.C.J. (2008). Resonance and Chaotic Dynamics. Singapore: Global Transversality World Scientific.

Marotto, F. (1979). Chaotic Behavior in the Henon Mapping. *Communications in Mathematical Physics, 68*, 187-194.

Matyas, L., & Barna, I. (2011). Geometrical origin of chaoticity in the bouncing ball billiard. *Chaos, Solitons & Fractals, 44*(12), 1111-1116.

May, R. (1976). Simple mathematical modals with very complicated dynamics. *Nature, 261*, 459-529.

Naylor, M., & Sanchez, P. (2002). Chaotic dynamics of an air-damped bouncing ball. *Physical Review E, 66*(5), 057201/1-057201/3.

Nordmark, A. (1991). Non-periodic motion caused by grazing incidence in an impact oscillator. *Journal of Sound and Vibration, 145*, 279-297.

Park, J., Wang, S., & Crocker, M. (2009). Mass load resonance of a single unit impact damper caused by impacts and the resulting kinetic energy influx. *Journal of Sound and Vibration, 323*, 877-895.

Pieranski, P. (1988). Direct evidence for the suppression of period doubling in the bouncing-ball model. *Physical Review A , 37*(5), 1782-1785.

Saif, F., Bialynicki-Birula, I., Fortunato, M., & Schleich, W. P. (1998). Fermi accelerator in atom optics. *Physical Review A, 58*, 4779-4783.

Schnurmann, R. (1941). Rate of energy loss from rebounding steel balls. *Proceedings of Physical Society, 53*(6), 662-673.

Shaw, S., & Holmes. (1983). A periodically forced piecewise linear oscillator. *Journal of Sound and Vibration, 90*, 129-155.

Wiesenfeld, K., & Tufillaro, N. (1987). Suppression of period doubling in the dynamics of a bouncing ball. *Physica D: Nonlinear Phenomena, 26*(1-3), 321-335.

Zaslavskii, G., & Chirikov, B. (1964). Fermi acceleration mechanism in the one-dimensional case. *Doklady Akademii Nauk SSSR, 159*, 306-309.

Zhusubaliyev, Z., Rudakov, V., Soukhoterin, E., & Mosekilde, E. (2000). Bifurcation Analysis of the Henon Map. *Discrete Dynamics in Nature and Society, 5*, 203-221.

APPENDICES

APPENDIX A

--G-Functions and Switching Conditions

As described in the theory of switchability (Luo, Discontinuous Dynamical Systems on Time-varying Domains, 2009), for a dynamic system consists of *N* sub-dynamic systems, a universal domain can be divided into *N* accessible sub-domains Ω_i plus the inaccessible sub-domains Ω_0. On the i^{th} sub-domain Ω_i, there is a C^{r_i}-continuous system ($r_i \geq 1$) in the form of

$$\dot{\mathbf{x}}^{(i)} \equiv \mathbf{F}^{(i)}(\mathbf{x}^{(i)}, t, \mathbf{p}_i) \in \mathbb{R}^n,\ \mathbf{x}^{(i)} = (x_1^{(i)}, x_2^{(i)}, ..., x_n^{(i)})^{\mathrm{T}} \in \Omega, \tag{A1}$$

where the time is t, and $\dot{\mathbf{x}}^{(i)} = d\mathbf{x}^{(i)}/dt$. $\mathbf{F}^{(i)}(\mathbf{x}^{(i)}, t, \mathbf{p}_i)$ is the C^{r_i}-continuous ($r_i \geq 1$) vector field with $\mathbf{p} = (p_i^{(1)}, p_i^{(2)}, ..., p_i^{(l)})^{\mathrm{T}} \in \mathrm{R}^l$ as the parameter vector. The boundary between the two domains Ω_i and Ω_j can be defined as

$$\partial\Omega_{ij} = \bar{\Omega}_i \bigcap \bar{\Omega}_j = \{\mathbf{x} \,|\, \varphi_{ij}(\mathbf{x}, t, \boldsymbol{\lambda}) = 0,\ \varphi_{ij} \text{ is } C^r\text{-continuous } (r \geq 1)\} \subset \mathbb{R}^{n-1}. \tag{A2}$$

Base on this boundary definition, $\partial\Omega_{ij} = \partial\Omega_{ji}$. And the dynamical system on the boundary Ω_{ij} is

$$\dot{\mathbf{x}}^{(0)} = \mathbf{F}^{(0)}(\mathbf{x}^{(0)}, t, \boldsymbol{\lambda}). \tag{A3}$$

The normal vector of the boundary $\partial\Omega_{ij}$ at point $\mathbf{x}^{(0)}(t)$ is given as

$$\mathbf{n}_{\partial\Omega_{ij}}(\mathbf{x}^{(0)}, t, \boldsymbol{\lambda}) = \nabla\varphi_{ij}(\mathbf{x}^{(0)}, t, \boldsymbol{\lambda}). \tag{A4}$$

The *G*-functions of the zero-order can be define as

$$G_{\partial\Omega_{ij}}^{(\alpha)}(\mathbf{x}_m, t_{m\pm}, \mathbf{p}_\alpha, \boldsymbol{\lambda}) \equiv \mathbf{n}_{\partial\Omega_{ij}}^{\mathrm{T}}(\mathbf{x}^{(0)}, t, \boldsymbol{\lambda}) \bullet [\mathbf{F}^{(0)}(\mathbf{x}^{(\alpha)}, t, \mathbf{p}_\alpha) - \mathbf{F}^{(0)}(\mathbf{x}^{(0)}, t, \boldsymbol{\lambda})]\Big|_{(\mathbf{x}_m^{(0)}, \mathbf{x}_m^{(\alpha)}, t_{m\pm})}. \tag{A5}$$

And the k^{th} order *G*-functions are defined as

$$\begin{aligned} &G_{\partial\Omega_{ij}}^{(k,\alpha)}(\mathbf{x}_t^{(0)}, t_\pm, \mathbf{x}_{t_\pm}^{(\alpha)}, \mathbf{p}_\alpha, \boldsymbol{\lambda}) \\ &\quad = \sum_{s=1}^{k+1} C_{k+1}^s D_{\mathbf{x}_t^{(0)}}^{k+1-s} \mathbf{n}_{\partial\Omega_{ij}}^{\mathrm{T}} \bullet [D_{\mathbf{x}}^{s-1}\mathbf{F}(\mathbf{x}, t, \mathbf{p}_\alpha) - D_{\mathbf{x}^{(0)}}^{s-1}\mathbf{F}^{(0)}(\mathbf{x}^{(0)}, t, \boldsymbol{\lambda})]\Big|_{(\mathbf{x}_m^{(0)}, \mathbf{x}_{m\pm}^{(\alpha)}, t_{m\pm})}. \end{aligned} \tag{A6}$$

Thus, the flow $\mathbf{x}^{(i)}(t)$ and $\mathbf{x}^{(j)}(t)$ to the boundary $\partial\Omega_{ij}$ is semi-passable from Ω_i to Ω_j as shown in Figure. A1 is given by Eq. (A7) (Luo, Discontinuous Dynamical Systems on Time-varying Domains, 2009). As illustrated in Figure A1, when the flow $\mathbf{x}^{(i)}(t)$ in domain Ω_i goes onto the boundary $\partial\Omega_{ij}$, if $G^{(i)}_{\partial\Omega_{ij}} < 0$ and $G^{(j)}_{\partial\Omega_{ij}} < 0$ for $\mathbf{n}_{\partial\Omega_{ij}} \to \Omega_i$, then the flow will pass the boundary and become $\mathbf{x}^{(j)}(t)$ in domain Ω_j, which forms a semi-passable flow from domain Ω_i to Ω_j.

$$\left.\begin{array}{l} \left.\begin{array}{l} G^{(i)}_{\partial\Omega_{ij}}(\mathbf{x}_m, t_{m-}, \mathbf{p}_i, \boldsymbol{\lambda}) > 0 \\ G^{(j)}_{\partial\Omega_{ij}}(\mathbf{x}_m, t_{m-}, \mathbf{p}_i, \boldsymbol{\lambda}) > 0 \end{array}\right\} \text{for } \mathbf{n}_{\partial\Omega_{ij}} \to \Omega_j, \\ \left.\begin{array}{l} G^{(i)}_{\partial\Omega_{ij}}(\mathbf{x}_m, t_{m-}, \mathbf{p}_i, \boldsymbol{\lambda}) < 0 \\ G^{(j)}_{\partial\Omega_{ij}}(\mathbf{x}_m, t_{m-}, \mathbf{p}_i, \boldsymbol{\lambda}) < 0 \end{array}\right\} \text{for } \mathbf{n}_{\partial\Omega_{ij}} \to \Omega_i. \end{array}\right\} \tag{A7}$$

Again, from the non-passable flow of the first kind (Luo, Discontinuous Dynamical Systems on Time-varying Domains, 2009), the sliding flow $\mathbf{x}^{(i)}(t)$ and $\mathbf{x}^{(j)}(t)$ on the boundary $\partial\Omega_{ij}$ is given by

$$\left.\begin{array}{l} \left.\begin{array}{l} G^{(i)}_{\partial\Omega_{ij}}(\mathbf{x}_m, t_{m-}, \mathbf{p}_i, \boldsymbol{\lambda}) > 0 \\ G^{(j)}_{\partial\Omega_{ij}}(\mathbf{x}_m, t_{m-}, \mathbf{p}_i, \boldsymbol{\lambda}) < 0 \end{array}\right\} \text{for } \mathbf{n}_{\partial\Omega_{ij}} \to \Omega_j, \\ \left.\begin{array}{l} G^{(i)}_{\partial\Omega_{ij}}(\mathbf{x}_m, t_{m-}, \mathbf{p}_i, \boldsymbol{\lambda}) < 0 \\ G^{(j)}_{\partial\Omega_{ij}}(\mathbf{x}_m, t_{m-}, \mathbf{p}_i, \boldsymbol{\lambda}) > 0 \end{array}\right\} \text{for } \mathbf{n}_{\partial\Omega_{ij}} \to \Omega_i. \end{array}\right\} \tag{A8}$$

This is also the onset condition for sliding motion on the boundary $\partial\Omega_{ij}$. On the other hand, the condition for sliding motion on the boundary $\partial\Omega_{ij}$ to vanish into domain Ω_i is given as

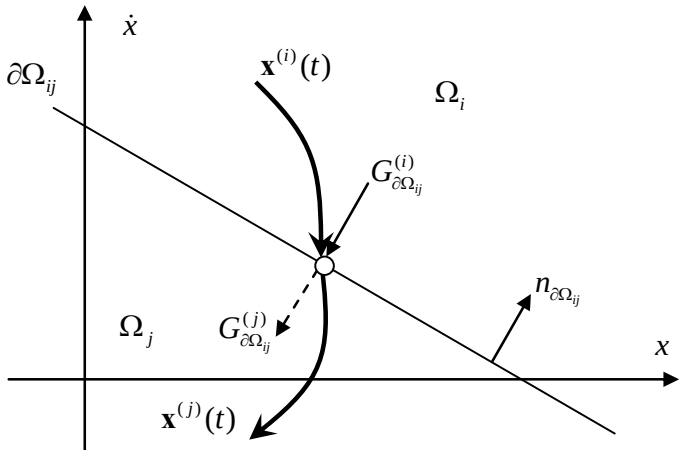

Figure A1: Semi-passable flow from Ω_i to Ω_j

$$\left.\begin{array}{l} G^{(0,i)}_{\partial\Omega_{ij}}(\mathbf{x}_m, t_{m\pm}, \mathbf{p}_j, \boldsymbol{\lambda}) = 0 \\ \left.\begin{array}{l} G^{(1,i)}_{\partial\Omega_{ij}}(\mathbf{x}_m, t_{m+}, \mathbf{p}_i, \boldsymbol{\lambda}) < 0 \\ G^{(0,j)}_{\partial\Omega_{ij}}(\mathbf{x}_m, t_{m\pm}, \mathbf{p}_i, \boldsymbol{\lambda}) < 0 \end{array}\right\} \text{for } \mathbf{n}_{\partial\Omega_{ij}} \to \Omega_j, \\ \left.\begin{array}{l} G^{(1,i)}_{\partial\Omega_{ij}}(\mathbf{x}_m, t_{m+}, \mathbf{p}_i, \boldsymbol{\lambda}) > 0 \\ G^{(0,j)}_{\partial\Omega_{ij}}(\mathbf{x}_m, t_{m\pm}, \mathbf{p}_i, \boldsymbol{\lambda}) > 0 \end{array}\right\} \text{for } \mathbf{n}_{\partial\Omega_{ij}} \to \Omega_i. \end{array}\right\} \quad \text{(A9)}$$

Figure A2 illustrates the onset, ongoing, and vanishing of a sliding motion. When the flow $\mathbf{x}^{(i)}(t)$ in domain Ω_i comes onto the boundary $\partial\Omega_{ij}$, if $G^{(0,i)}_{\partial\Omega_{ij}} < 0$ and $G^{(0,j)}_{\partial\Omega_{ij}} > 0$ for $\mathbf{n}_{\partial\Omega_{ij}} \to \Omega_i$, then the onset condition of sliding motion satisfies. And the flow turns into $\mathbf{x}^{(0)}(t)$ which moves on the boundary, until $G^{(0,j)}_{\partial\Omega_{ij}} = 0$, $G^{(0,i)}_{\partial\Omega_{ij}} < 0$, and $G^{(0,j)}_{\partial\Omega_{ij}} < 0$, which means the vanishing condition of sliding motion satisfy. And the flow will leave the boundary ($\mathbf{x}^{(j)}(t)$) and goes into domain Ω_j as shown in Figure A2.

Finally, the tangential flow (Luo, Discontinuous Dynamical Systems on Time-varying Domains, 2009) gives the grazing motion to the boundary $\partial\Omega_{ij}$ in domain Ω_i as follows:

$$\left.\begin{aligned} &G_{\partial\Omega_{ij}}^{(0,i)}(\mathbf{x}_m, t_m, \mathbf{p}_i, \boldsymbol{\lambda}) = 0 \\ &G_{\partial\Omega_{ij}}^{(1,i)}(\mathbf{x}_m, t_m, \mathbf{p}_i, \boldsymbol{\lambda}) < 0 \text{ for } \mathbf{n}_{\partial\Omega_{ij}} \to \Omega_j, \\ &G_{\partial\Omega_{ij}}^{(1,i)}(\mathbf{x}_m, t_m, \mathbf{p}_i, \boldsymbol{\lambda}) > 0 \text{ for } \mathbf{n}_{\partial\Omega_{ij}} \to \Omega_i. \end{aligned}\right\} \quad \text{(A10)}$$

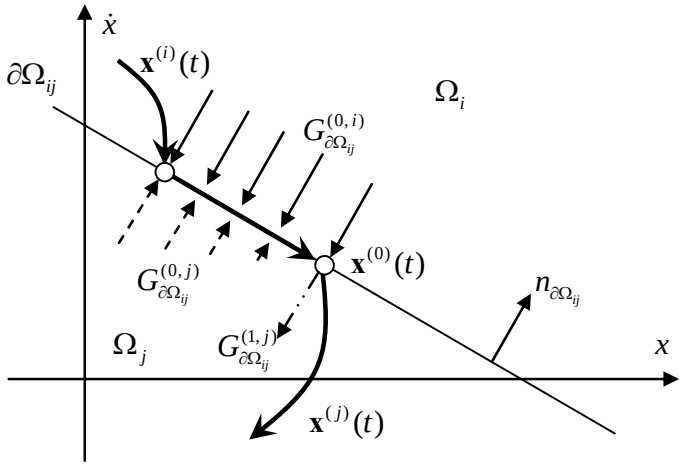

Figure A2: Sliding motion on the boundary $\partial\Omega_{ij}$.

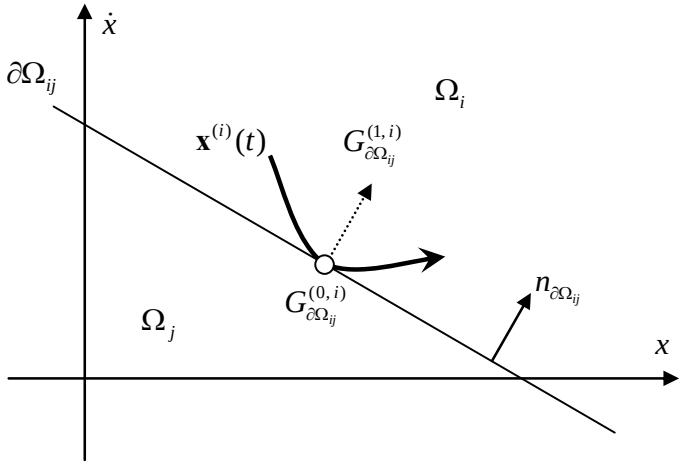

Figure A3: Grazing motion in domain Ω_i

Eq. (A10) also provides the grazing bifurcation conditions of the system as is illustrated in Figure 3: when the flow $\mathbf{x}^{(i)}(t)$ in domain Ω_i goes onto the boundary $\partial\Omega_{ij}$, if $G_{\partial\Omega_{ij}}^{(0,i)} = 0$ and $G_{\partial\Omega_{ij}}^{(1,i)} > 0$ for $\mathbf{n}_{\partial\Omega_{ij}} \to \Omega_i$, then the grazing motion condition satisfies. In this case, the flow

will tangentially touch the boundary and then goes back into domain Ω_i without passing the boundary.

VITA

Graduate School
Southern Illinois University

Yu Guo

gary.rain@gmail.com

South China University of Technology
Bachelor of Computer Engineering, September 2006

Southern Illinois University Edwardsville
Master of Mechanical Engineering, August 2008

Special Honors and Awards:

- Best Presentation Award in the 2011 Graduate Student Symposium at SIUE, 2011.
- Travel Grant for ASME International Mechanical Engineering Congress and Exposition (IMECE) 2009- 2011.
- Travel Grant for 12th Conference on Nonlinear Vibrations, Dynamics and Multibody Systems at Virginia Tech 2008.
- President of the Chinese Student Community at SIUE 08/2008-09/2011.
- Vice-president of the Chinese Student Community at SIUE 08/2006-08/2008.
- Excellent Student Scholarship at SCUT, 2002-2003 & 2003-2004.

Dissertation Title:

Bifurcation and Chaos of Nonlinear Vibro-Impact Systems

Major Professor: Albert C.J. Luo

Publications:

Journal Articles:

1. Y. Guo and A. C.J. Luo (2011), “Parametric analysis of a periodically driven horizontal impact pair”, International Journal of Bifurcation and Chaos, Vol 7, Issue 2, Article No. 021001.
2. Y. Guo and A. C.J. Luo (2011), “Analytical prediction of complex motions of a ball in a periodically shaken horizontal impact pair”, ASME Journal of Computational and Nonlinear Dynamics, Vol 7, Issue 2, Article No. 021001.
3. A. C.J. Luo and Y. Guo (2010), “Parameter Characteristics for Stable and Unstable Solutions in Nonlinear Discrete Dynamical Systems”, International Journal of Bifurcation and Chaos, Vol 20, Issue 10, pp. 3173-3191.
4. Y. Guo and A. C.J. Luo (2011), “Discontinuity and Bifurcation Analysis of Motions in a Fermi Oscillator under Dual Excitations”, Journal of Vibroengineering, Vol 13, Issue 1, pp. 66-101.
5. A. C.J. Luo and Y. Guo (2010), “Switching Mechanism and Complex Motions in an Extended Fermi-Acceleration Oscillator”, ASME Journal of Computational and Nonlinear Dynamics. Vol 5, Issue 4, pp. 1-14.

6. A. C.J. Luo and Y. Guo (2009), “Motion Switching and Chaos of a Particle in a Generalized Fermi-Acceleration Oscillator”, Mathematical Problems in Engineering, Paper No. 298906.

Monograph:

1. Albert C. J. Luo and Yu Guo (2013), “Vibro-Impact Dynamics”, Wiley.

Book Chapters:

1. Yu Guo and Albert C. J. Luo (2011), “Complex motions in a Fermi Oscillator”, Nonlinear Approaches in Engineering Applications (Eds. L. Dai, and R. Jazar, Springer) pp.105-134.
2. A.C.J. Luo and Y. Guo (2010), “Complete Bifurcation Behaviors of a Henon Map”, Dynamical Systems-Discontinuity, Stochasticity, and Time-Delay, (Eds. Albert C.J. Luo, Springer). pp.37-47.
3. A.C.J. Luo and Y. Guo (2009), “Switching and Stick Motions in an Extended Fermi-Acceleration Oscillator”, Vibro-Impact Dynamics of Ocean Systems and Related Problems, Lecture Notes in Applied and Computational Mechanics (Eds. Raouf A Ibrahim, Vladimor I Babitsky and Masaaki Okuma, Springer). pp.179-189.

Conference Articles:

1. A.C.J. Luo and Y. Guo, (2011), “Bifurcation Analysis of a Double-Excited Fermi-Acceleration Oscillator under Different Excitations”, ASME International Mechanical Engineering Congress and Exposition, Denver, Colorado, USA, Paper No. IMECE2011-62947.
2. Y. Guo and A.C.J. Luo, (2011), “Complex Motions in a Horizontal Impact Pair with Periodic Excitation”, ASME International Design Engineering Technical Conference & Computers and Information in Engineering Conference, Washington, DC, USA, Paper No. IDETC/CIE2011-47385.
3. A.C.J. Luo and Y. Guo, (2010), “Switchability and Bifurcation of Motions in a Double-Excited Fermi-Acceleration Oscillator”, ASME International Mechanical Engineering Congress and Exposition, Vancouver, British Columbia, Canada, Paper No. IMECE2010-39165.
4. A.C.J. Luo and Y. Guo, (2009), “On Stable and Unstable Periodic Solutions of N-Dimensional Discrete Dynamical Systems”, ASME International Mechanical Engineering Congress and Exposition, Florida, MA, USA, Proceedings 10 (PART B), pp. 945-953.
5. A.C.J. Luo and Y. Guo, (2008), “Switching Bifurcation and Chaos in an Extended Fermi-Acceleration Oscillator”, ASME International Mechanical Engineering Congress and Exposition, Boston, MA, USA, Proceedings 11, pp. (Vol 2) 293-304.

Conference Presentation:

1. A.C.J. Luo and Y. Guo, (2008), “Switching Mechanism of Periodic and Chaotic Motions in an Extended Fermi-acceleration Oscillator”, Presentation on 8th Understanding Complex Systems Conference at University of Illinois Urbana Champaign.
2. A.C.J. Luo and Y. Guo, (2008), “Switching Bifurcation and Chaos in an Extended Fermi-Acceleration Oscillator”, Presentation on 12th Conference on Nonlinear Vibrations, Dynamics and Multibody Systems at Virginia Tech.

3. A.C.J. Luo and Y. Guo (2008), “Switching and Stick Motions in an Extended Fermi-Acceleration Oscillator”, Presentation on International symposium on Dynamics of Vibro-Impact Systems, Troy Michigan, USA.